Homotypic and heterotypic interactions in the peripheral nervous system

Julian Jan Albert Hoving

Thesis submitted for the degree of Doctor of Philosophy

MRC Laboratory for Molecular Cell Biology

University College London

Declaration

I, Julian Jan Albert Hoving, confirm that the work presented in this thesis is my own. Where information has been derived from other sources, I confirm that this has been indicated in the thesis.

Signed…….....……. Date..……

Abstract

Peripheral nerves have a remarkable ability to regenerate following a transection injury. To achieve this, Schwann cells collectively migrate as cords, taking regrowing axons across newly formed tissue known as the bridge that forms to reconnect the two nerve stumps. The Schwann cell cords themselves are guided by a newly formed polarised vasculature that provides a conducive environment for Schwann cell migration. Here we show, that in addition to mediating Schwann cell clustering, N-cadherin is required for contact inhibition of locomotion (CIL) in Schwann cells, which may be required to produce an outward force within the cords of collectively migrating Schwann cells. Mechanistically we show that N-cadherin regulates CIL independent of its traditional mechanism of trans-homodimerisation and independent of adherence junction components. Instead, the extracellular domain of N-cadherin is sufficient to mediate CIL, which appears to present a repulsion (co-)signal to the other cell. We further show, that CIL is disrupted in Schwann cells expressing oncogenic Ras in a MEK-dependent manner, not through loss of N-cad, but through loss of a distinct signal. Ras-Raf-MEK-ERK signalling alters the mRNA expression levels of ephrins and Eph receptors, and we show using Co-IP and mass spectrometry, that oncogenic Ras changes the interaction profile of N-cadherin proteins and show a potential role for glypican-4 and ephrin-A1 in CIL. Finally, we show that migration of Schwann cells along the vasculature is independent of focal adhesion complexes, consistent with the more amoeboid-mode of migration observed along the blood vessels.

Acknowledgements

I would like to thank Alison Lloyd for her guidance throughout this project and her feedback on the first drafts of this thesis. I would also like to thank members of the lab, previous and past, for the discussions and their scientific feedback on this project. I am grateful to Lucie for proof reading my thesis and Anne-Laure for the countless scientific discussions and her advice on experiments, as well as, the members of my thesis committee Ewa Paluch, Buzz Baum and Karl Matter for their advice.

My appreciation goes out to all of my friends, here in London and back home in Amsterdam, for their support in different ways over the many years, you have been an inspiration to me. I would also like to express my deepest gratitude to my family back home in Amsterdam and Geneva, for their support and encouragement over the many years.

Finally, I owe my sincerest gratitude to my boyfriend Christopher Whale, who I could always rely on for support. You have been invaluable to me.

Table of Contents

Declaration 2
Abstract 3
Acknowledgements 4
Table of Contents 5
List of Figures and Tables 9
List of Abbreviations and Acronyms 12
Chapter One: Introduction 14
1.1. Cell migration during tissue formation and homeostasis 14
1.1.1. Principles of cell migration 15
1.1.2. Collective migration 18
1.1.3. Contact inhibition of locomotion 20
1.1.4. Repolarisation 21
1.1.5. From cell-cell recognition to intracellular signalling 22
1.1.6. CIL in collective migration 23
1.1.7. Neuronal-cadherin 25
1.1.7.1. Classification and function 25
1.1.7.2. Trans- and cis-interactions 27
1.1.7.3. Adherence junction components 29
1.1.8. Cadherins in collective migration and CIL 32
1.1.9. Guidance molecules 34
1.1.9.1. Eph receptors and their ligands 35
1.1.9.2. CIL in tumourigenesis 39
1.2. Schwann cell biology 42
1.2.1. Schwann cell development 43
1.2.2. Neural crest 44
1.2.3. Schwann cell precursors 46
1.2.4. Immature Schwann cells 47
1.2.5. Myelin regulators and structure 48
1.3. Nerve regeneration 54

1.3.1. Injury response 54
1.3.2. Schwann cell migration 59
1.4. Pathology 62
1.4.1. Neuropathies 62
1.4.2. NF1 and NF2 63
1.4.2.1. Neurofibromatosis Type I 63
1.4.2.2. Neurofibromatosis Type II 67
1.5. Thesis Aims 69
Chapter Two: Materials and Methods 70
2.1. Materials 70
2.1.1. Chemicals 70
2.1.2. Constructs and oligos 70
2.1.3. Buffers 73
2.1.4. Antibodies 73
2.1.5. Cell culture 74
2.1.5.1. Preparation tissue culture dishes 74
2.1.5.2. Schwann Cells 75
2.1.5.3. Raf-ER cells 76
2.1.5.4. DNp53-Ras cells 76
2.1.6. Fibroblasts 76
2.1.7. HUVECS 76
2.1.8. Retroviral infection 77
2.2. Methods 78
2.2.1. Cell Assays 78
2.2.1.1. Dorsal root ganglion neurons (DRG) preparation and co-cultures . 78
2.2.1.2. siRNA transfection 79
2.2.1.3. DNA transfection 79
2.2.1.4. Cell rounding assay 80
2.2.1.5. Repulsion assays 80
2.2.1.6. Repulsion quantification 81
2.2.1.7. Rescue experiments 82

2.2.1.8. Matrigel assays 83
2.2.1.9. 2D migration assays 83
2.2.1.10. Scratch assay 83
2.2.1.11. Cell tracking 84
2.2.2. Microscopy 84
2.2.2.1. Time Lapse Microscopy 84
2.2.2.2. Immunofluorescence 84
2.2.3. Protein Analysis 85
2.2.3.1. Protein extraction and quantification 85
2.2.3.2. Western Blotting 85
2.2.3.3. Co-immunoprecipitation (Co-IP) 86
2.2.4. Molecular biology 87
2.2.4.1. RNA extraction and cDNA synthesis 87
2.2.4.2. RT-qPCR 87
2.2.5. Cloning 88
2.2.5.1. Mutagenesis 88
2.2.5.2. Transformation 88
2.2.6. Mass spectrometry 89
2.2.7. Statistics 90
Chapter Three: Results I
Characterising the role of N-cad in contact inhibition of locomotion 91
3.1. Chapter introduction 91
3.2. Characterisation of Schwann cell-Schwann cell recognition 91
3.3. CIL is independent of trans-homodimerisation 100
3.4. Assessing the mechanism by which N-cad regulates CIL 103
3.5. The extracellular domain of N-cad mediates CIL in Schwann cells 117
3.6. Chapter discussion and conclusions 124
Chapter Four: Results II
Uncovering the mechanism of homotypic CIL 138
4.1. Chapter introduction 138
4.2. Assessing homotypic CIL of DNp53-Ras Schwann cells 141

4.3. Assessing homotypic CIL of DNp53-Ras Schwann cells 145
4.4. A candidate approach to determine the co-signal in CIL 149
4.5. The role of ephrins in homotypic CIL 155
4.6. Mass spectrometry 164
4.7. Chapter conclusions and discussion 176
4.7.1. Loss of cell-cell recognition in NF1 182
4.7.2. Repulsion signals 189
Chapter Five: Results III
Uncovering the mechanism of heterotypic Schwann cell-endothelial cell interactions 192
5.1. Chapter introduction 192
5.2. Assessing the role of β1-integrin on Schwann cell migration 193
5.3. β1-integrin is not required for Schwann cell migration along blood vessels 197
5.4. Chapter conclusion 205
Chapter Six: Conclusion 210
References 216
Appendix 234

List of Figures and Tables

Figure 1.1. Migrating cells adapt a front to rear polarity. ……..17
Figure 1.2. Cell polarity mediates single cell and collective migration. ……..20
Figure 1.3. The mechanism of CIL. ……21
Figure 1.4. Cell-cell recognition molecules that mediate CIL. ……24
Figure 1.5. The cadherin super family. ……...26
Figure 1.6. Formation of N-cadherin complexes. ……..28
Figure 1.7. Cadherin assembles in adherence junction complexes. …… 30
Figure 1.8. Eph and ephrin interactions can induce bidirectional signalling. ……...37
Figure 1.9. Structure of the peripheral nerve. ……44
Figure 1.10. The major differentiation steps of the Schwann cell lineage. ……...45
Figure 1.11. Structure of myelinated axons. ……...50
Figure 1.12. The assembly of the Nodes of Ranvier. ……53
Figure 1.13. Schwann cells orchestrate the regenerative process. ……55
Figure 1.14. Model of the multi-cellular processes involved in the regeneration of peripheral nerves. ……56
Figure 1.15: Schwann cells change their behaviour following heterotypic interactions with fibroblasts. ……58
Figure 1.16: Schwann cell migrate as cellular cords required for axonal regeneration. ……59
Figure 1.17. Neurofibromas mimic an unrepaired wound. ……65
Figure 3.1. Loss of cell-cell recognition is mediated by a loss of N-cadherin. ……93
Figure 3.2. CIL is dependent on N-cad. ……97
Figure 3.3. Outward migration is dependent on N-cad. ……..……97
Figure 3.4. N-cad is required for Schwan cell directionality. ..……101
Figure 3.5. N-cad mediates CIL independent of *trans*-homodimerisation. ……..104
Figure 3.6. N-cad mediates CIL independent of *trans*-homodimerisation. ……..105
Figure 3.7. Schwann cells express αE-catenin. ……...107
Figure 3.8. αE-catenin knockdown. ……109
Figure 3.9. CIL is mediated through αE-catenin independent mechanisms. ……...111
Figure 3.10. αE-catenin is required to form stable junctions. ……112
Figure 3.11. p120-catenin has a slow turnover. ……114
Figure 3.12. N-cad mediates CIL independent of p120-catenin. ……115
Figure 3.13. N-cad expression levels correlates to p120-catenin knockdown. ……118

Figure 3.14. Expression of N-cad full length and mutants in Schwann cells. …….120
Figure 3.15. The different N-cad constructs are functional. ……..125
Figure 3.16. Velocity analysis of Schwann cells overexpressing N-cad mutants. .126
Figure 3.17. N-cad full length rescues the N-cad knockdown phenotype. ……..127
Figure 3.18. The extracellular domain of N-cad is sufficient to mediate CIL. ……..128
Figure 3.19 N-cad mediates CIL independent of trans homodimerisation. …….130
Figure 3.20 Repulsion signal could induce outward forces, which could drive
the collective migration of Schwann cells. ……136
Figure 4.1. Raf-activated Schwann cells grab axons in an N-cad dependent
Manner. ……..139
Figure 4.2 N-cad regulates opposing behaviours in Schwann cells. ……140
Figure 4.3. Expression of oncogenic Ras induces loss of cell-cell recognition in
a MEK dependent manner. ……142
Figure 4.4. CIL in Schwann cell expressing Ras is lost in a MEK dependent
manner..……..146
Figure 4.5. Loss of CIL in DNp53-Ras-SCs is not due to aberrant expression of N-
cad. ……..147
Figure 4.6. The kinetics of PD184352 restoration of CIL in Ras-expressing cells
Is slow. …..……150
Figure 4.7. Oncogenic Ras induces changes in the mRNA expression of the
Eph receptor family in a MEK dependent manner. ……151
Figure 4.8. Oncogenic Ras induces changes in the mRNA expression of the
Eph receptor family in a MEK dependent manner. ……152
Figure 4.9. Raf-activation is sufficient to induce loss of cell-cell recognition
between Schwann cells. ……..156
Figure 4.10. Raf activation is sufficient to induce changes in the mRNA
expression levels of the Eph receptor family. ……..157
Figure 4.11. Homotypic CIL and heterotypic CIL in Schwann cells are
mediated through different mechanisms. ……159
Figure 4.12. Clustered Ephrin-A1 induces Schwann cell rounding. ……163
Figure 4.13. Fyn inhibition does not affect CIL. ……...165
Figure 4.14. Raf-activation does not affect the adherence junction complex. ……167
Figure 4.15. Mass Spec analysis of N-cad complexes. ……..170
Figure 4.16. Functional classification of proteins overlapping TMX and EtOH. …..171
Figure 4.17. Functional classification of proteins interacting with N-cad in only

the EtOH treated samples. ……172
Figure 4.18. Functional classification of proteins interacting with N-cad in TMX treated samples. ……173
Figure 4.19. Glypican-4 siRNA knockdown is extremely efficient. ……175
Figure 4.20. Glypican-4 is required for CIL in Schwann cells. ……177
Figure 4.21. Glypican-4 does not appear to affect N-cad levels at membrane junctions. ……178
Figure 4.22. Schematic overview of affects of oncogenic Ras on CIL..……181
Figure 4.23. Heterotypic and homotypic CIL between Schwann cells and fibroblasts are differentially mediated. ……...182
Figure 4.24 N-cad mediates repulsion possibly through interaction with a co-signal. ……191
Figure 5.1. β1 integrin is required for 2D Schwann cell migration. ……195
Figure 5.2. Talin1 and Talin2 integrin are required for 2D Schwann cell migration. 198
Figure 5.3. Schwann cell migrate along tubules ……199
Figure 5.4. Schwann cell migration along endothelial tubules is independent of β1 integrin. ……..202
Figure 5.5. Schwann cell migration along endothelial tubules is independent of talin. ……..203
Figure 5.6. Schwann cell migration along the blood vessels is independent of focal adhesion complexes. ……204
Figure 5.7 Amoeboid-like migration of Schwann cells along the vasculature. …….207
Table 2.1 siRNA oligos. ……..71
Table 2.2 Rt-qPCR primers. ……...72
*Table 2.3 western blot and Co-IP buffers. ……*73
Table 2.4. Immunofluorescence antibodies. ……74
Table 2.5. Western blot antibodies. ……..74
Table 4.1 Expression levels of Ephrin-A ligands in DNp53-Schwann cells and DNp53-Ras-Schwann cells. ……161
Table 4.2. Summary of identified proteins. ……168
Table 4-3. Overview of proteins overlapping in TMX and EtOH. Treated samples……171
Table 4-4. Overview of proteins interacting with N-cad in EtOH treated samples. .172
Table 4-5. Overview of proteins interacting with N-cad in TMX treated samples. ..173

List of Abbreviations and Acronyms

BSA	Bovine serum albumin
CAM	Cell adhesion molecules
CIL	Contact inhibition of locomotion
CIP	Contact inhibition of proliferation
CLEM	Correlative light electron microscopy
CMT	Charcot-Marie-Tooth disease
CNS	Central nervous system
Co-IP	Co-immunoprecipitation
CRC	Colorectal cancer
DNp53	Dominant negative p53
DNp53-Ras-SCs	Schwann cells expressing DNp53 and oncogenic Ras
DNp53-SC	Schwann cells expressing DNp53
DTSSP	3,3'-Dithiobis(sulfosuccinimidylpropionate)
EC domains	Extracellular cadherin domains
ECM	Extracellular matrix
ER	endoplasmic reticulum
Extra	Extracellular domain
E-cad	Epithelial cadherin
FGF	Fibroblast growth receptor
FL	Full length
GAP	GTPase activating protein
GEF	Guanine nucleotide exchange factors
GPCR	G-protein-coupled receptor
GPI	glycosylphosphatidylinositol
HAV-motif	Histidine-alanine-valine
HUVECs	Human umbilical vain endothelial cells
HRP	Horseradish peroxidase
IGF-2	Insulin growth factor-2,
Intra	Intracellular domain
LIF	leukaemia inhibitory factor
MAG	Myelin associated glycoprotein and
Mass Spec	Mass spectrometry

MPZ	Myelin protein zero gene
MPNST	Malignant Peripheral Nerve Sheath Tumours
M-cad	Muscle cadherin
Nck1	Non-catalytic region of Tyr kinase adaptor protein 1
Necl	Nectin-like proteins
NF1	Neurofibromatosis Type 1
NF155	Neurofascin
NF2	Neurofibromatosis Type 2
NRG	Neuregulin
NR-SCs	Schwann expressing Ras or a Raf-inducible construct
NT3	Neurotrophin3
N-cad	Neuronal cadherin
PDGF	Platelet-derived growth factor
PFA	Paraformaldehyde
pFib	primary fibroblasts
PI3K	Phosphoinositide 3-kinase
PNS	Peripheral nervous system
P-cad	Placental cadherin
RTK	Receptor tyrosine kinases
R-cad	Retinal cadherin
ROCK	Rho-associated protein kinase
SAM	Sterile alpha motif
SCR	Scrambled siRNA
SDS-Page	Sodium dodecyl sulphate-polyacrylamide gel electrophoresis
Sema4F	Semaphorin4F
siRNA	small interfering (si) RNA
SI	siRNA
TMX	tamoxifen
VE-cad	Vascular-endothelial cadherin
ZO1	Zonula occludens protein 1

Chapter One: Introduction

1.1. Cell migration during tissue formation and homeostasis

The development of organs and tissues requires the orchestration of multiple processes including cell growth, cell proliferation, survival and movement. Moreover, tissues consist of multiple cell types, domains and compartments, each with their own unique properties, which requires the cell sorting of initially intermingled cells into separate cell populations (Batlle and Wilkinson, 2012). This separation of cell compartments by a clear border occurs during a process called boundary formation and requires the coordination of multiple signals between different cells types, which can be mediated via homotypic or heterotypic interactions. Boundary formation is mediated by repulsive signals, which cause the separation of different cell populations away from each other, and adhesive signals, which mediates the sorting of cells into groups of cells (Batlle and Wilkinson, 2012; Steinberg, 2007). Once the boundaries are established they are further exposed to cell movement caused by growth and morphogenesis, which includes migrating cells, as well as cell movement caused by the proliferation of cells (Batlle and Wilkinson, 2012). In the adult, cellular movement occurs in some instances during homeostasis and can be further triggered during the regeneration of a tissue following injury and during an immune response. Control of cell migration to the appropriate areas to position cell populations is crucial to maintain the integrity of tissues. Intermingling of different populations is prevented by contact repulsion and contact inhibition of cell movement, however, differential adhesion also plays a role (Abercrombie and Heaysman, 1954b; Batlle and Wilkinson, 2012; Steinberg, 2007). The movement of cells into inappropriate areas is associated with many diseases including tumourigenesis and is central to tumour invasion and metastasis (Batlle and Wilkinson, 2012). Thus, it is important to

understand how cells recognise and communicate with each other and how these controls are lost during the tumourigenic process.

1.1.1. Principles of cell migration

Cellular movement is a key process during the development of tissues and organs and in the adult, cellular movement can be further triggered upon injury, and metastasis (Mayor and Etienne-Manneville, 2016). Cells can either migrate as single cells or as groups of cells. Single cell migration *in vitro* is well characterised; cells adopt a front to rear polarity, with F-actin-rich membrane protrusions such as lamellipodia and filopodia at the front the cell, and a contractile actomyosin rear (Figure 1.1) (Reig et al., 2014). Motility of cells is mediated by cycles of i. Actin dependent-protrusion extension at the front of the cell, where adhesions of the cell to the substrate are formed, ii. Contraction of the cell body, iii. Disassembly of focal adhesions at the rear of the cell and iv. Retraction of the rear (Figure 1.1) (Reig et al., 2014). This front to rear polarisation is achieved by a polarised cytoskeletal organisation, which in turn is set by a front to rear activation of RhoGTPases including active Rac-1 and Cdc42 at the front of the cell, and active Rho at the back of the cell (Figure 1.1) (Nobes and Hall, 1999). Moreover, the rear of the cell is defined by active myosin II, required for contraction of the cell body (Figure 1.1) (Reig et al., 2014).

Rho GTPases are the master regulators of the cytoskeletal changes that integrate multiple external cues that can control migration, such as adhesion to the ECM through integrins, cell-cell interactions and cytokines (Mayor and Etienne-Manneville, 2016). RhoGTPase family members cycle between the inactive GDP bound state and the active GTP bound state, in which they can bind to downstream effectors (Sadok and Marshall, 2014). GTPases are regulated by guanine nucleotide

exchange factors (GEFs) mediating the exchange from GDP to GTP, and GTPase-activating proteins (GAPs) that promote hydrolysis of GTP to GDP by increasing their intrinsic GTPase activity. Rac-1 and Cdc42 are active at the front of polarised migrating cells and promote lamellipodia and filopodia formation respectively by regulating actin polymerisation (Nobes and Hall, 1999) (Figure 1.1). RhoA is important for force generation by mediating contractility at the rear of the cell by regulating Rho-associated protein kinase (ROCK), but has also been shown to be active at the front of the cells where it is required for the initial actin polymerisation (Machacek et al., 2009; Narumiya et al., 2009; Pertz et al., 2006).

Integrin-dependent migration is important for migration along the extracellular matrix (Huttenlocher and Horwitz, 2011). Adhesion to substrates such as laminin, collagen and fibronectin, through integrins induces cytoskeletal reorganisation and the formation of protrusions (Huttenlocher and Horwitz, 2011). Moreover, integrins mediate traction forces, which allow the cells to migrate forward (Huttenlocher and Horwitz, 2011). Integrins are αβ heterodimers with a large extracellular domain through which they connect to the ECM and a cytoplasmic domain, which is connected via adaptor proteins to the actin cytoskeleton. Binding specificity for the type of substrate is determined by the combination of α and β subunits: e.g. fibronectin α5β1 and α4β1; laminin α3β1 and α2β1; collagen α1β1 and α2β1 (Huttenlocher and Horwitz, 2011).

As cells migrate, integrins are activated at the front of the cell, where they initially form small adhesion complexes named nascent adhesions (Figure 1.1). Nascent adhesions can then mature into the larger focal adhesion complexes that connect to the actomyosin network allowing traction forces to be exerted to the substrate (Figure 1.1) (Huttenlocher and Horwitz, 2011; Mayor and Etienne-Manneville, 2016). As the cells move forward, disassembly of focal adhesions occurs

at the rear of the migrating cells, allowing the cells to detach from the substrate. Activation of integrins through interactions with the ECM at the front of the cells induces the local activation of RhoGTPases Cdc42 and Rac, which subsequently regulate actin polymerisation through the WAVE/Arp2/3 complex (Campellone and Welch, 2010).

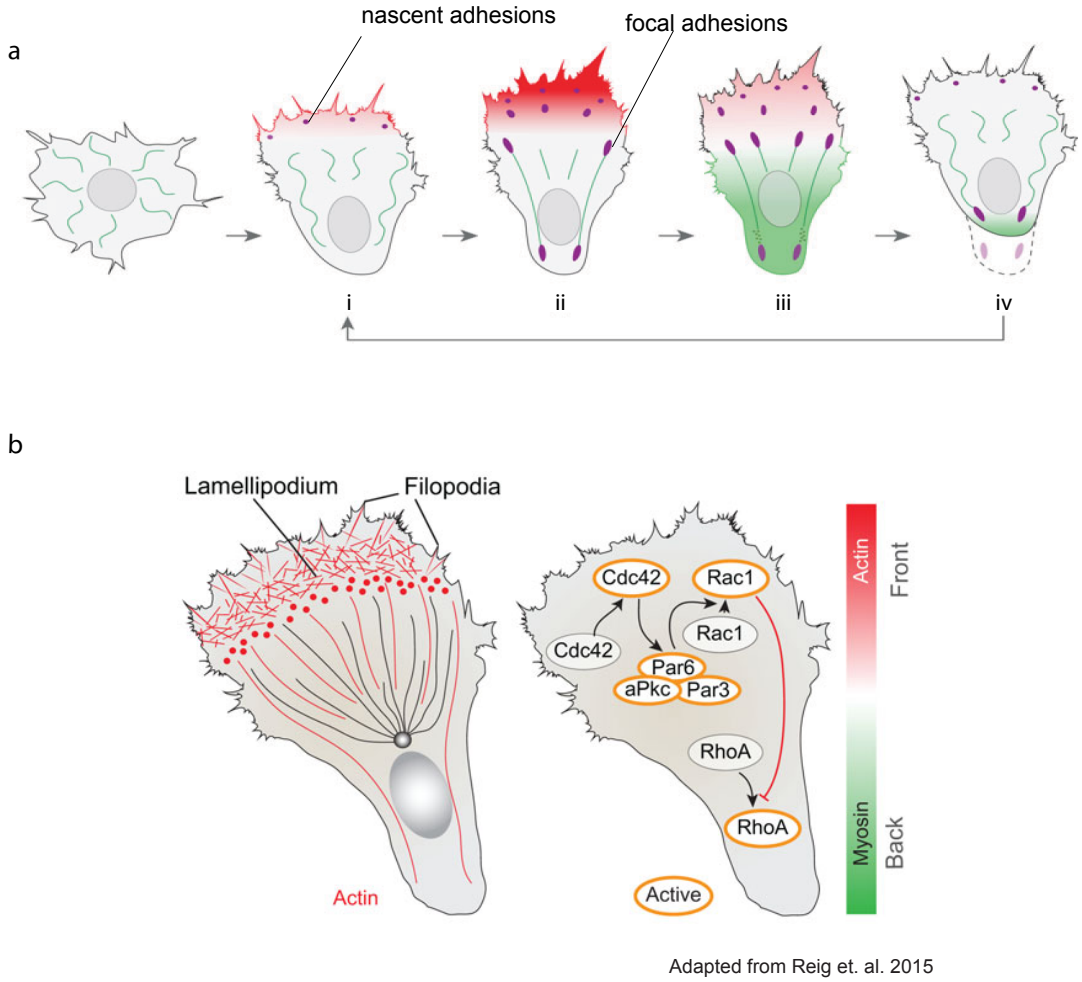

Adapted from Reig et. al. 2015

Figure 1.1. Migrating cells adapt a front to rear polarity.
Migrating cells adapt a characteristic shape with protrusions such as lamellipodia and filopodia at the front of the cell and a retractile rear. a) Migration goes through a cycle of i. formation of nascent adhesions to the substrate at the front of the cell. ii. protrusion extension and maturation of adhesions to focal adhesion complexes. iii. Contraction of the cell body forward. iv. Disassembly of the focal adhesion complexes and retraction of the rear. b). The polarised organisation of cells is mediated by a polarised cytoskeletal network, with actin polymerisation at the front of the cells that pushes the membrane forward and a high myosin activity at the rear of the cell. This is in turn set by a polarised activation of Cdc42 and Rac-1 at the front of the cell while RhoA is mainly active at the rear of the cell.

1.1.2. Collective migration

While single cell migration can occur *in vivo*, several studies have shown that cells often migrate as cohesive groups during embryogenesis, and in the adult during regeneration and tumourigenesis (Mayor and Etienne-Manneville, 2016). Different modes of collective migration have been described depending on the context (Etienne-Manneville, 2014). For example, epithelial cells migrate as large layered sheets during wound healing; primordium cells migrate as closely associated cells clusters along the lateral line organ in *Drosophila*; neural crest cells migrate during embryogenesis as a loose stream of cells, in which individual cells can be identified whilst maintaining constant interaction with each other; and during neo-angiogenesis endothelial cells migrate as cords, in which a single tip cell guides the rest of the cluster (Aman and Piotrowski, 2010; Etienne-Manneville, 2014; Mayor and Carmona-Fontaine, 2010; Valentin et al., 2007). Moreover, Schwann cells appear to migrate as cellular cords during peripheral nerve regeneration (Parrinello et al., 2010). Although the modes of collective migration can differ in organisation, cell types and size, there are two common features found in all types of collective migration; firstly the cells at the front of the group, the leading edge, are polarised with protrusions emerging from the cells in the direction of migration (Mayor and Etienne-Manneville, 2016). Secondly, the cells need to interact continuously to maintain a cluster, while the interactions need to be dynamic to allow cellular rearrangements to occur. How migrating cells can maintain a coherent group while allowing cellular rearrangements is a long-standing question.

The mechanisms of collective migration rely on the same principles as single cell migration. However, in collective migration, the polarisation of individual cells is altered due to cell-cell interactions (Figure 1.2) (Mayor and Etienne-Manneville, 2016). These cell-cell interactions create two types of cells in the group: the leading

cells which are located on the outside of the group and the follower cells, which are located in the middle of the group (Figure 1.2), though follower cells and leader cells can interchange position. The leading cells are polarised and have protrusions in the direction of migration (Theveneau et al., 2010). In contrast, the follower cells are not polarised which is due to cell-cell interactions with the leader cells and the surrounding follower cells. Moreover, the polarisation of the leading cells, caused by the direct cell-cell interactions with the follower cells allows them to be more responsive to extracellular signals such as secreted molecules, which in turn can further polarise the cells (Theveneau et al., 2010).

In addition to direct cell-cell interactions, secreted molecules play a role in collective migration (Theveneau et al., 2010; Valentin et al., 2007). For example, the chemoattractant SDF-1 stabilises protrusions at the leading edge of neural crest cells, which contributes further to the global polarisation of the clusters, which is required for directional migration (Theveneau et al., 2010). Moreover, neural crest cells migrate as a loose cluster, which means that occasionally cells escape the direct interactions and migrate away from the cluster. To counteract this, neural crest cells secrete complement factor C3a and express the receptor C3aR (Carmona-Fontaine et al., 2011). These “co-attraction” molecules attract neural crest cells that have migrated away, back to the cluster to maintain the collective migration (Carmona-Fontaine et al., 2011).

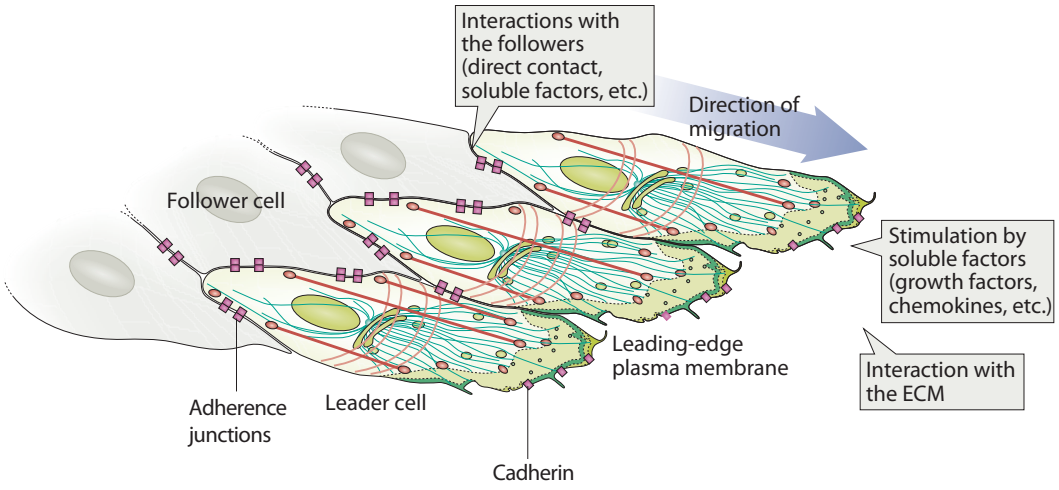

adapted from Mayor and Etienne-Manneville, (2016).

Figure 1.2. Cell polarity mediates single cell and collective migration.
In a coherent cluster, leader cells have a polarised morphology based on the same mechanisms as single cell migration. Polarity in leader cells is stimulated by chemokines, interactions with the ECM and interactions with the follower cells. Note non-engaged cadherin at the front of the leading cell where it could regulate CIL (see below).

1.1.3. Contact inhibition of locomotion

Contact inhibition of locomotion (CIL) describes the process in which cells upon contact stop their migration and change their direction of migration (Figure 1.3) (Abercrombie and Heaysman, 1953, 1954b). This process was first described in explants of chick heart fibroblast in the 1950s by Abercrombie, who reasoned that CIL is required for the directional outward migration of the fibroblasts (Abercrombie and Heaysman, 1954b). Indeed, loss of CIL leads to the decreased directional migration of several cell types such as neural crest cells and macrophages, causing defects in embryogenesis, and the spreading of macrophages respectively (Carmona-Fontaine et al., 2008; Stramer et al., 2010). CIL, like axonal guidance, cell sorting, cell segregation and boundary formation, prevents intermingling of cells through mediating a repulsive force, causing the cells to separate from each other, suggesting similar mechanisms could be in place to regulate these different

processes (Abercrombie and Heaysman, 1954b; Bashaw and Klein, 2010; Batlle and Wilkinson, 2012). A failure of CIL has been associated with tumourigenesis in which loss of CIL in cancer cells can lead to the invasion of normal tissues (Abercrombie, 1979; Astin et al., 2010). Thus, it is important to understand how CIL is regulated.

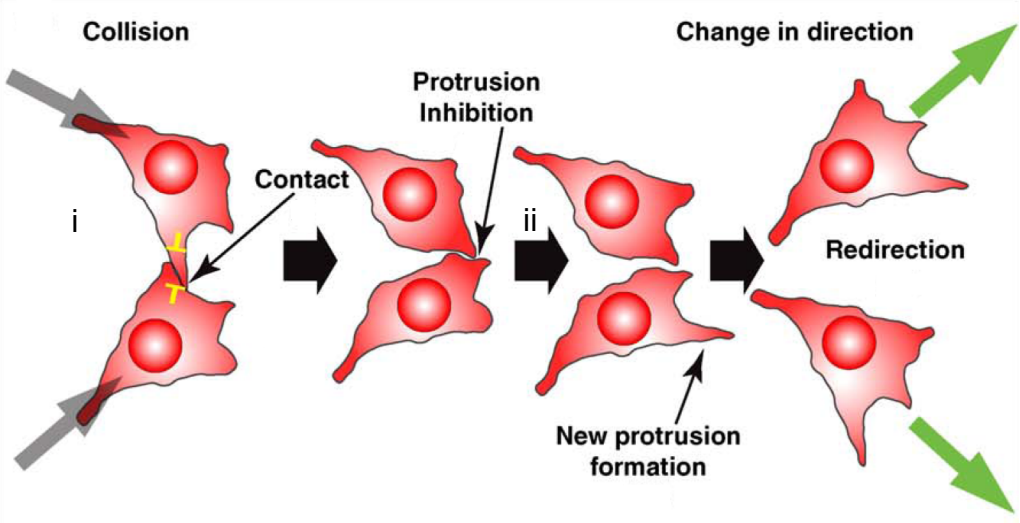

Adapted from Mayor and Carmona -Fontaine (2010).

Figure 1.3. The mechanism of CIL
CIL is the process by which migrating cells are redirected upon collision, which is mediated by a repolarisation of the cell. i) When migrating cells collide, protrusions are inhibited at the site of cell-cell contact. ii) New protrusions are formed away from the site of cell-cell contact and in the direction of subsequent migration. As a result, the cells change their direction of migration.

1.1.4. Repolarisation

CIL is mediated by a repolarisation of the cells which involves two steps: i) Once contact has been made between two cells, protrusions or filopodia at the site of cell-cell contact are inhibited and collapse; ii) Formation of new protrusions or filopodia away from the site of the contact in the direction of migration (Figure 1.3). Repolarisation of cells is mediated by a reorganisation of the actin cytoskeleton (Nobes and Hall, 1999). Indeed, it has been observed that the actin cytoskeleton is disassembled at the site of cell contact, while actin polymerisation is induced at the

free edge of the cell, which induces newly formed protrusions (Davis et al., 2015; Scarpa et al., 2015). In addition, microtubules have also been shown to play a role in CIL as microtubule destabilisation is induced upon cell-cell contact (Batson et al., 2014) and microtubules are required for repolarising the cell (Kadir et al., 2011; Moore et al., 2013).

Rho GTPases play a key role in CIL by locally modulating the cytoskeleton. For example in neural crest cells, a polarised local activation of RhoA induces collapse of the protrusions at the site of cell-cell contact and induces repolarisation (Carmona-Fontaine et al., 2008). Whereas polarised activation of Rac-1 induces formation of protrusions at the free edge of the cell (Scarpa et al., 2015; Theveneau et al., 2010). Moreover, in the prostate cancer cell line, PC3, the homotypic repulsive response is regulated by activating RhoA through the GEF VAV2 at the site of cell-cell contact (Astin et al., 2010; Batson et al., 2014). In contrast, the attractive signalling is mediated through Cdc42, which is also activated at the site of cell-cell contact and regulates filopodia extension (Astin et al., 2010).

1.1.5. From cell-cell recognition to intracellular signalling

An important feature of CIL is the initial cell-cell contact made when two cells collide, which requires recognition followed by a change in the polarisation and direction of cell migration. Cell recognition can be mediated by direct contact via surface molecules such as adhesion and guidance molecules, which have been implicated in CIL during which cell polarity is modulated by locally regulating the activity of Rho GTPases (Figure 1.4). For example, repulsive and guidance molecules such as robo and slit have been shown to inhibit protrusion formation at cell-cell contacts in fibroblasts (Fritz et al., 2015). While in PC3 cells, EphA and EphB receptors and their ligands regulate CIL by activating RhoA and Cdc42 respectively (Astin et al., 2010).

In contrast, in neural crest cells, the non-canonical Wnt pathway induces a polarised RhoA activation (Carmona-Fontaine et al., 2008). Intriguingly, it has recently been indicated that adhesive molecules such as cadherins and nectins can regulate CIL in neural crest cells and glioblastoma cells (Becker et al., 2013; Matthews et al., 2008; Scarpa et al., 2015; Takai et al., 2008; Tanaka et al., 2012; Theveneau et al., 2010). Although CIL and adhesion seem to be opposing processes, it could explain how the initial contact is made and maintained, while eliciting a downstream repulsive response. However, how adhesion receptors can mediate these opposing responses remains unclear.

1.1.6. CIL in collective migration

Although CIL was originally described in single migration, it is now apparent that it is required for the collective migration of specific cells during development and for the spreading of other cell types. During the collective migration of neural crest cells, it has been shown that CIL regulates the polarity of the cells by inhibiting protrusion formation at the site of cell-cell contact and by inducing the formation of protrusions at the free edge of the outer cells of the cluster (Figure 1.4) (Theveneau et al., 2010). This causes a global polarity of the cluster in which the inner cells lack polarity whereas the outer leading cells at the front of the group have protrusions in the direction of migration. This group behaviour is important for the cluster to be responsive to locally secreted molecules and to migrate in a directional manner to a gradient of chemotactic factors. Importantly, loss of CIL within the cluster abrogates the directional migration of a neural crest cell cluster in response to the chemoattractant SDF-1 (Theveneau et al., 2010).

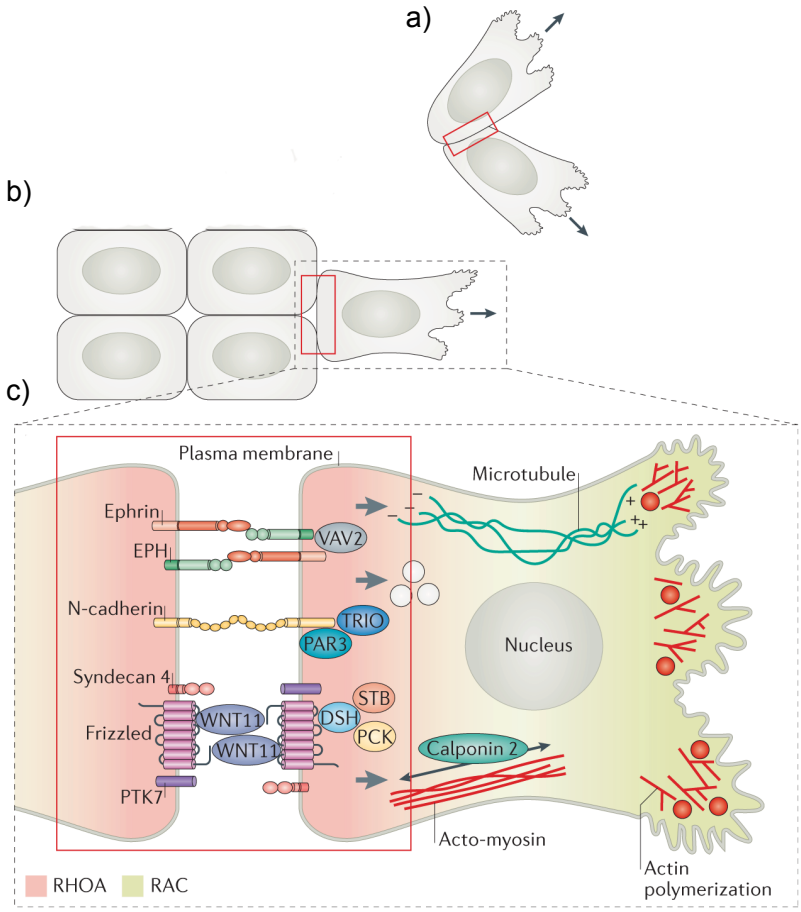

Adapted from Mayor and Etienne-Manneville, (2016)

Figure 1.4. Cell-cell recognition molecules that mediate CIL

CIL is required for (a) repolarising cells to redirect cells and (b) polarising the leader cells in collective migration. (c) Enlarged inset of (a and b) Showing that CIL is regulated by direct cell-cell interactions mediated by various types of surface receptors that inactivate Rac-1 and/or activate RhoA through various adaptor proteins. This results in actin depolarisation and disassembly of focal adhesions resulting in the collapse of protrusions at the site of contact. Rac-1 and Cdc42 are activated at the leading edge inducing the polymerisation of actin and a repolarisation of the cell in a different direction.

CIL has also been shown to be required for the spreading of several cell types including macrophages in *Drosophila*, fibroblasts and prostate cancer cells *in vitro* and for neural crest cells during development in zebrafish and *Xenopus* (Batson et al., 2014; Carmona-Fontaine et al., 2008; Fritz et al., 2015; Moore et al., 2013; Stramer et al., 2010). In these cases, contact-dependent cell repulsion mediates the dissemination of individual cells at the edge of the group, away from the denser area

of cells within the group, resulting in a force, which drives their outward migration and the spreading of the cells.

1.1.7. Neuronal-cadherin

1.1.7.1. Classification and function

The cadherin superfamily generally plays a role in adhesion and cell-cell recognition and has been shown to be important in a wide range of processes such as CIL, morphogenesis, cell sorting, cell migration, cell survival, cell proliferation and cell signalling (Brasch et al., 2012; Harris and Tepass, 2010). Moreover, aberrant expression is associated with tumourigenesis (van Roy, 2014). Cadherins are best known as calcium dependent transmembrane surface receptors that cluster together in adherence junction complexes and are important for transmitting adhesion forces between adjacent cells (Brasch et al., 2012).

The cadherins are clustered together in the cadherin superfamily based on their distinctive and highly conserved extracellular cadherin (EC) domains. The superfamily is divided into subtypes based on the number and arrangement of the EC domains (Figure 1.5) (Brasch et al., 2012). Neuronal-cadherin (N-cad) which has been shown to play a role in CIL, is a Type I classical cadherin. These are single-pass transmembrane receptors with ectodomains consisting of five tandem EC domains and a highly conserved cytoplasmic domain that is indirectly connected to the actin cytoskeleton. There are two classes of classical cadherins: Type I consisting of six cadherins and Type II consisting of 13 cadherins. There are structural differences in the Type I classical cadherins in the distal EC1 domain resulting in stronger homophilic adhesions compared to Type II classical cadherins. Type I classical cadherins include epithelial cadherin (E-cad) which is mostly expressed in epithelial cells, placental cadherin (P-cad), retinal cadherin (R-cad),

muscle cadherin (M-cad), vascular endothelial (VE-cad) and N-cad which is expressed in neuronal tissues and in heart muscle cells, amongst others.

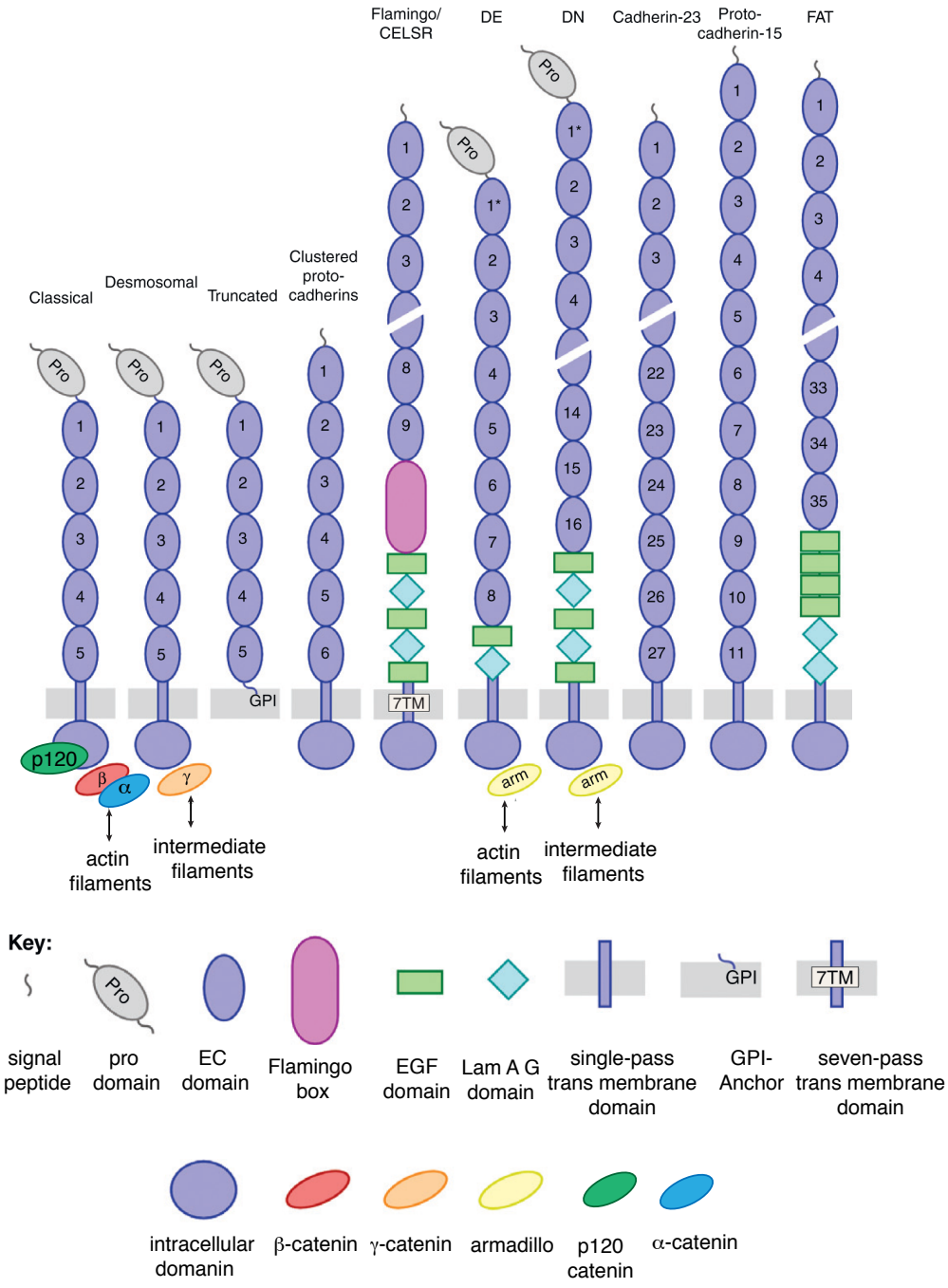

Adapted from Brasch et. al.(2012).

Figure 1.5. The cadherin super family

Cadherins are a large class of calcium dependent adhesion receptors with five or more highly conserved EC domains. Classical cadherins, by far the most studied cadherins, are connected through the cytoplasmic domain to the actin cytoskeleton via its adaptor proteins α-catenin, β-catenin and p120-catenin.

1.1.7.2. Trans- and cis-interactions

Classical cadherins form homophilic cell-cell interactions and often aggregate in adherence junction complexes, linking adhesion to the actin cytoskeleton. Both Type I and Type II use the same mechanism to establish homophilic *trans*-interactions (Brasch et al., 2012), however, there are slight differences in the homophillic *trans*-interactions due to differences in the EC1 domain between the Type I and Type II cadherins. Of the five EC domains, only the EC1 domain is engaged in *trans*-interactions between the two cadherin molecules (Brasch et al., 2012; Halbleib and Nelson, 2006). This interaction is mediated by 'strand swapping' between the two EC1 domains of the two interacting cadherin molecules. However, the resulting bond is only a weak hydrophobic affinity bond (Figure. 1.6). To obtain stronger adhesion, molecules aggregate together in micro clusters via: (i) passive diffusion, thought to be formed by already present Nano clusters (Yap et al., 2015). The mechanisms remain unclear, but trapping in the actin cytoskeleton, lipid driven segregation and endocytosis have been suggested to play a role (Brasch et al., 2012; Yap et al., 2015). (ii) *cis*-interactions between two cadherins. Unlike *trans*-interactions, *cis*-interactions require the interface between the base of the EC1 domain and the EC2 domain of the adjacent cadherin (Figure 1.6). *Cis*-interactions are only formed between Type I classical cadherins, as Type II lack the *cis* interface domains (Brasch et al., 2012).

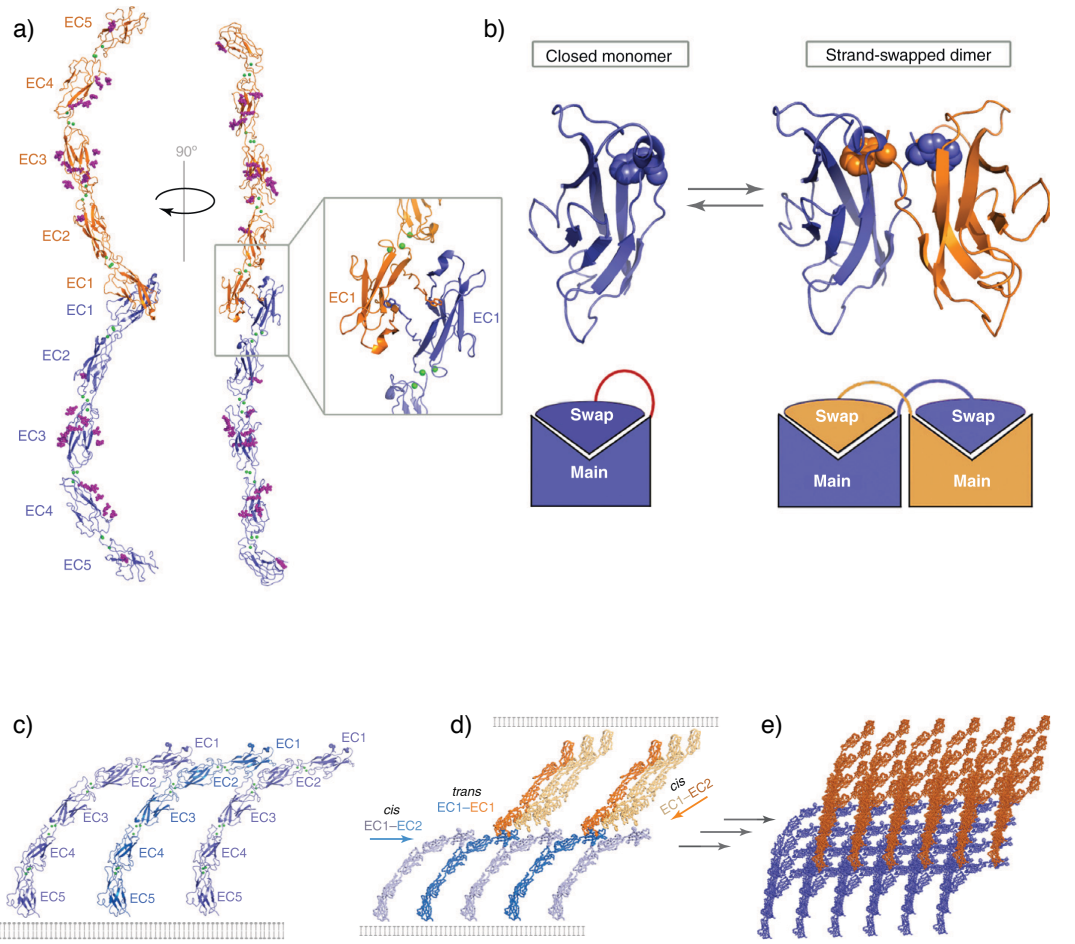

Adapted from Brasch et. al. 2012.

Figure 1.6. Formation of N-cadherin complexes

a) Homophilic *trans*-interactions are mediated by "strand swapping" of the EC1 domain. b) Free monomers are closed. This creates a relatively weak affinity bond between the two cadherin molecules. c) *Cis*-interactions between the EC1 and the EC2 of adjacent molecules further strengthen adhesion by aggregating multiple cadherin molecules into adherence junction complexes. *Cis*- and *trans*-interactions are dependent on the binding of three calcium ions to each linker between the EC domains. d and e) Cadherins in *trans*-interactions and *cis*-interactions cluster together.

Though cadherins preferentially make homophilic *trans*-interactions, Type I cadherins can make heterotypic *trans*-interactions with other members of the subtype. However, due to differences in the EC1 domain they cannot interact with Type II cadherins (Brasch et al., 2012). Intriguingly, cadherins have also been shown to make heterotypic *cis*-interactions with other types of molecules. For example N-cad can interact with the fibroblast growth (FGF) receptor, to regulate growth, contact

dependent cell survival and cell motility (Brasch et al., 2012; Suyama et al., 2002; Trolice et al., 1997). This interaction is mediated between the EC4 domain of N-cadherin and the histidine-alanine-valine (HAV)-motif of the FGF receptor (Williams et al., 2001). Other studies suggest that N-cadherin interacts through adaptor proteins, via its cytoplasmic tail with the Wnt co-receptor Lrp5, to negatively regulate Wnt signalling and thereby inhibits osteoblast differentiation (Hay et al., 2009). Moreover, interaction of the cytoplasmic tail of robo to N-cadherin via the abl/cable complex results in decreased adhesion between neural retinal cells, which is important for axonal outgrowth (Rhee et al., 2007; Rhee et al., 2002). It has also been reported that E-cad can interact through its extracellular domain with the metalloproteinase ADAM10, which cleaves and sheds the extracellular domain of E-cad, thereby decreasing adhesion which is required for Ephrin/ephB mediated segregation (discussed below) (Solanas et al., 2011).

1.1.7.3. Adherence junction components

Cadherin-mediated adhesion is dependent on its three intracellular interacting partners α-catenin, β-catenin, p120-catenin, which are key components of the adherence junction complex and which mediate connections to the microtubule and actin cytoskeleton (Figure 1.7).

p120-catenin regulates cadherin stability at the membrane by control of cadherin trafficking and degradation (Peglion and Etienne-Manneville, 2013). Downregulation of p120-catenin results in decreased cadherin expression in several tissues (Davis et al.). Within the p120-catenin binding site there is an endocytic dileucine motif and an E3 ubiquitin ligase recognition site. Therefore, when p120-catenin is not bound to cadherin, endocytosis of the cadherin complex is induced (Miyashita and Ozawa, 2007). Moreover, p120-catenin masks two phosphorylation

sites within the juxtamembrane domain that can be recognised by the E3 ubiquitin ligase Hakai, which targets cadherin for proteasomal degradation (Fujita et al., 2002). Though the endocytic signal required for E-cad internalisation is lacking in N-cad, some data suggest that p120-catenin can regulate N-cad internalisation and recycling in astrocytes (Peglion and Etienne-Manneville, 2013; Peglion et al., 2014). P120-catenin has also been found to bind via kinesins to microtubules and this interaction has been shown to be important for the export of N-cad from the endoplasmic reticulum (ER) to the plasma membrane. In addition to cadherin bound p120-catenin, there is a cytoplasmic pool of p120-catenin that can modulate the actin cytoskeleton via regulating Rho-GTPases (Peglion and Etienne-Manneville, 2013). For example, p120 can directly interact with and inhibit RhoA and has been found to activate Cdc42 and Rac-1 by binding to the guanine exchange factor VAV2 (Anastasiadis et al., 2000; Grosheva et al., 2001; Noren et al., 2000).

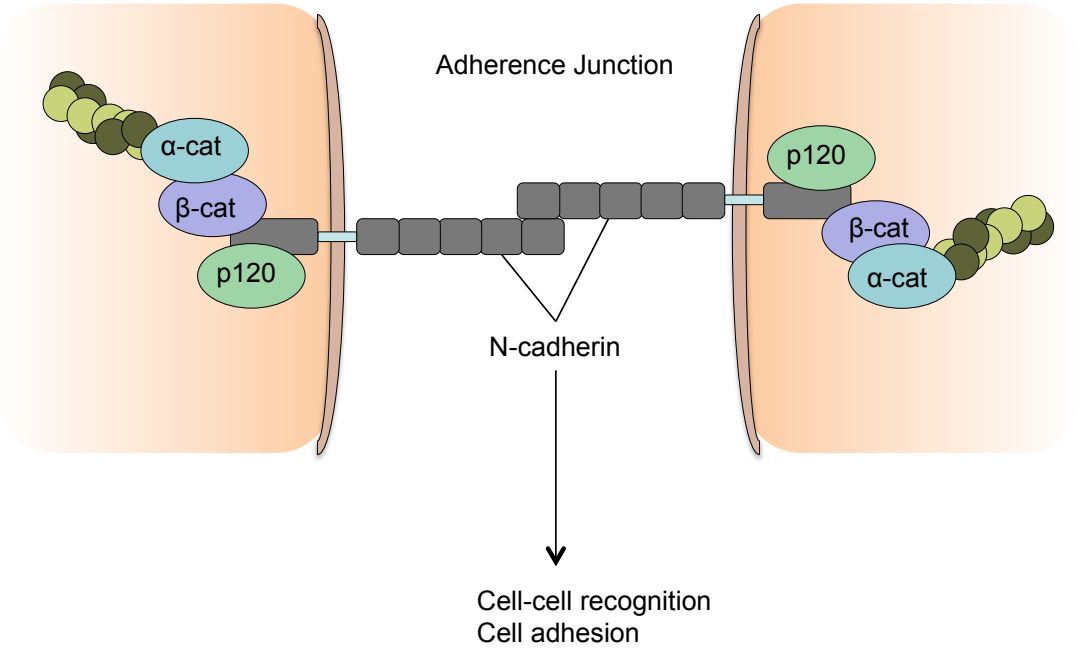

Figure 1.7. Cadherin assembles in adherence junction complexes.
Cadherins interact with α-catenin, β-catenin, p120-catenin to form the adherence junction complex, through which cell-adhesion is linked to the cytoskeleton, the main function of cadherins. Other roles of cadherins are cell-cell recognition, cell sorting, cell migration, cell survival, cell proliferation CIL, and cell signalling.

A major function of β-catenin is to link N-cad to α-catenin, which in turn directly interacts with actin. β-catenin initially binds to cadherins in the endoplasmic reticulum and this binding is important for the proper translocation of cadherin to the membrane and to recruit α-catenin to the adherence junctions (Desai et al., 2013; Harris and Tepass, 2010). Moreover, loss of β-catenin can lead to decreased adhesion, and thus β-catenin is required for destabilising adherence junctions (Rhee et al., 2007; Rhee et al., 2002). Other work has suggested roles for β-catenin in cadherin endocytosis (Delva and Kowalczyk, 2009).

α-catenin is the link that couples cadherins to the actin cytoskeleton, which allows pulling forces applied on adherence junctions to be transmitted onto the actin cytoskeleton (Buckley et al., 2014; le Duc et al., 2010; Nelson and Weis, 2016; Yonemura et al., 2010). However, the means by which α-catenin mediates the interaction between cadherins and actin remained controversial until recently, as α-catenin was shown using co-immunoprecipitation (Co-IP) to interact with cadherin and β-catenin, but a quaternary complex of actin, N-cad and β-catenin could not be shown to interact simultaneously with actin to form a quaternary complex (Aberle et al., 1994; Yamada et al., 2005). This showed that α-catenin binds in an allosteric fashion, and alternates between binding to β-catenin and actin filaments (Yamada et al., 2005). However, this model does not explain how α-catenin can relay pulling forces applied on adherence junctions onto the actin cytoskeleton, as this requires a simultaneous physical interaction between α-catenin, actin filaments and β-catenin (Buckley et al., 2014; Desai et al., 2013; le Duc et al., 2010; Yonemura et al., 2010). Recent reports have shown that external tension relayed onto α-catenin, induces a conformational change of α-catenin, activating the binding to actin allowing it to simultaneously bind to the cadherin/ β-catenin complex and the actin (Buckley et al., 2014; Yao et al., 2014). Stretching α-catenin to the non-folded protein, also allows for

the subsequent binding of vinculin, a tension sensor protein that can localise at the adherence junction complexes (le Duc et al., 2010; Yonemura et al., 2010). Vinculin binding to α-catenin, in turn prevents folding of opened α-catenin (Yao et al., 2014), suggesting vinculin stabilises the open α-catenin form. However, other work has shown that α-catenin can form homodimers, which mainly binds to actin and which cannot bind to β-catenin, as dimerisation of α-catenin masks the β-catenin-binding domain within α-catenin homodimerisation domain (Pokutta and Weis, 2000). The role of α-catenin dimers and homodimers is unclear, however they may be important for regulating the actin cytoskeleton organisation at the cell contacts (Nelson and Weis, 2016), possibly through other adaptor proteins which bind to α-catenin such as formin, α-actinin, zonula occludens protein 1 (ZO1), afadin and spectrin (Harris and Tepass, 2010).

1.1.8. Cadherins in collective migration and CIL

Cadherins are required for the collective migration of several cell types such as Schwann cells, neural crest cells, astrocytes, endothelial cells, epithelial cells and border cells in the *Drosophila* egg chamber (Kametani and Takeichi, 2007; Parrinello et al., 2010; Peglion et al., 2014; Theveneau et al., 2010). Moreover, several reports have shown that cadherins plays a role in CIL (Becker et al., 2013; Scarpa et al., 2015; Tanaka et al., 2012; Theveneau and Mayor, 2010). For instance, in neural crest cells a system in which CIL is well characterised, N-cad mediates CIL within the neural crest cells cluster by inhibiting protrusion formation at the site of cell-cell contact (Theveneau et al., 2010). N-cad locally inhibits Rac-1, thereby establishing a polarised activation of Rac-1 in the leader cells. Moreover, this polarisation is required for the directional migration in response to SDF-1. However, how N-cad regulates Rac-1 is unknown. Previous work by the same group showed that the Wnt

signalling pathway is also required for CIL (Carmona-Fontaine et al., 2008). In this case, Wnt signalling activates RhoA upon collision at the site of cell contact, locally inhibiting protrusion formation. The authors suggest there is a link between the two mechanisms, though this remains to be clarified.

In contrast, other work has shown that cad-11 is required for CIL in neural crest cells (Becker et al., 2013). The mechanism by which Cad-11 regulates CIL is unknown, but the authors suggest that cadherin-mediated adhesion of two adjacent cells is required for CIL, indicating *trans*-homodimerisation of N-cad is needed to induce the repulsion response. Moreover, the authors find that Wnt signalling pathway also is required for CIL in neural crest cells, and propose signalling that has a similar effect on CIL. Though a direct link between the pathways is not shown.

In addition, E-cad has also been shown to regulate CIL (Scarpa et al., 2015). In contrast to N-cad, E-cad inhibits CIL in non-migratory neural crest cells (an earlier developmental stage), which have diminished CIL compared to their migratory neural crest cell counter parts. Like N-cad, E-cad regulates CIL by controlling a polarised activation of Rac-1. However, in contrast to N-cad, E-cad redistributes Rac-1 activity towards the site of cell contact thereby promoting formation of protrusions at the site of cell-cell contact, which results in the loss of CIL. Mechanistically the authors show that E-cad regulates Rac-1 by sequestering p120-catenin to the junction, which subsequently induces Rac-1 activation.

N-cad has also been shown to regulate heterotopic CIL between U87MG glioblastoma cells and normal glial cells (Tanaka et al., 2012). In contrast to the mechanism in neural crest cells, in U87MG, it is reported that N-cad controls CIL via *α*-catenin by sequestering Nm23-H1 a nucleotide diphosphate kinase that supresses Tiam1 a guanine exchange factor (GEF). Inactive Tiam1 in turn can then no longer activate Rac-1, thereby blocking the formation of protrusions at the site of contact.

However, cadherins also mediate strong adhesions within collectively migrating cells to maintain a cluster. How cadherins can both mediate strong adhesion as well as mediate CIL during collective migration remains unclear. Recent work in astrocytes has indicated that polarised N-cad expression in migrating cells could play a role in mediating both strong adhesion within the cluster while allowing cellular rearrangements to occur (Peglion et al., 2014). Free N-cad complexes accumulate at the front of the leading cells, whereas N-cad forms adherence junctions with adjacent cells at the lateral sides of the leading cells. The adherence junctions on the lateral sides are dynamic in the leading cells and undergo constant retrograde flow, from the front to the rear of the cell. In contrast, adherence junctions are stable in the follower cells. In addition to the polarised recycling of N-cad along the lateral sides of the leading cells, there is a high rate of N-cad internalisation at the rear of the cells, which is recycled back to the front of the leading cells. Here, N-cad can re-engage in junctions and go through the same cycle (Peglion et al., 2014). Overall, this causes a strong adhesion at the front and weaker adhesion at the back of the lateral junctions. The weaker interactions between leading and trailing cells could trigger a polarisation in the trailing cells inducing them to migrate, whereas in the front of the leading edge the free pool of N-cad could regulate protrusions and mediate new interactions and importantly could mediate CIL.

1.1.9. Guidance molecules

Another set of molecules reported to regulate CIL are the so called guidance molecules, that are maybe best known for their repellent or adhesive properties in the nervous system (Bashaw and Klein, 2010). A major role in the pathfinding of growing axons is to guide axons to their target. Guidance molecules include membrane bound proteins as well as secreted molecules and include Eph receptors and their ligands,

semaphorins and slits (Hung and Terman, 2011). Although CIL implies contact dependent communication, local secreted signalling also appears to play a role in CIL, as the secreted ligand slit and Wnt are required for CIL between fibroblasts and NC cells respectively (Carmona-Fontaine et al., 2008; Fritz et al., 2015).

1.1.9.1. Eph receptors and their ligands

EphA and EphB receptors are a large class of receptor tyrosine kinases (RTK) that preferentially bind to the ligands ephrin-A and ephrin-B respectively (Kania and Klein, 2016). Eph signalling largely results in repulsion responses but in some cases it has also been shown to result in adhesion, and as such plays a crucial role in boundary formation and compartmentalisation. Moreover, ephrins have been implicated in proliferation, apoptosis, cell migration and differentiation. There are ten EphA receptors that can bind to five ephrin-A ligands and five EphB receptors that can bind to three ephrin-B ligands. Though, EphA4 and EphB2 have been shown to bind the ephrin-B ligands and ephrin-A5 respectively (Gale et al., 1996; Himanen et al., 2004). The ephrin-A and ephrin-B classes of ligand differ in that ephrin-As are attached to the membrane through a glycosylphosphatidylinositol (GPI) anchor, while ephrin-Bs have a transmembrane domain and cytoplasmic domain containing a PDZ domain through which it can signal into the cell (Figure 1.8). Signalling can occur in both directions through receptor “forward signalling” and through ligand “reverse signalling” (Figure 1.8).

Eph receptors are transmembrane proteins that consist of an extracellular globular ligand binding domain, a Cys domain, fibronectin domains, transmembrane domains, an intracellular Tyr kinase domain, a sterile alpha motif (SAM) and a PDZ domain (Kania and Klein, 2016). To activate the Eph receptors efficiently, ephrins must bind in the form of multimers, which results in large signalling clusters (Davis et

al., 1994). The size of the signalling clusters correlates to the strength of the signal (Egea et al., 2005). Upon ligand binding, the kinase domain gets activated which leads to autophosphorylation at the juxtamembrane Tyr residues (Kullander et al., 2001; Zisch et al., 1998). Once activated, Eph receptors can interact with several proteins including Vav2, Vav3, ephexin, phosphoinositide 3-kinase (PI3K), and the non-catalytic region of Tyr kinase adaptor protein 1 (Nck1) and Nck2 (Kania and Klein, 2016). This generally results in cytoskeletal rearrangements through regulation of Rho-GTPases, but Eph signalling has also been shown to affect the Ras MAP kinase signalling pathway (Kania and Klein, 2016; Lisabeth et al., 2013).

Forward signalling can be abrogated through dephosphorylation of the cytoplasmic domain of the Eph receptor by phosphotyrosine phosphatases. Intriguingly, the whole ephrin-Eph complex can be endocytosed into both ephrin and Eph expressing cells (Marston et al., 2003). Signalling through the Eph receptor can still occur once endocytosed until it is either dephosphorylated and degraded or recycled back to the membrane. However, endocytosis is also thought to terminate ephrin-Eph signalling (Mann et al., 2003; Marston et al., 2003; Zimmer et al., 2003).

Reverse signalling occurs through the ephrin-B ligands (Figure 1.8) (Kania and Klein, 2016). Contact with the EphB receptor induces phosphorylation of the ligand by Src kinases, leading to the recruitment of proteins with PDZ domains. Although ephrin-A ligands lack an intracellular domain, some work has suggested they can also signal through binding to other membrane bound molecules as well. These include p75 receptors, which are expressed by Schwann cells, the neutrophin receptor, TrkB and the Ret receptor, which are required for synaptogenesis and axonal repulsion (Bonanomi et al., 2012; Lim et al., 2008; Marler et al., 2008).

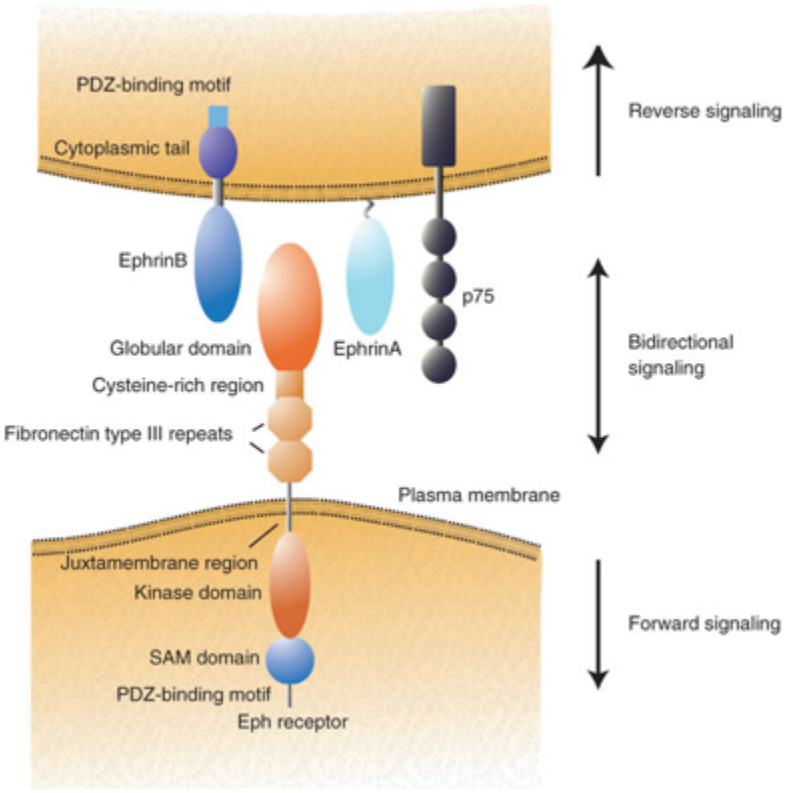

Figure 1.8. Eph and ephrin interactions can induce bidirectional signalling.
The Eph receptor kinase domain is activated upon interaction with ephrins, which induces the recruitment of various adaptor proteins such as GEFs to Vav2 that can regulate the activity of Rac-1 and as such protrusion formation and CIL {Kania, 2016 #251}{Astin, 2010 #8}. Ephrin-A ligands lack an intracellular domain but can signal through co-receptors such as p75 {Lim, 2008 #36}. In contrast, the ephrin-B ligands do have a cytoplasmic domain that contains a PDZ domain through which it can signal to Src kinases {Kania, 2016 #251}.

Importantly, ephrins have been shown to have key roles in axonal path finding and cell sorting/segregation and CIL (Astin et al., 2010; Batlle and Wilkinson, 2012; Hattori et al., 2000; Lisabeth et al., 2013; Parrinello et al., 2010). Eph signalling can mediate cell segregation through regulating repulsion, attraction, as well as adhesion and often the processes are associated with each other. For example, Eph signalling can decrease adhesion via endocytosis of the ephrin-Eph complexes and adjacent adhesive molecules, inducing repulsion and separation of cells. Eph receptors and ephrins can also interact and activate metalloproteases such as the ADAM family

members (Hattori et al., 2000). Upon binding of EphA to ephrin-A ligands, ADAM10 interacts in *cis* with ephrin-A ligands and cleaves them, resulting in a repulsion response (Hattori et al., 2000). In another recent report, in MDCK cells, ADMAM10 has also been shown to interact in *cis* with the EphB3 receptor and E-cad (Solanas et al., 2011). In this instance, ADAM10 gets activated upon binding of ephrin-B1 to EphB3, inducing E-cad shedding between the ephrin-B and EphB expressing cells. This causes differential adhesion between the ephrin-B and the EphB expressing cells and induces cell sorting of the two different populations. The authors propose that this mechanism could be important for the appropriate compartmentalization of different cell types within the epithelial layer of the intestine, as both the knockout of EphB3 or the specific expression of a dominant negative form of ADAM10 (CR2-ADAM10$^{\Delta MP}$) in a specific cell type called the Paneth cell, which normally are compartmentalised within the stem cell niche of the epithelium, results in the aberrant migration of the Paneth cells into unwanted areas of the epithelium (Batlle et al., 2002; Solanas et al., 2011). Thus, Eph-ephrin signalling can control migration of cells by inhibiting their movement into unwanted regions. This is similar to how CIL has been suggested to halt migration and prevent cells from invading into other tissues (Abercrombie and Heaysman, 1954a), and thus Eph/ephrin signalling could be involved in CIL. Indeed, the Eph-ephrin interaction has been shown to promote either CIL by inducing a repulsion response at the site of cell-cell contact, or promote forward migration by inducing filopodia extension at the site of contact, through regulating RhoGTPases activity (Astin et al., 2010). Interestingly, the decision between undergoing CIL or continuing forward migration is dependent on the concentration and array of ephrins and their receptors present on cells (Astin et al.). For example, PC3 cells express both EphA and EphB receptors and express ephrin-A ligand but only a small amount of ephrin-B2, whereas fibroblasts express low

levels of ephrin-A ligands and high levels of ephrin-B2. When two PC3 cells collide there is strong activation of the repulsive EphA pathway, inducing RhoA and inhibiting protrusion formation, resulting in homotypic CIL. However when a PC3 cell meets a fibroblast there is stronger ephrin-B/Ephb3/4 signalling, inducing the activation of Cdc42, which promotes forward migration by inducing filopodia formation. Thus, Eph receptors and ephrins can have differential effects on CIL.

1.1.9.2. CIL in tumourigenesis

Loss of cell-cell recognition can cause unwanted movement and intermingling of cells, which is fundamental to tumourigenesis, invasion and metastasis. To induce tumour spreading, cells need to acquire the ability to migrate and also to lose the ability to recognise other cell types (Friedl and Alexander, 2011). Compartmentalisation can be mediated through repulsive signals such as ephrins. It is therefore not surprising, that aberrant ephrin signalling is associated with tumourigenesis (Pasquale, 2010). For example, EphB2 silencing in colorectal cancer (CRC) is associated with a poor prognosis (Batlle et al., 2005; Batlle et al., 2002), while EphA4 and EphA2 are overexpressed in prostate cancer (Astin et al., 2010; Pasquale, 2010). Proper expression of EphB2 and EphB3/ephrin-B1 is required for the correct compartmentalisation of different domains in the epithelial layers of the intestine (Batlle et al., 2002; Cortina et al., 2007). Interestingly, EphB/ephrinB expression is retained in adenomas, which are benign tumours of the intestine, and their expression keeps the tumours compartmentalised (Batlle et al., 2002; Cortina et al., 2007). However progression of the tumours into aggressive carcinomas is associated with the downregulation of EphB2/EphB3/EphB4, with the loss of EphB3 resulting in the invasion of the epithelium into the muscle layer (Batlle et al., 2005). Moreover, ephrin-B expression in tissues surrounding adenomas prevents them from

migrating into the ephrin-B expressing tissues, as loss of ephrin-B results in expansion of adenomas into the surrounding normal epithelium layer (Cortina et al., 2007).

Loss of heterotypic CIL has been proposed to be fundamental for the invasion and thus the metastasis of tumours (Abercrombie, 1979; Astin et al., 2010). For example, heterotypic CIL between prostate cancer cells PC3 cells and fibroblasts is lost (Astin et al., 2010), while mouse sarcoma cells and mouse melanoma cells have diminished or lost CIL and are able to invade chick fibroblasts (Abercrombie, 1979). However, homotypic CIL has been proposed to remain intact in tumour cells which may allow cells to disseminate, similarly to how cells spread during development (Astin et al., 2010; Mayor and Carmona-Fontaine, 2010). Homotypic CIL between PC3 cells has recently been shown to remain intact and this is required for their dissemination, which is mediated by EphA2 and EphA4 (Astin et al., 2010; Batson et al., 2014). However, whether homotypic CIL is intact in the majority of cancer cells remains to be investigated.

Many tumour cells are thought to migrate collectively, similarly to migrating cells during development. To induce migration in non-motile tumour cells, they need to gain the ability to migrate, which includes disrupting existing adhesions (Wells et al., 2011). This is often compared to epithelial to mesenchymal transition (EMT) in which non-migratory epithelial cells differentiate into migratory mesenchymal cells (Scarpa et al., 2015; Theveneau and Mayor, 2012b). EMT is characterised by a change from E-cad, which mediates stronger adhesion, to N-cad expression, which is associated with lower adhesion and increased cell migration (Scarpa et al., 2015; Wells et al., 2011). It is therefore not surprising that tumours change expression in adhesion molecules, specifically E-cad to N-cad (Wells et al., 2011). Expression of N-cad in breast cancer cells induces their motility, invasion and metastasis (Hazan et

al., 2000; Nieman et al., 1999; Suyama et al., 2002). Interestingly, the increase of migration and invasion is dependent on FGF (Hazan et al., 2000; Nieman et al., 1999); FGF receptor binding to N-cad, prevents internalisation of the FGF receptor and therefore causes sustained signalling (Hazan et al., 2000; Suyama et al., 2002). Furthermore, upregulation of N-cadherin could provide the cells with a less adhesive but more dynamic phenotype, which is required for collective cell invasion in a 3D matrix (Shih and Yamada, 2012). More recently, it has been shown that EMT transition of NC cells in *Xenopus leavis* is mediated by a switch from E-cad to N-cad, inducing CIL, which is required for the dispersal of these cells (Scarpa et al., 2015). Whether N-cad has a similar role in CIL during tumourigenesis, remains to be investigated.

1.2. Schwann cell biology

The structure of a tissue can be compromised upon injury and during the process of regeneration, cell movement and proliferation are induced and structures and boundaries must be re-established. Regeneration of a tissue is thought to recapitulate aspects of developmental processes, however, in contrast to during development when tissues grow in a concerted fashion as the organism grows, regeneration requires the reforming of appropriate structures within the existing structures of the tissue and organism (Poss, 2010). However, very few tissues in the adult mammal retain the capability to regenerate following injury. This has been attributed to the lack of a suitable a stem cell population, differences in signalling in the local environment, and in some cases by the formation of scar tissue (Gurtner et al., 2008; Poss, 2010).

One of the very few tissues in the adult mammal that is capable of some regeneration following injury is the peripheral nervous system (PNS). This is especially remarkable, as peripheral nerves are highly complex structures that can extend over long distances. However, though axonal regeneration has been shown to be efficient following mild injuries such as crush of the nerve, regeneration is less efficient following a full transection of the nerve, possibly the result of incorrect entry of axons into the endoneurial tubes or the growing of axons outside the endoneurial tubes (Nguyen et al., 2002).

The regeneration of a nerve requires coordination of movement and growth of several cell types over long distances (Zochodne, 2008). Key to this process are the Schwann cells, which upon injury dedifferentiate, proliferate, migrate and remodel the local environment (Napoli et al., 2012; Zochodne, 2008). To achieve this, Schwann cells must interact intercellularly as well as with other cells within the local environment. Moreover, existing interactions in the quiescent nerve must change to

allow cellular rearrangement to occur. To understand how Schwann cells can regulate the regenerative process, it is important to understand how homotypic and heterotypic interactions between Schwann cells and their surrounding cells are mediated, both during the development and maintenance of the nerve, as well as in the regenerating nerve.

Schwann cells are the main glial cells of PNS that in the adult exist as two types, myelinating Schwann cells, which enwrap and myelinate large calibre axons in a 1:1 ratio, and non-myelinating Schwann cells, which can enwrap multiple smaller axons in structures called Remak Bundles (Zochodne, 2008). Myelination provides efficient saltatory conduction of nerve impulses and therefore, loss or defects in myelination leads to loss of conduction and neuropathies (Conforti et al., 2014).

The nerves in the PNS consist of groups of axons enwrapped by Schwann cells, which are bundled together and organised into fascicles (Zochodne, 2008) (Figure 1.9). Each fascicle is enclosed by a layer of specialised fibroblasts, called the perineurium. Within the fascicles, the endoneurium, which in addition to the axons and Schwann cells, consists of ECM, macrophages, fibroblasts, and blood vessels. Several fascicles, in turn, are grouped together to make up a larger nerve, and are surrounded by the epineurial sheath.

1.2.1. Schwann cell development

The development of Schwann cells is well characterised, Schwann cells derive from neural crest cells through two differentiation intermediates: Schwann cells precursors and immature Schwann cells, each characterised by expression of specific expression markers (Figure 1.10) (Jessen and Mirsky, 2005).

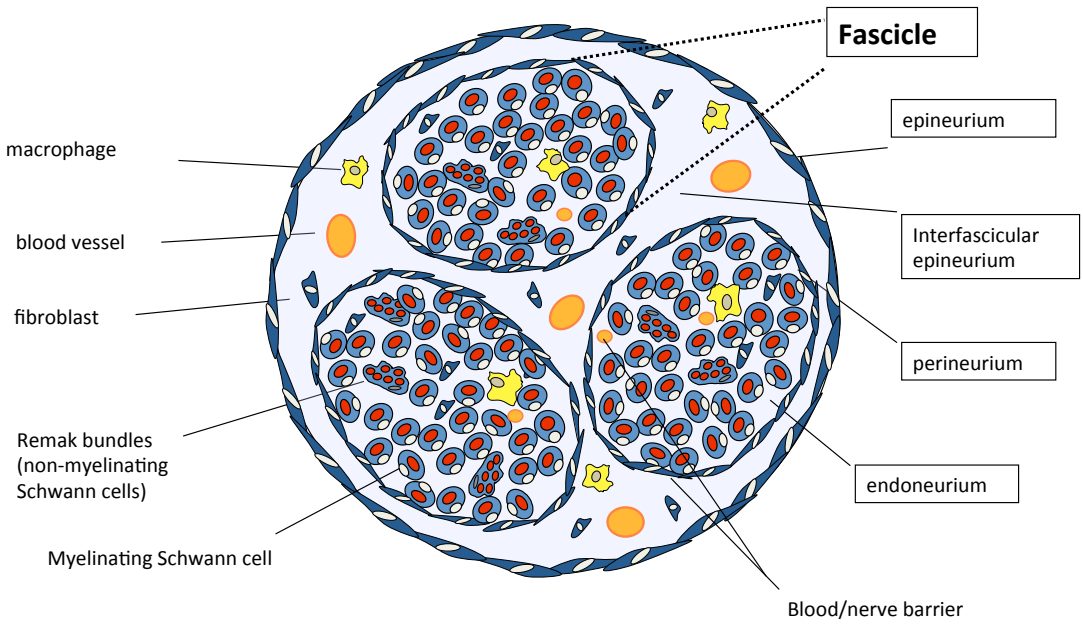

Figure 1.9. Structure of the peripheral nerve
This cross section of the peripheral nerve shows the complexity of the nerve. The peripheral nerve consists of multiple layers, the outer layer the epineurium, which can contain several fascicles that are enclosed by the perineurium. Within the fascicles is the endoneurium, a densely packed structure, containing groups of myelinated axons, Remak bundles, blood vessels, ECM and macrophages.

1.2.2. Neural crest

Little is known about how neural crest cells differentiate into Schwann cell precursor cells. During neurulation, a process occurs whereby neural crest cells separate from the neuroepithelial in a process called delamination and migrate away from the neural tube in two major streams, to give rise to the glial cells and some neurons of the PNS and also differentiate into melanocytes, fibroblasts, smooth muscle cells and in the head to cartilage and bones (Theveneau and Mayor, 2012b). Several factors have been shown to regulate the differentiation state of neural crest cells. The transcription factor Sox-10 is expressed by neural crest and is required for the generation of Schwann cell precursor cells (Jessen and Mirsky, 2005). However, it is

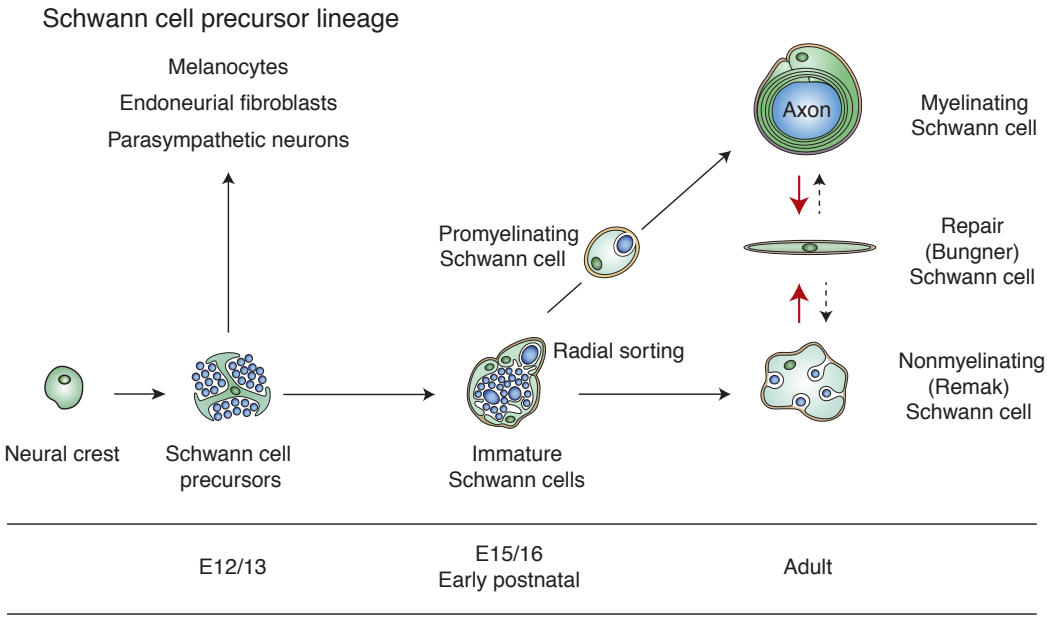

Adapted from Jessen et. al. 2015

Figure 1.10. The major differentiation steps of the Schwann cell lineage
Neural crest cells can differentiate into Schwann cell precursors that associate with axons, which can group together in bundles. At this stage, axons and Schwann cells are tightly packed and there is little ECM, endothelial cells or fibroblasts, which all appear at the time of the transition to immature Schwann cells. Note that Schwann cell precursors can also give rise to melanocytes, endoneurial fibroblasts and parasympathetic neurons. At the stage of immature Schwann cells, radial sorting begins, and Schwann cells associate in a 1:1 ratio and myelinate the larger axons, while several smaller axons are bundled together in Remak bundles by non-myelinating Schwann cells.

expressed by most early neural crest cells and therefore is not solely associated with glial cells. Sox-10 is not expressed by neurons and acts to inhibit neurogenesis and indirectly regulates gliogenesis through regulation of the ErbB3 receptor, which is an important signal in Schwann cell identity (Britsch et al., 2001). ErbB3 is strongly expressed by neural crest cells but is down regulated in derivatives with the exception of Schwann cells (Birchmeier, 2009). FoxD3 is another transcription factor associated with the differentiation of neural crest cells to the Schwann cell lineage, as it is expressed by both neural crest cells and Schwann cell progenitors and inhibits differentiation into neurons and melanocytes (Nitzan et al., 2013).

1.2.3. Schwann cell precursors

Schwann cell precursors first appear around E12/13 in the mouse (E14/15 rat) and are characterised by an upregulation of cadherin-19 (Cad19), which is exclusively expressed by the Schwann cell precursors and may play a role in the compaction of early nerves (Jessen et al., 2015; Woodhoo and Sommer, 2008). A crucial signalling pathway in the developing nerves, is the Neuregulin (NRG)/ErbB pathway. Moreover, survival of Schwann cell precursors is dependent on ErbB3, which is also important for Schwann cell precursor migration along the developing axon tract and for control of cell number and progression of differentiation into Schwann cells (Birchmeier, 2009; Heermann and Krieglstein, 2012; Jessen et al., 2015; Lyons et al., 2005). The ErbB3 receptor is activated upon binding of NRG1, which is expressed by axons (Birchmeier, 2009). ErbB3 knockout mice lack Schwann cell precursors and therefore indirectly cause nerve degeneration, as axons degenerate in the absence of Schwann cell precursors (Hoke, 2006; Riethmacher et al., 1997). As Schwann cell precursors are reduced in mice in which neuregulin signalling is absent, the development of Schwann cells is dependent on NRG1. In addition, Notch signalling between axons and Schwann cell precursors is important for controlling the speed of conversion to Schwann cells as Notch signalling controls the upregulation of ErbB3 receptors on the Schwann cells, making them more susceptible to NRG signalling (Woodhoo et al., 2009). Other markers associated with the differentiation step of neural crest to Schwann cell precursors are the negative regulators endothelin and AP2α (Brennan et al., 2000; Stewart et al., 2001). Aberrant expression of endothelin and AP2α leads to either premature appearance of Schwann cell precursors or slows down the progression into Schwann cells, respectively.

Apart from being an intermediate between neural crest and Schwann cells, Schwann cell precursors also have functions in the fasciculation of nerves, a process

in which axons are grouped together (Jessen et al., 2015). The development of axons is initially normal without Schwann cell precursors, however at later stages axons become defasciculated and project aberrantly into the target tissues (Birchmeier, 2009). Moreover, knockout studies showed that axons die without the support of Schwann cells, illustrating the importance of the interdependency between Schwann cells and axons (Hoke, 2006; Riethmacher et al., 1997).

1.2.4. Immature Schwann cells

Immature Schwann cells can be detected in the developing nerve around E15/16 in the mouse (E17/18 rat) (Jessen et al., 2015). In contrast to neural crest cells, Schwann cell precursors and immature Schwann cells are associated with axons and there is an interdependency on the survival between axon and the different Schwann cell intermediates (Jessen and Mirsky, 2005). However, unlike Schwann cell precursors, immature Schwann cells survival is independent of NRG1, but secrete factors including insulin growth factor-2 (IGF-2), platelet-derived growth factor (PDGF) and neurotophin3 (NT3), leukaemia inhibitory factor (LIF) and lysophophatidic acid, which can enhance the survival of the cells in the absence of axons *in vitro* (Dowsing et al., 1999; Meier et al., 1999; Weiner and Chun, 1999). However, prolonged periods of no contact with axons after injury results in cell death of Schwann cells in the adult (Hoke, 2006; Sulaiman and Gordon, 2009). The transition of Schwann cell precursors to immature Schwann cells is further characterised by structural changes of the nerve, which include vascularisation of the nerves and the appearance of endoneurial fibroblasts and ECM (Jessen and Mirsky, 2005). At this time, immature Schwann cells also envelop groups of axons into bundles of axons/Schwann cells. In preparation for myelination, Schwann cells start a process known as radial sorting, in which individual larger axons associate with

Schwann cells in a 1:1 relationship, while several smaller axons are enwrapped by single Schwann cells to form the Remak bundles. The mechanism underlying this process include interactions between α6β1, α7β1 integrins on the surface of the Schwann cells with laminins, which are required for the ensheathment of axons by Schwann cells (Berti et al., 2011; Feltri et al., 2002; Pellegatta et al., 2013). Concurrently, after birth, Schwann cells begin myelination of the larger axons, while non-myelinating Schwann cells continue constructing the Remak bundles.

1.2.5. Myelin regulators and structure

Myelination of peripheral nerves is important for salutatory conduction and defects in myelination are associated with neuropathies, and thus control of the myelination process is key for the development of peripheral nerves (Salzer, 2015). Several transcriptional regulators have been implicated in the progression of immature Schwann cells into myelinating Schwann cells including Krox20, Sox10, Nab1/2 and SREBP, which regulate the expression of factors important in the myelination process or directly regulate myelin genes (Salzer, 2015). Moreover, Krox20 is a key regulator during PNS myelination and regulates the transcription of biosynthetic components of myelin lipid synthesis and myelin structural proteins. The heterotypic interactions between axons and Schwann cells are crucial for myelin initiation and maintenance. The levels of expression of type III NRG1 on the axons sets a threshold for myelination by the Schwann cells, and determines the extent of myelination (Taveggia et al., 2005). Other molecules are implicated in controlling myelination including the adhesion G-protein-coupled receptor (GPCR) Gpr126, which is required for radial sorting and initiating myelination but is dispensable for the maintenance of myelination (Glenn and Talbot, 2013; Salzer, 2015). Mechanistically, Gpr126 increases levels of cAMP (Mogha et al., 2013), an important myelination

signal (Glenn and Talbot, 2013). cAMP in turn can increase of expression of the pro-meylinating transcription factor Pou3f1 (Monuki et al., 1989) and can drive Krox20 expression (Kipanyula et al., 2013), and via activation of PKA can activate transcription factors, including NF-kB and the CREB family, the latter has been suggested to have a role in differentiation of Schwan cells (Arthur-Farraj et al., 2011).

Another signalling pathway key for initiation of myelination is the PI3K signalling pathway, which is downstream from NRG/ErbB signalling (Salzer, 2015). Activation of the PI3K pathway results in hypermyelination of axons, which is thought to occur via activation of Akt and the subsequent activation of mTOR (Goebbels et al., 2010; Goebbels et al., 2012).

In addition, binding of Lgi4 protein, expressed by Schwann cells, to Adam22 on the surface of the axon has a role in promoting myelination, as deletion of either result in major defects in myelination (Ozkaynak et al., 2010; Sagane et al., 2005). However, Lgi4 and Adam22, appear to be modulators that advance myelination beyond the promyelination phase (Bermingham et al., 2006; Kegel et al., 2013; Ozkaynak et al., 2010), while NRG1 and Gpr126 are absolutely required for initiation of myelination and appear to be the major signals that control myelination.

The myelin sheath is a polarised structure, both longitudinally as well as radially, and can largely be divided into different segments including the Nodes of Ranvier, nodes, paranodes, juxta paranodes and internodes (Figure 1.11), each with specific physiological functions and array of ion channels, cell adhesion molecules, and cytoplasmic adaptors (Corfas et al., 2004). The longest domain is the internode, in which the membranes of the Schwann cell and of the axons are in intimate contact. Adhesion molecules present in the internode include myelin associated glycoprotein (MAG) and Nectin-like (Necl) proteins Necl-1, Necl-2 and Necl-4 that mediate interactions between Schwann cells and axons (Maurel et al., 2007; Rasband and

Peles, 2015; Spiegel et al., 2007). Interactions between Necl-1 on the axon and Necl-4 on the surface of Schwann cells are required for myelination, as knockdown of either molecule *in vitro* results in decreased axonal myelination (Maurel et al., 2007; Spiegel et al., 2007). Though, Necl1 and Necl4 mediate the myelination of the axons, they do not appear to be required for the initial contact between Schwann cells and axons (Spiegel et al., 2007).

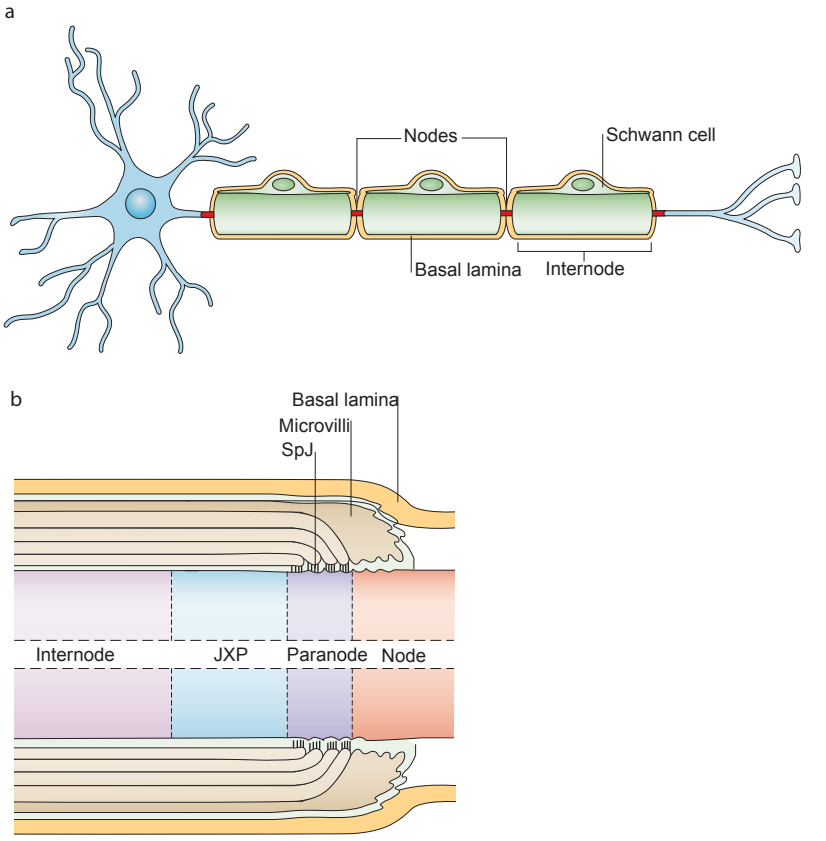

Adapted from Poliak and Peles, 2003

Figure 1.11. Structure of myelinated axons.
a) Large diameter axons in the PNS are myelinated by Schwann cells in a 1:1 ratio. Each segment of a myelinating Schwann cell around the axon is called the internode and two myelinating Schwann cells are intersected by nodes. b). Schematic longitudinal cut in which the internode, juxtaparanode, paranode and node are labelled. At the paranode, Schwann cells interact with axons through paranodal junctions. Microvilli emerging from myelinating Schwann cells interact with axons at the node. Schwann cells are surrounded by a layer of basal lamina.

The Nodes of Ranvier intersect adjacent Schwann cells along the length of the axon, and are characterised by the accumulation of Na+ channels and K+ channels on the surface of the axons, that are fundamental for salutatory conduction (Rasband and Peles, 2015). The Na+ channels are concentrated at the node on the surface of the axon by ankyrin G and βIV spectrin that connect the channels to the actin cytoskeleton (Berghs et al., 2000; Kordeli et al., 1995). Clustering of Na+ channels and K+ channels at the Nodes of Ranvier is mediated through interactions between the axonal surface and Schwann cell microvilli, which are structures emanating from both ends of the myelinating Schwann cells flanking the internode. The interactions between the Schwann cells microvilli and the axon are mediated by the cell adhesion molecules (CAM) NF186 on the axon and nrCam on the Schwann cells that interact via their ligand gliomedin, which in turn clusters the Na+ channels on the axonal membrane through a complex of the ion channels with ankG (Figure 1.12) (Eshed et al., 2005; Rasband and Peles, 2015). While Gliomedin is required for the node formation, it does not effect the myelination process, (Eshed et al., 2005), consistent with the relatively late appearance of microvilli (Rasband and Peles, 2015).

Other proteins that mediate Schwann cell/axonal interactions include neurofascin (NF155), which is located on the surface of Schwann cells at the paranodal junctions, which flank the Nodes of Ranvier (Charles et al., 2002). NF155 interacts with an axonal complex consisting of GPI-anchored contactin and Caspr. These complexes are crucial for the formation of the paranodal loops, as loss of Caspr leads to aberrant nerve conductions (Laquerriere et al., 2014). Other molecules that are important for Schwann cell/axonal interactions are N-cad and E-cad, which are expressed by Schwann cells and play roles in Schwann cell migration, proliferation and myelination (Crawford et al., 2008; Fannon et al., 1995; Lewallen et al., 2011; Parrinello et al., 2010; Tricaud et al., 2005; Wanner et al., 2006; Wanner and Wood,

2002). E-cad is expressed in mature myelinating Schwann cells, where it forms autotypic junctions between membranes of a single Schwann cells and plays a role in maintaining the architecture of several structures such as the paranodal loops at the Nodes of Ranvier and at Schmidt-Lanterman incisures, a structure important for the transport of molecules between periaxonal and pericellular cytoplasm (Crawford et al., 2008; Fannon et al., 1995; Tricaud et al., 2005). In contrast, N-cad is expressed in Schwann cell precursors during the development of the nerve and is important for the outgrowth of the nerve (Wanner et al., 2006). Interestingly, after injury, N-cad is re-expressed upon the dedifferentiation of Schwann cells and has been suggested to provide a scaffold to promote axonal growth and is required to initiate remyelination of the axons (Lewallen et al., 2011; Parrinello et al., 2010; Wanner et al., 2006; Wanner and Wood, 2002). Moreover, we have previously shown that N-cad is required for sorting Schwann cells into clusters, which is important for their collective migration, which promotes axonal regrowth following injury (Parrinello et al., 2010).

In addition, Semaphorin 4F (Sema4F) plays a role in the heterotypic interaction between Schwann cells and axons, it is required for the alignment of Schwann cells to axon, and controls Schwann cell proliferation (further discussed in Chapter 5) (Parrinello et al., 2008).

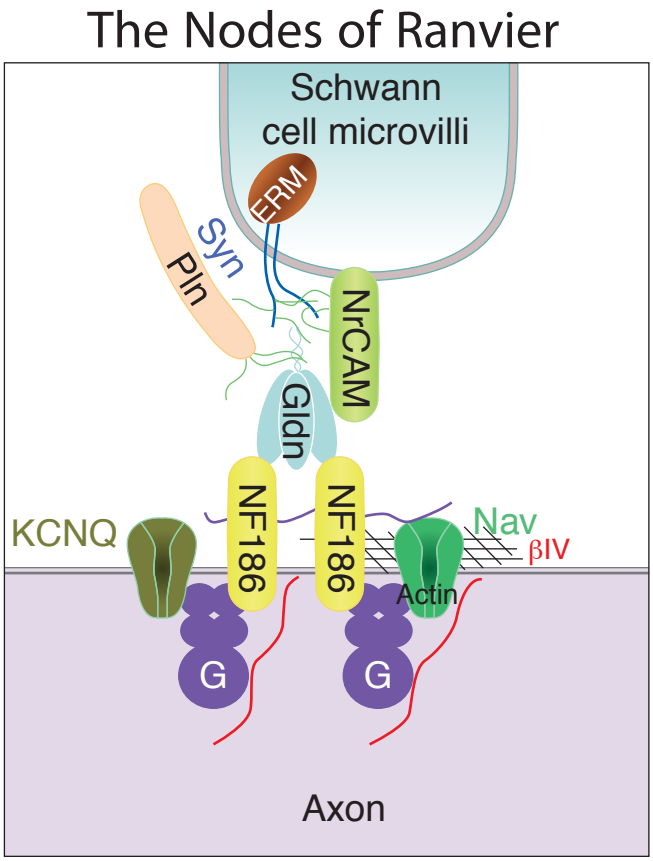

Adapted from Rasband and Peles 2015

Figure 1.12. The assembly of the Nodes of Ranvier.
Interaction between the axon and the Schwann cell microvilli, which emanate from myelinating Schwann cells that are flanking the internode, are required for assembly of the Nodes of Ranvier. These interactions are mediated by NF186 and nrCAM on the axon and Schwann cells respectively, which are connected via Gliomedin (Gldn). NF186 in turn via interaction of ankG (G), clusters the Na+ channels in the axonal membrane, which are concentrated at the Nodes of Ranvier.

1.3. Nerve regeneration

1.3.1. Injury response

Unlike nerves of the central nervous system (CNS), the nerves of the PNS can regenerate following an injury and are able to reconnect to their original targets (Navarro, 2009; Nguyen et al., 2002; Zochodne, 2008). Upon injury of the nerve, a complex process called Wallerian degeneration is induced, which includes degeneration of the axons downstream from the site of injury and Schwann cell dissociation, dedifferentiation and proliferation (Conforti et al., 2014). Proximal to the site of injury, polarised growth of axons is induced in order to allow regrowth back towards their targets (Cattin and Lloyd, 2016). Remarkably, during the regeneration process, the normally quiescent, myelinating Schwann cells are triggered to dedifferentiate to a more progenitor-like state. Dedifferentiation of Schwann cells is mediated by the Ras/Raf/ERK signalling pathway, that induces the reprogramming of the cells - including the down regulation of myelin genes (Figure 1.13) (Harrisingh et al., 2004). Moreover, the dedifferentiated Schwann cells provide a proliferative pool, which are capable of clearing the myelin and axonal debris through phagocytic processes, opening of the blood nerve barrier and inducing an inflammatory response (Napoli et al., 2012). Other pathways important for the dedifferentiation-state of Schwann cells include c-Jun, which is induced by ERK and drives the dedifferentiation process by negatively regulating the transcription of the myelin genes (Parkinson et al., 2008; Woodhoo and Sommer, 2008). In addition, c-Jun has a role in axonal regeneration, by promoting axonal survival through regulating expression of the secreted neurotrophic factors GDNF and Artemin in Schwann cells (Arthur-Farraj et al., 2012; Fontana et al., 2012). Notch signalling has also been shown to negatively regulate the myelin genes and its expression is sufficient to

revert the myelinating Schwann cells to a demyelinating state (Woodhoo et al., 2009).

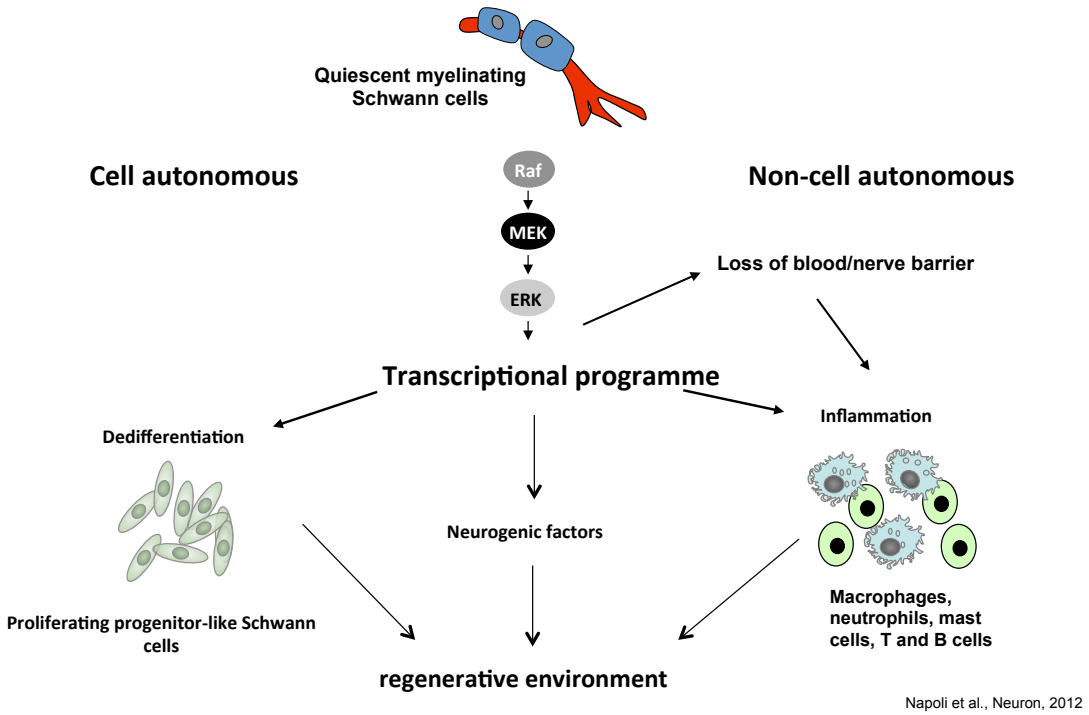

Figure 1.13. Schwann cells orchestrate the regenerative process.
Ras activation in Schwann cells, following injury, plays a key role during the regenerative process, which has multiple affects, including the dedifferentiation to a more progenitor like state, secretion of neurogenic factors, opening of the blood/nerve barrier and the induction of the immune response.

Following full transection of the nerve, the nerves stumps retract leaving a gap, which axons need to cross in order to grow back to their original target (Figure 1.14). Distal to the cut, Schwann cells within the distal stump form tube-like structures within their original basement membranes called Bands of Büngner, which provide a track through which axons can regrow to their original target (Figure 1.14) (Cattin and Lloyd, 2016). However, to reach the Bands of Büngner axons face some hurdles; axons must pass through a densely packed tissue that forms, through unknown mechanisms, at the cut site between the proximal and distal stump, called “the bridge”. The bridge consists of a mixture of inflammatory cells, fibroblasts and matrix and appears a hostile and non-directional environment that can extend over several

millimetres (Figure 1.14). Until recently it was unclear how axons crossed this bridge. However, we have shown that Schwann cells play a crucial role in guiding the axons across the bridge (Parrinello et al., 2010).

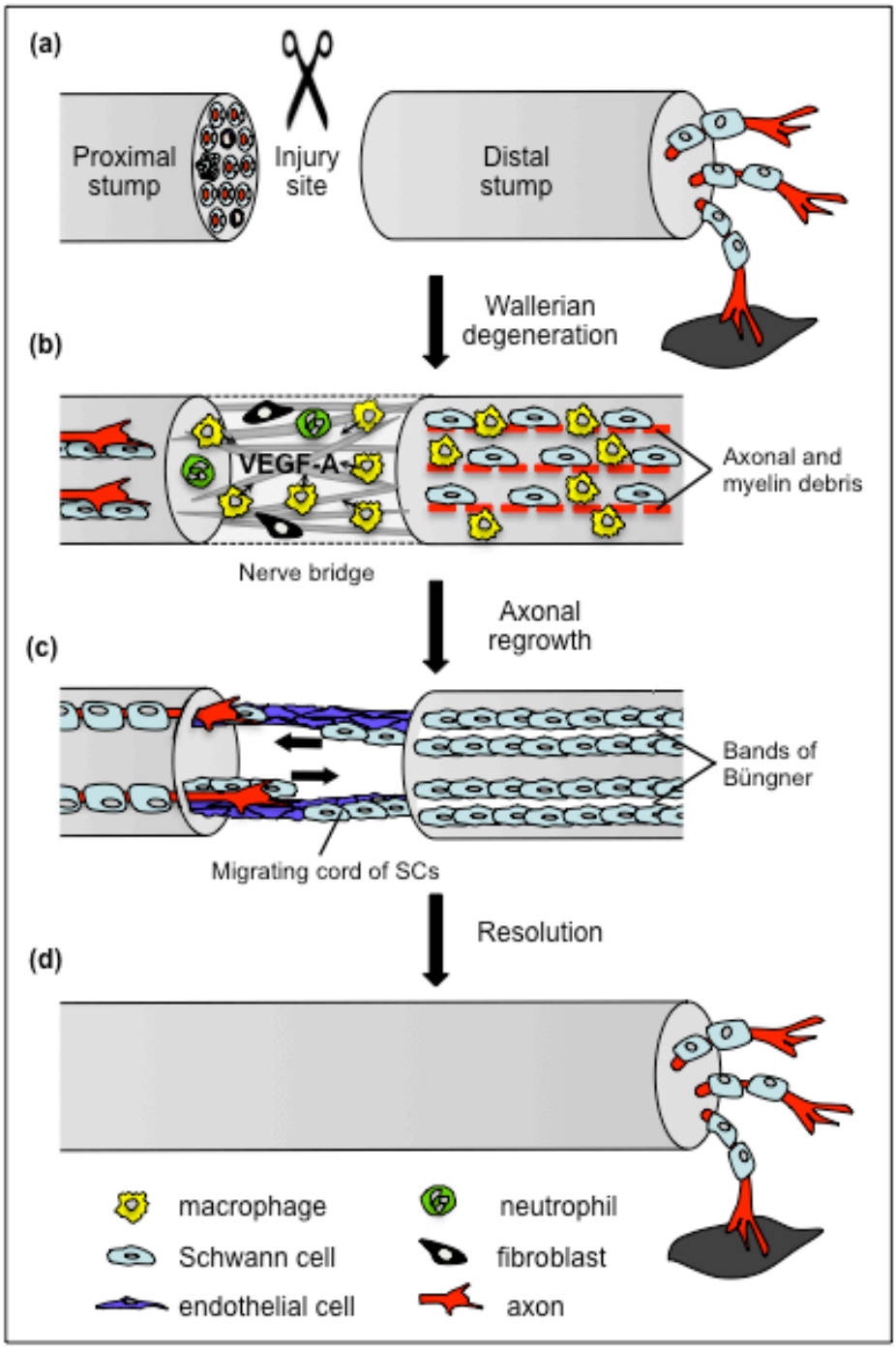

Figure 1.14. Model of the multi-cellular processes involved in the regeneration of peripheral nerves.

a) Injury of the nerve induces the degeneration of axons distal to the site of injury; both nerve stumps retract leaving a gap. b) At the site of injury a structure is formed called “the bridge”, which consists of matrix, fibroblasts, neutrophils, and

macrophages (the majority cell type). The bridge becomes hypoxic which is specifically sensed by the macrophages, which subsequently secrete VEGF-A. c) VEGF-A induces the formation of new blood vessels in the bridge that are polarised in the direction of subsequent Schwann cell migration. Schwann cells migrate along the blood vessels using them as a track, taking axons along with them across the bridge. Once the axons re-enter the distal stump they grow through the Bands of Bungner back to their targets. d) Axons are remyelinated by Schwann cells and the inflammatory response resolves.

To guide axons back to their target, Schwann cells migrate collectively as cellular cords, emerging from both stumps until they fully extend across the bridge. We showed that the migration of Schwann cells as a collective is fostered by heterotypic interactions with fibroblasts, which induce the sorting of the Schwann cells (Parrinello et al., 2010). Schwann cells cultured alone, undergo CIL and thus normally repulse each other upon contact causing individual cells to migrate away from each other. In contrast, in co-cultures of Schwann cells with fibroblasts, Schwann cells switch their behaviour from repulsive to adhesive, following a heterotypic interaction with a fibroblast, causing the Schwann cells to cluster (Figure 1.15 and 1.16). This heterotypic interaction is mediated by EphrinB/EphB2 signalling between fibroblasts and Schwann cells, which induces re-localisation of N-cad to the cell-cell junctions between Schwann cells, through activation of the transcription factor Sox-2 (Figure 1.15). Interestingly, Sox-2 does not regulate the mRNA expression levels of N-cad, nor does it affect protein levels, but instead induces, through unknown mechanisms, N-cad re-localisation to the site of cell-cell junctions. Moreover, this EphB2-mediated process is required for nerve regeneration, as loss of EphB2 signalling *in vivo* results in loss of cord formation and loss of directional Schwann cell migration and axonal growth (Parrinello et al., 2010). Interestingly, time-lapse analysis of the Schwann cells clusters formed in co-cultures with fibroblasts, show that while Schwann cells become more adhesive, they don't become static, but appear very motile and dynamic and appeared to attempt to migrate away from each other, reminiscent of

repulsive behaviour (Parrinello et al., 2010). This suggests, that the repulsion signalling may still be active in the collectively migrating Schwann cells, which could be important for the cells to exert forces and move the Schwann cell collective forward. This is reminiscent of collectively migrating neural crest cells during development, in which CIL is required for mediating the global polarisation of individual cells in the direction of migration and also appears to mediate a repulsive force outward from the cluster (Scarpa et al., 2015; Theveneau and Mayor, 2010). Although, it is clear that Schwann cell clustering is mediated by N-cad re-localisation, what mediates homotypic CIL between Schwann cells, and if other homotypic interactions between the collectively migrating Schwann cells are required, is unknown.

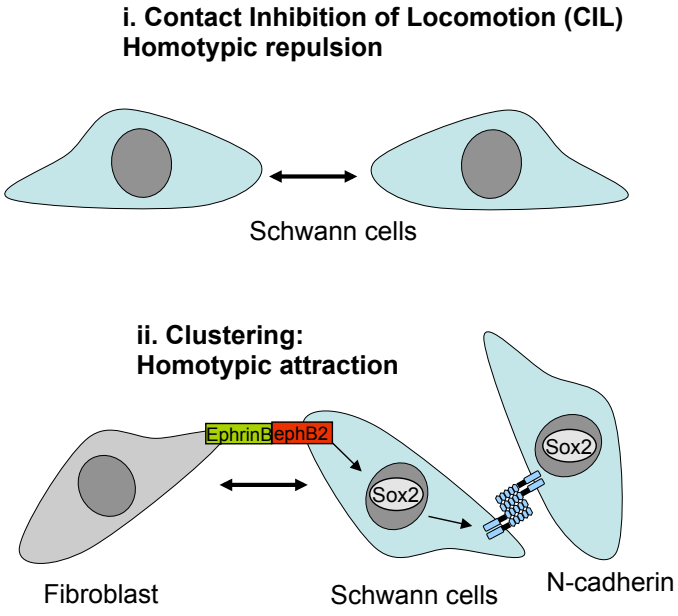

Figure 1.15: Schwann cells change their behaviour following heterotypic interactions with fibroblasts.
i. *In vitro*, Schwann cells repulse each other upon collision. ii. Upon heterotypic contact with fibroblasts, mediated through EphrinB/EphB2 signalling, Schwann cells change their behaviour from repulsive to adhesive, inducing Schwann cell clustering. Mechanistically we showed that this is mediated by the activation of the transcription factor Sox-2 in Schwann cells, which by an unknown mechanism induces the re-localisation of N-cad to the site of cell-cell junctions (Parrinello et al., 2010).

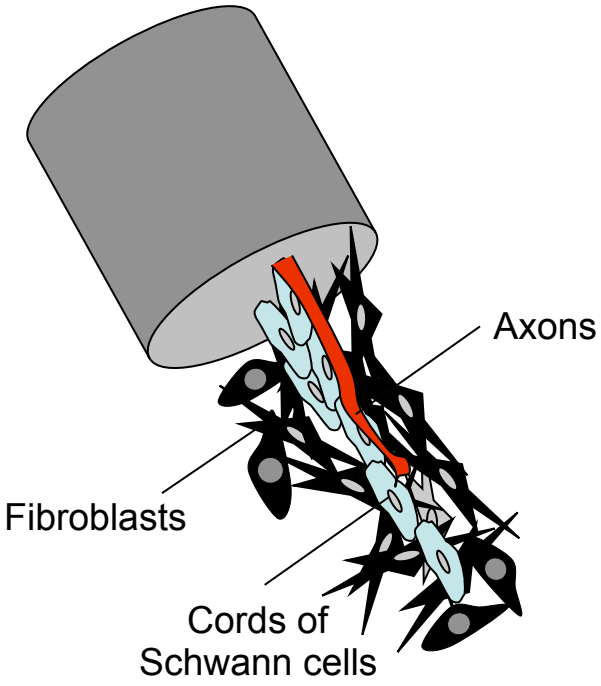

Figure 1.16: Schwann cells migrate as cellular cords required for axonal regeneration.
Schwann cells emerge from both the proximal and distal stumps, into the bridge, where they come into contact with fibroblasts. The heterotypic interactions with fibroblasts are required to induce Schwann cell sorting into cellular cords. Schwann cell migration extends across the bridge, taking along the axons, to guide them back to their targets.

1.3.2. Schwann cell migration

Schwann cell migration plays a key role both during the development of peripheral nerves and during the regeneration process (Cattin and Lloyd, 2016; Heermann and Schwab, 2013). Little is known about the signals controlling Schwann cell migration with most studies focusing on the migration that occurs during the development of the peripheral nerve. During development, Schwann cell precursors migrate along the growing axons, from the nerve roots to the periphery (Heermann and Schwab, 2013). Thus Schwann cells must migrate over long distances in order to populate the the entire length of the axon. Several studies have shown a crucial role for NRG1 type III/ ErbB2/3 signalling in Schwann cells migration. NRG1 type III is expressed by

the growing axon and induces directional Schwann cell migration along the lateral line in zebra fish, and along explants of sympathetic axons (Heermann et al., 2011; Lyons et al., 2005). However, inhibition of NRG1 besides blocking migration also results in increased apoptosis, but when both apoptosis and NRG1 signalling are inhibited Schwann cell migration is restored, suggesting that the effect of NRG1 type III on Schwann cell motility is indirect through survival of the Schwann cells (Heermann et al., 2011). The authors, suggest that apoptosis might lead to loss of contact between neighbouring Schwann cells, resulting in the stalling of migrating Schwann cells, with surviving cells migrating backwards to re-contact the group of migrating Schwann cells. This phenotype is reminiscent of the collective migration of Neural crest cells, which are kept together by the co-attraction molecule C3a (Carmona-Fontaine et al., 2011), however, this needs to be further investigated.

The neurotrophins BDNF and NT3 have also been shown to play a role in Schwann cell migration *in vitro* (Yamauchi et al., 2003, 2004). BDNF is secreted by axons and signals via p75 expressed by the Schwann cells, which inhibits Schwann cell migration along explants of axons, in a Src-kinase dependent manner (Yamauchi et al., 2004). In contrast, neurotrophin NT3 induces Schwann cell migration along the axon, through activating the Rho-GTPases Cdc42, and Rac-1 (Yamauchi et al., 2003, 2004). Other proteins that have been shown to promote Schwann cell motility in Boyden chamber assays *in vitro* are integrins, and GDNF (Cornejo et al., 2010; Inoue et al., 2010; Milner et al., 1997). Moreover, erythropoietin has been shown to regulate Schwann cell migration, by promoting β1-integrin-dependent Schwann cell migration on fibronectin, which is mediated by the direct recruitment of β1-integrin to the cell-cell surface of Schwann cells, upon stimulation with erythropoietin (Inoue et al., 2010).

In contrast to during development, during regeneration Schwann cells migrate across the bridge prior to axonal growth, suggesting different mechanisms are in place to mediate directional Schwann cell migration (Parrinello et al., 2010). We recently showed, how Schwann cells migrate directionally through the apparently non-directional environment of the bridge (Cattin et al., 2015). Following severing of the nerve, macrophages, along with other inflammatory cells, are recruited to the bridge with macrophages being the majority cell type in the bridge (Figure 1.14). The bridge region initially lacks blood vessels, and thus becomes hypoxic, which is sensed specifically by the macrophages resulting in the subsequent secretion of VEGF-A, which in turn induces the formation of a polarised vasculature (Figure 1.14). Moreover, while VEGF-A is sufficient to induce the formation of the blood vessels, it is not required for Schwann cell migration. However, we also found that macrophages secrete unknown factors that increase Schwann cell migration (Cattin et al., 2015).

We also showed that interactions between Schwann cells and blood vessels are important for the directionality of the subsequent migrating Schwann cells (Figure 1.14) (Cattin et al., 2015). Blood vessels promote directional Schwann cell migration in two ways, they provide a surface for Schwann cells to migrate on, as *in vitro* analysis showed that Schwann cells cannot migrate within a 3D matrix, but required the interaction with the surface of the endothelial cells to move forward (further explained in Chapter 5). Moreover, the polarised vasculature provides Schwann cells with directionality. This was shown most convincingly, by directing blood vessel formation into surrounding tissues which redirected Schwann cell migration and axonal growth along the redirected vessels into the surrounding tissue. However, what attracts Schwann cells into the bridge and how the blood vessels provide a conducive migratory environment remains unclear.

1.4. Pathology

1.4.1. Neuropathies

As described in the preceding sections, the development and maintenance of healthy peripheral nerves is mediated by the interdependent Schwann cell/axon relationship. It is therefore not surprising that underlying many neuropathies is aberrant Schwann cell/axonal communication (Juarez and Palau, 2012). Charcot-Marie-Tooth disease (CMT) is a heterogenous group of inherited peripheral neuropathies that affect both motor and sensory nerves and affects 17-40 per 100,000 people. Neuropathies are primarily caused by myelination defects, which ultimately lead to axonal degeneration. However, there are Schwann cell induced neuropathies that cause axonal degeneration independent of demyelination. Alternatively, the disease can be the result of a defect in the axon. The affected genes underlying the neuropathies are often related to myelin processes including compaction and maintenance of myelin, trafficking, transport through myelin, myelin related transcription regulation, as well as genes in axonal transport, cell signalling and cytoskeleton formation (Juarez and Palau, 2012).

There are different types of CMT, CMT Type I are demyelinating forms which are characterised by a reduction in nerve conduction velocity, segmental demyelination and remyelination, and CMT Type II in which the defect is primarily in the axon, which often results in a mild reduction of nerve conduction, and loss of axons (Juarez and Palau, 2012). CMT Type I is by far the most prevalent peripheral neuropathy and results from autosomal dominant or X-linked mutations, caused by mutations in genes including PMP22 that encodes for myelin protein 22, which is mainly expressed in compact myelin of Schwann cells (Lupski et al., 1991; Raeymaekers et al., 1991), and the myelin protein zero gene (MPZ), which is the major protein in the myelin sheath (there are more than 150 mutations in MPZ

associated with CMT1B) (Juarez and Palau, 2012), CMTX1, an X-linked gene encoding for gap junction protein connexin-32, which is located within the myelin sheath, and is important for the transport of ions and nutrients between cells (Bergoffen et al., 1993).

Other types of CMT that occur less frequently include Type II, which are disorders caused by autosomal dominant mutations in axonal genes, CMT Type III which is characterised by the thinning of myelin and segmental demyelination, and CMT Type IV, which is a rare autosomal recessive neuropathy (Juarez and Palau, 2012; Suter and Scherer, 2003).

1.4.2. NF1 and NF2

Additional disorders associated with Schwann cell dysfunction arise in patients with Neurofibromatosis Type 1 (NF1) and Type 2 (NF2), which are inherited dominant autosomal disorders, in which there is a high risk of tumour formation (Ferner, 2007). These are of particular interest for this study, as tumourigenesis is associated with loss of heterotypic and homotypic interactions, which can cause loss of inhibition of cell movement and CIL, and ultimately result in invasion and metastasis. Indeed, the development of the tumours in NF1 and NF2 is characterised by the loss of cell-cell recognition molecules (Morrison et al., 2001; Parrinello et al., 2008).

1.4.2.1. Neurofibromatosis Type I

Though the tumours associated with both NF-1 and NF-2 consist of Schwann cells, they are genetically and clinically different. NF1 is a very common disease that affects 1 in 3500 people world wide, and is characterised by skin disorders and the manifestation of peripheral nerve tumours. NF-1 results from the heterozygous loss of the NF1 gene and mainly affects the peripheral nervous system, in which there is

an increased risk of developing peripheral nerve sheath tumours called neurofibromas (Ferner, 2007). However, loss of NF1 also results in several other clinical manifestations such as café au lait macules, Lisch nodules, optic gliomas, neoplasias of the haematopoietic system, skin deformation and learning disorders. Neurofibromas are benign tumours that can occur along the length of the peripheral nerve, they can either be located within the dermis (dermal neurofibromas) or are located deeper towards the nerve roots (plexiform neurofibromas). Although benign, the plexiform type of neurofibroma can continuously grow, is locally invasive, spreads into the surrounding tissue and can affect whole limbs or organs (Figure 1.17) (Woodruff, 1999). Furthermore, in 7-13% of NF-1 patients the tumours can transform into highly malignant Malignant Peripheral Nerve Sheath Tumours (MPNSTs), which usually arise from a pre-existing plexiform neurofibromas, that can invade and metastasise (Figure 1.17) (Evans et al., 2002). Thus like during the regenerative process Schwann cells appear to become migratory during the tumourigenic process (Figure 1.17).

The *NF1* gene encodes for neurofibromin, a cytoplasmic protein containing a Ras-GAP domain, which regulates Ras, by promoting the hydrolysis of GTP to GDP, thereby inactivating Ras and terminating downstream signalling. Thus loss of *NF1* results in hyperactivation of Ras (Martin et al., 1990; Xu et al., 1990). Neurofibromas are complex tumours that contain multiple cell types including increased numbers of Schwann cells, fibroblasts and mast cells, and an increase in ECM. Importantly, Schwann cells are dedifferentiated and dissociated from the axons. Although neurofibromas are a mixture of cells, it is well understood that neurofibromas arise from the loss of NF1 in Schwann cells, resulting in the hyper activation of Ras (DeClue et al., 1992; Kim et al., 1997). However, genetic studies have suggested that

other cell types are also important during the development of the tumours, as well as the local environment (Ribeiro et al., 2013; Yang et al., 2008; Zhu et al., 2002).

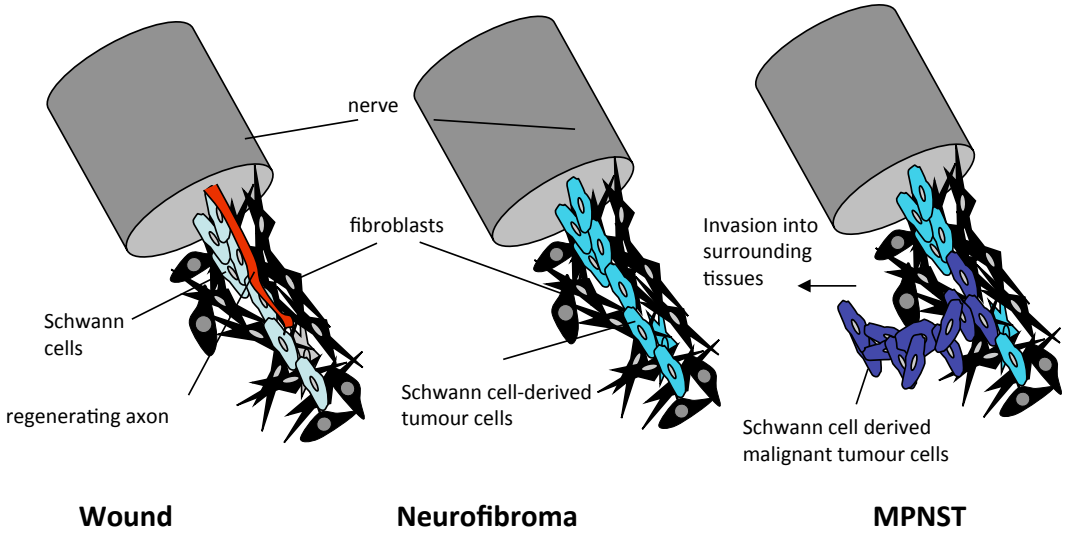

Figure 1.17. Neurofibromas mimic an unrepaired wound.
Neurofibromas have a similar cellular composition to a regenerating nerve, including dedifferentiated and dissociated Schwann cells, inflammatory cells and fibroblasts. During nerve regeneration Schwann cells collectively migrate. Similarly, plexiform neurofibromas can spread over long distances and are locally invasive, suggesting Schwann cells become motile. While, in MPNST the malignant tumour cells become highly invasive and are able to invade into surrounding tissues and metastasise.

Owing to their similar cellular composition, neurofibromas have been described as mimicking the injured state and have been referred to as unrepaired wounds (Figure 1.17) (Lassmann et al., 1976). Interestingly, similarities can be made between Ras signalling during the formation of neurofibromas and peripheral nerve regeneration. Activation of the Ras pathway is sufficient to induce many aspects of the regenerative response (Napoli et al., 2012). This results in the dedifferentiation of the Schwann cells and dissociation from axons. Acting cell-autonomously, Ras activation induces Schwann cell dissociation from axons, which is mediated by a loss of Sema4F expression by the Schwann cells which indirectly mediates hyper proliferation (Parrinello et al., 2008). Non-cell autonomous effects include the loss of

the BNB and the induction of the inflammatory response (Napoli et al., 2012), the latter is thought to be important for the development of the tumour as there is a large influx of inflammatory cells, such as mast cells which changes the tumour development (Yang et al., 2008), and thus this suggests that the microenvironment of tumours plays an important role in their development.

Indeed, a large body of evidence suggest that the tumours do not just develop from cell-autonomous effects. Studies have shown that loss of NF-1 in Schwann cells alone is not sufficient for the formation of neurofibromas, as tumours only develop in a *Nf-1* heterozygous background, suggesting interactions of *Nf-1-/-* Schwann cells with other *Nf-1+/-* cell types are required for tumour formation (Yang et al., 2003; Zhu et al., 2002). Moreover, *in vivo* work showed that knockout of *NF1* in Schwann cells during development does not result in the early formation of tumours, moreover, the nerves develop normally (Joseph et al., 2008; Wu et al., 2008; Zheng et al., 2008). However, tumours did develop in the adult, when Schwann cells can be seen to start dissociating from axons, which ultimately give rise to neurofibromas (Wu et al., 2008; Zheng et al., 2008). Interestingly, however, loss of *NF1* in the adult does not result in many tumours (Joseph et al., 2008). This suggests that loss of *NF1* is not sufficient to disrupt heterotypic interactions between Schwann cells and axons or lead to the dedifferentiation of the cells. Moreover, these results showed that the timing of the loss of *NF1* at a specific stage during development could also be important to predispose Schwann cells to tumour formation at a later stage and suggest additional tumour promoting signals from the microenvironment, such as from a inflammatory response, are required to trigger the primed Schwann cells for tumour development (Parrinello and Lloyd, 2009).

Recent work from our lab showed that the injury response can play a role in the development of tumours and provided further evidence for the importance of the

microenvironment in neurofibroma development (Ribeiro et al., 2013). In this study we showed that the wound site provides a tumour-promoting environment, as tumours formed with high frequency specifically at the site of injury in mice in which NF1 was specifically lost in myelinating Schwann cells in the adult, both in a *Nf1+/+* and a *Nf1+/-* background. In contrast, the structure distal to the injury site was not affected, indicating that additional (loss of) signals, or interactions of *NF1-/-* Schwann cells with microenvironment at the site of injury are required for the formation of tumours (Ribeiro et al., 2013). Thus, this shows that *NF1-/-* Schwann cells need a conducive microenvironment for the development of neurofibromas.

Although the importance of changes in normal Schwann cell homotypic and heterotypic interactions in the development of neurofibromas appears clear, there is still surprisingly little known about what mediates these changes in cell/cell interactions.

1.4.2.2. Neurofibromatosis Type II

In contrast to NF1, NF2 is a disease that is characterised by the development of benign bilateral Schwannomas and meningiomas, and has a lower incidence of approximately 1 in 25,000 (Petrilli and Fernandez-Valle, 2016). NF2 results in manifestations both in the CNS and the PNS, which include bilateral vestibular schwannomas, peripheral nerve schwannomas, spinal tumours, cranial meningiomas and ocular abnormalities (Ferner, 2007). NF2 results from mutations or the loss of heterozygosity of the *NF2* gene. In Schwannomas loss-of-function or deletion of *NF2* results from the heterozygous loss of the *NF2* gene in Schwann cells, with tumours resulting through the loss of the two alleles, causing benign tumours that are exclusively composed of Schwann cells.

The NF2 gene encodes for Merlin, a protein structurally related to the ERM proteins ezrin, moesin and radixin, which link the actin cytoskeleton to the cell surface (Li et al., 2012). Consistent with the function of ERM proteins, Merlin's activity is dependent on localisation at the cell surface (Shaw et al., 1998). Merlin plays a major role in cell-cell recognition, as it has been shown suppress mitogenic signalling in a cell density-dependent manner. Merlin has been shown to mediate contact inhibition of proliferation (CIP), downstream of the cell-cell cell/substrate adhesion receptor CD44, and can localise at the membrane where it is able to bind to adherence junction complexes (Morrison et al., 2001; Morrison et al., 2007). However, Merlin affects multiple pathways including cell adhesion, integrin signalling, ErbB2/ErbB3, Rac signalling, mTOR, pI3K/akt, Wnt signalling and the Hippo pathway, to regulate cell survival, proliferation and contact inhibition of cell growth (Petrilli and Fernandez-Valle, 2016).

Thus, loss of cell/cell interactions between Schwann cells appears to play a critical role in the development of Schwann cell derived tumours associated with NF1 and NF2. As discussed in the preceding sections, CIL prevents intermingling of different cell populations and can be lost during tumourigenesis, thereby contributing to the development and spreading of the tumour. However, whether CIL is lost in Schwann cells in NF1 and NF2, and how this attributes to the development of tumours is unknown.

1.5. Thesis Aims

In the previous sections, I described the importance of heterotypic and homotypic interactions in maintaining the healthy and organised structure of peripheral nerves, as well as during cellular movements triggered upon injury of the nerve, and how (loss of) these interactions can contribute to the tumourigenesis associated with NF1 and NF2. I also discussed the importance of Schwann cell migration both during development, as well as during the regenerative process, and the role of homotypic and heterotypic interactions of Schwann cells. Schwann cells normally undergo CIL *in vitro,* and recent reports showed that CIL is required for cell dispersal and collective migration of certain cell types *in vivo*, suggesting CIL may play a role in mediating the collective migration of Schwann cells. However, how CIL is mediated in Schwann cells remains unknown. I further discussed how N-cad, a well known cell/cell recognition molecule, plays an important role during the collective migration of Schwann cells by maintaining a cluster, and has been shown to regulate CIL in neural crest cells. However, whether N-cad is required for CIL in Schwann cells, and how N-cadherin can mediate these opposing behaviours remains unclear.

Moreover, I described the importance of the migrating Schwann cells with the vasculature, required for the directionality of the migrating cells during the regenerative process. However, what mediates the Schwann cell/blood vessel interactions, to mediate Schwann cell migration along the vasculature is unknown.

The principle aim of this thesis was to understand the mechanism by which homotypic CIL in Schwann cells is mediated and if CIL is lost during the tumourigenic processes associated with NF1. We also wished to understand what mediates the heterotypic interactions needed for the efficient migration of Schwann cells along blood vessels.

Chapter Two: Materials and Methods

2.1. Materials

2.1.1. Chemicals

All chemicals unless stated otherwise were bought from Sigma. Inhibitors were bought from: Erk inhibitor PD184352 (0.75μM Axon), Fyn inhibitor SU6656 (250nM, Santa Cruz).

2.1.2. Constructs and oligos

Constructs

N-cadherin full length, the extracellular and intracellular domain of N-cadherin tagged with ptdTomato on the C-terminus and inserted into a GFP-N1 expression plasmid, in which the GFP was replaced by the dtTomato, were a kind gift from Prof. S. Yamada at the University of California (Shih and Yamada, 2012).

Retroviral constructs

The Raf-ER and dominant negative form of p53 (human $p53^{175}$ cDNA) construct were in pLXSN retroviral plasmid. H-RasV12 was in pBabe retroviral plasmid.

siRNA oligos

Double stranded RNA oligos were designed and supplied by Qiagen, scrambled siRNA was used a control. Refer to table 2.1 for target sequence and concentration used for each oligo.

Table 2.1 siRNA oligos

Gene	Target sequence	Concentration
αE-catenin siRNA 1	AAGAACGCCTGGAAAGCATAA	4nM
αE-catenin siRNA 2	CAACCGGGACTTGATATACAA	4nM
β1-integrin siRNA 1	ACAGCTGATTATCGATGCCTA	5nM
β1-integrin siRNA 2	CAAATTGTGGGTGGTGTACAA	5nM
Cadherin 2 siRNA 1	TCCCAACATGTTTACAATCAA	1*-2nM
Cadherin 2 siRNA 2	CAGTATACGTTAATAATTCAA	1*-2nM
EphB2 siRNA1	CTGGGTGGCCGCGTCATGAA	3nM
p120-catenin siRNA 1	AGGTCAGATCGTGGAAACCTA	2.5nM
p120-catenin siRNA 2	ATGCTCGGAACAACAAAGAGTTAA	2.5nM
Talin 1 siRNA1	CTGAGCGTCGTACAGAATCTA	3nM
Talin 1 siRNA2	CTGGTCGCTTGCAAGGTCAAA	3nM
Talin 2 siRNA1	ACCGGGCAAGCTTCTGACTAT	5nM
Talin 2 siRNA2	ACCGGGCAAGCTTCTGACTAT	5nM
Glypican-4 siRNA1	CCGACTGGTTACTGATGTCAA	2.5nM
Glypican-4 siRNA2	CGGTGTAGTTACAGAACTGTA	2.5nM

** 1nM was used for rescue experiments. 2nM was used for all other experiments.*

qPCR Primers

Primers were designed using Pimer3 tool to specifically target the mRNA by annealing to sequences in two exons that are flanking one or more intron(s). Refer to table 2.1 for the sequence.

Table 2.2 Rt-qPCR primers

Gene	Forward primer (5'-3')	Reverse primer (5'-3')
EphA1	ACACCCCTGTACATGTACCA	GCTTCCTCTCCTCGGTAGAT
EphA2	GTTTACCACCGAGATCCACC	TTCAGCGTCTTGATAGCCAC
EphA3	CACCAACATAGCCATCGACA	GATGTTGGGGTGGTCAAACT
EphA4	CACCATCATCCATTGCTTTG	AAAGGGTTCAGGCCTTTGAT
EphA5	CACAGAGACCTTGCTGCTAG	TTGCCTCCCCTTGTGGTATA
EphA6	CCACCTTCTATGGCGTGTAC	ATGAATCGAAGTCCTGCACC
EphA7	CAACGGAGTCATCACGGAAT	TTAATGGAGGCTGAGGTGGA
EphA8	GCATGGTGCTTCACATGAAC	TGGGACCTCATTGTCTGGAT
EphB1	TTCAGCATTACAGCACAGGC	CAATCGGCCCTTGTACACTT
EphB2	CAACTGGCTACGGACCAAAT	TCTCCATCCAGTTGGGAAAG
EphB3	TCGCACAGTAGCAGGTTACG	GCAGACAAGAGCAATGACCA
EphB4	CATCAAGGTGGACACAGTGG	AAAGAGATGCAAGGAGAGCA
EphB6	TCCTTCACCA TGACCAGTGA	AACCAA TCACCAAGGACAGC
Ephrin-A1	GAAGGTGACTGTCAATGGCA	TGACCAATGCTGTGCAAAAC
Ephrin-A2	CTTTTCCCTGGGCTTTGAGT	TGGACGCACGTAAACTTTCA
Ephrin-A3	TGGGCTATGAATTCCATGCC	AGCAGACGAACACCTTCATC
Ephrin-A4	GAGACTCCAGGTGTCTGTCT	GCAGAAGACGGAGTATTGGG
Ephrin-A5	GCTGCTCTTTCTGGTGCTCT	GTGGTAGTCACCCCTCTTGGA
Ephrin-B1	GGAAATCCGCTTTACCATCA	CGTTACGGCATTTGGATCTT
Ephrin-B2	TCCCTTTGTGAAGCCAAATC	GTCTCCTGCGGTACTTGAGC
Ephrin-B3	CTGGTGTCTGGACTCAGCCT	AACTTAGGAGAGGAGTGGGGG
B2M	TGACCGTGATCTTTCTGGTG	ATTTGAGGTGGGTGGAACTG
Glypican-4	CATGCTGATGGTGGCAGAGA	TCCACAGCCTTGGAAAACCT

2.1.3. Buffers

Table 2.3 western blot and Co-IP buffers

Solutions	**Components**
RIPA lysis buffer*	1% Triton X-100, 0.5% sodium deoxycholate, 50mM Tris pH7.5, 100mM NaCl, 1mM EGTA pH8, 20mM NaF, 100µg/ml PMSF, 15µg/ml aprotonin, 1mM Na3VO4.
NP40 buffer*	50mM Tris pH 7.5, 150mM NaCl, 1% NP40.
s100 buffer**	20mM Tris, 150mM NaCl, 2.5mM EDTA, 1mM EGTA PH 7.5.
4x Sample buffer	200mM Tris pH 6.8, 8% SDS (BioRad), 40% glycerol, 400mM DTT, 0.25% bromophenol blue.
10x Running buffer	50mM Tris pH, 500mM Glycine, 0.1% SDS.
10x Transfer buffer	200mM Tris, 1.5M Glycine, 20% methanol.
5% milk/ TBS-T.	Skimmed milk powder in 1X TBS-T.
Stripping buffer	200mM Glycine, pH2.5, 0.4% SDS.
20X TBS	200mM Tris base pH8, 3M NaCl.
20X TBS-T	200mM Tris base pH8, 3M NaCl 0.02% Tween-20.

* Add fresh 1/100 protease cocktail inhibitor mix.

** Add fresh 1/100 protease cocktail inhibitor mix 1/200 phosphatase inhibitor cocktail mix 2, 0.5mM PMSF and 1mM DTT.

2.1.4. Antibodies

Primary antibodies were used against: N-cadherin (BD transduction); Alpha-catenin (Sigma); β-catenin (BD transductions); p120-catenin (BD Transduction); ERK1/2 (Sigma), mCherry (BioLegend); AKT 1/2/3 (Santa Cruz); β1-integrin (Abcam); Talin (Sigma); Alexa-Fluor secondary antibodies were obtained from Invitrogen.

Horseradish peroxidase (HRP)-linked antibodies were obtained from GE-healthcare.

Table 2.4. Immunofluorescence antibodies

	Antibody	Dilution	Species	Secondary
N-cadherin	610920	1:1,000	Mouse	1:1,000
α-catenin	C2081	1:1,000	Rabbit	1:1,000
β-catenin	610153	1:2,000	Mouse	1:1,000
p120-catenin	61034	1:2,000	Mouse	1:1,000
Talin	T3287	1:500	Mouse	1:1,000
alexa fluor phalloidin	A22283	1:1,000	N/A	N/A
Hoechst		1:1,000	N/A	N/A

Table 2.5. Western blot antibodies

	% acrylamide gel	Antibody	Dilution	Species	Secondary
ERK1/2	7.5	M5670	1:5,000	Rabbit	1:5,000
AKT 1/2/3	7.5	H-136	1:2,000	Rabbit	1:5,000
N-cadherin	7.5	610920	1:10,000	Mouse	1:5,000
mCherry	7.5	677702	1:1,000	Mouse	1:5,000
α-catenin	7.5	C2081	1:1,000	Rabbit	1:5,000
β-catenin	7.5	610153	1:2,000	Mouse	1:5,000
β1-integrin	7.5	ab52971	1:500	Rabbit	1:5,000
p120-catenin	7.5	61034	1:500	Mouse	1:5,000

2.1.5. Cell culture

2.1.5.1. Preparation tissue culture dishes

For culturing Primary rat Schwann cells, dishes were coated with 80µg/mL poly L-lysine hydrobromide (PLL) for 20 min at room temperature, washed twice with water (Baxter) and dried over night.

Cell migration assays and experiments performed on glass coverslips required double coating with PLL and laminin. To double coat, the plastic tissue culture dishes and glass coverslips were first coated with PLL as described above followed by incubating them with 0.01mg/mL laminin in MEM for 1 hour at room temperature and aspirated just before seeding the cells.

2.1.5.2. Schwann Cells

Primary rat Schwann cells were extracted from sciatic nerves of postnatal 7 days Sprague-Dawley rats. Sciatic nerves were dissected from 10 rats, chopped with a scalpel and forceps, re-suspended in digestion buffer (EBSS, 7900 U/mL DNase Type IV, 2mg/mL collagenase, 2.5% Trypsin) and agitated 5 times using a 1 mL Gilson, before incubating for 15 min at 37C in the water bath to digest the tissue. Subsequently the sample was mixed again using 1 mL Gilson, before stopping the trypsin reaction using 900 µL of FCS (10%). The cells were centrifuged for 5 min at 264g, resuspended.in 4 mL panning buffer (0.1%BSA (Invitrogen), L15 medium (Gibco)) and filtered using a 40µm strainer (Falcon). Panning of the cells was performed by adding the cells to two bacterial dishes coated with CD11b/c (Harlan sera Lab mouse anti-rat (MAS 370p clone Ox42) and incubated for 10 min at room temperature to filter out the macrophages. Subsequently, the supernatant is incubated on two bacterial plates coated with Thy1 antibody (clone Ox7, home made) for 10 min at room temperature, to pan out the fibroblasts. These two panning steps were performed 3 times, before adding 0.5% BSA to the cells and collecting them by spinning for 5 min at 264g. The pellet containing Schwann cells, were subsequently re-suspended in low culture DMEM (Lonza) supplemented with 3% FBS, 1 µM Forskolin (Abcam), 200mM L-Glutamine (Gibco), GGF, 100µg/mL kanamycin (Gibco) and 800µg/mL gentamicin (Gibco). Schwann cells were seeded on to PLL-coated and laminin-coated dishes until 3 passages, upon which the cells were cultured on PLL-coated plates. Schwann cells were maintained in 10% CO_2 and 20% humidity at 37ºC. Cells were seeded at $5x10^5$ or $1.5x10^6$ per 10cm or 15cm culture plates respectively, the medium was replaced the next day and after this every two days until confluent.

2.1.5.3. Raf-ER cells

Raf-ER inducible Schwann cells (NR-SC) were produced using retroviral infection (see below). NR-SCs were cultured in normal Schwann cell medium without phenol red, which has been shown to activate the estrogen receptor. To activate NR, 0.1 µM tamoxifen (TMX) dissolved in ethanol (EtOH) was added to the culture for 24, 36 or 48 hours, ethanol was used as a control solvent.

2.1.5.4. DNp53-Ras cells

Schwann cells expressing DNp53 and Schwann cells expressing oncogenic Ras (H-Ras^{V12}) (DNp53-Ras) were produced using retroviral infection as described below. DNp53 and DNp53-Ras were cultured in the same conditions as normal Schwann cells, but were seeded at 3 $x10^5$ cells per 10cm dish.

2.1.6. Fibroblasts

Fibroblasts were collected from the sciatic nerves of 7 days old rats with the immunopanning (plates coated with Thy1 antibody) as described above. Upon harvesting of the Schwann cells, Fibroblast medium (DMEM containing 10% FBS, 200mM L-Glutamine, 100µg/mL kanamycin (Gibco) and 800µg/mL gentamicin (Gibco)) was added to the plates, and cells were grown to confluency before passaging on tissue culture dishes. The cells were cultured in 3% O_2, 10% CO_2 and 95% humidity at 37ºC.

2.1.7. HUVECS

Human umbilical vain endothelial cells (HUVECs) were cultured on gelatin coated plastic culture dishes in endothelial cell growth medium-2 (ECGM2, PromoCell) containing 100µg/mL kanamycin and 800µg/mL gentamicin (Gibco) in 5% CO_2 and

20% humidity at 37ºC. Dishes were coated with EmbryoMax 0.1% Gelatin Solution (EMD Millipore) for 10 min at 37ºC.

2.1.8. Retroviral infection

Phoenix ecotrophic retroviral producer cell line were cultured in phoenix DMEM containing 10% FBS, 200mM L-Glutamine, 100µg/mL kanamycin (Gibco) and 800µg/mL gentamicin (Gibco). Cells were passed through an 18G needle to dissociate cells and seeded in a 10 cm culture dish at $5x10^6$. The next day the medium was replaced with 4mL of phoenix medium and the cells were transiently transfected by dropping on 1860 µL of lipid complexes containing the retroviral constructs, and incubating for 4 hours at 37C, before replacing the complexes with 6mL of Schwann cell media for 24 hours, to concentrate the virus. Subsequently the media was collected and filtered through a 0.45µm filter to remove cells and cell debris, before adding polybrene (8 µg/mL), which stimulates the infection by the virus into the Schwann cells. Schwann cells, which were seeded the previous day at $5x10^6$, were incubated with the virus for 2 hours at 37C, to infect the cells with the construct, before washing the cells with media and replacing it with 10mL of Schwann cell media to let the cells recover. This procedure of collecting the virus and infecting the Schwann cells was repeated three times over three days, before antibiotic selection of the infected Schwann cells using Puromycine (0.5µg/mL) for the pBabe construct, G418 0.4 mg/ml for the LXSN constructs. pBird-GFP control vector, which lack antibiotic selection, was used to asses the transfection efficiency and as a control for the efficacy of the antibiotic-selection of infected cells. For infection of both DNp53 and

Rasv12 the cells were infected with DNp53 and the infected cells were subsequently infected using the retroviral construct LXSN expressing the H-Ras-12 construct or the empty LXSN.

Formation of complexes: 6.2 μg retroviral construct, was premixed with 15 μL Attractene reagent (Qiagen) in 1860 μL DMEM and incubated for 15 min at room temperature, before adding to the cells drop by drop.

2.2. Methods

2.2.1. ***Cell Assays***

2.2.1.1. Dorsal root ganglion neurons (DRG) preparation and co-cultures

DRGs were obtained from the vertebrae of postnatal day 0/1 Sprague Dawley rats. In brief the vertebrae was openen antero-posteriorly using surgical scissors, and subsequently the spinal cord was removed to expose the DRG capsules. DRGs were extracted using forceps, transferred into icecold L-15 media, and contaminating tissue was removed. DRG capsules were then explanted into the centre of PLL- and laminin-coated 12 well plates or glass coverslips in 4-well plates. DRG explants were incubated at 37C, 95% humidity and 5% CO2 in basal media (F-12 DMEM without phenol red, 100ng/mL, 20μg/mL, 100μg/mL transferrin, 100μg/mL BSA Fraction V, 60ng/mL progesterone, 16μg/mL putrescine, 40ng/mL selenium, 50ng/mL thyroxine, 50ng/mL tri-Iodo-thyrine). To remove all endogenous mitotic Schwann cells and fibroblasts, after 18 hours the media was supplemented with 10M S-phase inhibiter β-cytosine-D-arabinofuranoside (AraC). The media was replaced with basal media after 24 hours to remove all dead cells, and was continued to be replaced every two days upto 5-6 days until the DRG were used.

For the association assays Schwann cells were seeded onto 5/6 days old DRG on coverslips ($1.5x10^4$ cells) and fixed and stained for immunofluorescence after 8 hours

or seeded onto 12 well plates ($2x10^4$ cells) and imaged for 20 hours using time lapse microscopy. Schwann cells infected with Val12 mutant H-Ras or empty vector were produced as described previously and seeded onto DRGs 24 hours after infection. Scrambled or N-cad siRNA treated Schwann cells were seeded 48 hours post transfection.

2.2.1.2. siRNA transfection

For siRNA transfection 10^5 cells or $2x10^5$ Schwann cells were seeded per 6 well plate or 60mm dish respectively. The next day, medium was replaced prior to transfection with fresh 2.3mL or 4.6mL medium per well or dish respectively. siRNA or scrambled siRNA were mixed in plain DMEM completed to 100µL before adding 6µL Hiperfect (Qiagen) mixed by tapping and incubated for 10 min at room temperature to allow complexes to form. For 60mm dishes, the siRNA's were mixed in a total volume of 200µL DMEM and 12µL Hiperfect was added. Cells were incubated with the complexes for 16 hours and washed once with normal Schwann cell medium. Cells were then further maintained in at 37ºC before either harvesting or seeding for further experiments. Knockdown efficiency was determined using western blot analysis, Real-Time PCR (RT-qPCR) or immunofluorescence. See table 2.1 for target sequence and concentrations used.

2.2.1.3. DNA transfection

DNA was transfected using Attractene protocol (Qiagen). Briefly $2x10^5$ Schwann cells were seeded onto 60mm plate 24 hours prior to transfection. 250ng plasmid of interest and 2.25µg carrier vector DNA was incubated with 3.7µL Attractene for 15 min at room temperature to allow complexes to form. Complexes were then added onto the Schwann cells drop by drop and were incubated for 2 hours at 37ºC. pBird

was used as control for transfection efficiency.

2.2.1.4. Cell rounding assay

Schwann cells were seeded at $4x10^3$ onto laminin-coated coverslips. The next day, Schwann cells were serum starved and grown in defined media, which contains no factors (SATO) (DMEM containing: BSA 100µg/mL, progesterone 60ng/mL, Putrescine 800 µg/mL, selenium 2µg/mL, Thyroxine 2.5µg/mL, Triiodothyrine 50ng/mL). To do this, cells were washed twice quickly and once for 10 min with SATO to remove all factors and medium was then replaced with 300µL SATO supplemented with IGF (0.1µg/mL) and transferrin (100µg/mL). 18 hours later the Ephrin-A1-FC ligands (R&D Systems, 602-A1-200) or Ephrin-A4 FC ligands (R&D Systems 569-a4-200) were clustered by premixing ligand 1µg/mL final concentration with 10µg/mL affinipure goat anti human IgG (Stratech, Jackson ImmunoResearch, 109-005-008) (2:1 ligand:Fc ratio) in 100µL PBS. Clusters were allowed to form for 30 minutes at 37°C, dropped onto Schwann cells and incubated for 20 min at 37°C. This was followed by PFA fixation, immunolabeling for Fc and co-staining with phalloidin to stain the actin cytoskeleton to visualise the cells morphology.

Cell rounding was measured using Fiji, by measuring the length and the width of the cells and the cell-rounding index was obtained by dividing the shortest measurement through the longest.

2.2.1.5. Repulsion assays

For repulsion assays $8x10^3$ or $4x10^3$ Schwann cells were seeded onto PLL and laminin coated 6 well plates or 12 well plates respectively. Cells were allowed to adhere for at least 6 to 18 hours hours before starting the time-lapse microscopy. For knockdown experiments cells were seeded either 24 hours, 36 hours, or 69 hours

post transfection for N-cad and glypican-4, α-catenin, and p120-catenin siRNA respectively.

To analyse interactions between scrambled and N-cad knockdown cells, cells were treated with 1μM Cell Tracker Red CMTPX Dye or Green CMFDA dye (Invitrogen) respectively for 30 min at 37°C and washed once with 3% medium. Subsequently, 1 hour after treatment 4 $x10^3$ scrambled treated cells were mixed with 4 $x10^3$ N-cad knockdown cells, incubated for at least 16 hours before starting live-imaging using time-lapse microscopy.

To analyse the effects of oncogenic Ras on CIL, DNp53 and DNp53-Ras cells were cultured for 18 hours either in the presence of the inhibitor PD184352 (0.75 μM) or DMSO. Cells were then seeded at 3 $x10^3$ onto PLL and laminin coated 12 well plates in medium containing PD184352 or DMSO. For time-point analysis DNp53 and DNp53-Ras were imaged for 6 hours before adding the inhibitor PD184352 and further imaged for 48 hours.

For Schwann cells and fibroblasts co-culture experiments, $2.5x10^3$ cells fibroblasts and $3x10^3$ Schwann cells were seeded on to laminin-coated dishes in 5:1 fibroblast medium to Schwann cells medium ratio.

2.2.1.6. Repulsion quantification

Volocity was used to quantify repulsion. Single cells that were not dividing or engrossed by debris were tracked until contact with another cell and the initial response upon contact was determined. Three types of events were defined: Repulsion, cells retract protrusions and change direction of migration; No-repulsion, interact for longer than five hours and don't change direction of migration; Invasion, cell migrate on top of another cell with their protrusion and or cell bodies. To ensure a specific readout only single cell-cell interactions were quantified. Analysis was done

by eye and where possible blind, moreover some experiments were analysed by colleagues to avoid unconscious bias.

For the mixing experiments, the response of scrambled-treated cells, were quantified upon contact with N-cad knockdown cells and vice versa. Similarly, for the rescue experiments only the response of N-cad knockdown cells were quantified upon contact with a cell expressing, either GFP, the full length of N-cad, the extracellular domain of N-cad or the intracellular domain of N-cad.

2.2.1.7. Rescue experiments

Rescue experiments were performed in a two faceted protocol, first siRNA transfection was performed using 1nM of N-cad siRNA1 as described above, incubated overnight, and the complexes were removed in the morning and replaced with 2mL medium. The following day approximately 4-5 hours after removing siRNA complexes, DNA was transfected using Attractene protocol (Qiagen). Briefly, 575ng carrier vector, 25ng pBird were and 80ng plasmid DNA carrying either N-cad full length, the extracellular domain or the intracellular domain of N-cad were mixed in a total volume of 240 µL plain DMEM and incubated with 0.9µL Attractene for 15 min at room temperature to allow complexes to form. Complexes were dropped onto scrambled-treated or N-cad knockdown cells and were incubated for 2 hours at 37ºC. pBird was used as control for transfection efficiency. The following day cells were seeded for repulsion assays, or $15x10^3$ cells per 4 well plate were seeded for immunofluorescence. Time-lapse was started approximately 6 hours after seeding and were imaged for 24 hours. For immunofluorescence the cells were fixed and stained 18 hours after seeding. Alternatively, cells were harvested for western blotting at 48 hours after knockdown.

2.2.1.8. Matrigel assays

HUVECs tubules were formed by coating 150µL matrigel (Cornig) onto 24 well plates on ice, which was subsequently allowed to polymerise at 37ºC for 30 min before seeding $2.5x10^4$ HUVECS in normal HUVEC media. Tubules were allowed to form for 14 hours when $5x10^3$ GFP-labelled Schwann cells treated with either scrambled or siRNA targeting Talin or β1-integrin were seeded onto the tubules and immediately live-imaged using time-lapse microscopy. Schwann cells were seeded in HUVEC media supplemented with 20µg/mL recombinant human neuregulin1-β1 (NRGI) (R&D systems) to allow the Schwann cells to migrate. β1-integrin knockdown cell or Talin 1 and 2 knockdown cells were seeded 36 hours and 60 hours after knockdown respectively and were imaged for 24 hours.

2.2.1.9. 2D migration assays

For the 2D migration assays, scrambled or siRNA treated (Refer to table 2.1 for concentration) cells were seeded at low density ($8x10^3$) on PLL and laminin-coated dishes and allowed to adhere for approximately 18 hours. Cells were imaged for with time-lapse microscopy for 24 hours. β1-integrin knockdown cell or Talin 1 and 2 knockdown cells were then imaged 36 hours and 60 hours after knockdown respectively.

2.2.1.10. Scratch assay

For the scratch assays cells were seeded for a siRNA knockdown at $1x10^5$, cells, and the siRNA transfection was performed as described above (Refer to table 2.1 for concentration), and the cells were grown to confluence. At 48 hours after treatment a scratch was induced with a sterile tip. The cells were gently washed twice with medium to remove any debris and imaged using time-lapse microscopy for 24 hours.

Cells at the leading edge were imaged.

2.2.1.11. Cell tracking

Cells were tracked by their nucleus using velocity for 8 - 12 hours, except for dividing cells. Velocity and the directionality were then measured from these tracks using macro plugin in excel as described in (Gorelik and Gautreau, 2014).

2.2.2. ***Microscopy***

2.2.2.1. Time Lapse Microscopy

Life-imaging was performed at 10x or 20x using a Zeiss Axiovert 200M microscope equipped with a Hamamatsu Orca AG camera controlled by Volocity software (Improvision) and an environmental chamber which maintained the temperature at 37ºC and provided a humidified stream of 5% or 10% CO_2 in air. Images were taken every 10 minutes for 24 or 48 hours 72 hours.

2.2.2.2. Immunofluorescence

Cells grown on glass coverslips were fixed in 4% paraformaldehyde (PFA) for 10 minutes at room temperature, permeabilised with 0.3% Triton in PBS for 10 minutes at room temperature and blocked with 3% Bovine serum albumin (BSA) in PBS for 1 hour at room temperature. Coverslips were incubated with primary antibodies (Refer to table 2.4 for dilutions) overnight at 4ºC, washed with PBS, incubated with secondary antibodies conjugated to Alexa Fluor (Refer to table 2.4 for dilution) for one hour at room temperature and washed with PBS before mounting onto microscope slides using fluoromount-g (Southern Biotech). All solutions, except fluoromount-g, were supplemented with 1mM $CaCl_2$ and 0.5mM $MgCl_2$ to prevent disruption of the Ca dependent complexes such as N-cadherin and the cytoskeleton.

2.1.1.1. Confocal microscopy

All images were acquired using an inverted Leica TCS SPE confocal microscope. For each experiment the same volume, number of Z-stack and the same setting of acquisition were used. All image processing and analysis was done using FIJI software. For each image, a projection of the z-stacks was made using Fiji software using the maximal intensity.

2.2.3. Protein Analysis

2.2.3.1. *Protein extraction and quantification*

For protein extraction cell media was aspirated from cells which were then washed on ice with PBS, followed by snapfreezing at -80ºC to break membranes and harvested in 100-150µL RIPA buffer (see table 2.3). Cells were then lysed on ice for 30 minutes, vortexed every 10 minutes and homogenised using a 26 gauge needle (Beckton Dickinson). Cell debris were pelleted by spinning down at 750g for 5 min at 4ºC, the supernatant was collected and quantified using BCA assay (Pierce, Thermo Scientific).

2.2.3.2. Western Blotting

Western blotting was performed using Hoefer Scientific Instrument apparatus or Biorad western blot running kit. 20 to 30µg of proteins were resolved using a Sodium Dodecyl Sulfate - polyacrylamide gel electrophoresis (SDS-PAGE). As a size reference 5µL of PageRuler Plus Prestained Protein Ladder (Thermo Scientific) was loaded. Protein was transferred onto nitrocellulose membrane (Millipore-Immobilon), which was then blocked for one hour at room temperature using 5% milk-TBST. The membrane was incubated with primary antibodies (refer to table 2.5 for dilutions) overnight at 4ºC, washed 3 times for 5 minutes at room temperature with TBST, followed by incubation with a secondary antibody conjugated to Horseradish

peroxidase (HRP) (refer to table 2.5 for dilutions). Subsequently, membranes were washed three times for 10 minutes at room temperature before chemiluminescence detecting using Pierce-ECL western blot substrate (Thermo Scientific) or Luminata Crescendo Western HRP substrate (EMD-Millipore). Refer to table 2.3 buffer composition.

2.2.3.3. Co-immunoprecipitation (Co-IP)

NR-SCs were seeded at $1.2x10^6$ onto 15cm dishes in duplicate. EtOH or TMX was added the following day and incubated for 36 hours before harvesting. Medium was aspirated and cells were once washed with 10mL PBS. Cells were scraped in approximately 360µL NP40 buffer, lysed on ice for 30 minutes and membranes were broken using a 23G needle. Debris was pelleted, by centrifuging at 750g for 5 min at 4ºC and the supernatant was collected into a fresh tube. Protein concentration was then quantified using BCA assay. All subsequent steps were performed at 4ºC. Approximately 300µg (1mg for mass spectrometry) protein was pre-cleared using 10µL of 50% protein G Beads (GE healthcare) (20µL for mass spectrometry analysis) by rotating for 15 minutes. Beads were collected and discarded by centrifuging at 750g for 1 minute. Pre-cleared supernatant was incubated with primary antibodies targeting N-cad (1ug for normal Co-IP or 2ug for mass spectrometry) for 2 hours by rotating. The antibody-protein complexes were pulled down by rotating the mixture with 20µL of 50% Protein G beads (40 µL for mass spectrometry) slurry for 1 hour. Beads were washed 4 times with 500µL NP40 buffer by rotating for 5 minutes and were collected by centrifuging at 750g for 1 minute and transferred to a clean tube. Finally, the beads were resuspended in 30 µL of 2x Leamlli buffer and boiled for 10 minutes at 95C. Refer to table 2.3 buffer composition.

2.2.4. ***Molecular biology***

2.2.4.1. RNA extraction and cDNA synthesis

RNA extraction was performed using Tri-Reagent according to manufactures protocol. RNA concentration was determined using Nanodrop and 500-1000ng of RNA was used to synthesize complementary DNA using Superscript II kit (Invitrogen). Briefly, RNA was incubated with 0.25µM random hexamers and 0.5µM dNTP's for 5 minutes at 65ºC. Subsequently, the mixture was quickly cooled on ice before further incubation with 40U RNaseOUT, 0.02M DTT and 1x first strand buffer for 2 min at 25ºC. Superscript II was added at 20U/µL for an initial incubation for 10 minutes at 25ºC, followed by incubating for 50 minutes at 42ºC and the enzyme inactivated by incubating for 20 minutes at 70ºC.

2.2.4.2. RT-qPCR

For RT-qPCR the MESA Blue qPCR MasterMix Plus kit was used (Eurogentec). For each gene MESA Blue was mixed with 100nM forward and reverse primers (refer to table 2.2), 23uL was pipetted in to a 96 well. 2µL of template cDNA was added to mix, ddH2O was used as a negative control.

Cycle parameters:

MeteorTaq activation	5 min 95 º	
Amplification (40 cycles):		
Denaturation	15 min	95 ºC
Annealing/extension	1 min	58 ºC
Dissociation curve	60-98ºC	

2.2.5. Cloning

2.2.5.1. Mutagenesis

NEB Q5 Site-Directed Mutagenesis Kit (NEB) was used according to manufacturers protocol to introduce silent mutations in the N-cad siRNA1 targeting sequence (see table 2.1) in the constructs expressing either N-cad full length, or the extracellular domain of N-cad, to disrupt the annealing of N-cad siRNA to the constructs. This was achieved by introducing four silent mutations in the four codons of the target sequence. Primers were designed using the primer design software NEBaseChanger and synthesised by sigma:

Forward primer	5'-CACGATAAACAATGAGACTGGGGACATC-3'
Reverse primer	5'-AACATATTGGGTGAAGGTGTGCTGGG-3'

Cycle parameters

Initial denaturation	98ºC	
Amplification step (25 cycles):		
Denaturation	98ºC	30 sec
Annealing	65ºC	10 sec
Extension	72ºC	2 min
Final extension	72ºC	2 min
Hold	4ºC	

2.2.5.2. Transformation

High efficiency 10-beta competent *E.coli* (NEB) were transformed using 5µL of PCR product, according to manufacturers protocol. Bacteria were then spread onto Agar plates consisting of Lysogeny-broth agar supplemented with 30µg/mL Kanamycin

(Gibco) and incubated overnight. Subsequently several colonies were picked and grown overnight for a DNA miniprep.

DNA was extracted from the bacteria using Zyppy prep (Zymo research) according to manufacturers protocol. DNA was then digested with restriction endonucleases XhoI (Promega) and NotI (Promega) in the appropriate buffer for 2 hours at 37°C to determine if the correct plasmid was obtained. The digested DNA, was resolved on 0.8% agarose gel. The correct plasmids were sequenced at Eurofins MWG operon to determine if mutations were inserted. Subsequently, bacteria transformed with plasmids positive for the mutations were grown up for a maxiprep, and DNA was extracted using Endo Free maxi prep Kit (Qiagen).

2.2.6. Mass spectrometry

Similar conditions described for the Co-IP were used to prepare samples for qualitative Mass Spec analysis. One sample per condition was used for the Co-IP, and 1mg protein as input was used. The proteins were eluted from the beads using Laemli buffer. The proteins were then separated on a gel, extracted from the gel, digested with trypsin and analysed using the LTQ Orbitrap Velos Pro Mass-spec systems (Performed by Proteomics Facility, University of Dundee). The obtained data was analysed using the Mascot search engine using the Uniprot DB with Rat as the taxonomic filter (Performed by Proteomics Facility, University of Dundee).

The obtained N-cad pull down lists were compared to the IgG control lists with http://www.cmbi.ru.nl/cdd/biovenn/ to filter for background proteins, which were removed. Alternatively, as p120-catenin and alpha-catenin were both identified in the IgG controls but were associated with a lower protein score than in the N-cad pull down lists. These scores range from 1-11,000, in which the higher the score the greater confidence that the protein ID is correct and a higher likelihood of a higher

abundance in the sample. The N-cad pull down lists were compared to the IgG controls, and all protein with a ≥2.5 fold increase in the N-cad pull down lists were included. Subsequently, the resulting protein lists from the control (EtOH) and TMX-treated condition were compared to each other to determine which proteins were overlapping and which were specifically identified in each condition and were functionally classified and mapped for protein ID using http://pantherdb.org.

2.2.7. Statistics

Statistics were performed using GraphPad (Prism) software. For all repulsion assays grouped analysis was performed using unmatched two-way ANOVA to examine the effect of two (or more) independent factors on the response of the protrusions. To correct for multiple comparisons, the Sidak method was used, assuming that the comparisons are independent. Every (selected) mean were compared to every other mean, or in the case of the repulsion assay in the p120 catenin knockdown every mean to the control mean.

For all velocity analysis and the directionality ratio analysis, where the distribution was gaussian, the T-test was performed. In the cases where there was no gaussion distribution, the Mann-Whitney test was performed to compare two unmatched groups.

For the cells rounding analysis the non-parametric Kruskal-Wallis test was performed to compare three unmatched groups.

For all western quantifications and qPCR analysis one-way ANOVA was performed, except for the qPCR analysis of the expression levels of the Eph receptors and ligands in the NR-SCs, where the T-Test was performed.

In all cases p *< 0.05, **<0.01, *** <0.001, n.s. = not significant.

Chapter Three: Results I

Characterising the role of N-cad in contact inhibition of locomotion

3.1. Chapter introduction

In the adult peripheral nervous system, Schwann cells make both homotypic interactions as well as heterotypic interactions with the axons. These interactions are disrupted upon injury of the nerve when the axons degenerate and Schwann cells dedifferentiate and express a new array of surface molecules through which they establish new interactions with the surrounding cells in the environment. We have previously shown that Schwann cells in the bridge make heterotypic interactions with fibroblasts, which induces the cell sorting of Schwann cells into cellular cords (Parrinello et al., 2010). *In vitro* analysis of Schwann cell sorting showed that these interactions are mediated by ephrin-B to EphB2 signalling between the fibroblasts and Schwann cells, which induces a switch in Schwann cell behaviour from repulsive to attractive. This attractive homotypic interaction between Schwann cells is mediated by a Sox-2 dependent re-localisation of N-cad to the cell-cell junctions. Though we observed that Schwann cells normally undergo CIL *in vitro,* the mechanism by which this is regulated is unknown. Moreover, CIL has been shown to be important for directional migration and collective migration *in vivo* (Carmona-Fontaine et al., 2008; Theveneau et al., 2010). This led to the hypothesis that CIL could be important for Schwann cells to migrate *in vivo* as a collective. Thus, it is important to understand the mechanism by which CIL between Schwann cells is regulated.

3.2. Characterisation of Schwann cell-Schwann cell recognition

To understand how Schwann cells recognise each other, Schwann cells were initially cultured *in vitro* and grown to confluence to observe their behaviour and to determine

if they form junctions. Schwann cells at low density are singular entities and distribute randomly but evenly in the dish. When grown to confluence, Schwann cells form a monolayer with wave-like patterns. Importantly, Schwann cells appear to form junctions between each other (Figure 3.1A). N-cad is an adhesion and cell-cell recognition molecule that can aggregate in adherence junctions (Brasch et al., 2012). Moreover, N-cad is expressed in Schwann cells during development and is re-expressed upon injury in dedifferentiated Schwann cells (Parrinello et al., 2010; Wanner et al., 2006; Wanner and Wood, 2002). To test if N-cad mediates cell-cell recognition between Schwann cells *in vitro*, cells were treated either with scrambled, or two previously published (Parrinello et al., 2010) independent small interfering RNA (siRNA) oligos targeting N-cad for 48 hours and the knockdown was assessed using western blot analysis (Figure 3.1B). The efficacy of the knockdown was extremely efficient in cells treated with siRNA1 while siRNA2 was slightly less efficient but N-cad was still barely detectable compared to control (Figure 3.1B left). The knockdown efficiency was quantified, and showed that N-cad was downregulated in N-cad knockdown cells by greater than 90% by siRNA1 and greater than 85% for siRNA2 (Figure 3.1B right). Moreover, whereas in scrambled-treated cells N-cad localised at the junctions between Schwann cells, in siRNA treated cells N-cad was not detectable at the junctions or within the cell body (Fig 3.1C, arrows). In addition, the actin cytoskeleton was reorganised to a more cortical distribution upon N-cad knockdown, consistent with N-cad regulating the actin cytoskeleton, which is a classical feature of N-cad junctions (Fig 3.1C).

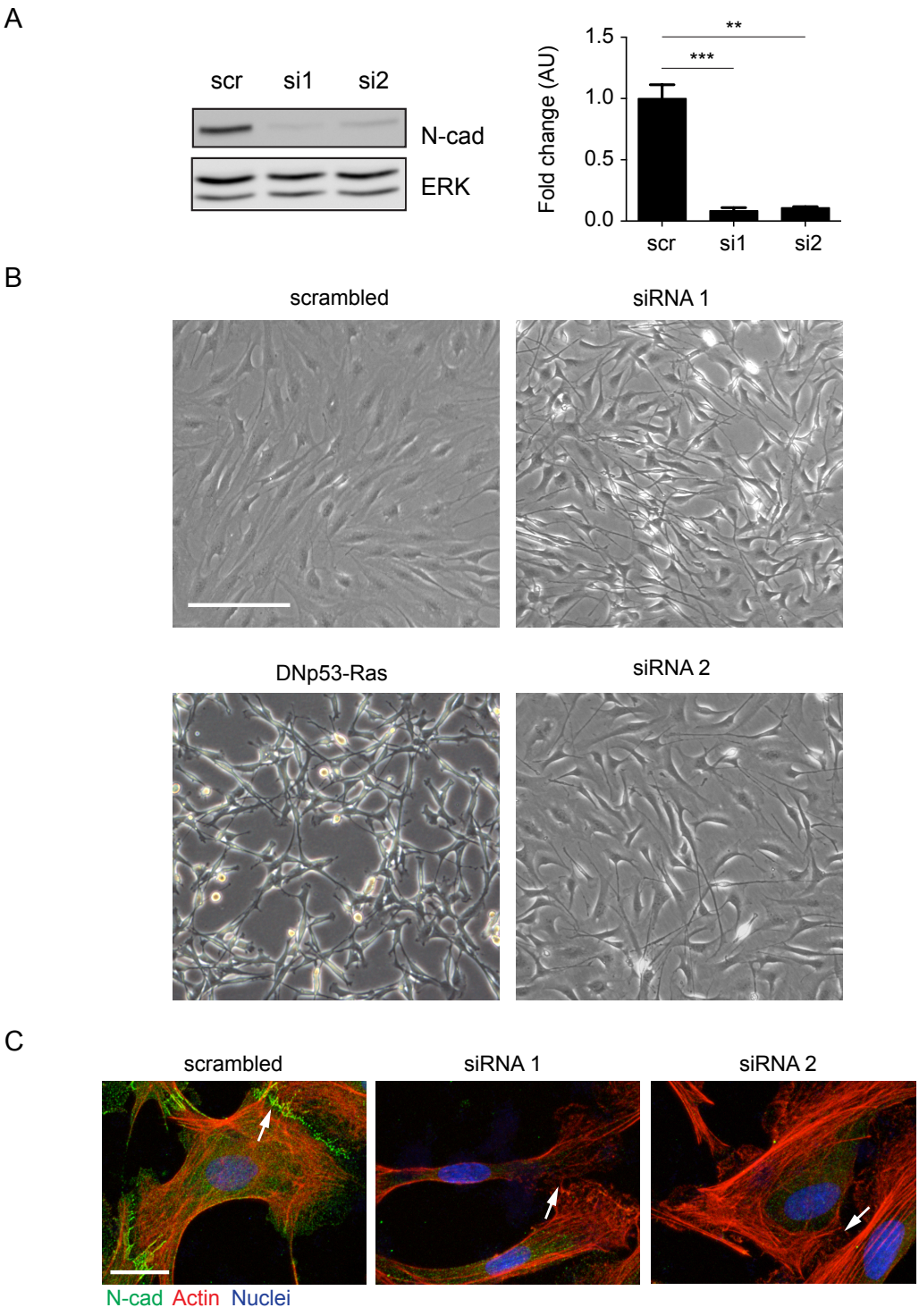

Figure 3.1. Loss of cell-cell recognition is mediated by a loss of N-cadherin. **(A)** Left: Representative western blot of 3 independent experiments showing N-cad protein levels in Schwann cells treated with either 2nM Scrambled (scr), siRNA1 (si1) or siRNA2 (si2) for 48 hours. Erk was used as a loading control. Right, quantification of N-cad protein expression levels normalised for Erk; Graph represents three experiments ± SEM. One-way ANOVA, Dunnett's multiple comparison test was performed. **(B)** Representative phase contrast images of scr, siRNA1, siRNA2 and Schwann cells expressing dominant-negative p53 (DNp53) and oncogenic Ras

(DNp53-Ras-SC). Schwann cells expressing oncogenic Ras were obtained through retroviral infection of a Ras expressing construct in a dnp53 background to prevent exit from the cell cycle (Lloyd et al., 1997). Scale bar 100µm. **(C)** Representative confocal images of scrambled, siRNA1 or siRNA2 treated cells at 36 hours, immunostained to detect N-cad (green), F-actin (red) and the nuclei (blue). White arrows indicate the cell contacts. Scale bar 20 µM.

Interestingly, the Schwann cells lost the ability to recognise each other to such an extent that they grew on top of each other, indicating a potential loss of cell-cell recognition (Figure 3.1A). The effect was stronger with siRNA1 compared to siRNA2, but this could be due to the differences in the knockdown efficiency. Interestingly, the loss of cell-cell recognition in N-cad knockdown cells was reminiscent how Schwann cells expressing oncogenic Ras grow on top of each other (Lloyd et al., 1997) (Figure 3.1A). Ras is a known oncogene whose aberrant activity can result in loss of contact inhibition of proliferation and contact inhibition of locomotion (Abercrombie, 1979; Ridley et al., 1988), indicating that the loss of cell-cell recognition in N-cad knockdown cells could also result in loss of CIL.

To determine the behaviour of N-cad knockdown cells in terms of CIL, an *in vitro* assay was established in which scrambled or siRNA treated Schwann cells were seeded at low density onto laminin-coated dishes and imaged for 24 hours using time-lapse microscopy. This allowed us to study the role of N-cad following single cell-cell interactions. Migrating control Schwann cells have broad lamellipodia in the direction of migration (Movie 3.1). Furthermore, Schwann cells are highly protrusive cells that randomly extend and retract many protrusions in different directions, even in the absence of other cells (Movie 3.1). Schwann cells can also be found interacting with each other through their protrusions. Importantly, Schwann cells retract their protrusions upon contact and this is usually followed by a change in their direction of migration, which are two features typical of CIL (Movie 3.1) (Abercrombie and Heaysman, 1954b). Thus, this indicated that Schwann cell-cell contact elicits a

repulsion response. Still images of a video show two migrating cells indicated by the blue and green dot colliding upon contact (arrowhead) followed by a change in the direction of migration (arrows) (Figure 3.2A). Interestingly, N-cad knockdown Schwann cells can be seen to have even more dynamic protrusions (Movie 3.1). However, strikingly, in contrast to scrambled treated cells, both cells treated with siRNA1 and siRNA2 failed to retract their protrusions upon contact and in many cases the cells migrated on top of the other cell (Movie3.1; Figure 3.2A arrow heads), suggesting that the normal repulsive behaviour is lost upon loss of N-cad.

To quantify this behaviour, we looked at single cell-cell interactions and determined three different responses of the protrusions after the initial contact was made: Repulsion, Schwann cells retract their protrusions and change the direction of migration; No-repulsion, Schwann cells interact for longer than 5 hours, do not change their direction of migration, or do not migrate away following contact; Invasion, Schwann cells continue to migrate with their protrusions or cell bodies invading over each other. Using these parameters, as expected, we found that almost all scrambled-treated Schwann cells repulsed each other upon contact, while only a small proportion of the cells were invasive and almost no no-repulsion could be seen (Figure 3.2B; Movie 3.1). This is consistent with previously published results (Parrinello et al., 2010). In contrast, when N-cad was downregulated using either treated siRNA1 or siRNA2 there was a marked reduction in repulsion events, while there was a striking increase in invasion events, indicating that N-cad is required for CIL. Importantly, there was hardly any change seen in no-repulsion, suggesting that the repulsion signal inhibits forward migration. That the repulsion signal was not completely lost can partly be explained by the highly dynamic protrusions that are randomly extended and retracted by Schwann cells, even when they are not interacting with other cells, which leads to an overestimation of the repulsion events

(Figure 3.2A). Together, these results suggest that N-cad regulates CIL between Schwann cells by both mediating a repulsion response and blocking forward migration, which is consistent with confluent knockdown cells that are on top of each other as shown in earlier figure. These findings have parallels with previous studies showing N-cad is required for CIL in neural crest cells by inhibiting protrusion formation at sites of cell-cell contact (Tanaka et al., 2012; Theveneau et al., 2010).

Contact dependent repulsion during CIL has been shown to be important to drive outward migration of fibroblasts, PC3 cells and neural crest cells during development (Batson et al., 2013; Carmona-Fontaine et al., 2008; Fritz et al., 2015; Theveneau et al., 2010). Thus, indicating that the dispersal of cells can be an indication of CIL. To test if N-cad can block the outward migration of Schwann cells, a scratch assay or wound healing assay was performed, by inducing a gap in confluent monolayers of cells of scrambled or N-cad siRNA1-treated cells with a tip and their behaviour was observed using time-lapse microscopy (Movie 3.2; and Figure 3.3). Scrambled-treated Schwann cells migrated efficiently into the gap when a scratch was induced, with only a few migrating away from the gap or to the side (Movie 3.2; Figure 3.3). This suggests Schwann cells collectively migrate forward into the gap. Moreover, when the cells collided upon closure of the gap, scrambled treated cells appeared to be repulsed in that they changed direction of migration. In contrast, Schwann cells treated with siRNA1 migrated in all directions in a more random fashion and many more cells migrated backwards and sideways compared to controls (Movie 3.2; Figure 3.3). Importantly, N-cad knockdown Schwann cells migrating into the gap did not migrate as far as control cells, which can be seen in the still images of the movie (Figure 3.3), suggesting migration is not as efficient and as directional due to the loss of the repulsive signal.

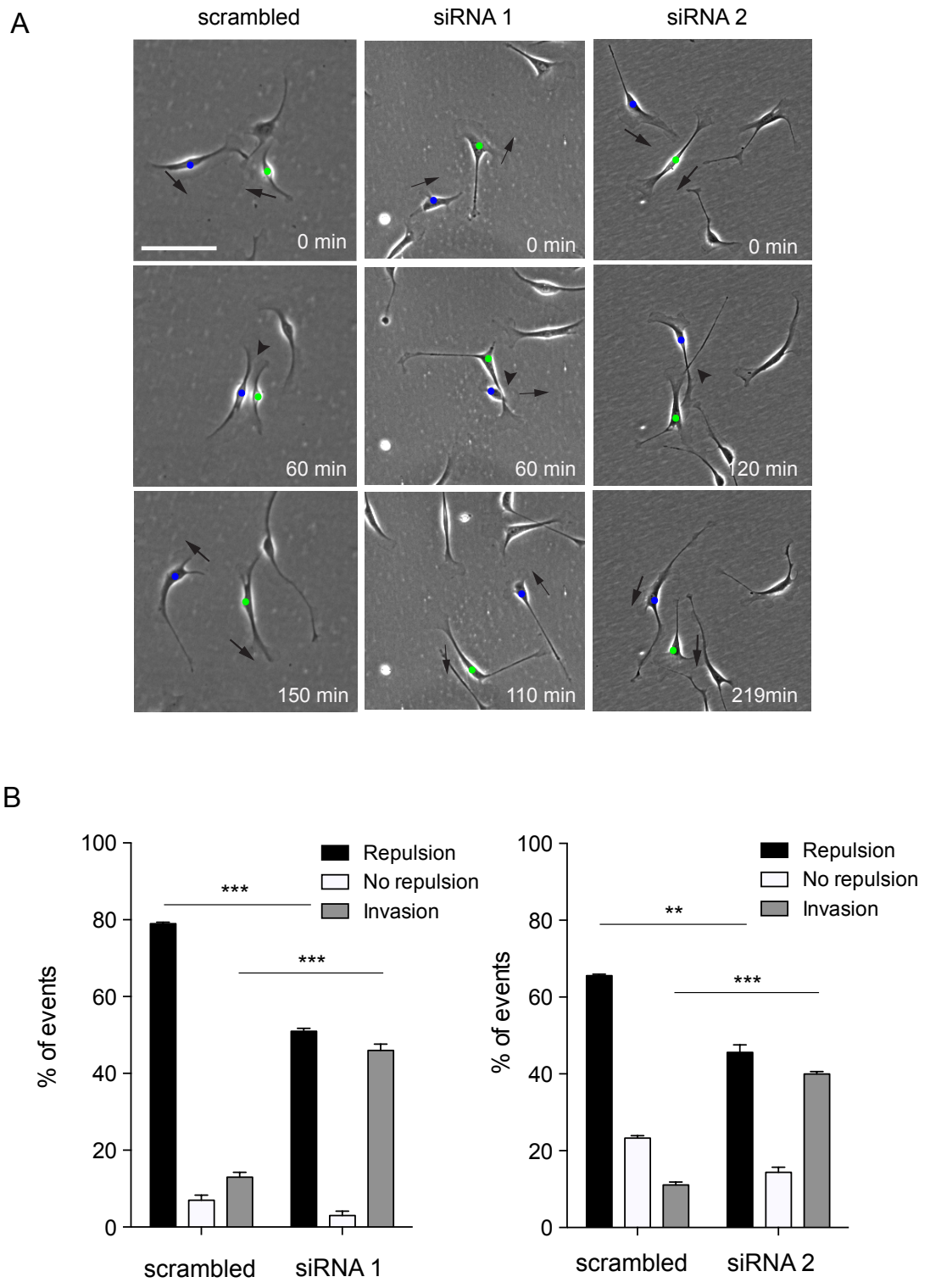

Figure 3.2. CIL is dependent on N-cad.
(A) Representative time-lapse images of a CIL assay, showing scrambled or N-cad knockdown cells, treated with siRNA1 or siRNA2, that are repulsed or invading respectively (arrow heads). The blue and green dots indicate the two interacting cells. Arrows indicate the direction of migration. Scale bar 100µm. **(B)** Quantification of A, bar represents the mean of three independent experiments ± SEM in which 30 cells per experiment were analysed. Related to movie 3.1.

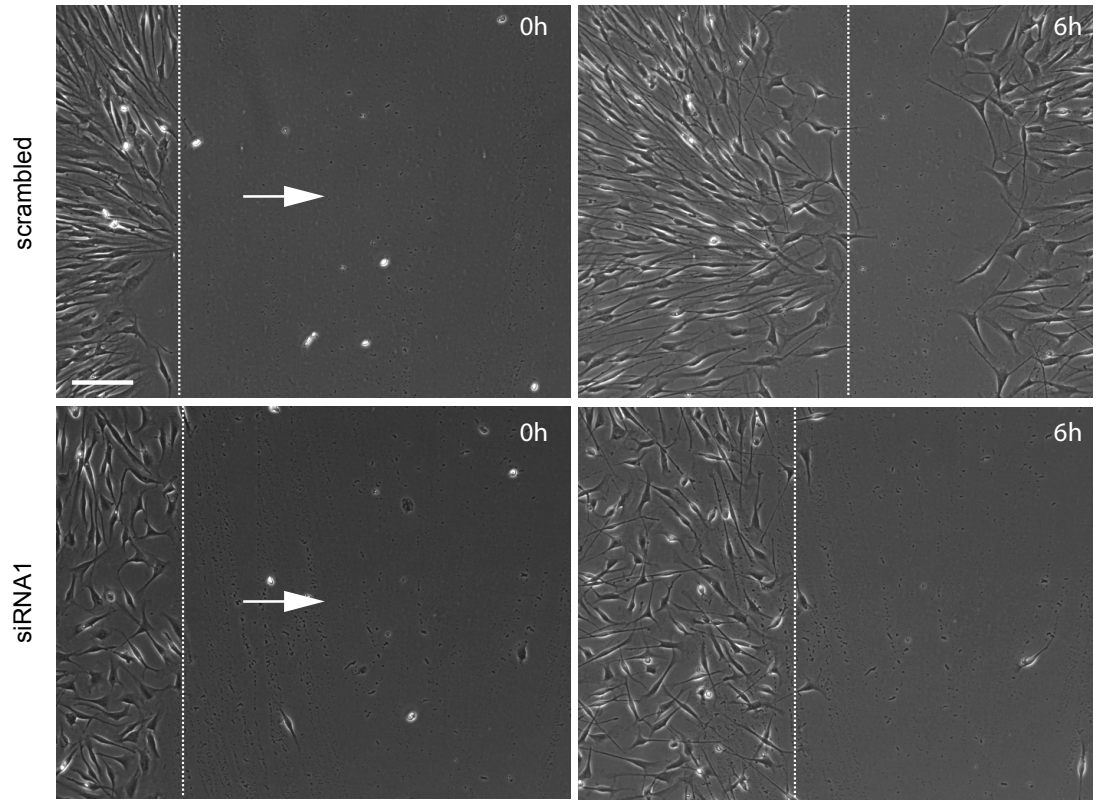

Figure 3.3. Outward migration is dependent on N-cad.
Representative still images from a time-lapse of a scratch assay of scrambled treated Schwann cells or N-cad knockdown Schwann cells treated with siRNA1. Dashed line indicates the leading edge of the migrating cells. Arrow indicates direction of the gap that was introduced with a pipette. Scale bar 100µm. Related to movie 3.2.

To quantify this behaviour, cells were tracked using the nucleus for 12 hours and the directionality ratio index (which measures the shortest distance between start and end point divided by the length of the trajectory) was calculated. A representative graph of the tracks of scrambled cells from a single experiment shows, that most of the tracks were orientated towards the gap and that the direction of the tracks does not appear to change very often, though a few cells can be found migrating backwards towards the end of the track, which is possibly due to repulsion upon collision with other cells upon closing the gap (Figure 3.4). This suggested that scrambled-treated cells migrate towards the gap without changing their direction of

migration. In contrast, there was a striking difference in the tracks of the N-cad knockdown cells, which were orientated in multiple directions and the tracks appeared to change directions more often, suggesting N-cad knockdown cells have lost their directionality (Figure 3.4A). To quantify this, the directionality ratio was calculated from the tracks of three experiments. A high directionality equals 1 and a low directionality equals 0. The vast majority of the scrambled-treated cells showed a high directionality ratio, with only a few cells showing a low directionality with an average of ±0.5, suggesting scrambled-treated cells migrate in a directional manner towards the gap (Figure 3.4B). In contrast, the directionality ratio of N-cad knockdown cells was completely shifted to a low directionality ratio, suggesting that N-cad and cell-cell repulsive signals are required for directional migration towards the gap (Figure 3.4B).

Moreover, the loss of directionality following N-cad knockdown was not due to a decreased velocity, as N-cad knockdown cells appeared to migrate faster than scrambled-treated control cells (Movie 3.2). To quantify this, the velocity was calculated from the tracks, which showed that there was a marked increase in velocity following N-cad knockdown (Figure 3.4C). This suggests that the loss of directionality is not due to loss of migration speed. Moreover, similar to N-cad knockdown cells at low density, the N-cad knockdown cells in the scratch assay appeared to migrate on top of each other, indicating that the loss of directionally could be due to loss of CIL (Figure 3.2A, and 3.3; Movie 3.2).

In addition, the loss of cell recognition is consistent with unpublished work performed by a former PhD student, who showed that N-cad knockdown cells maintained a high level of proliferation at high density (Wingfield-Digby et. al. unpublished thesis). Patrick Wingfield-Digby showed, that in N-cad knockdown cells there was a two-fold increase of proliferation at high-density compared to scrambled-

control, while in low-density, N-cad knockdown had no effect on proliferation. Thus suggesting an additional role for N-cad in contact-dependent inhibition of Schwann cell proliferation, which is consistent with previous reports in which E-cad is required for CIP in epithelial cells (Perrais et al., 2007). Moreover, this suggests that N-cad links CIL and CIP at high density, but that additional signals are required to regulate CIP.

Taken together, this data strongly indicate that N-cad is required for cell-cell recognition between Schwann cells and for homotypic CIL.

3.3. CIL is independent of trans-homodimerisation

Next we determined how N-cad regulates CIL. N-cad can transmit adhesive forces between neighbouring cells by forming homodimers through interactions in *trans* (Brasch et al., 2012). These homotypic junctions are required for collective migration in several cell types including neural crest cells, astrocytes and primordium on the zebra fish lateral line and are required for Schwann cell sorting (Parrinello et al., 2010; Peglion et al., 2014; Theveneau et al., 2010; Theveneau and Mayor, 2012a). To understand if CIL requires *trans*-interactions between N-cad molecules, CIL between scrambled-treated cells and N-cad knockdown cells were analysed. To do this, scrambled-treated cells were mixed with siRNA1 treated cells and imaged using time-lapse microscopy to analyse their response to each other following contact. To distinguish the different cell populations scrambled and N-cad siRNA1-treated cells were labelled with cytotracker red fluorescence or green fluorescence respectively. First, as a control, the response between two scrambled-treated cells was analysed (Movie 3.3; Figure 3.5). As expected, the two red-labelled scrambled-treated cells (eg. S1 and eg. S2) repulsed each other upon contact (Movie 3.3; Figure 3.5). Next, in the same movie, the response between two green-labelled N-cad

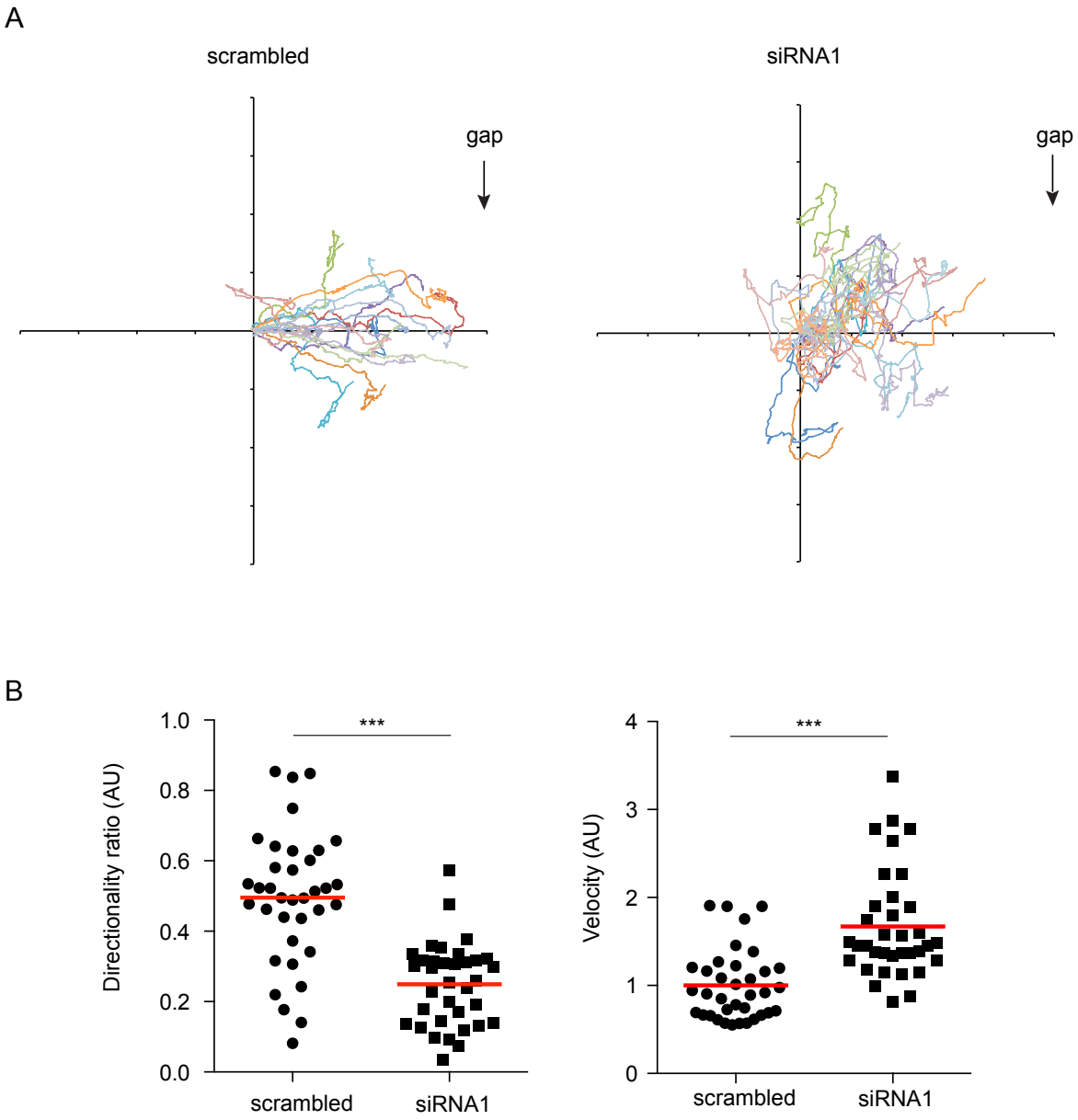

Figure 3.4. N-cad is required for Schwan cell directionality.
(A) A representative graph of three independent experiments showing the trajectories of scrambled treated cells or N-cad knockdown cells treated with siRNA1. The arrow indicates where the gap was introduced. (N=30). **(B)** Quantification of the directionality ratio from the tracks in (A). Mean is indicated by the red line. A total of 30 cells from three different experiments were quantified. Statistics: T-Test. **(C)** Quantification of the cell velocity using the tracks in (A). Mean is indicated by the red line. A total of 30 cells from three different experiments were quantified. Statistics: Mann-Whitney test.

knockdown cells (N1 and N2) was analysed, which as expected, invaded each other (Movie 3.3; Figure 3.5). Subsequently, the response of a green-labelled knockdown cell (eg. S2) was analysed. Surprisingly, while the N-cad knockdown cell (eg. N2) invaded another N-cad knockdown cell (N1), it was repulsed upon subsequent contact with a scrambled-treated cell (S2). This suggests that N-cad is required to present a repulsion signal and induce repulsion, but is not required for the cell to be repulsed (Movie 3.3; Figure 3.5). In contrast, when analysing the response of the scrambled- treated cells (eg. S2) upon contact with an N-cad knockdown cells (eg. N2), in the many of the cases the scrambled-treated cells were not repulsed (Movie 3.3; Figure 3.5). This confirms that N-cad is required to present a repulsion signal and induce repulsion, but not to be repulsed (Movie 3.3; Figure 3.5).

These different behaviours between scrambled-treated cells and N-cad knockdown cells were quantified as shown in the graph in Figure 3.6A. As expected, the vast majority of the scrambled-treated cells repulsed each other upon contact, while only a few no-repulsion or invasion events were seen (Figure 3.6A). In the N-cad knockdown cells there was a marked increase in invasion and a decrease in repulsion events, while there was no change in no-repulsion events (Figure 3.6A). Interestingly, the response of N-cad knockdown cells upon contact with scrambled-treated cells was similar to how the scrambled control behaved; in that there were high levels of repulsion and low levels of invasion. This shows that N-cad knockdown cells were still repulsed by scrambled cells meaning a Schwann cell does not need to express N-cad to be repulsed (Figure 3.6A). In contrast, there was a distinct phenotype in the scrambled cells contacting the N-cad knockdown cells, in that the scrambled cells were no longer efficiently repulsed by N-cad knockdown cells and did not migrate away following contact, but they also did not invade them as the N-cad

knockdown cell had migrated away (Figure 3.5B). This suggests N-cad is required to present a repulsion signal.

Taken together, this indicates that N-cad is required to provide a repulsion signal to the other cell, but it is not required for the cell to be repulsed in a N-cad dependent manner (Figure 3.6B). Moreover, it suggests that N-cad mediates CIL independent of *trans*-homodimerisation, through which it is known to classically signal.

3.4. Assessing the mechanism by which N-cad regulates CIL

Previous work has indicated that CIL inhibits the formation of protrusions at the site of cell-cell contact, which is accomplished by locally rearranging the actin cytoskeleton through the cytoskeletal regulators Cdc42, RhoA and Rac-1 (Astin et al., 2010; Carmona-Fontaine et al., 2008; Scarpa et al., 2015; Theveneau et al., 2010). N-cad has been shown to inhibit protrusion formation at the site of cell-cell contact by locally inhibiting Rac-1 and redistributing Rac-1 activity to the free edge of the cell (Theveneau et al., 2010). Moreover, recent work suggests that E-cad represses CIL by distributing Rac-1 activity in a p120-catenin dependent manner (Scarpa et al., 2015). Other work indicates that N-cad mediates heterotypic CIL between glia and the glioblastoma cell line U87MG through α-catenin, which binds to nm23-H1, which in turn interacts and inhibits the GEF Tiam1 and therefore inactivates Rac-1. Thus, this indicates that N-cad could regulate CIL through its intracellular binding partners α-catenin and p120-catenin. However, our data shows that the repulsion signal is independent of N-cad *trans*-homodimerisation and the repulsed cell does not require N-cad. Thus, this might suggest that the repulsion signal would be independent of the adherence junction complex including the components α-catenin, β-catenin and p120-catenin. To test this, a series of knockdowns were performed.

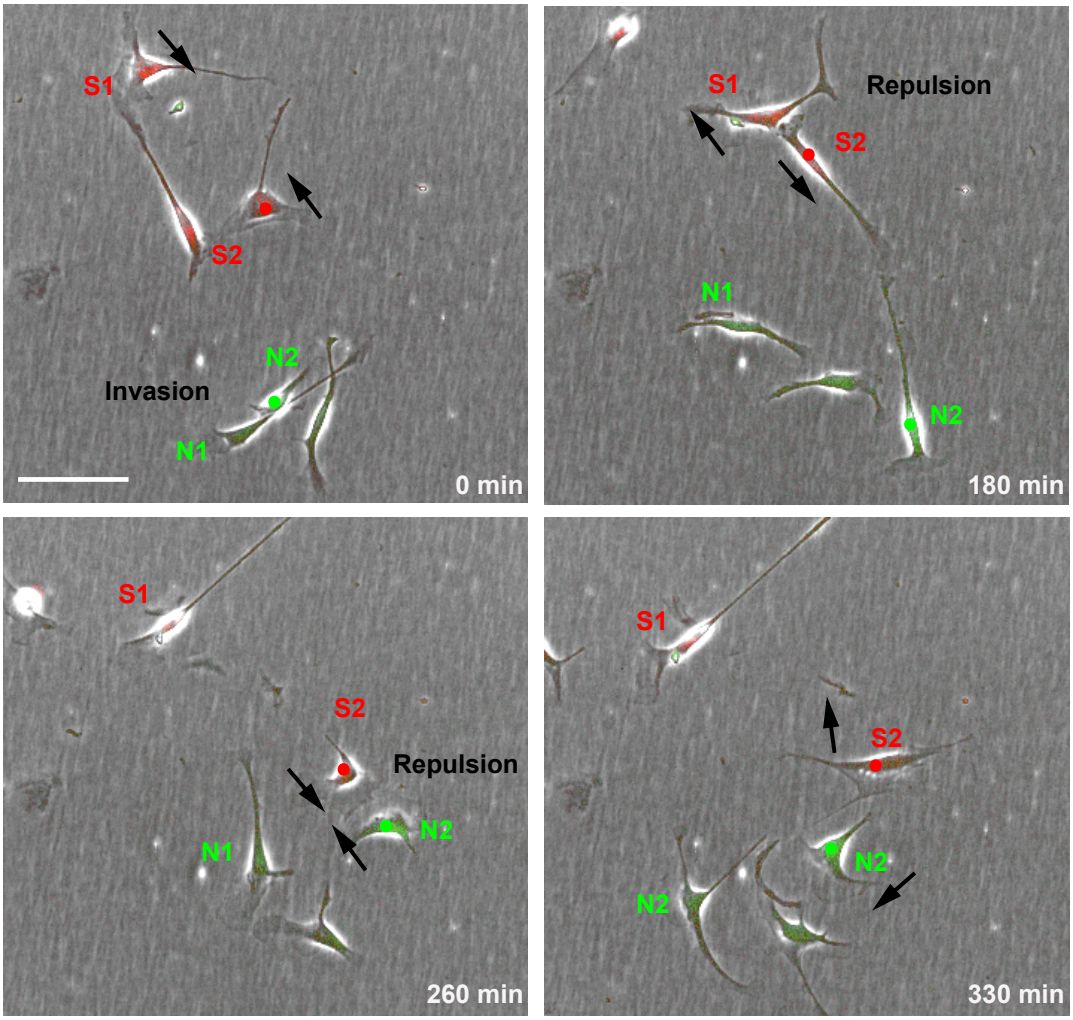

Figure 3.5. N-cad mediates CIL independent of *trans*-homodimerisation.
(A) Representative still images from a time-lapse of a CIL assay in which red fluorescence-labelled scrambled-treated cells (S1 and S2) were mixed with green fluorescence-labelled N-cad knockdown cells (N1 and N2). Cells of interest are indicated with a red or green dot for scrambled and N-cad knockdown cells respectively. Arrows indicate direction of migration. Invasion and repulsion events are indicated. Scale bar 100µm. Related to movie 3.3.

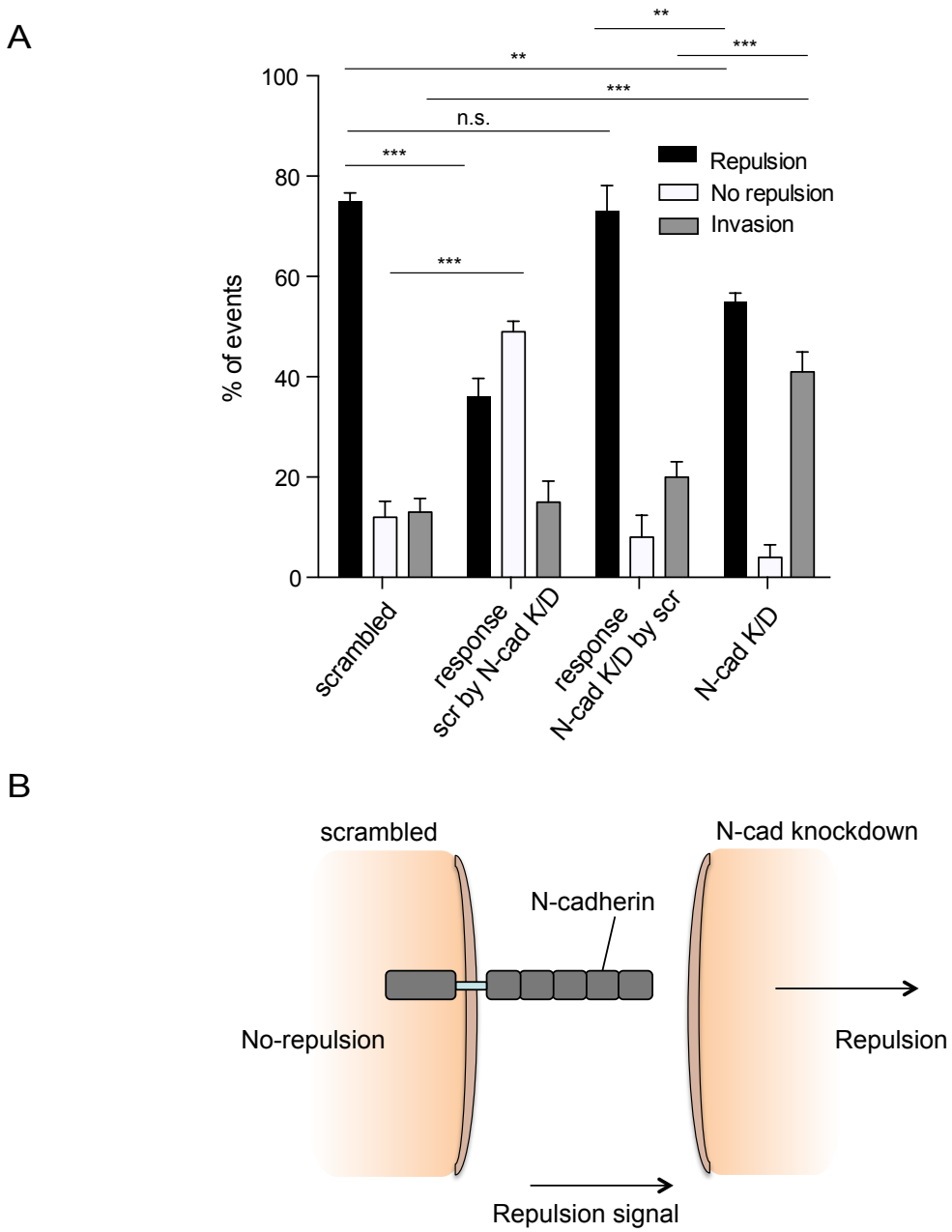

Figure 3.6. N-cad mediates CIL independent of *trans*-homodimerisation.
(A) Quantification of Figure 3.5 in which repulsion, no repulsion and invasion was measured between scrambled-treated cells, N-cad knockdown cells or the response of scrambled-treated cell by N-cad knockdown cells and vice versa. Graph represents mean of three independent experiments in which 30 cells per condition were quantified ± SEM. (B) Schematic overview of how N-cad mediates CIL between Schwann cells; while N-cad is required to induce a repulsion response it is not required for the cell to be repulsed. Related to movie 3.3.

In collaboration with an undergraduate student, Mariana Campana, siRNA oligos for α-catenin were tested for knockdown efficiency. α-catenin binds to β-catenin and is the physical link between the actin cytoskeleton and N-cad. There are three α-catenin genes: αE-catenin, αN-catenin and αT-catenin which are primarily expressed in epithelial, neuronal and heart tissue respectively (Kobielak and Fuchs, 2004). N-cad can interact with both αE-catenin and αN-catenin (Kobielak and Fuchs, 2004) and in the adult sciatic nerve E-cad interacts with αE-catenin in myelinating Schwann cells (Murata et al., 2006). To test which α-catenin gene is expressed by Schwann cells in culture, αE-catenin levels were determined in the different tissues and in Schwann cells using RT-qPCR and normalised to the heart (which expresses αT-catenin and αE-catenin) for αE-catenin (Figure 3.7A) or the cortex (which mainly expresses αN-catenin) for αN-catenin (Figure 3.7B). As expected, αE-catenin is expressed by the heart and the sciatic nerve, which is consistent with previous reports (Kobielak and Fuchs, 2004; Murata et al., 2006). Importantly, in Schwann cells in culture there was a strong expression of αE-catenin compared to the heart and sciatic nerve, suggesting dedifferentiated Schwann cells express high levels of αE-catenin (Figure 3.7A). In contrast, while αN-catenin could be detected in the cortex, it was not detected in sciatic nerve or Schwann cells in culture, suggesting Schwann cells do not express αN-catenin (Figure 3.7B). Thus Schwann cells in culture express high levels of αE-catenin, while αN-catenin cannot be detected, indicating that Schwann cells in culture express αE-catenin.

Subsequently, αE-catenin was downregulated using two independent siRNA oligos for 36 hours and protein expression was analysed using western blot analysis, which was probed with an antibody recognising αE-catenin or ERK as a loading control. The knockdown was efficient in both Schwann cells treated with siRNA1 or

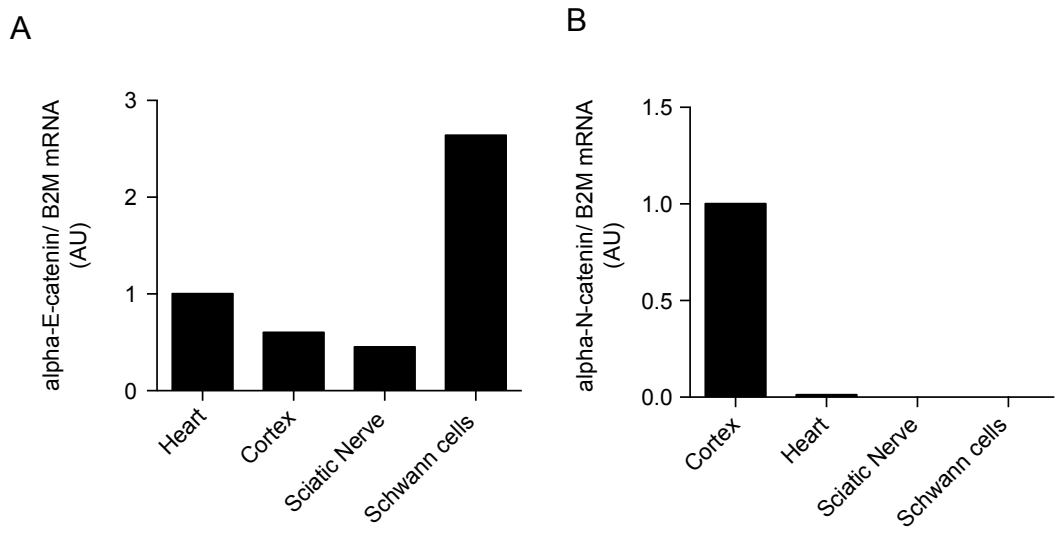

Figure 3.7. Schwann cells express αE-catenin.
(A) Rt-qPCR analysis of the mRNA expression levels of αE-catenin Schwann cells, heart, cortex and sciatic nerve, in which the expression was compared to expression levels in the heart. **(B)** Analysis of mRNA expression levels of αN-catenin in Schwann cells, heart, cortex and sciatic nerve, in which the expression was compared to expression levels in the heart. Shown are representative graphs of two independent experiments.

siRNA2 (Figure 3.8A). However, treating the cells using both siRNA1 and siRNA2 was extremely efficient, as following knockdown less than 10% of the protein could be detected (Figure 3.8A). Therefore, for the following experiments the combination of siRNA1 and siRNA2 was used. Importantly, using immunostaining, αE-catenin could be detected at the junctions between the scrambled treated cells that are in contact with each other, though some perinuclear αE-catenin expression could also be detected (Figure 3.8B). However, Schwann cells treated with both siRNA1 and siRNA2 no longer appeared to interact with each other and αE-catenin was not detectable at the cell junctions (Figure 3.8B, arrow). In addition, loss of αE-catenin resulted in more cortical F-actin and stress fibres, suggesting αE-catenin is required for modulating the actin cytoskeleton (Figure 3.8B).

We subsequently determined whether αE-catenin is important for Schwann cell-Schwann cell recognition. Intriguingly, although the cells appeared to be unable

to form stable junctions, αE-catenin knockdown Schwann cells were still repulsed by each other and were indistinguishable from the controls. Thus indicating that αE-catenin is not required for CIL (Figure 3.9A; Movie 3.4). This was quantified, as shown in the graph in Figure 3.9B, which showed that there was no significant difference in repulsion, no-repulsion and invasion between Schwann cells treated with scrambled or siRNA1 and siRNA2. Thus, αE-catenin is not required for CIL, which is consistent with the finding that the repulsion signal is independent of N-cad *trans*-homodimerisation.

Though knockdown of αE-catenin had no effect on CIL between Schwann cells, it appeared that the αE-catenin knockdown cells were migrating faster when seeded at low density. To quantify this, the cells were tracked using the nucleus as described previously. Scrambled-treated cells behaved normally and migrated as expected (Figure 3.9). In contrast, there was an increase in migration speed in αE-catenin knockdown cells, suggesting that αE-catenin knockdown cells migrate faster. We have shown that CIL between Schwann cells is independent of αE-catenin and independent of *trans*-homodimerisation, suggesting N-cad mediates CIL through mechanisms independent of its classical function. To test if αE-catenin affects N-cad localisation at the membrane, scrambled-treated cells and αE-catenin were fixed and immunolabled for N-cad, αE-catenin and stained with phalloidin to visualise the actin cytoskeleton. As expected in control cells, junctions were observed between the cells (arrowheads) in which N-cad and αE-catenin co-localise, indicating that N-cad and αE-catenin are interacting (Figure 3.10A). In contrast, in αE-catenin knockdown cells, αE-catenin appears to be completely absent from cell contacts, while N-cad is still present at the contact points (arrowheads), suggesting that N-cad is still at the cell surface and can homodimerise (Figure 3.10A). Moreover, Western blot analysis showed that N-cad expression levels were not changed in Schwann cells following

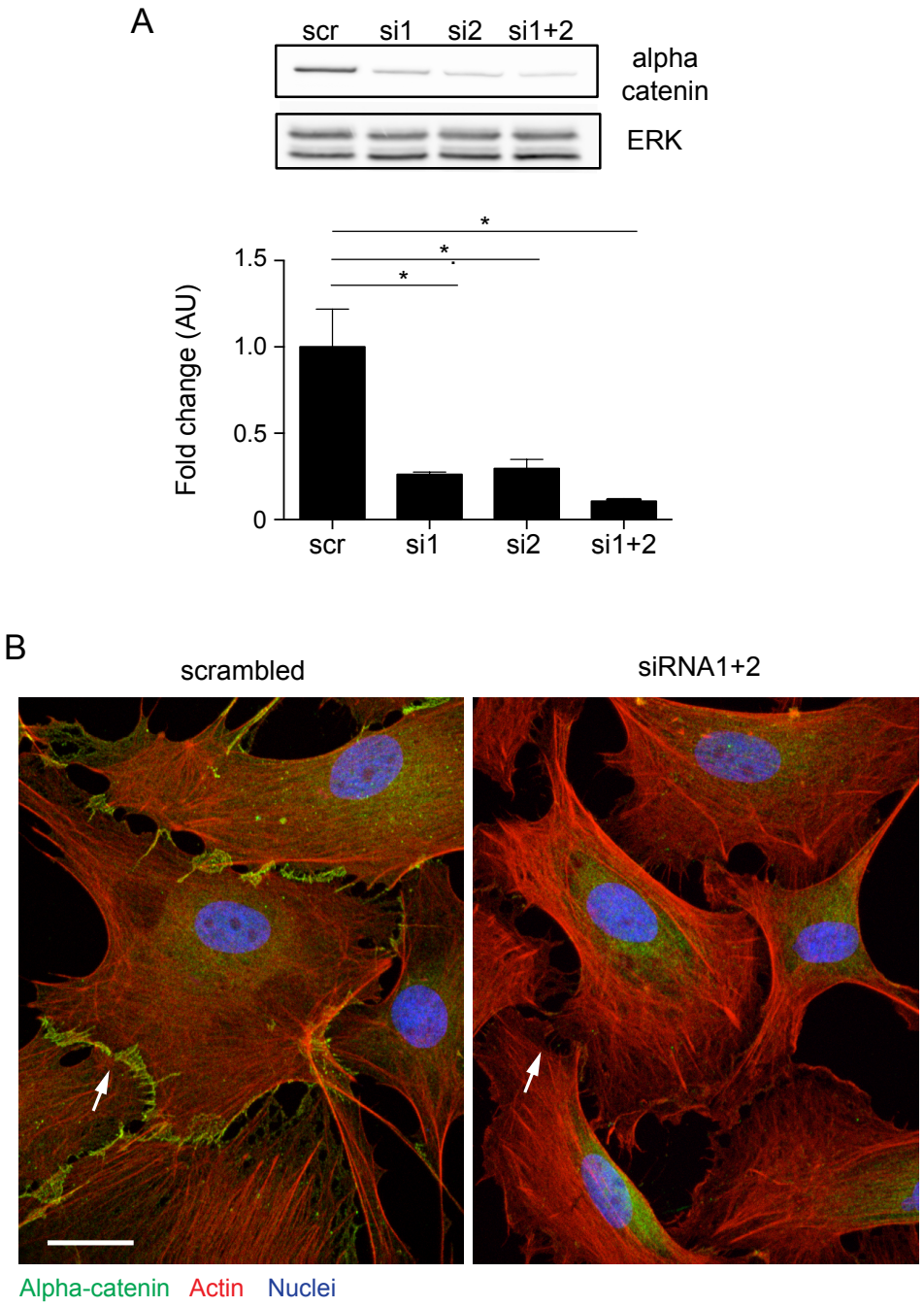

Figure 3.8. αE-catenin knockdown.
(A) Upper panel: Representative western blot showing the efficiency of αE-catenin knockdown with two independent siRNAs compared to scrambled control at 36hours. ERK was used a loading control. Lower panel: Quantification of αE-catenin expression levels corrected for ERK levels. Bars represent mean of three independent experiments ± SEM. One-way ANOVA, Dunnett's multiple comparison test. **(B)** Representative confocal images of Schwann cells treated with scrambled or siRNA1+2 for 36 hours, immunostained for αE-catenin (green), F-actin (red) and the nuclei (blue). Cell-contact points are indicated by white arrows that are positive for αE-catenin in scrambled treated cells but no αE-catenin can be detected in siRNA1 + 2 treated cells.

knockdown of αE-catenin, suggesting αE-catenin does not affect N-cad expression levels (Figure 3.10B). Moreover, while in control cells the actin appears to go into the junctions, the actin cytoskeleton appears to be no longer connected to the junctions in the majority of the αE-catenin knockdown cells (arrowheads). Thus, this data indicates that αE-catenin is required to form stable junctions but is not required for CIL.

We next determined if N-cad mediated CIL requires p120-catenin. p120-catenin can mediate cytoskeletal changes by regulating Rho-GTPases (Peglion and Etienne-Manneville, 2013). Moreover, inhibition of protrusion formation at the site of cell-cell contact of non-migratory neural crest by E-cad is dependent on p120-catenin (Scarpa et al., 2015). To understand if p120-catenin is regulating CIL in our system, we performed a knockdown experiment. Initially, the knockdown for p120-catenin was set up using two independent siRNA oligos and a good knockdown of protein levels was detected at 72 and 96 hours using western blot analysis, indicating p120-catenin has a slower turnover than αE-catenin (Figure 3.11A). The protein levels at 96 hours were quantified using densitometry. The knockdown efficiency was reasonable in Schwann cells treated with siRNA1 (>70%), while the knockdown in cells treated with siRNA2 was extremely efficient (>85%) (Figure 3.11B). Immunofluorescence of p120-catenin showed that in scrambled-treated cells, p120-catenin was at the cell-cell junctions and in the cytoplasm (Figure 3.11C). Strikingly, in p120-catenin knockdown cells, p120-catenin was not detectable in either the cytoplasm nor the at the cell-cell contact points (Figure 3.11C, arrows). Moreover, while scrambled-treated cells were densely packed and had many junctions, gaps could be observed between the p120-catenin knockdown cells, suggesting the cells interact in a different way than the scrambled-treated cells. There was also a striking change in

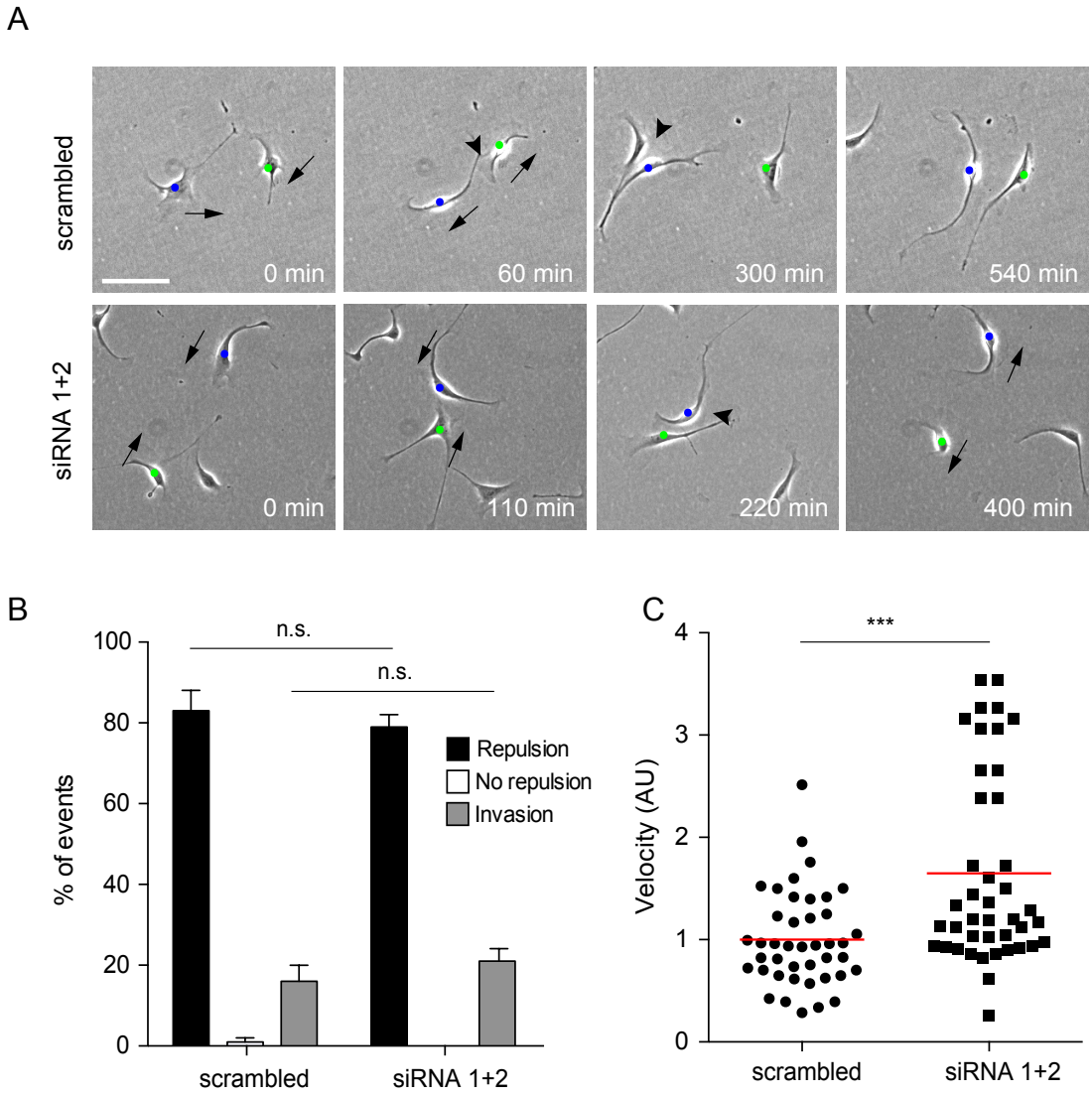

Figure 3.9. CIL is mediated through αE-catenin independent mechanisms.
(A) Representative still images from time-lapse microscopy of a CIL assay in which Schwann cells were treated with either 5nM scrambled siRNA or αE-catenin siRNA1+2 for 36 hours before imaging. Repulsion events are indicated by black arrow heads, black arrows indicate the direction of migration. Cells of interest that are undergoing a repulsion event are indicated by green and blue dots. Scale bar 100µm. **(B)** Quantification of A, bar represents mean of three experiments ± SEM. 50 cells per condition were quantified. **(C)** Graph showing the velocity of the tracks form scrambled treated cells (dots) or siRNA1+2 treated cells (squares). For each condition 30 cells per experiment were tracked for 12 hours. The Red lines represent the mean. T-test. Related to movie 3.4.

A

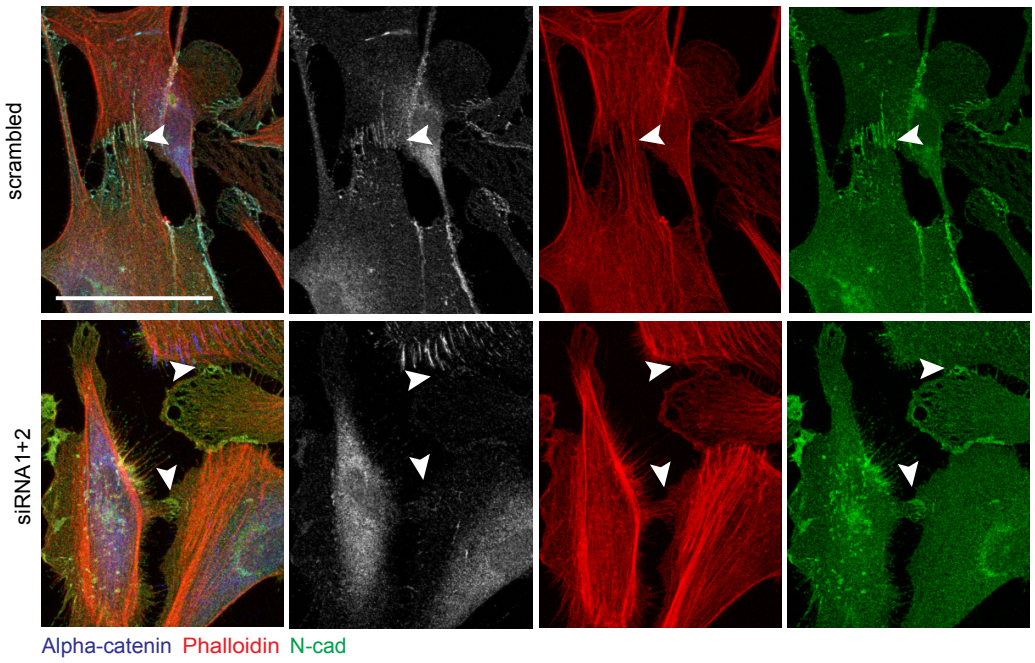

B

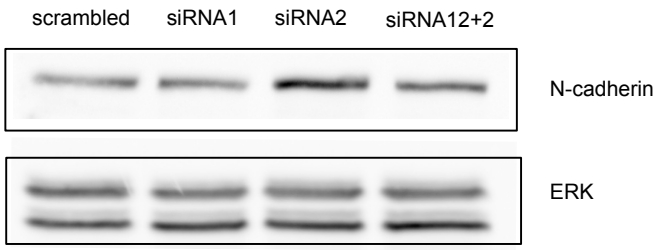

Figure 3.10. αE-catenin is required to form stable junctions.
(A) Representative confocal images of scrambled-treated and αE-catenin knockdown cells at 36 hours, immunostained to detect α-catenin (grey), N-cad (green) and co-stained for f-actin (red). Note N-cad is still localised at the junctions following αE-catenin knockdown (arrows). Scale bar 50μm. **(B)** Representative Western blot showing no change in expression of N-cad protein following αE-catenin knockdown at 36 hours. ERK was used a loading control.

the actin cytoskeleton, which appeared more cortical following p120-catenin knockdown, consistent with p120-catenin regulating the actin cytoskeleton (Figure 3.11B).

To determine the role of p120-catenin in CIL, scrambled-treated and p120-catenin knockdown cells were seeded at 72 hours onto laminin coated dishes at low density and imaged, using time-lapse microscopy. Scrambled-treated cells behaved normally and were repulsed (arrowheads) upon contact, though some events of no-repulsion were observed (Figure 3.12A). P120-catenin knockdown cells had broader lamellipodium than control cells (Figure 3.12A; Movie 3.5). Interestingly, siRNA1 treated Schwann cells behaved similarly to control cells and were also repulsed (arrowheads) upon contact (Movie 3.5; Figure 3.12A and quantified in Figure 3.12B). In contrast, in cells treated with siRNA2 repulsion events were less frequent and invasion events were slightly more frequent, suggesting a possible role for p120-catenin in CIL (Movie 3.5; Figure 3.12A and quantified in figure 3.12B). Interestingly, this difference in the effect on repulsion and invasion correlated to the differences in p120-catenin knockdown.

To further analyse this effect, the migration speed was analysed in the different conditions. Scrambled-treated cells migrated as expected, and there was no difference in migration speed in the cells treated with siRNA1 (Figure 3.12C). Interestingly, while knockdown of p120-catenin using siRNA2 had a small effect on CIL, it had no effect on the velocity of the cells, suggesting that the difference in CIL between the two siRNA's was not due to a difference in migration speed (Figure 3.12C).

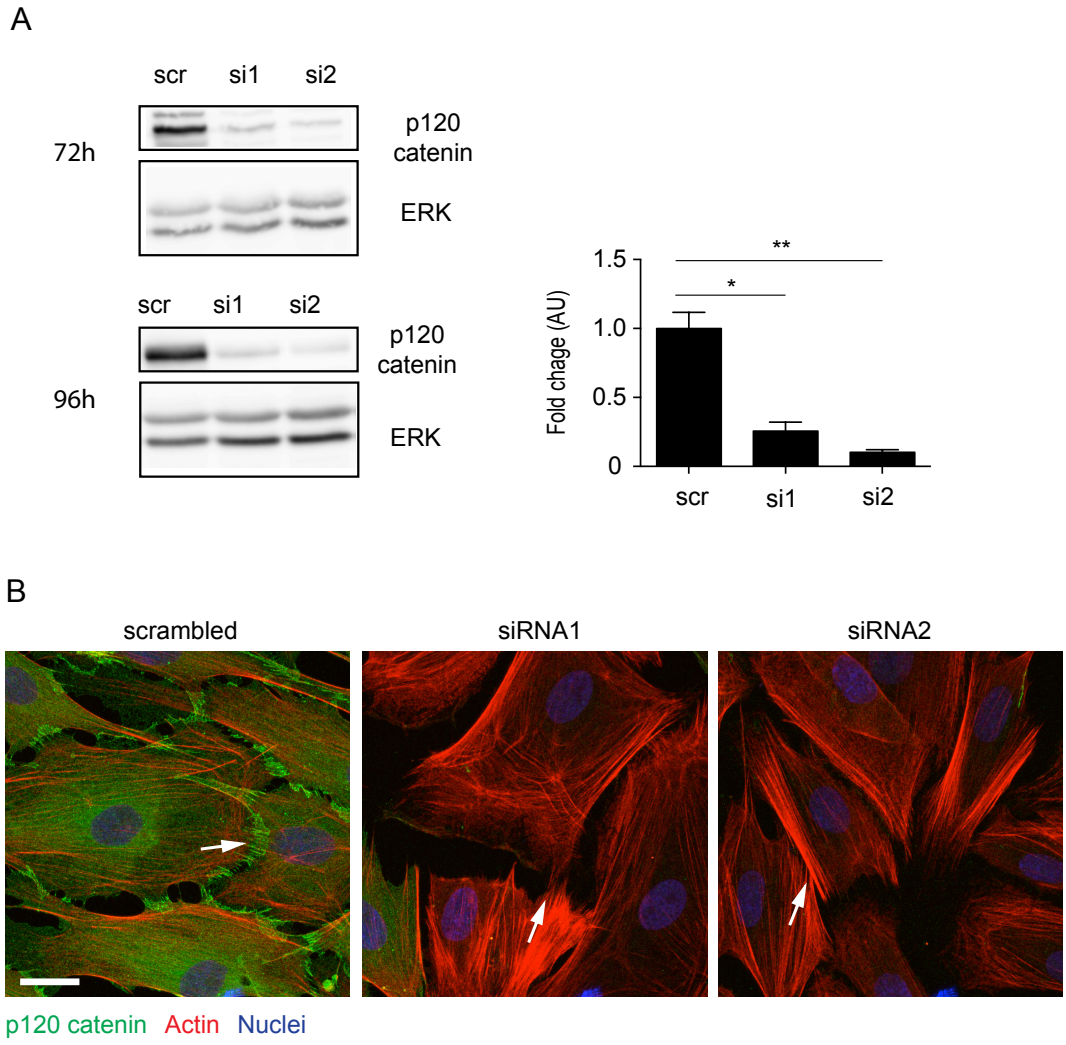

Figure 3.11. p120-catenin has a slow turnover.
(A) Left: Western blot showing the knockdown of p120-catenin using two independent siRNAs at 72 hours or 96 hours. ERK was used a loading control. Right: quantification of p120-catenin expression levels corrected for ERK, and compared to the p120-catenin expression levels in scrambled control. Bars represent the mean of three experiments ± SEM. One-way ANOVA, Dunnett's multiple comparisons test. **(B)** Immunostaining of p120-catenin (green), F-actin (red) and the nuclei (blue) in scrambled, siRNA1 and siRNA2 treated cells, at 96 hours. Arrows indicate junctions between two cells that are p120-catenin positive in scrambled-treated cells but lost following knockdown. Scale bar 20µm.

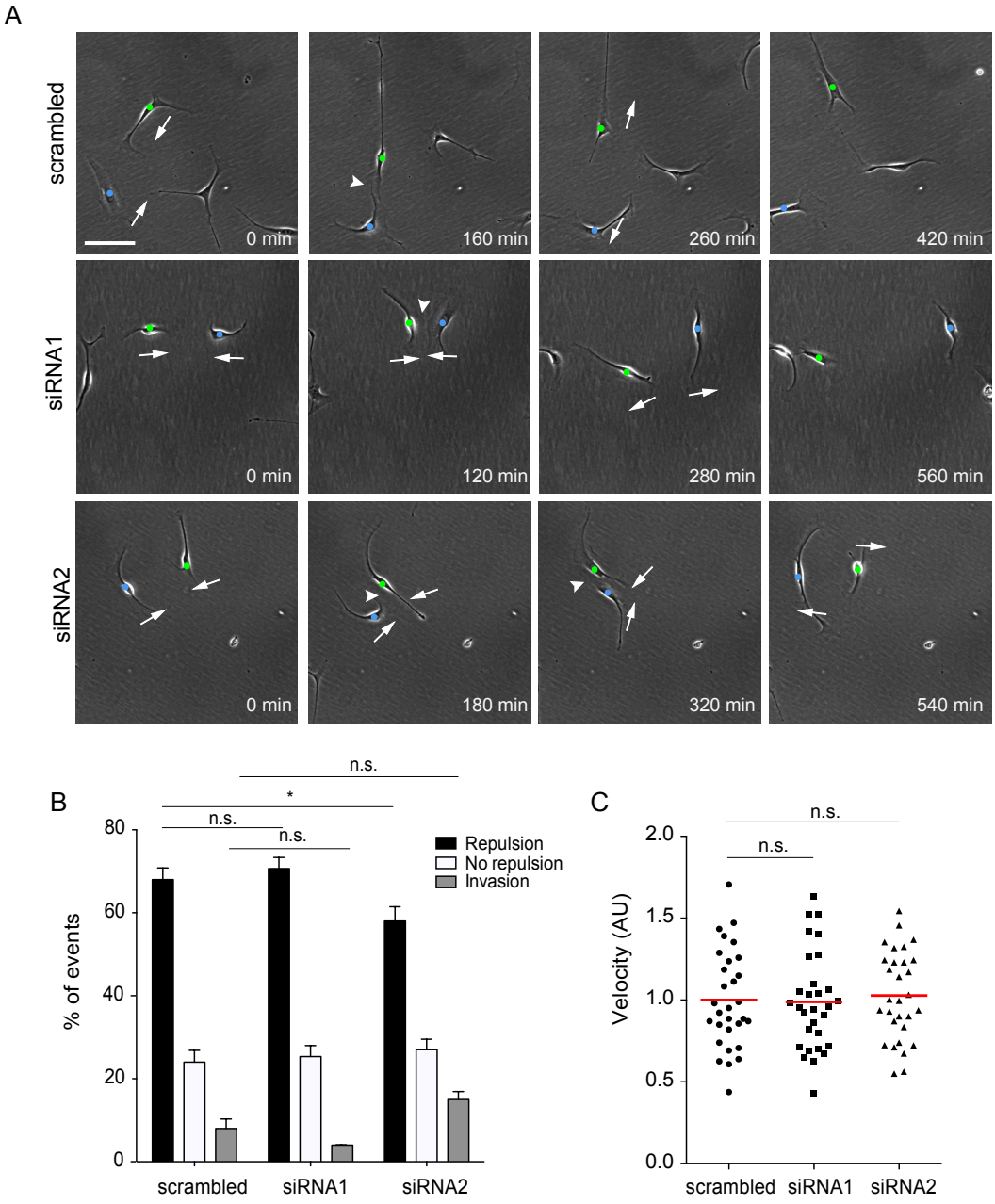

Figure 3.12. N-cad mediates CIL independent of p120-catenin.
(A) Representative still images from time-lapse microscopy of a CIL assay in which cells were treated with either 2.5 nM scrambled siRNA, or p120-catenin siRNA1 or siRNA2 for 96 hours before imaging for 24 hours. White arrows indicate direction of migration. White arrowheads indicate repulsion events. Cells of interest which are undergoing a repulsion event are indicated by green and blue dots. Scale bar 100µm. **(B)** Quantification of A. Bar represents four independent experiments ± SEM for scrambled and siRNA2. Bar represents mean of three independent experiments ± SEM for siRNA1 ≥90 cells from ≥3 experiments were quantified. **(C)** Velocities from the tracks of scrambled (N=30), siRNA1 (N=30) or siRNA2 treated cells (N=30). The red lines indicate the mean. One-way ANOVA, Sidak's multiple comparisons test.. Related to movie 3.5.

Subsequently we assessed whether there was a difference in the levels of N-cad, as p120-catenin has been reported to be important for the regulation of endocytosis and recycling of cadherins from the membrane (Peglion and Etienne-Manneville, 2013). Moreover, p120-catenin binding to cadherins masks a degradation domain, regulating the proteasomal degradation of cadherins (Fujita et al., 2002). Therefore, the decrease in repulsion could be due to a decrease in N-cad expression levels. To test if p120-catenin has affects on N-cad levels in Schwann cells, protein levels were analysed using Western blot analysis at 96 hours after treatment and we found a strong downregulation in N-cad levels, correlating with the levels of p120-catenin knockdown (Figure 3.13A). This suggests p120-catenin regulates N-cad expression levels in Schwann cells, which is consistent with previous reports in other cell types (Nanes et al., 2012; Wehrendt et al., 2016). As p120-catenin appears to regulate N-cad, we tested if p120-catenin affects N-cad localisation at the membrane using immunofluorescence. As expected, in scrambled-treated cells N-cad localised at the membrane and at cell-cell junctions (arrow) (Figure 3.13B). In contrast, in Schwann cells treated with siRNA1 there was a striking decrease of N-cad in the cell, although some could still be detected in small puncta at cell-cell contacts, consistent with the finding that siRNA1 treated cells can still repulse (Figure 3.13B and Figure 3.12B). In Schwann cells treated with siRNA2, there was a further decrease of N-cad, with only discrete points of N-cad at the cell-cell contact observable, correlating with the decrease in repulsion in these cells (Fig 3.13B and Figure 3.12B). This suggests that p120-catenin regulates N-cad stability at the cell surface in Schwann cells, which could be through masking the E3 ubiquitin binding sites, endocytosis or gene expression, which is consistent with previous reports performed in astrocytes, epithelial cells and HUVECs (Nanes et al., 2012; Peglion and Etienne-Manneville, 2013; Wehrendt et al., 2016). Moreover, it suggests

that the differential effect on CIL between the cells treated with siRNA1 and siRNA2, could be due to differences in N-cad levels at the cell surface. In addition, this suggests that low levels of N-cad at the cell-surface are sufficient to mediate CIL between Schwann cells.

Taken together, these data show that CIL is independent of p120-catenin, a known intracellular binding partner of N-cad, which is consistent with CIL being independent of *trans*-homodimerisation and independent of α-catenin.

3.5. The extracellular domain of N-cad mediates CIL in Schwann cells

So far we have shown that N-cad mediates CIL in Schwann cells, which is independent of *trans*-homodimerisation and independent of its cytoplasmic binding partners molecules αE-catenin and p120-catenin. To further understand how N-cad mediates CIL, we determined which domains of N-cad are required for CIL. To do this, constructs expressing different domains of N-cad were expressed in Schwann cells lacking endogenous N-cad. N-cad is a transmembrane receptor that has five EC domains through which it mediates adhesion and a cytoplasmic tail through which it can modulate the actin cytoskeleton (Brasch et al., 2012). To test which domain(s) of N-cad are required for CIL, either a mouse full length N-cad or mutants which either lack the intracellular domain or the extracellular domain were introduced into Schwann cells (Figure 3.14A) (Shih and Yamada, 2012).

To do this the constructs were expressed in N-cad knockdown cells for two reasons: firstly, we have previously shown that overexpression of N-cad in normal Schwann cells induces Schwann cells to cluster (Parrinello et al., 2010), thus it is important to express physiological levels of N-cad; secondly, we showed here that N-cad knockdown cells are still repulsed upon contact with an N-cad-expressing cell.

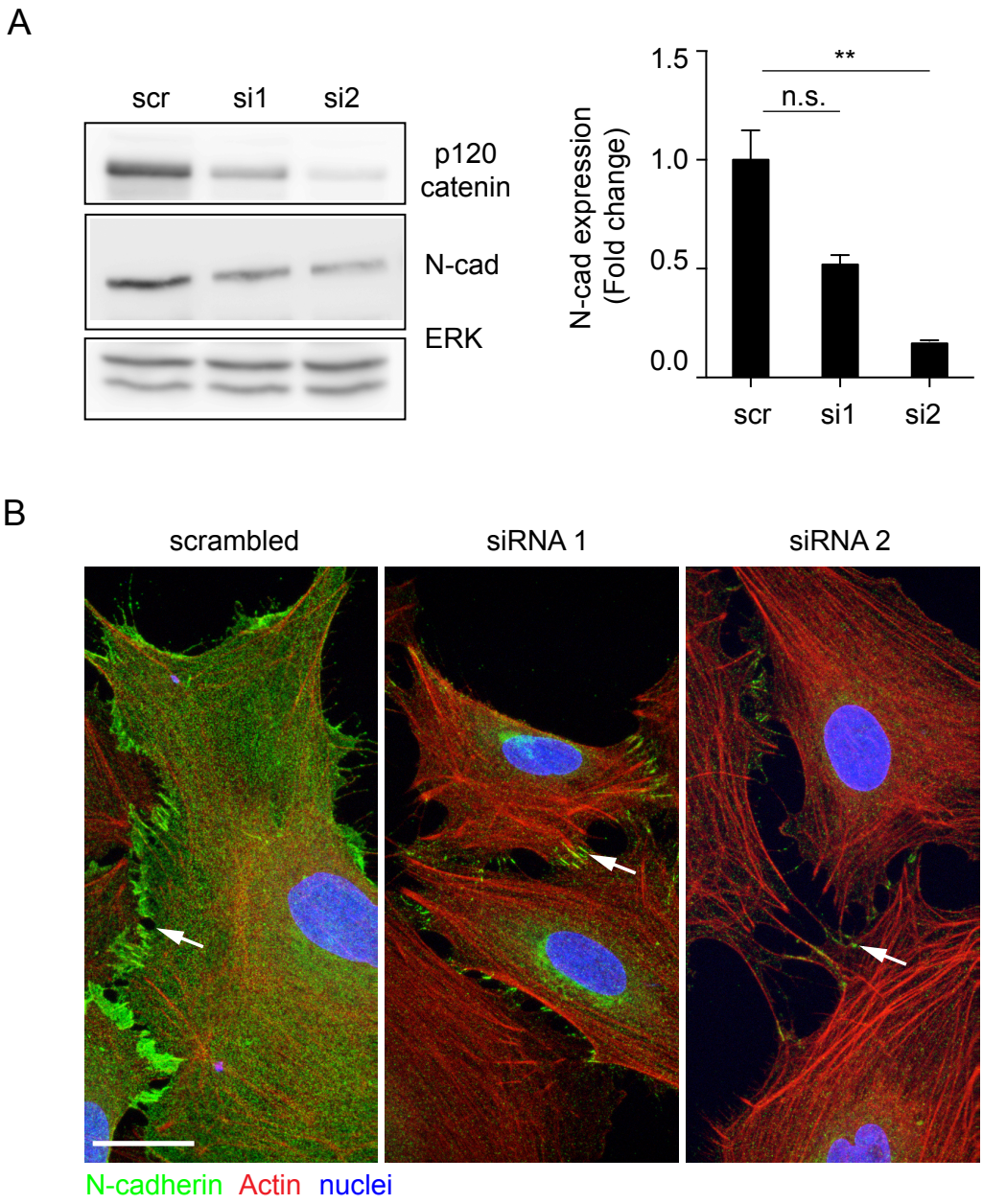

Figure 3.13. N-cad expression levels correlates to p120-catenin knockdown. **(A)** Left: Western blot showing the levels of N-cad following p120-catenin knock down. ERK was used a loading control. Right: quantification of Western blot of N-cad expression levels in p120-catenin knockdown cells compared to expression levels of N-cad in scrambled controls at 96 hours. Bar represents mean of three independent experiments ± SEM. One-way ANOVA, Dunnett's multiple comparisons test. **(B)** Representative confocal images of scrambled or p120-catenin knockdown cells at 96 hours, immunostained for N-cad (green), and costained for F-actin (red) and the nuclei (blue). Arrows indicate N-cad positive cell-contacts, which are downregulated following p120-catenin knockdown. Scale bar 20µm.

Therefore, ideally the response of an N-cad knockdown cell to a cell expressing one of the constructs should be measured. To test which domains are involved, the following mouse N-cad constructs were used that have been fully characterised (Shih and Yamada, 2012): Full length N-cad, N-cad with only the extracellular domain AA1-746 (Extracellular) and N-cad with only the cytoplasmic domain AA747-906 (Intra cellular) that were all tagged with tomato on the C-terminus (Figure 3.14A) (Shih and Yamada, 2012). Because the siRNA targeting sequence in the extracellular domain of N-cad is highly conserved between mouse and rat, four silent mutations were introduced into four codons of the siRNA target sequence, which should inhibit binding of the siRNA but should not alter the amino acids and therefore the structure of the proteins.

To test if the proteins were functional in the Schwann cells, the constructs were expressed in N-cad knockdown cells in a two step protocol: first N-cad was down regulated using siRNA1 which targets nearly all cells, followed by transfection of the constructs or empty vector after 24 hours, which targets approximately 20-30% of the cells. GFP was co-transfected to follow the successfully transfected cells. After a further 24 hours of expression, the proteins were extracted and assessed for the levels of the constructs using an antibody recognising the intracellular domain of N-cad. As expected, endogenous N-cad was down regulated, while low levels of full length N-cad could be detected running higher than controls, which was expected due to the tomato tag (Figure 3.14B). The extracellular domain fusion protein could not be detected, as the antibody recognises the intracellular domain. The intracellular domain fusion protein could be detected running lower than control, which would be expected due to the lack of the extracellular domain. Moreover, these bands were specific as the proteins were also detected using a mCherry antibody that also recognises pdtTomato (Figure 14B). Two bands of extracellular domain were

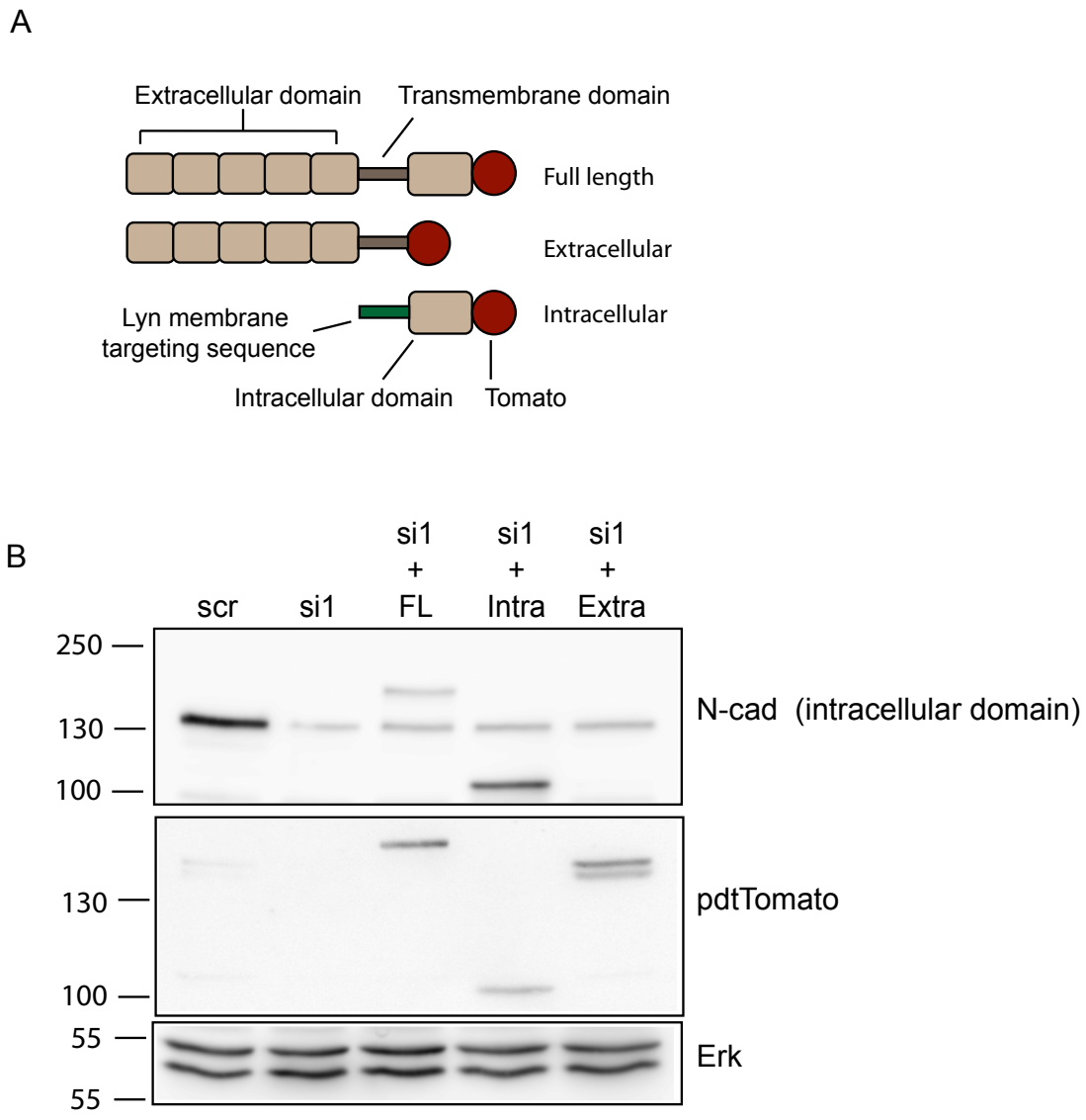

Figure 3.14. Expression of N-cad full length and mutants in Schwann cells.
(A) Illustration of the different N-cad constructs, full length, extracellular and intracellular domains tagged with ptdTomato on the C-terminus. The intracellular domain of N-cad has an additional Lyn membrane targeting sequence on the N-terminus to target it to the membrane **(B)** Representative western blot of N-cad and mCherry (that also recognises ptdTomato), showing the expression levels of N-cad and the different constructs following N-cad knockdown and overexpression of the different constructs 24 hours after overexpression (48 hours after knockdown). ERK was used a loading control.

detected, one of which ran slightly lower than the full length, which could possibly be a breakdown product. Importantly, the different domains have similar expression levels. The lower expression levels of the constructs could be explained by the low

efficiency of the DNA transfection, in which, depending on the transfection, only 20-30% of the cells were targeted. Moreover, the species of the constructs are mouse while the endogenous N-cad is rat therefore, there could be a difference in antibody binding efficiency between the two species, which could affect the detection of the fusion proteins.

To test if the full length and intracellular constructs are localised at the membrane and were able to bind intracellular binding partners, the cells were seeded on coverslips, fixed and immunolabelled for tomato, p120 and α-catenin. Full length N-cad can be observed engaging in junctions (insets) and as expected p120-catenin and α-catenin co-localise at the junctions (insets), suggesting the full length N-cad can interact with p120-catenin and α-catenin (Figure 3.15, left panel). In contrast, while the intracellular domain of N-cad localised at the membrane (insets) and at the sites of cell contact, it does not appear to form junctions, as might be expected (Figure 3.15, middle panel). Importantly, there is a strong localisation of p120-catenin and α-catenin at the cell contact (insets), which appears to co-localise with the intracellular domain of N-cad, suggesting the intracellular domain of N-cad can still interact with the intracellular binding partners p120-catenin and α-catenin and behaves as might be expected (Figure 3.15, middle panel). The extracellular domain of N-cad was localised at the membrane but appeared to have a more vesicular localisation than the full length of N-cad and the intracellular domain of N-cad. Importantly, the extracellular domain was able to localise at cell-cell contacts and appeared to form junctions, suggesting the extracellular domain can homodimerise (insets) though to a lesser extent than the full length (Figure 3.15, middle panel). However, as would be predicted, p120-catenin appears to be cytoplasmic and does not co-localise with the extracellular domain of N-cad at the junctions (inset) (Figure 3.15, right panel). Moreover, α-catenin could barely be detected in the cells and does

not appear to be localised at the cell junctions (inset), which is similar to N-cad knockdown cells in which no α-catenin could be detected, suggesting the intracellular domain of N-cad does not interact α-catenin (Figure 3.15, middle panel). Thus, this shows that the different N-cad constructs are localised and behaving as expected.

Next we tested if the different constructs affected migration behaviour. To do this, the full length of N-cad, the intracellular domain and the extracellular domain were expressed in N-cad knockdown cells. As shown earlier, the N-cad knockdown cells migrated faster than the scrambled-treated cells (Figure 3.16A). Interestingly, cells expressing the full length of N-cad have a similar velocity as the N-cad knockdown cells, suggesting that the full length of N-cad could not rescue the migration effect (Movie 3.6; quantified in Figure 3.16). Similarly, cells expressing the intracellular domain of N-cad had a slight but not significant increase in migration, suggesting they behave similarly to N-cad knockdown cells (Movie 3.6; quantified in Figure 3.16B). In contrast, cells expressing the extracellular domain of N-cad migrated faster than N-cad knockdown cells (Movie 3.6; quantified in Figure 3.16B). One reason why the full length may not rescue the increased velocity phenotype of N-cad knockdown cells could be the low expression levels of the full-length construct.

To understand if N-cad full length could rescue the loss of repulsion, it was expressed in the N-cad knockdown cells. As the N-cad expressing cell provides a repulsion signal to the other cell, but is not required for the N-cad expressing cell to be repulsed, only the response of the N-cad knockdown cells to the rescued cells were quantified. The controls behaved as expected: GFP-transfected scrambled treated cells (green dot) induced repulsion (black arrowhead) to the other cells (blue dot) upon contact, while GFP-transfected N-cad knockdown cells (green dot) were invasive (white arrowhead) upon contact with knockdown cells (blue dot), suggesting transfection does not affect CIL (Figure 3.15A). Crucially, while an N-cad knockdown

cell (blue dot) could invade another N-cad knockdown cell (green dot), it was subsequently repulsed upon collision with a cell expressing full-length N-cad (red dot), these events are now more common and invasion events became less frequent compared to N-cad knockdown control (Movie 3.6, Figure 3.17A). Quantification of CIL showed, that the rescued cells expressing the full length N-cad, behaved similar to scrambled-treated control cells in that they have many repulsion events and only a few invasion events, confirming that the loss CIL is specific for N-cad (Figure 3.15A and B).

Subsequently, the intracellular domain and extracellular domain were transfected into N-cad knockdown cells and imaged for 24 hours to observe their behaviour. Tomato-labelled intracellular domain expressing cells (red dot) were very dynamic, evidenced by the and extension and retraction of many protrusions, and in many events invaded (white arrowheads) N-cad knockdown cells (blue dot), suggesting that the intracellular domain is not sufficient to confer CIL (Movie 3.6; Figure 3.18A). In contrast, the tomato-labelled extracellular domain expressing cells (red dot) appeared to behave like scrambled-treated control cells (Movie 3.6 Figure 3.18A). While a N-cad knockdown cell (blue dot) could be observed invading another N-cad knockdown cell (green dot) upon contact, the same cell (blue dot) was repulsed (black arrowhead) upon contact with a cell expressing the extracellular domain of N-cad (red dot), suggesting the extracellular domain is sufficient to mediate CIL and that the intracellular domain is not required for this signal (Movie 3.6; Figure 3.18A). Quantification of CIL showed, that the intracellular-domain expressing cells behaved as N-cad knockdown cells in that there were fewer repulsion events compared to scrambled-treated cells, and many invasion events (>40%), suggesting the intracellular domain is not sufficient to induce CIL (Figure 3.16B). In contrast, the extracellular domain behaved similarly to scrambled control

cells and rescued the N-cad knockdown effect on CIL, with a decrease in invasion events and an increase of repulsion events, suggesting that the extracellular domain of N-cad is sufficient to mediate CIL (Figure 3.18B).

Taken together, these results show that the extracellular domain is sufficient to mediate CIL and that the intracellular domain is not required. This is consistent with the findings that CIL is independent of the adherence junction complex partners p120-catenin and α-catenin. Rather, it shows that the extracellular domain of N-cad provides a repulsion signal to mediate CIL.

3.6. Chapter discussion and conclusions

CIL is an important process that prevents intermingling of cells, and is important for the directional migration of cells in several systems. We showed that loss of N-cad results in a loss of cell-cell recognition and junction formation between Schwann cells, leading to the Schwann cells growing on top of each other, which is similar to the loss of cell-cell recognition observed between Schwann cells expressing oncogenic Ras. N-cad mediates cell-cell interactions in two ways: firstly, we showed that N-cad mediates CIL between Schwann cells by regulating repulsion and inhibiting the formation of forward protrusions. Moreover, N-cad is required for the directional migration of Schwann cells seen in a wound-healing assay. Secondly, in unpublished work, it was shown that N-cad regulates CIP, which inhibits the proliferation of cells at high density. While, N-cad is classically known to mediate adhesion between cells through homophillic *trans*-homodimersation and does so in Schwann cells (Brasch et al., 2012; Parrinello et al., 2010), we also showed that N-cad regulates CIL independently of *trans*- homodimersation and of the classical adherence junction complex (Figure 3.19). Rather, N-cad is required to provide a repulsion signal to repulse a cell, but is not required for the cell to be repulsed in an

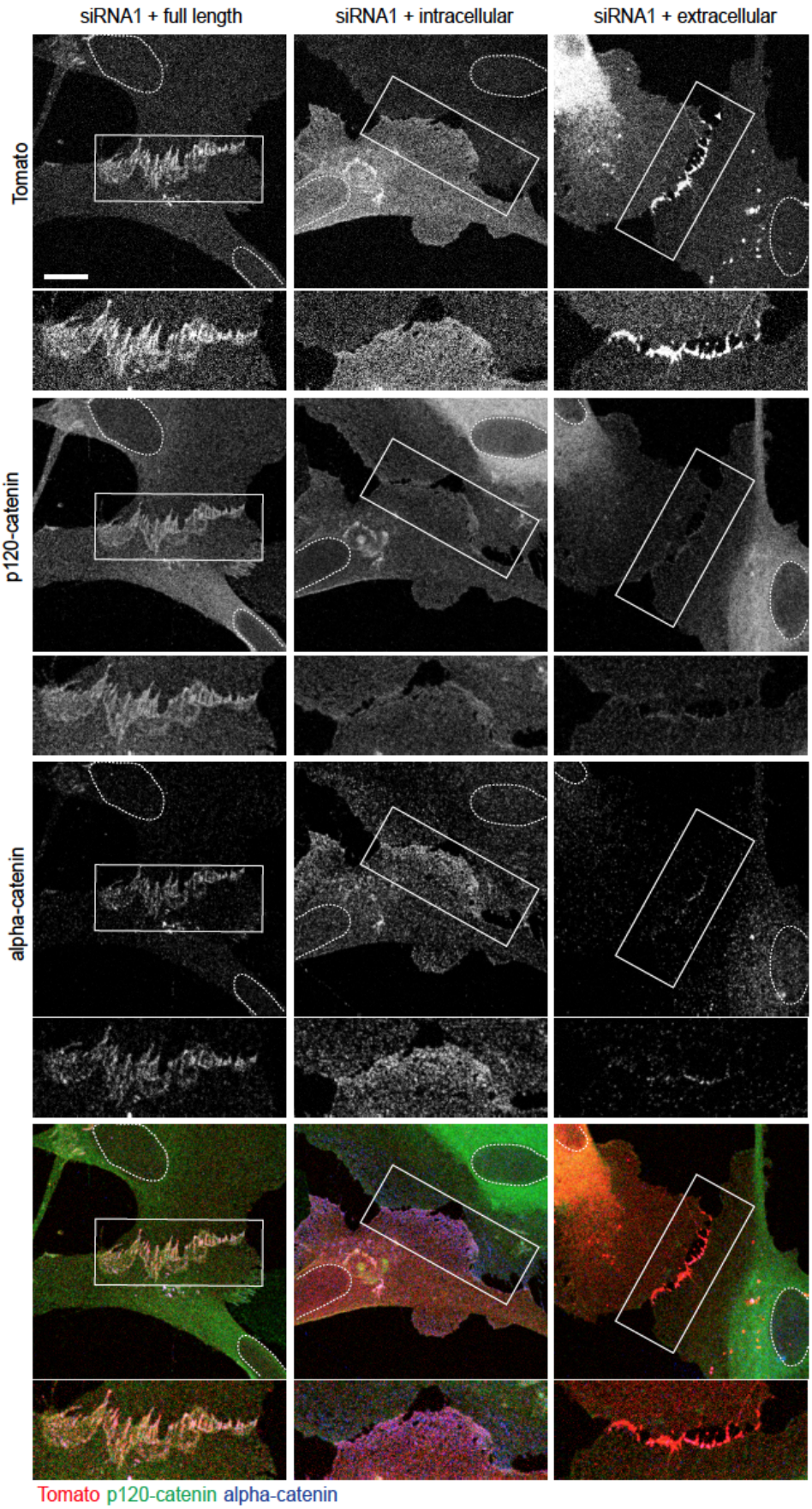
siRNA1 + full length
siRNA1 + intracellular
siRNA1 + extracellular
Tomato
p120-catenin
alpha-catenin
Tomato p120-catenin alpha-catenin

Figure 3.15. The different N-cad constructs are functional.
Representative confocal images showing N-cad knockdown cells overexpressing the different ptdTomato tagged (red) N-cad full length, extracellular domain or the intracellular domain, immunolabelled with p120-catenin (green) and α-catenin (blue). Enlarged insets show area of cell-contacts where the constructs are localised. Scale bar 20µm.

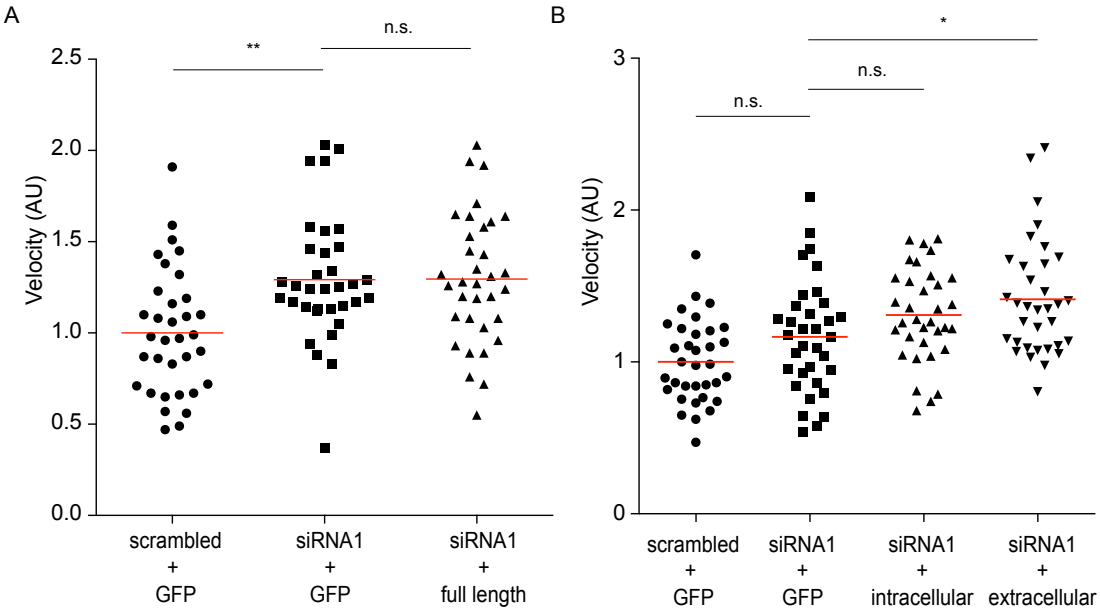

Figure 3.16. Velocity analysis of Schwann cells overexpressing N-cad mutants.
(A and B) Velocity of scrambled-treated cells, N-cad knockdown cells treated with siRNA1 and **(A)** siRNA1 N-cad knockdown cells overexpressing the full length of N-cad (full length) or **(B)** the extracellular domain of N-cad (extracellular) or the intracellular domain of N-cad (intracellular). Cells were tracked for 12 hours. The red lines represent the mean. 34 cells per condition from ≥3 independent experiments were quantified. Statistics: One-way ANOVA (A) or Two-way ANOVA (B), Sidak's multiple comparisons test

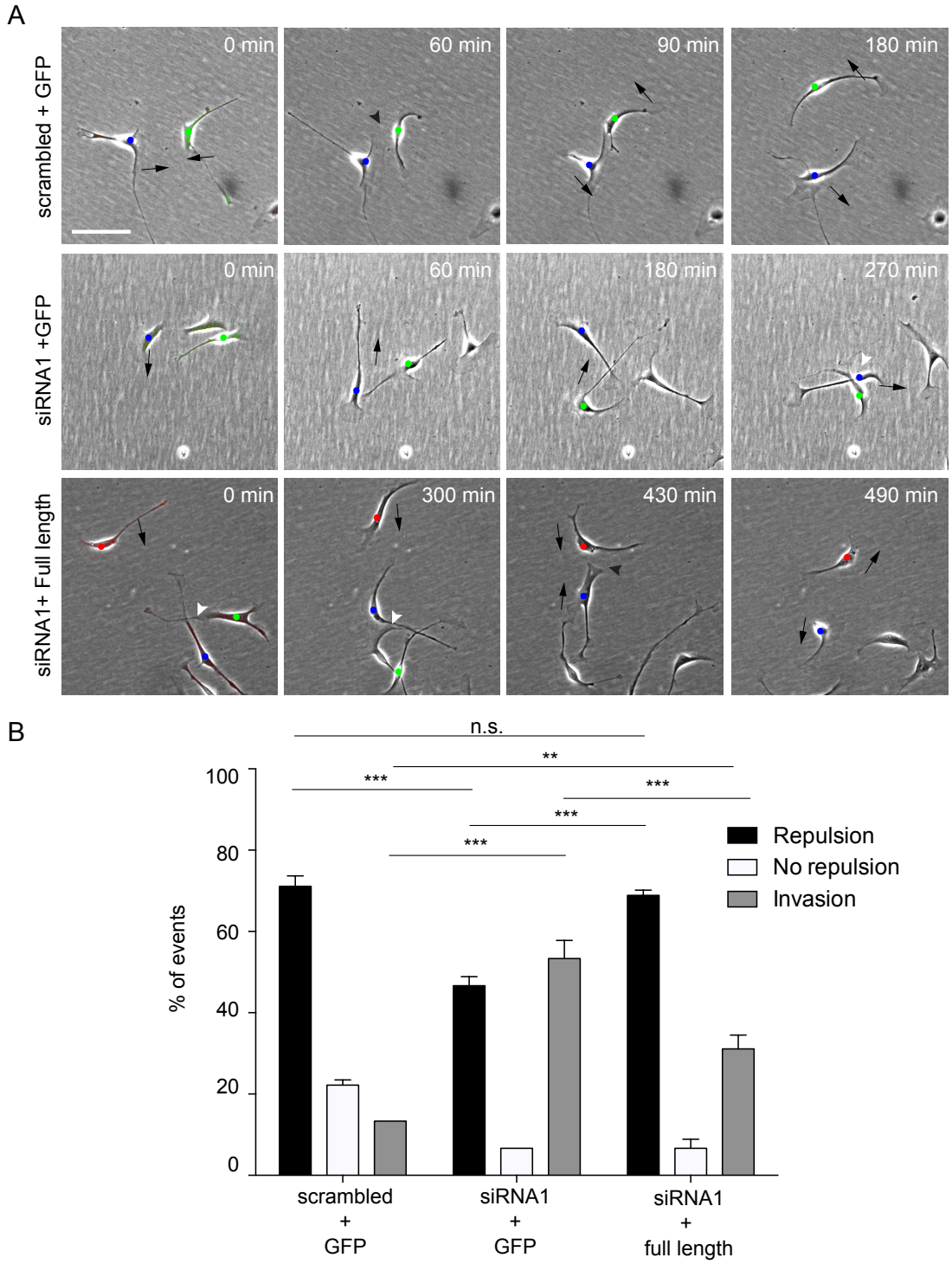

Figure 3.17. N-cad full length rescues the N-cad knockdown phenotype.
(A) Representative still images from a time-lapse movie in which scrambled-treated and N-cad knockdown cells were transfected with cytoplasmic GFP and/or ptdTomato-tagged full-length of N-cad. Arrows indicate direction of migration. Black arrowheads indicate repulsion events. White arrowheads indicate invasion events Interacting cells are indicated by blue and green dots (scrambled, siRNA1) or blue, green, and red dots (siRNA1+full length). Scale bar 100µm. **(B)** Quantification of A in which 45 cells from three independent experiments were quantified. Bars represent the mean ± SEM.

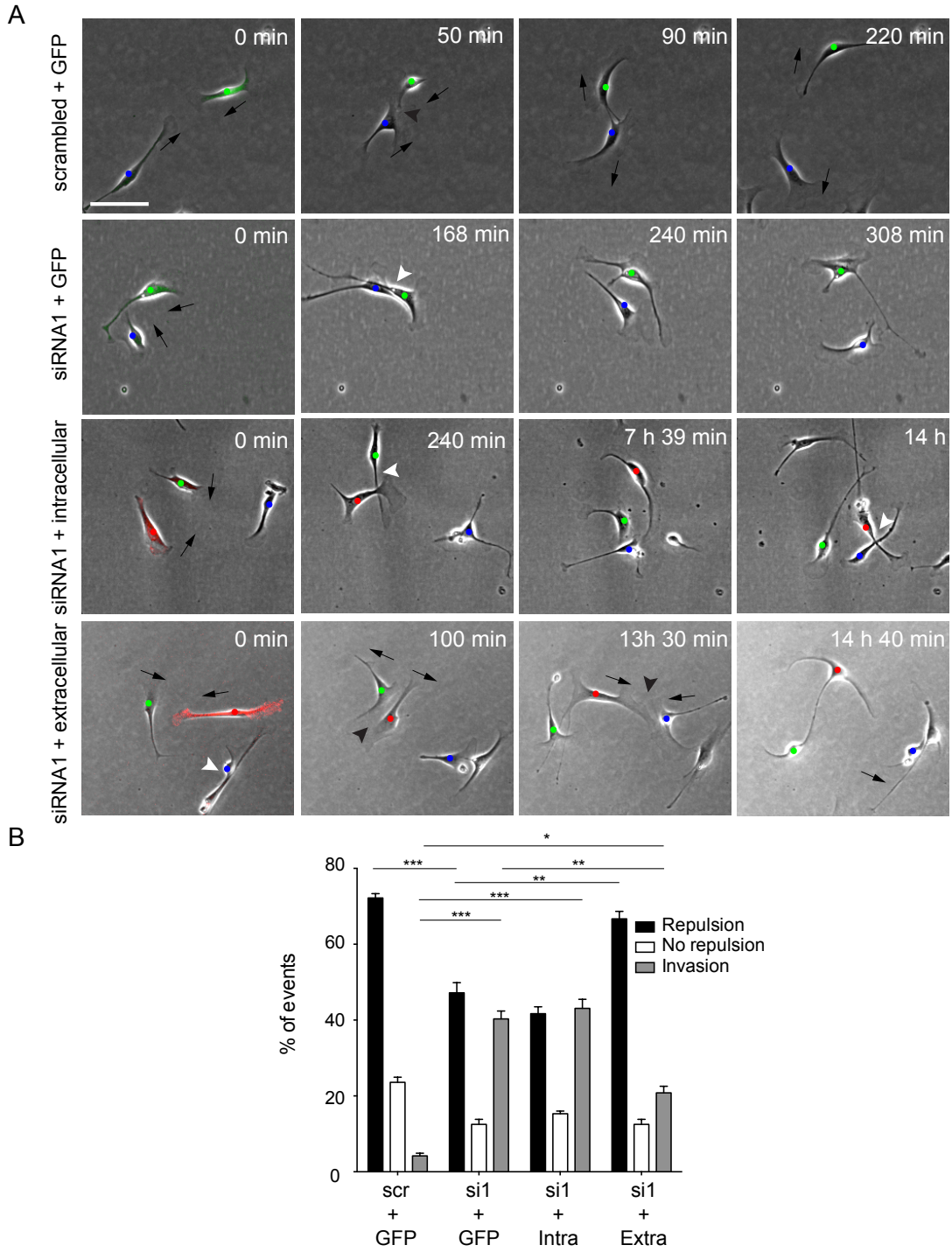

Figure 3.18. The extracellular domain of N-cad is sufficient to mediate CIL.
(A) Representative still images from a time-lapse movie in which scrambled-treated cells and N-cad knockdown cells were transfected with cytoplasmic GFP and/or the extracellular domain of N-cad (siRNA1+extracellular) or the intracellular domain of N-cad (siRNA1+intracellular) tagged with ptdTomato. Arrows indicate the direction of migration. Black arrowheads indicate repulsion events. White arrowheads indicate invasion events. Interacting cells are indicated by blue and green dots (scrambled and siRNA1) or blue, green and red dots (siRNA1+extracellular and siRNA1+intracellular). Scale bar 100µm. **(B)** Quantification of A in which 72 cells

from four independent experiments were quantified. Bars represent the mean ± SEM of four independent experiments. Related to movie 3.6.

N-cad dependent manner (Figure 3.19). Consistent with this, adherence junction components α-catenin and p120-catenin are not required for CIL between Schwann cells. Though p120-catenin does regulate N-cad levels at the membrane, which showed that even low levels of N-cad were sufficient to induce CIL. In agreement with this, we showed that only the extracellular domain of N-cad is sufficient to mediate CIL.

CIL is thought to have multiple roles, giving cells directionality during collective migration, preventing the intermingling of different cell populations and in boundary formation preventing the migration of cells into unwanted tissues. Many cells types such as fibroblasts migrate *in vitro* in a directional manner and change direction upon contact with another cell (Paddock and Dunn, 1986). Therefore, classical CIL quantifications measures the change of direction of migration of the cells following contact, by quantifying the vector displacement of a cell before and after collision with another cell (Astin et al., 2010; Carmona-Fontaine et al., 2008; Paddock and Dunn, 1986). These quantifications, which were originally described for fibroblasts, assume the cells will migrate in the same direction unless it meets another cell (Paddock and Dunn, 1986). This technique turned out to be inadequate for measuring Schwann cell CIL for two reasons: firstly, Schwann cells lack an intrinsic directionality and often change their direction of migration randomly, even without contact with other cells. Secondly, Schwann cells are highly dynamic cells and extend and retract many protrusions, even without the contact of other cells, which is even more exaggerated in N-cad knockdown Schwann cells. For this reason, it was decided to quantify CIL between Schwann cells by assessing the response of protrusions immediately following contact with another cell. To avoid

unconscious bias, colleagues who used the same parameters to quantify the same experiments, obtained similar results. Moreover, many of the experiments were analysed blind and the same results were obtained.

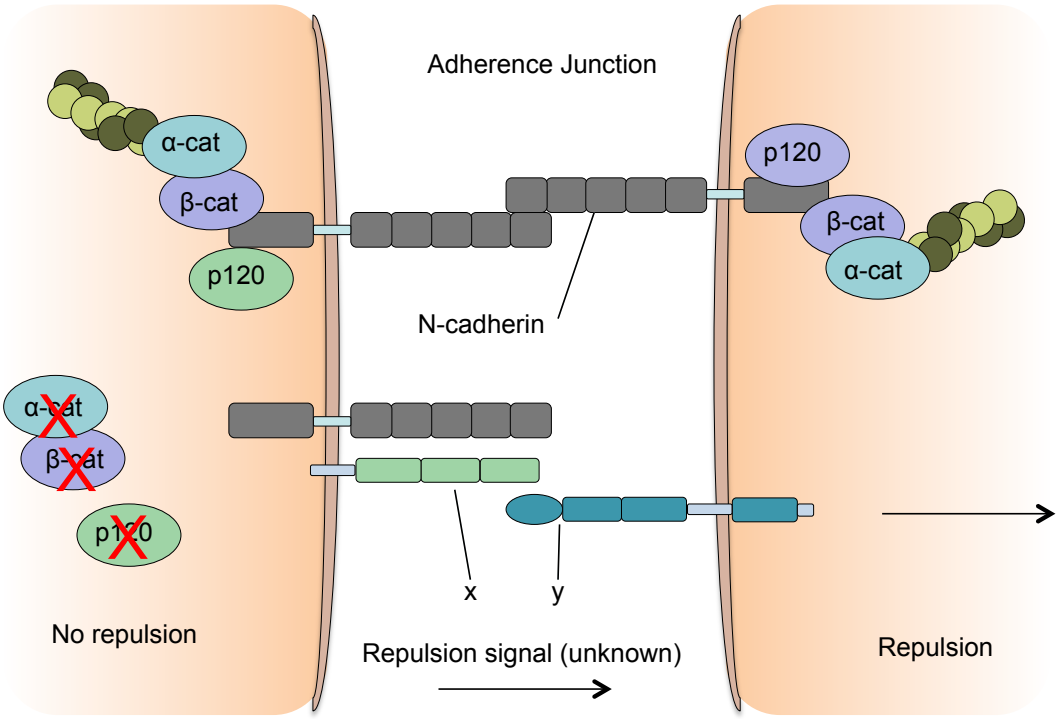

Figure 3.19 N-cad mediates CIL independent of trans homodimerisation.
N-cad is classically known to relay signalling, via *trans*-homodimerisation, into the cell through interacting proteins including α-catenin, β-catenin and p120-catenin. In contrast, CIL in Schwann cells is mediated by N-cad through a mechanism independent of trans-homodimerisation and of its interacting molecules α-catenin, p120-catenin and β-catenin. Rather, N-cad provides a repulsion signal to a second cell, which is then repulsed.

These findings have shown that in Schwann cells, CIL is regulated through N-cad, which inhibits the formation of forward protrusions and mediates repulsion, which is consistent with findings to a role of N-cad in CIL between neural crest cells and the heterotypic CIL seen between glia and glioblastoma cells (Becker et al., 2013; Scarpa et al., 2015; Tanaka et al., 2012; Theveneau et al., 2010). In neural crest cells, N-cad inhibits protrusions at the site of cell-cell contact within a cell cluster, repolarising the cells, resulting in the formation of new protrusions at the free

edge of the cell (Theveneau et al., 2010). Similarly, N-cad mediates heterotypic CIL between glia and a glioblastoma cell line by inhibiting forward migration. In agreement with these findings we have found that N-cad is required for CIL, by inhibiting protrusions at the site of cell-cell contact and thus blocking forward migration.

CIL is mediated by a repolarisation of cells, which results in a change in direction of migration of single cells, or repolarising the formation of protrusions to the free edge of cells, of cells migrating as a group (Theveneau et al., 2010). Moreover, recent work in neural crest cells showed that inducing protrusions at the free edge of the cell, by locally activating Rac, a regulator of protrusions, was sufficient to repolarise the cells, disassemble junctions at the cell-cell contact sites and trigger CIL (Scarpa et al., 2015). Though it was not directly addressed in this chapter, it appears from the movies that CIL in Schwann cells is associated with a change in polarisation, as it appears that protrusions are formed at the free edge away from the side of cell contact, however further analysis needs to be done to determine whether collapse of protrusions at the site of cell-cell contact is accompanied with protrusion formation at the free edge of the cell. Moreover, it would be interesting to see if, similarly to other systems such as in neural crest cells, glioblastoma, prostate cancer cells PC3, and fibroblasts whether Rho-GTPases are involved in mediating CIL (Astin et al., 2010; Carmona-Fontaine et al., 2008; Fritz et al., 2015; Scarpa et al., 2015; Tanaka et al., 2012; Theveneau et al., 2010).

Using two separate methodologies we showed that, CIL is independent of α-catenin and p120-catenin. This was shown first by knocking down α-catenin and p120-catenin using siRNA oligos, which did not affect CIL. Secondly, a rescue experiment in which the extracellular domain of N-cad was expressed in N-cad knockdown cells, showed that is was sufficient to confer CIL. In contrast, while the

intracellular domain could interact with α-catenin and p120-catenin, it could not rescue CIL. However, in previous studies using neural crest cells, p120-catenin was shown to have a role in inhibiting cell-cell repulsion in neural crest cells (Scarpa et al., 2015). E-cad supresses repulsion by sequestering p120-catenin, which leads to the redistribution of active Rac-1 and formation of protrusions away from the free edge of the cell. While not directly addressed by the authors, this could suggest that in N-cad expressing migratory neural crest cells, free p120-catenin could play a role in CIL by inducing the formation of protrusions at the free edge of the cell. However, they showed that p120-catenin knockdown does not affect protrusion formation at the free edge of migratory neural crest cells, suggesting that similarly to Schwann cells it may not play a role in CIL (Scarpa et al., 2015).

A separate mechanism was reported in studies in glioblastoma, in which the interaction of the nucleotide diphosphate kinase nm23-H with α-catenin, was shown to be required to mediate heterotypic CIL between glioblastoma and glial cells (Tanaka et al., 2012). In glioblastoma cells, nm23-H suppresses the activity of tiam-1 a GEF for rac-1 thereby inhibiting Rac-1 activity, which the authors propose blocks protrusion formation and mediates CIL. In contrast, we have shown that α-catenin is not required for homotypic CIL between Schwann cells. Differences between the mechanisms of CIL in glioblastoma in Schwann cells could be attributed to cell type differences, or could reflect that homotypic CIL and heterotypic CIL are regulated differently.

Studies of neural crest cells also showed that, overexpression of the intracellular domain of E-cad inhibits CIL in migratory cells in a p120-catenin dependent manner. Interestingly, similar to neural crest cells prior to EMT, quiescent myelinating Schwann cells express E-cad (Fannon et al., 1995). However, whether CIL is inhibited in myelinating Schwann cells and if E-cad can inhibit CIL in a similar

manner to NC in Schwann cells in unclear. However, as p120-catenin is not required for CIL between Schwann cells, this may suggest that E-cad regulates CIL in myelinating Schwann cells independently of p120 catenin.

Though, this work shows that the intracellular binding partners of N-cadherin are not involved in CIL, we have not completely excluded this. For example, we have not shown whether β-catenin, which is the physical link between N-cad and α-catenin, is involved in CIL between Schwann cells. However, as the extracellular domain of N-cad is sufficient to confer CIL it would seem unlikely. Nevertheless, we will test if β-catenin has a role in CIL.

The somewhat surprising result was that CIL is independent of *trans*-homodimerisation and independent of the adherence junction complex, which suggests that N-cad may need to interact with another molecule to present a repulsion signal. Though N-cad is classically known to *trans*-homodimerise and aggregate in adherence junction complexes, some reports have shown that N-cad can interact in *cis* with other membrane proteins (Suyama et al., 2002; Williams et al., 2001). Studies in cerebellar neurons have shown that, N-cad can modulate the function of the FGF receptor by directly interacting with the FGF binding site (the HAV motif of the FGF receptor), which promotes neurite outgrowth (Williams et al., 2001). Another study in the breast cancer cell line MCF-7, indicated that the interaction of the activated FGF receptor with the extracellular domain of N-cad prevents internalisation of the receptor, and therefore causes sustained signalling through the FGF receptor, resulting in high levels of ERK signalling, which results in increased invasion and cell growth (Suyama et al., 2002).

In contrast, other work suggests that N-cad can modulate signalling by binding through its intracellular domain to other receptors such as Robo and LRP5 (Hay et al., 2009; Rhee et al., 2007). Work done in osteoblasts showed that N-cad

interacts indirectly through its intracellular domains via an unknown protein to axin, which in turn binds to the Wnt co-receptor LRP5 (Hay et al., 2009; Rhee et al., 2007). This interaction, results in increased β-catenin degradation, thereby negatively regulating Wnt signalling, which inhibits osteoblast differentiation and bone formation. In a different study, it was shown in neural retina cells, that binding of the ligand slit to its receptor Robo leads to interactions with N-cad via an intracellular complex of β-catenin, cables (a cycling-dependent kinase binding protein) and Abl, resulting in decreased adhesion of the neurons (Rhee et al., 2007). However, as we have shown that CIL can be mediated in Schwann cells by the extracellular domain of N-cad, this may suggest these types of interactions are not relevant for the regulation of Schwann cell CIL.

How could N-cad regulate CIL between Schwann cells? Our work suggests that N-cad provides a repulsion signal, which is dependent on the extracellular domain. Thus it would be tempting to speculate that in Schwann cells, similar to other systems, N-cad interacts via its extracellular domain in *cis* with a co-signal such as the FGF-receptor or another molecule to mediate CIL (see next chapter). Another possibility is that N-cad regulates the stability or levels of a co-signal at the cell surface in a more indirect manner. To further elucidate how N-cad regulates CIL, it will be important to determine which EC domain(s) of the extracellular domain of N-cad are involved in CIL, by expressing mutants lacking these different EC domains in N-cad knockdown Schwann cells.

What is the role of CIL in Schwann cells? During development, Schwann cells need to migrate outwards along axons to reach their final target, similarly to neural crest cells, which migrate away from the neural tube to their destination (Carmona-Fontaine et al., 2008; Heermann and Schwab, 2013). Several studies of neural crest cells, fibroblasts and PC3 cells have shown that outward migration requires contact-

dependent repulsive signals resulting in the cells migrating away from each other for the dispersal of cells (Batson et al., 2014; Fritz et al., 2015; Theveneau et al., 2010). Outward migration in Schwann cells was induced, by inducing a gap in a confluent monolayer. This showed that contact dependent migration mediated by N-cad is the efficient outward required for migration of Schwann cells, potentially suggesting a role for the outward migration of Schwann cells during development. The situation is different in the adult following injury when the Schwann cells form clusters mediated by increased N-cad at the membrane, and migrate as cellular cords (Parrinello et al., 2010). This re-localisation of N-cad to the cell junctions between Schwann cells is important for the Schwann cells to migrate as a collective and thus appear to have purely an adhesive role. However, although Schwann cells switch behaviour from repulsive to adhesive, live-imaging of co-cultures of Schwann cells with fibroblasts show that the Schwann cells within clusters adhere to each other, but still appear to attempt to migrate away from each other (Parrinello et al., 2010). Moreover, the cluster as a whole is not static; rather it is dynamic and appears to still move around the dish, while remaining as a cluster. This might suggest that the repulsive signal is still active in the cluster. In recent work studying neural crest cells, it was suggested that traction forces within the migratory cluster are exerted outwards to the edge of the clusters (Scarpa et al., 2015). This could also suggest that similar to the role of in NC, in Schwann cells CIL could prevent formation of protrusions at side of contact and provide a repulsive outward force within the cluster, which could mediate forward migration *in vivo* (Figure 3.2) (Theveneau et al., 2010). These ideas will be tested in future experiments.

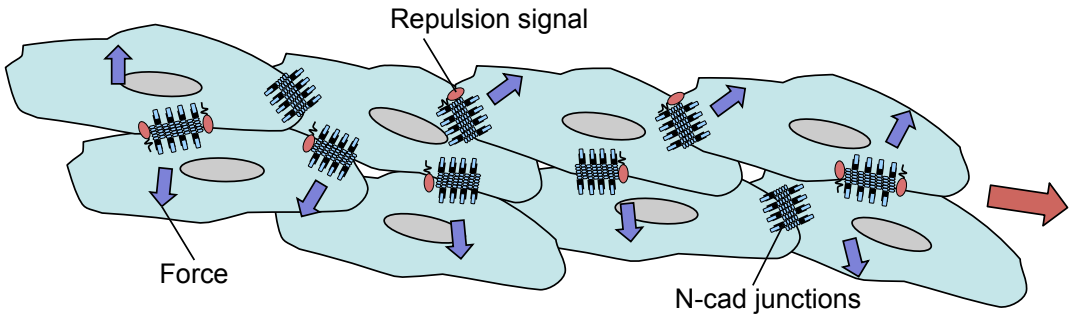

Figure 3.20 Repulsion signal could induce outward forces, which could drive the collective migration of Schwann cells.

During collective migration the cells within the cluster need to coordinate cell movement, cell speed and the direction of migration. This requires continuous communication between neighbouring cells, maintaining continuous strong contacts while these interactions may need to remain plastic to allow cellular rearrangements to occur. N-cad has been shown in many cell types to mediate adhesion and collective migration. Furthermore, N-cad has also been shown to mediate CIL within cell clusters and mediate directional migration. However, how N-cad can mediate these seemingly contradictory functions is not understood. Here we provide a simple solution in which N-cad controls these processes by two distinct mechanisms: firstly, N-cad could mediate cell adhesion maintaining a cell cluster through *trans*-homodimerisation, transducing adhesive forces onto the actin cytoskeleton through adherence junction components α-catenin and β-catenin. Secondly, N-cad could mediate inhibition of protrusions and mediate repulsive forces to drive the cluster forward, independent of *trans*-homodimerisation and the adherence junction complex, and requiring only the extracellular domain of N-cad and a co-signal (Figure 3.20). Therefore, it would be interesting to test if Schwann cell clustering is dependent on α-catenin, β-catenin and p120-catenin, and determine whether N-cad mediates cell clustering and CIL through different mechanisms and the role of all off these processes for Schwann cells to successfully guide axons *in vivo.*

In conclusion, these data showed that homotypic CIL between Schwann cells *in vitro* is required for cells to recognise each other, and contact dependent migration is required for directional migration during “collective” migration. We showed that N-cad mediates homotypic CIL between Schwann cells, which is independent of the classical adherence junction complex, independent of the intracellular domain of N-cad and the interacting molecules α- catenin and p120-catenin. Moreover, N-cad is not required for a Schwann cell to be repulsed. Rather N-cad provides a repulsion signal, possibly through interaction with a co-signal. Moreover, the repulsion signal is specifically mediated by the extracellular domain of N-cad, which is sufficient to mediate CIL. N-cad could possibly mediate both repulsion and adhesion by differentially mediating these processes; adhesion is mediated through the adherence junction complex, while CIL is mediated independent of the adherence junction complex but requires the extracellular domain to present a repulsion signal.

Chapter Four: Results II

Uncovering the mechanism of homotypic CIL

4.1. Chapter introduction

In the previous chapter, we showed that N-cad regulates CIL through a mechanism independent of *trans*-homodimerisation and the proteins associated with the intracellular domain. The data suggested that a co-signal is required to present the repulsive signal and mediate CIL. To further explore the mechanism by which N-cad regulates CIL, we decided to investigate Schwann cells expressing oncogenic Ras. These cells, similarly to N-cad knockdown cells, have lost the ability to recognise each other (Fig 3.1C). However, previous work from our laboratory has shown that this is not due to loss of N-cad, as Ras-expressing cells still express N-cad which appeared to be functional. In these unpublished studies, performed by a previous PhD student in the lab (Dr. Patrick Wingfield-Digby), it was shown that in co-cultures of Schwann cells and DRGs, Schwann cells grab axons in an N-cad dependent manner (data not shown), a process important for initial recognition both during development and after injury (Jessen and Mirsky, 2005). In addition, Dr. Patrick Wingfield-Digby, showed that Schwann cells expressing Ras or a Raf-inducible construct (NR-SCs), in which Raf signalling can be hyperactivated upon addition of tamoxifen (TMX), can still grab axons (Figure 4.1A), suggesting that hyperactive Raf signalling does not impair axonal grabbing by the Schwann cells. This process was dependent on N-cad as NR-SCs treated with N-cad siRNA lost the ability to grab axons (Figure 4.1B). These results indicate that cells with hyperactivated Ras/Raf signalling retain functional N-cad, suggesting that loss of cell-cell recognition in Schwann cells expressing oncogenic Ras is due to a separate mechanism. Moreover, these findings show that N-cad can mediate very distinct processes depending on the context, in that N-cad can regulate Schwann cell clustering,

Schwann cell CIL and axonal grabbing (Figure 4.2). How N-cad can regulate these three very different processes is unclear, but is likely to involve distinct co-signals.

A

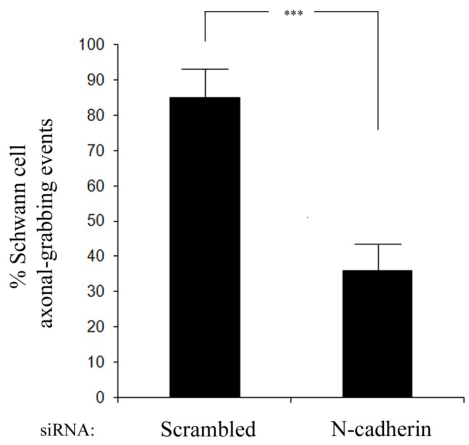

B

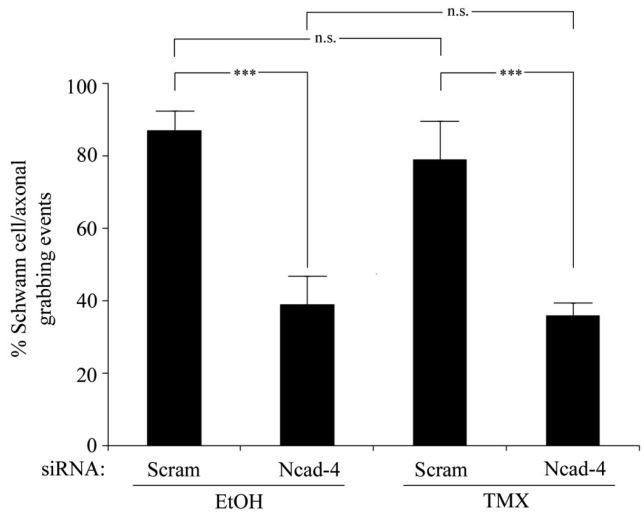

Figure 4.1. Raf-activated Schwann cells grab axons in an N-cad dependent manner.

(A) Quantification of Schwann cell/axonal grabbing events. Three videos were analysed per experiment in which 15-20 Schwann cells were scored. Bars show three experiments ± SD. Statistics: two tailed T-test. **(B)** Quantification of axonal grabbing events by control Schwann cells (EtOH) or Raf activated Schwann cells (TMX) that were either treated with scrambled siRNA (Scram) or N-cad targeting siRNA2 (Ncad-4). Bars represent SD of triplicate videos (n>15). Shown is a representative of two data sets. Statistics: one-way ANOVA Turkey-Kramer Multiple comparison T-Test.

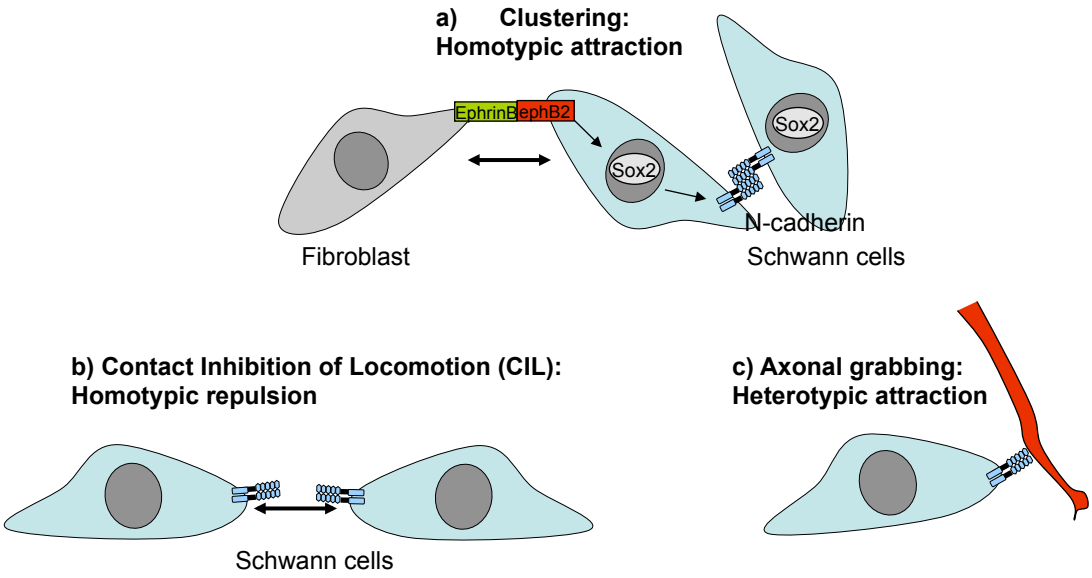

Figure 4.2 N-cad regulates opposing behaviours in Schwann cells.
Depending on the context, N-cad mediates a) Schwann cell clustering as a result of EphB2-induced relocalisation of N-cad to the cell-junctions. b) CIL by mediating homotypic repulsion between Schwann cells. c) Axonal grabbing by Schwann cells.

Neurofibromatosis Type I (NF1) is associated with the formation of neurofibromas, which are heterogeneous benign tumours consisting of a mixture of Schwann cells, axons, inflammatory cells, vascular cells and perineurial-like cells and enriched in extracellular matrix (Parrinello and Lloyd, 2009). Though neurofibromas are benign, plexiform neurofibromas can progress to MPNSTs that are highly malignant and frequently fatal (Parrinello and Lloyd, 2009). NF1 results from the loss of neurofibromin, a Ras GAP, which leads to the hyperactivation of Ras signalling (DeClue et al., 1992; Martin et al., 1990; Xu et al., 1990). Though neurofibromas are composed of multiple cell types, neurofibromas have been shown to originate from Schwann cells (Serra et al., 2000; Zhu et al., 2002).

Loss of heterotypic interactions between Schwann cells and axons is likely to be a key event in tumour formation, as Schwann cells are dedifferentiated and are found dissociated from axons in Neurofibromas (Zheng et al., 2008). We have previously shown that loss of this heterotypic interaction is partly mediated by loss of

Semaphorin 4F (Sema4f) expression, as a result of hyperactive Ras/Raf/MEK/ERK signalling. This results in increased proliferation of Schwann cells, as they lose the cell-cycle inhibitory signal associated with axonal interaction (Parrinello et al., 2008). Thus while Ras-expressing Schwann cells still grab axons, due to N-cad mediated interactions, loss of Sema4F expression results in unstable interactions as the cells no longer align along the axons.

Whilst loss of stable axonal interactions is likely to be tumour promoting, Ras-expressing Schwann cells also no longer recognise each other or other cells such as fibroblasts and it is likely that these changes in cell/cell interactions also contribute to tumour formation and spread. Thus it is important to understand how Ras deregulates homotypic and heterotypic interactions and how these may contribute to the onset of tumour formation.

4.2. Assessing homotypic CIL of DNp53-Ras Schwann cells

In the previous chapter, we briefly described that DNp53-Ras Schwann cells, like N-cad knockdown cells, lose the ability to form homotypic junctions. As discussed in the previous chapter, we use cells in which oncogenic Ras is expressed in Schwann cells expressing dominant negative p53 (DNp53) in order to prevent the cells from entering into senescence (Lloyd et al., 1997). The lab has previously shown that Schwann cells expressing DNp53 (DNp53-SC) behaved like normal cells in respect to cell growth (Collins et al., 2012). To determine whether expression of DNp53 affects cell recognition, DNp53-SCs and DNp53-Ras-SCs were cultured *in vitro* and grown to confluence in the same culture conditions as normal Schwann cells. DNp53-SCs formed a confluent monolayer, suggesting they behave like normal Schwann cells in respect to cell-cell recognition (Figure 4.3 see also Figure 3.1A). In contrast, DNp53-Ras-SCs grew on top of each other, as was described for N-cad

knockdown cells, suggesting that they can no longer form junctions and are invasive (Figure 4.3).

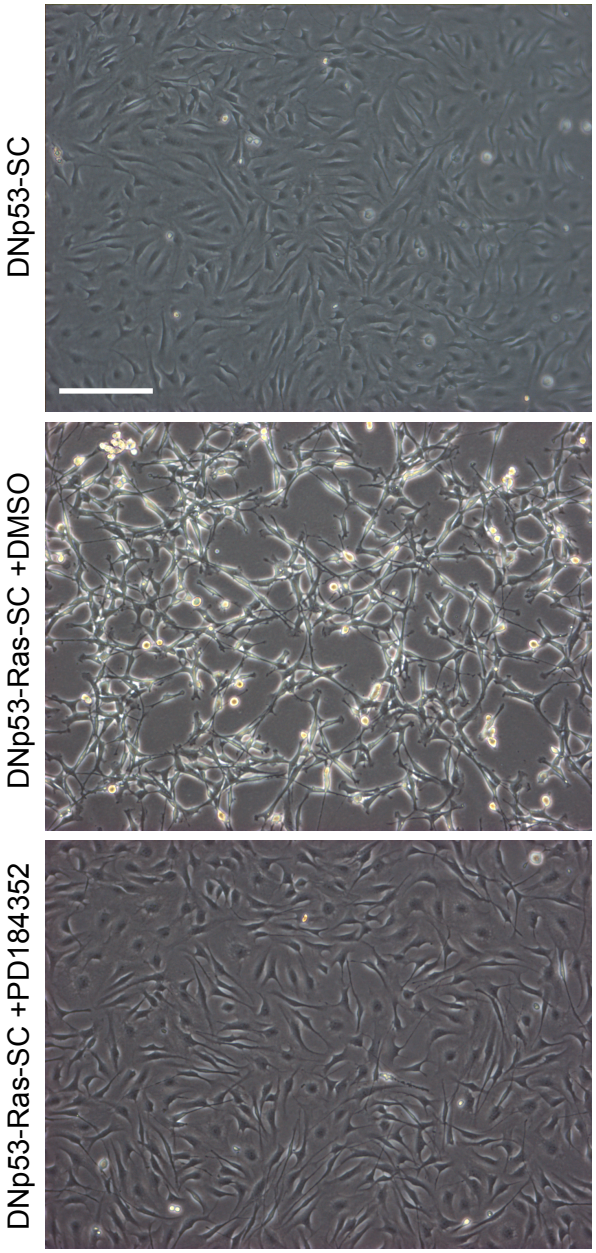

Figure 4.3. Expression of oncogenic Ras induces loss of cell-cell recognition in a MEK dependent manner.
(A) Phase contrast images of Schwann cells expressing DNp53 (DNp53-SC) or DNp53 and oncogenic Ras (DNp53-Ras-SC) in the presence of control solvent (DMSO) or the MEK1/2 inhibitor PD184352 (0.75µM). Scale bar 100µm.

To determine if DNp53-Ras-SCs, like N-cad knockdown cells, have lost CIL, DNp53-SC and DNp53-Ras-SCs were seeded at low density and CIL was analysed. As expected, DNp53-SCs behaved like normal Schwann cells and were repulsed upon contact; additionally, very few no-repulsion and invasion events were detected, demonstrating that CIL is maintained in DNp53 expressing cells (Movie 4.1; Figure 4.4A). Strikingly, Schwann cells became highly invasive, following expression of oncogenic Ras, recapitulating the phenotype of N-cad knockdown cells, demonstrating that they have lost CIL (Movie 4.1; Figure 4.4). However, they do not behave identically to the N-cad knockdown cells, in that they appear to be even more invasive and their behaviour appears more dynamic, in that they protrude and retract their protrusions more rapidly and frequently, apparently independently of contact with other cells (Movie 4.1; Figure 4.4A). The repulsion, invasion and no-repulsion events were quantified for DNp53-SCs and DNp53-Ras-SCs, which showed that DNp53-SCs, like normal cells were repulsed (≥80%) upon contact, with very few invasion (≤5%) and no repulsion (≤15%) events observed, indicating DNp53 cells behaved like normal cells and CIL remains intact (Figure 4.4B also see Figure 3.2B). In contrast, there was a marked decrease in repulsion events (≥2 fold) upon expression of oncogenic Ras, and a dramatic increase of invasion events (≥6 fold), while no no-repulsion events could be detected (Figure 4.4B). This indicates that CIL is lost in Schwann cells expressing oncogenic Ras, which become highly invasive. Moreover, the repulsion response is most likely an over representation of real repulsion events, as DNp53-Ras-SCs have highly dynamic protrusions, and frequently retract their protrusions independently of cell contact, possibly leading to the misinterpretation of retraction events upon contact with another cell.

To elucidate through which pathway Ras abrogates cell-cell recognition we added PD184352 (0.75 μM), a specific pharmacological inhibitor of MEK1/2, to

DNp53-Ras-SC (Collins et al., 2012). Strikingly, over time, the cells appeared to adopt a similar morphology to control cells (Figure 4.3). Importantly, cell-cell contacts were restored to control levels as the cells formed a confluent monolayer, indicating that oncogenic Ras disrupts cell-cell recognition through MEK dependent mechanisms possibly through regulating CIL. To test this, DNp53-Ras-SC or DNp53-SC were cultured for 18 hours in the presence of PD184352 or control solvent (DMSO), subsequently seeded on laminin-coated dishes at low density in the presence of inhibitor and imaged for 24 hours using time-lapse microscopy to observe their behaviour. Strikingly, treatment of DNp53-Ras-SCs with the MEK inhibitor completely restored normal Schwann cell CIL behaviour demonstrating that Ras disrupts CIL in a MEK dependent manner (Movie 4.1; Figure 4.4A and quantified in 4.4B).

Thus DNp53-Ras-SC have a similar phenotype to N-cad knockdown cells, in that they lose the repulsion signal and become invasive, however Schwann cells expressing hyperactive Raf-signalling can still grab axons in an N-cad dependent manner suggesting that the Ras/Raf response involves a distinct mechanism. One possibility was that loss of CIL in DNp53-Ras-SC was due to the specific loss of N-cad at sites of homotypic cell-cell contacts. To test this possibility, N-cad protein expression levels were first assessed by culturing DNp53-Ras or DNp53-Ras-SC, either in the presence of DMSO or PD184352 for 36 hours and the protein was harvested for Western blot analysis. As expected, N-cad was expressed by DNp53-SCs, but the levels were not significantly changed in the DNp53-Ras-SCs or by the presence of the MEK inhibitor (Figure 4.5A). This suggests that loss of CIL in DNp53-Ras-SCs is not the result of aberrant expression levels of N-cad. To analyse whether N-cad could be found at cell-cell contact points, DNP53-SCs and DNp53-Ras-SCs were treated with DMSO or PD184352 for 24 hours before fixing and

immunolabelling for N-cad. As expected, control DNp53-SCs had a similar morphology to normal Schwann cells and N-cad localised at the junctions (arrows) (Figure 4.5B). In contrast, DNp53-Ras-SCs appeared to have a more rounded morphology, and while most of the N-cad localised perinuclearly, it could still be found at contact-points between DNp53-Ras-SCs (Figure 4.5B). However, these contacts appeared not to be stable, as DNp53-Ras-SCs are highly dynamic and invasive (Figure 4.5B; Movie 4.1). Strikingly, junctions were completely recovered upon inhibition of MEK, confirming that oncogenic Ras disrupts stable junction formation in a MEK dependent manner.

4.3. Assessing homotypic CIL of DNp53-Ras Schwann cells

N-cad is classically known to form adhesion complexes in which it interacts with other cadherin molecules in *trans* or *cis* (Brasch et al., 2012). However, as described in the previous chapter, N-cad has been shown make heterophilic interactions in *cis* with other molecules such as the FGF receptor, to regulate axonal growth and the invasion of MCF-7 cells. Moreover, it has been shown that the FGF receptor interacts in *cis* with a motif present in the EC4 domain of N-cad (Williams et al., 2001). In a separate study in epithelial cells, E-cad has been shown to form a complex with ADAM10, and EphB2 (Solanas et al., 2011). The interaction of E-cad with ADAM10 and EphB2 is required for the sorting of EphB2-expressing epithelial cells. Cleavage of E-cad by ADAM10 following activation of EphB2 by Ephrin B induces cell sorting of the EphB-expressing cells through differential adhesion.

In initial experiments, we determined how long it takes for DNp53-Ras-SC to regain the ability to recognise each other following inhibition with the MEK1/2 inhibitor, PD184352, in order to determine the kinetics of the mechanisms involved. DNp53-Ras-SCs were seeded at low density and imaged for 6 hours before adding

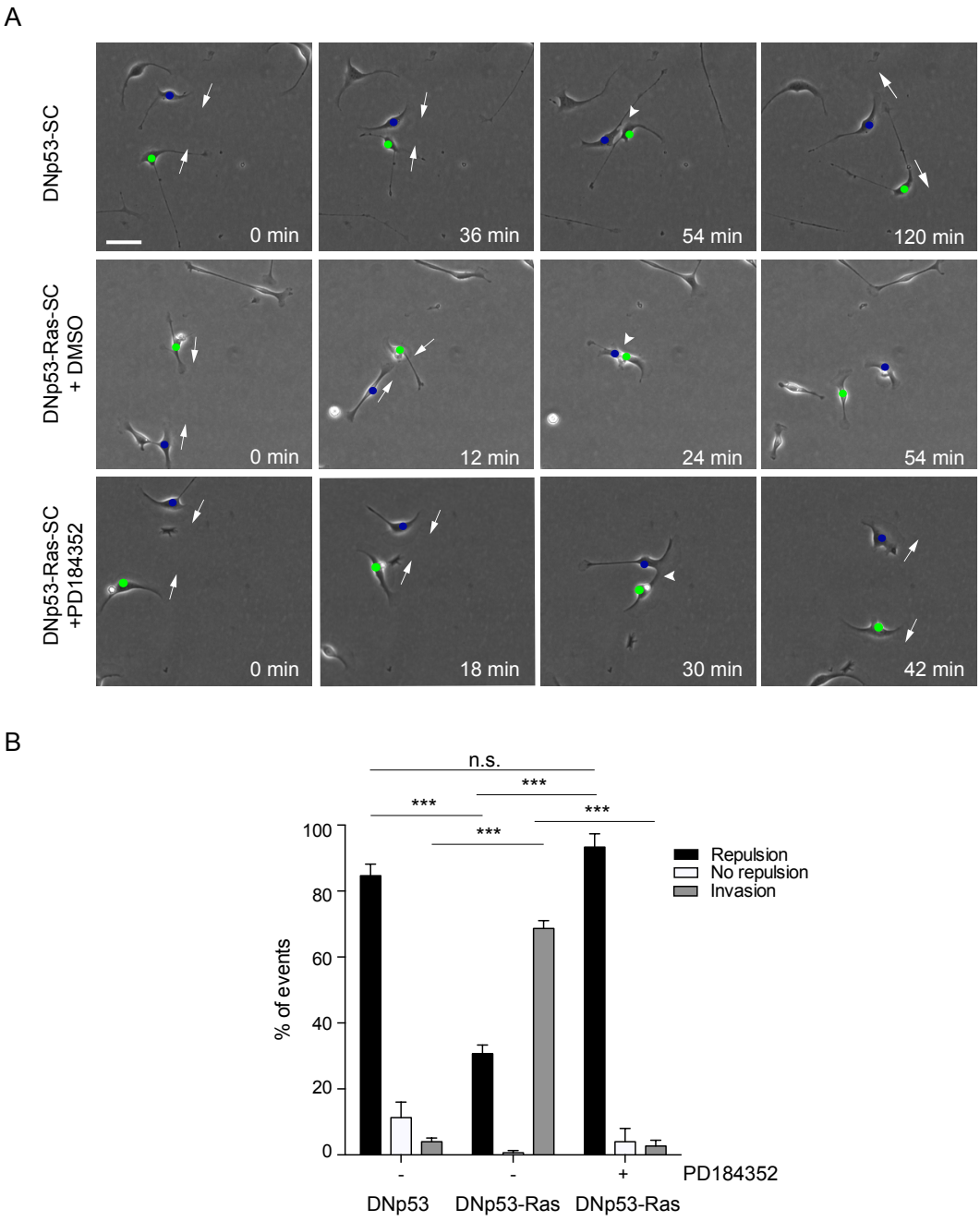

Figure 4.4. CIL in Schwann cells expressing Ras is lost in a MEK dependent manner.

(A) Time-lapse microscopy images of DNp53-SCs or DNp53-Ras-SCs in the presence of control solvent (DMSO) or MEK inhibitor PD184352 (0.75 µM) for 18 hours before imaging for a further 24 hours. Interacting cells are indicated by blue and green dots. White arrows indicate direction of migration. Black arrowheads indicate a repulsion response for DNp53-SC or DNp53-Ras-SC + PD184352 or invasion for DNp53-Ras-SC+DMSO. Scale bar 100µm. **(B)** Quantification of A in which 50 cells per condition were analysed. Graph shows the mean ± SEM of three independent experiments. Related to movie 4.1.

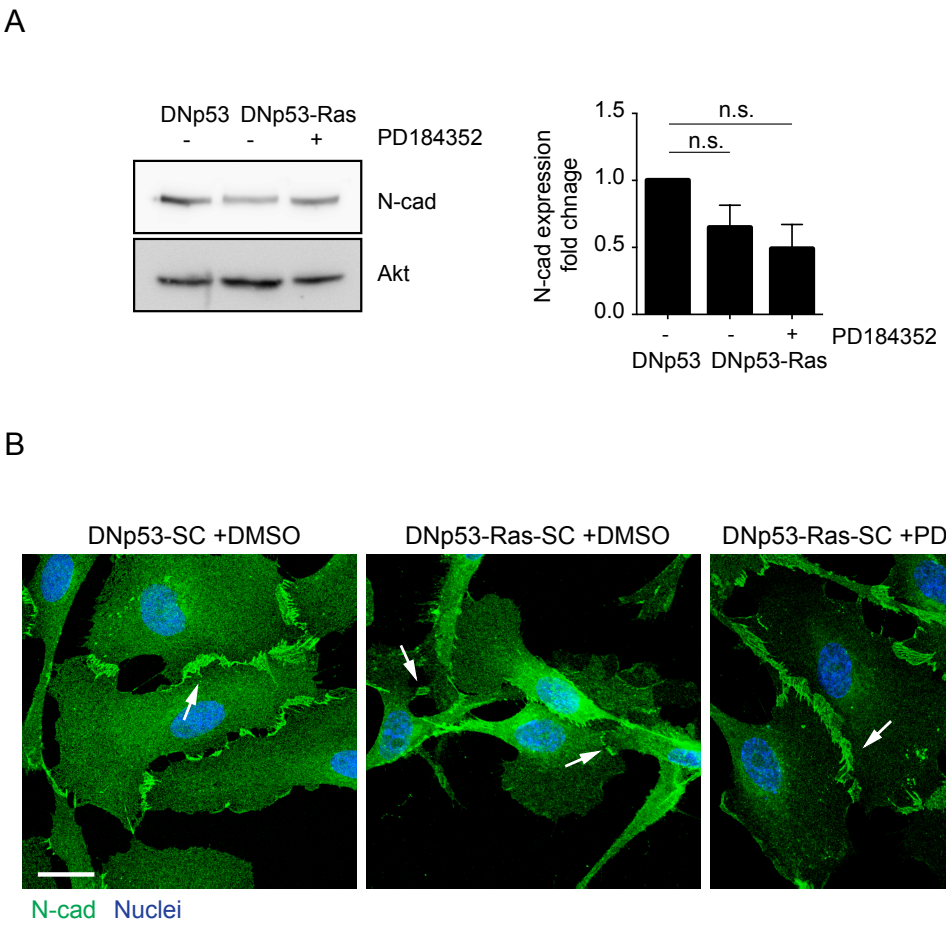

Figure 4.5. Loss of CIL in DNp53-Ras-SCs is not due to aberrant expression of N-cad.
(A) Left: Western blot showing N-cad expression levels in DNp53-SCs (DNp53) or DNp53-Ras-SCs (DNp53-Ras) in the presence of DMSO or PD184352 (0.75µM) at 48 hours. Akt was used a loading control. Right: Quantification of N-cad expression. Graph shows three experiments ±SD. Statistics: One-way ANOVA, Dunnett's multiple comparisons test. **(B)** Representative confocal images of DNp53-SCs or DNp53-Ras-SCs either in the presence of DMSO or PD184352 for 24 hours, immunostained for N-cad (green) and costained with Hoechst to label the nuclei (blue). Arrows indicate N-cad positive cell-cell contacts. Scale bar 20µm.

DMSO or PD184352 and then further imaged for another 24 hours. Interestingly, DNp53-Ras-SCs treated with PD184352 were initially invasive, however after approximately 10 to 14 hours their behaviour changed: cells appeared to slow down, spin around in circles, and changed the direction of migration more frequently, before starting to migrate again, suggesting a sort of reprogramming of the cell (Movie 4.2).

Importantly, while DNp53-Ras-SCs were initially invasive, over time more repulsion events could be detected, suggesting MEK inhibition does not affect CIL immediately but rather, restores CIL slowly, consistent with a change in gene expression (Movie 4.2). These results are also consistent with the observation that NR-SCs treated with TMX take several hours (>8h) to show a CIL phenotype (unpublished observations). To quantify this change in behaviour over time, repulsion, invasion and no repulsion events were measured between 0-12 hours and 12-24 hours after adding PD184352 or control-solvent (DMSO). Between 0-12 hours in PD184352-treated cells there was a small increase in repulsion events (from ~20% to ~40%) compared to DMSO control, while there was a decrease of invasion events (from ~70% to ~50%), suggesting that CIL was restored in some of the cells (Figure 4.6A). From the movies however, it could be seen that the majority of these changes took place towards the end of the time frame. To quantify this, CIL was measured between 0-8hours after adding PD184352 or control-solvent (DMSO). This showed that between these time-points there was no significant change in repulsion or invasion, consistent with longer-term changes being required (Figure 4.6B; Movie 4.2). In contrast, in PD184352-treated cells, CIL was completely restored to control levels between 12-24 hours (Figure 4.6A). This suggests that CIL is restored slowly, indicating that loss of CIL in Schwann cells expressing oncogenic Ras is mediated through MEK-dependent changes in gene expression.

Strong molecular candidates for a playing role in CIL are the Eph receptors and their ligands. They have been shown to play a role in CIL between PC3 cells and glioblastoma cells and play a crucial role in cell sorting, such as we observed in Schwann cells and has been extensively studied in the sorting of epithelial cells in the intestine (Astin et al., 2010; Batlle et al., 2002; Parrinello et al., 2010; Solanas et al., 2011; Tanaka et al., 2012). To test if the mRNA expression levels of the Eph

receptor family are regulated through the Ras-ERK pathway, DNp53-SCs and DNp53-Ras-SC were cultured in the presence of DMSO or PD184352 for 36 hours before RNA extraction. Subsequently the mRNA expression levels were assessed by RT-qPCR.

There are in total 10 EphA receptors and six EphB receptors that preferentially bind six Ephrin-A ligands and three Ephrin-B ligands respectively. We designed primers for the Ephrin-A ligands, Ephrin-A1, -A2, -A3 and -A4, and EphA receptors EphA1, A2, A3, A4, A5, A6, A7 and A8. In addition, we used primers previously validated by our lab for EphB1, B2, B3, B4, B6, A4, Ephrin-B1, -B2, -B3 and -A5 (Parrinello et al., 2010). The expression of EphA9, EphB5 and Ephrin-B6 appear not to be present in the human or mouse genome and so were not analysed (Figure 4.7A) (Cunningham et al., 2015).

4.4. A candidate approach to determine the co-signal in CIL

The expression of EphA6, EphA10, EphB5, Ephrin-A5, and Ephrin-B3 could not be detected in either DNp53-SC or DNp53-Ras-SC, suggesting they are not expressed in these cells (Figure 4.7A). Moreover, the lack of expression of Ephrin-A5 and Ephrin-B3 in DNp53-SCs is consistent with previous results (Parrinello et al., 2010).

Interestingly, Ras expression had multiple, dramatic effects on the expression levels of ephrin ligands and receptors of both families.

Ephrin-A ligands: All ephrin A ligands were downregulated by Ras expression in a MEK-dependent manner. Ephrin-A2 was more strongly downregulated than ephrin-A1, Ephrin-A3 and Ephrin-A4, and was only partially rescued by MEK inhibition indicating other pathways may be involved (Figure 4.7C).

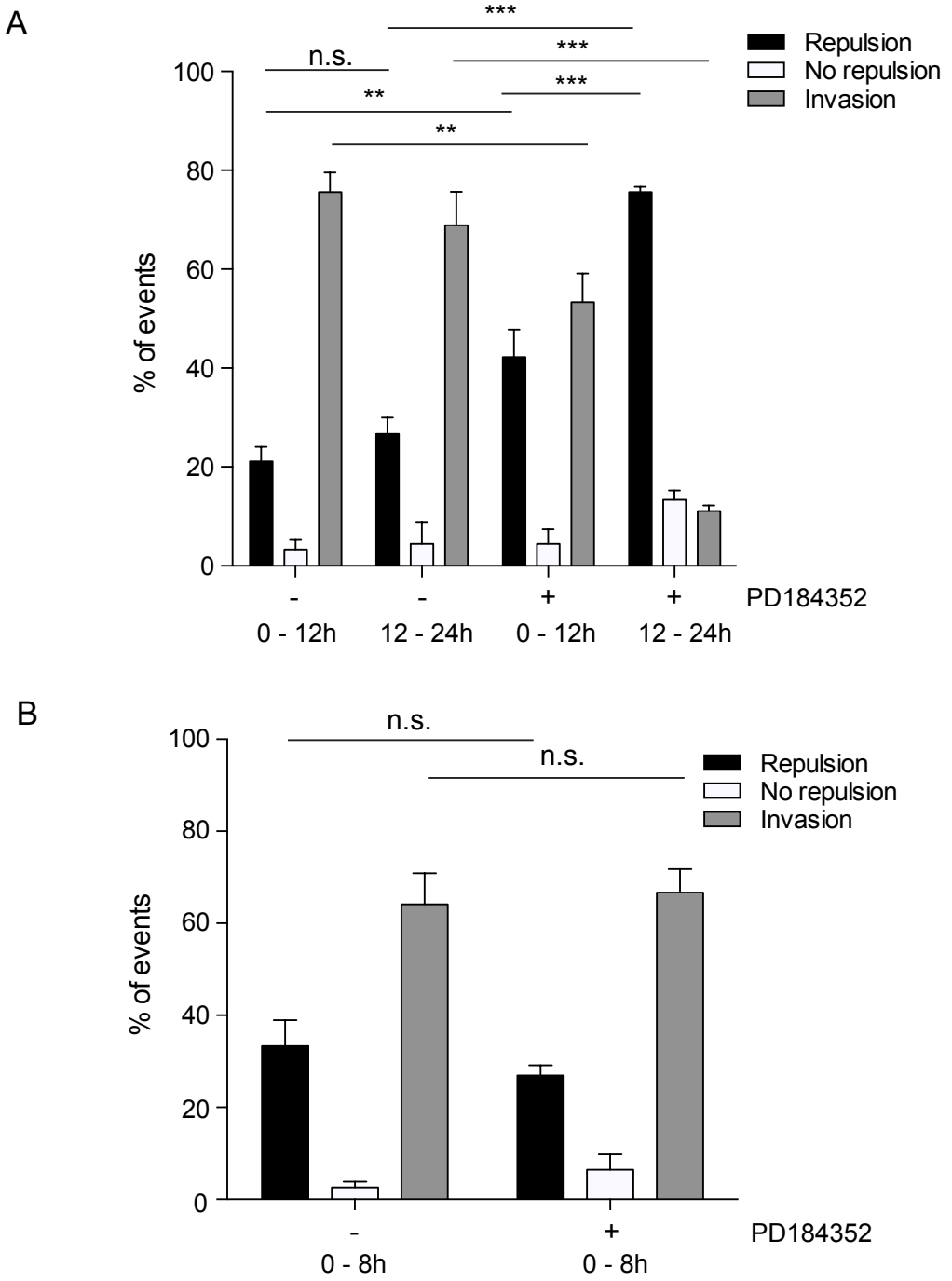

Figure 4.6. The kinetics of PD184352 induced CIL restoration in Ras-expressing cells is slow.

A) Graph showing a time-course of homotypic CIL between DNp53-Ras-SCs in the presence of control solvent (DMSO) or the MEK inhibitor PD184352 (0.75µM). Repulsion, no repulsion and invasion events of 30 cells were quantified in two timeframes 0-12 hours and 12-24 hours. B) Similar experiment as in (A) in which repulsion, no repulsion and invasion events of 26 cells were quantified between 0-8 hours. Bars represent three independent experiments ±SEM. Related to Movie 4.2.

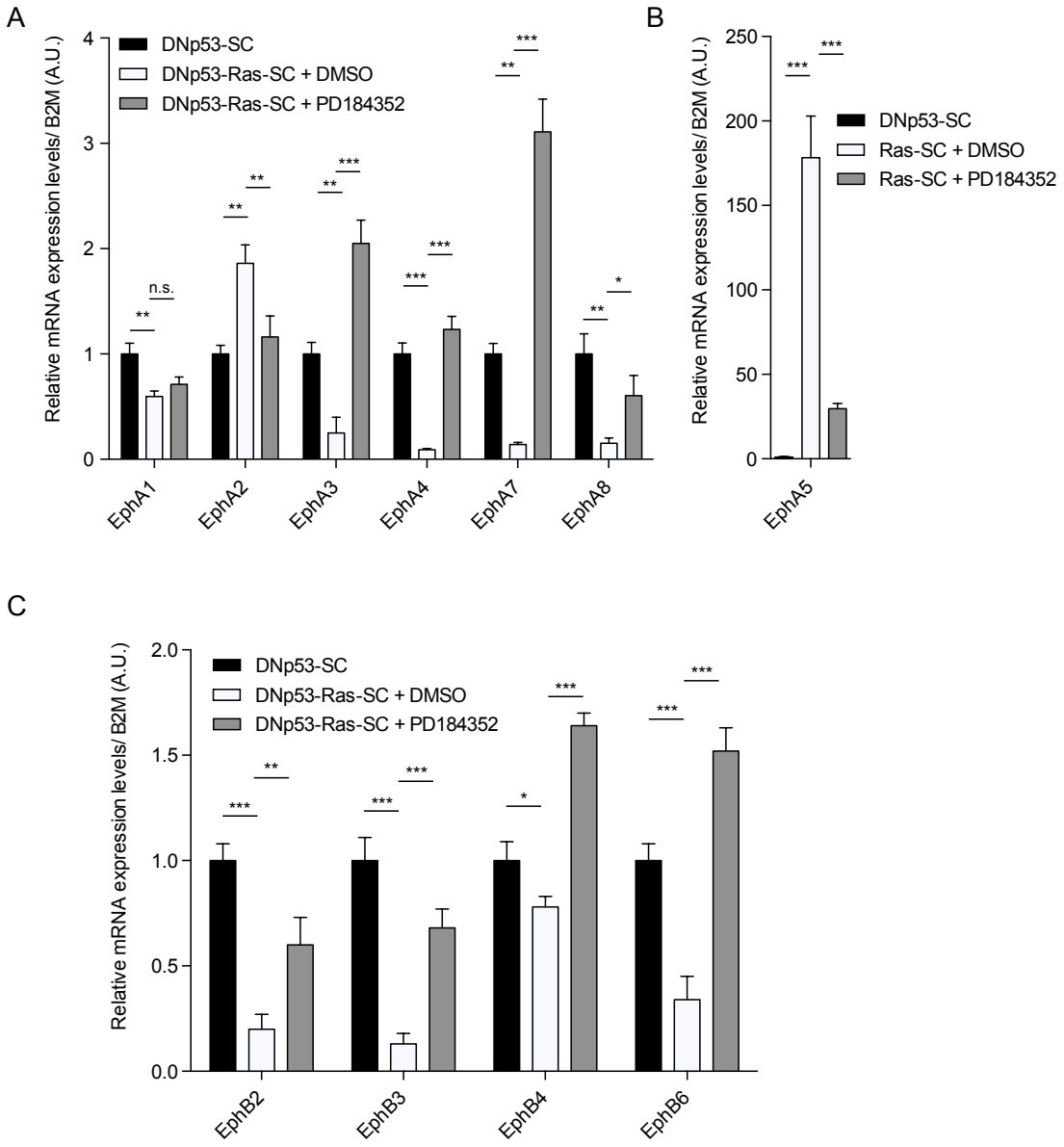

Figure 4.7. Oncogenic Ras induces changes in the mRNA expression of the Eph receptor family in a MEK dependent manner.

(A) Table of Eph receptors and ligands that appear to not be present in the human or mouse genome, and not expressed by DNp53-SCs and DNp53-Ras-SCs**. (B-C)** Quantitative RT-q-PCR analysis of Ephrin-A ligands and Ephrin-B ligands in DNp53-SCs and DNp53-Ras-SCs treated with DMSO or PD184352 (0.75μM) for 36 hours. Bars show the mean ±SEM of three experiments. Statistics: Two-way ANOVA Sidaks' multiple comparison test

A

Not expressed in human, mouse or rat	Undetectable in DNp53-SC
EphA9	EphA6
EphB5	EphB1
Ephrin-A6	EphB5
	EphB10
	Ephrin-A5
	Ephrin-B3

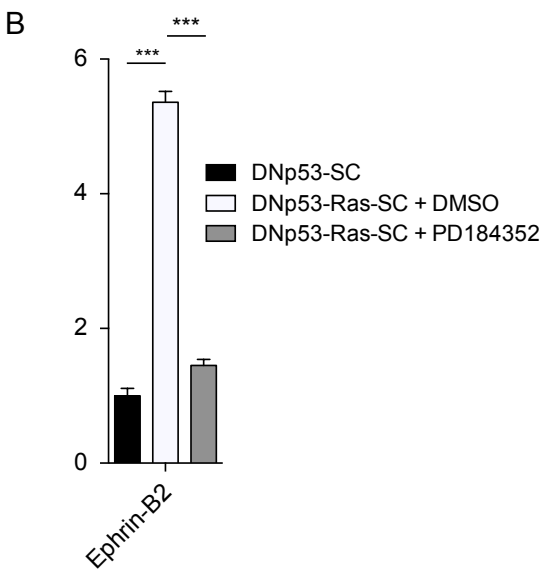

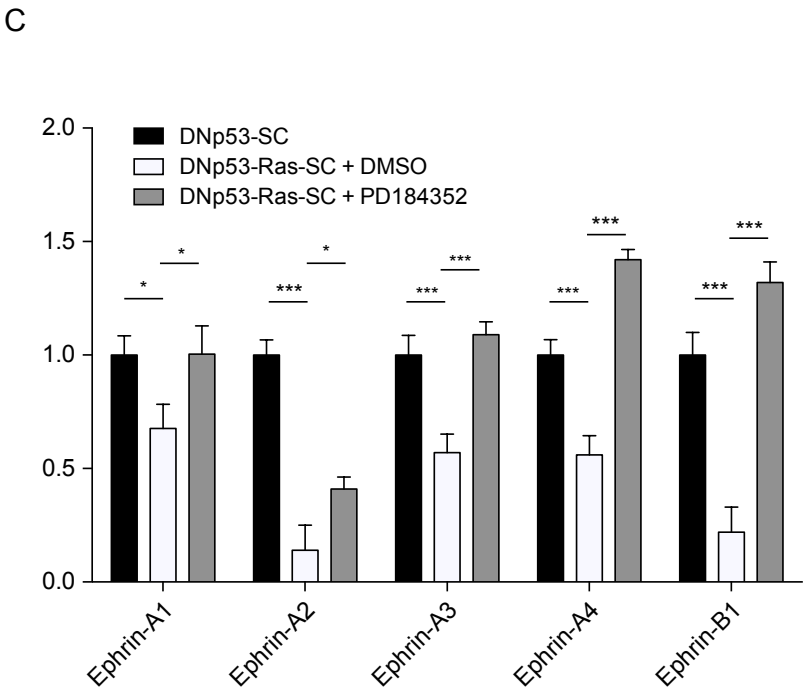

Figure 4.8. Oncogenic Ras induces changes in the mRNA expression of the Eph receptor family in a MEK dependent manner.

(A-C) Quantitative RT-q-PCR analysis of EphA receptors (A and B) and Eph-B receptors (C) in DNp53-SCs and DNp53-Ras-SCs treated with DMSO or PD184352 (0.75µM) for 36 hours. Results are shown relative to the expression in DN-p53SCs. Bars show the mean ±SEM of three experiments. Statistics: Two-way ANOVA Sidaks' multiple comparison test

Ephrin B ligands: Ephrin-B1 is downregulated in response to Ras, while Ephrin-B2 is strongly upregulated, suggesting they respond differentially to Ras signalling (Figure 4.7B and C). However, both Ephrin-B1 and Ephrin-B2 are regulated by Ras in a MEK dependent manner, as expression can be restored to control levels (Figure 4.7B and C).

EphA receptors: The majority of these receptors were downregulated following Ras expression (EphA1, EphA3, EphA4, EphA7 and EphA8) (Figure 4.8A). EphA1 was only slightly down regulated, while EphA3, EphA4, EphA7 and EphA8 were strongly downregulated, suggesting the latter are important downstream targets of Ras (Figure 4.8A). In contrast EphA2 and EphA5 were upregulated (Figure 4.8A and B). There was a dramatic increase in EphA5 expression, in part due to undetectable levels in DNp53-SCs, suggesting it is not expressed in these cells and is thus unlikely to be involved in regulating CIL between DNp53-SCs (Figure 4.8B). Interestingly, apart from EphA1, all expression levels could be restored to control levels following MEK inhibition, suggesting Ras regulates these receptors in a MEK-dependent manner and so are potential candidates for having a role in CIL (Figure 4.8A). EphA1 is not regulated by Ras in an ERK dependent manner, suggesting other signals regulate its expression and it does not play a role in CIL (Figure 4.8A).

EphB receptors: EphB receptors are all downregulated upon expression of oncogenic Ras, though there is only a weak effect on the expression of EphB4, suggesting it is not such an important target of Ras (Figure 4.8C). Interestingly, EphB2 and EphB3 are strongly downregulated, which can be rescued almost to control levels upon inhibition of MEK, suggesting they have a similar response to Ras and are regulated in a MEK dependent manner (Figure 4.8C). EphB6 is also down

regulated, though the effect is not as strong compared to EphB2 and EphB3 (Figure 4.8C).

All together this shows that Ras regulates the expression of the majority of Eph receptors and their ligands, the vast majority in a MEK dependent manner, correlating to the regulation of CIL by Ras in a MEK dependent manner.

Next, we wanted to understand if activating the Raf/MEK/ERK pathway is sufficient to induce a change in expression patterns of the ephrins and Eph receptors. To test this, NR-SCs were used which express a Raf-inducible construct. Initially, cultures of NR-SCs were treated for 36 hours in the presence of TMX (0.1μM) or control solvent (ETOH) and grown to confluence to observe their behaviour. As expected, control-treated cells formed a confluent monolayer (Figure 4.9). In contrast, NR-SCs treated with TMX adopted a more 'spiky' phenotype, lost their homotypic junctions and grew on top of each other, suggesting they lost cell-cell recognition and that they behave similar to DNp53-Ras-SCs and N-cad knockdown Schwann cells (Figure 4.9). Moreover, it suggests that activation of Raf is sufficient to induce loss of cell-cell recognition, consistent with previous studies (Lloyd et al., 1997).

Subsequently, it was tested if activating Raf induces a change in the expression pattern of the Eph receptors and their ligands. NR-SCs were cultured either in the presence of EtOH or TMX for 36 hours before harvesting mRNA and analysing the expression of the Eph receptors and theirs ligands using RT-qPCR. Interestingly, the ephrin-A ligands were all downregulated showing that activating Raf is sufficient to regulate their expression (Figure 4.10 and Figure 4.7C). Importantly, the extent of downregulation of Ephrin-A2, Ephrin-A3, and Ephrin-A4 ligands appeared to be similar to that seen in DNp53-Ras-SCs (Figure 4.10A and Figure 4.7C) confirming that regulation of these ligands is through the Ras/Raf/MEK/ERK

pathway. In contrast, Ephrin-A1 appeared more strongly downregulated in NR-SCS treated with TMX compared to the DMSO-treated DNp53-SCs, which could be due to the stronger activation of the ERK signalling pathway in NR-SCs compared to Ras-expressing cells (Figure 4.10A and Figure 4.7C).

Moreover the Ephrin-B ligands were also regulated similarly, as ephrin-B1 is down regulated while Ephrin-B2 is upregulated, confirming that regulation of these ligands is through the Raf/MEK/ERK pathway and that Raf differentially regulates these ligands (Figure 4.10A and B and Figure 4.7B and C).

Of the EphA receptors, EphA2 and EphA-5 were upregulated, while EphA-1, EphA3, EphA4 EphA47 and EphA8 were all downregulated, recapitulating the expression patterns in Schwann cells expressing oncogenic Ras. This suggests that activating Raf is sufficient to regulate the expression of these receptors. Similarly, all the EphB receptors were down regulated similarly to how Ras regulated the EphB receptors. However EphB6 was not as strongly downregulated compared to Ras, suggesting Raf activation is not sufficient to inhibit the expression of EphB6 (Figure 4.10C see also Figure 4.8C).

All together, these data demonstrates that Ras signalling has a fundamental role in controlling the expression levels of ephrin receptors and their ligands which is likely to have dramatic effects on the behaviour of Ras-expressing cells. This regulation acts mostly via the Raf/ERK signalling pathway. It remains to be determined how these changes affect the behaviour of these cells and the role in tumourigenesis.

4.5. The role of ephrins in homotypic CIL

We have previously shown that cell sorting of fibroblasts and Schwann cells is dependent on Ephrin-B to EphB2 signalling, which induces the translocation of N-cad

to the membrane in a Sox-2 dependent manner, which causes the Schwann cells to cluster (Parrinello et al., 2010). This showed that Ephrin-B to EphB2 signalling is important in heterotypic signalling between fibroblasts and Schwann cells. Although we showed in co-cultures that upon heterotypic interactions of Schwann cells with fibroblasts, Schwann cells switch their behaviour from repulsion to attraction, it does

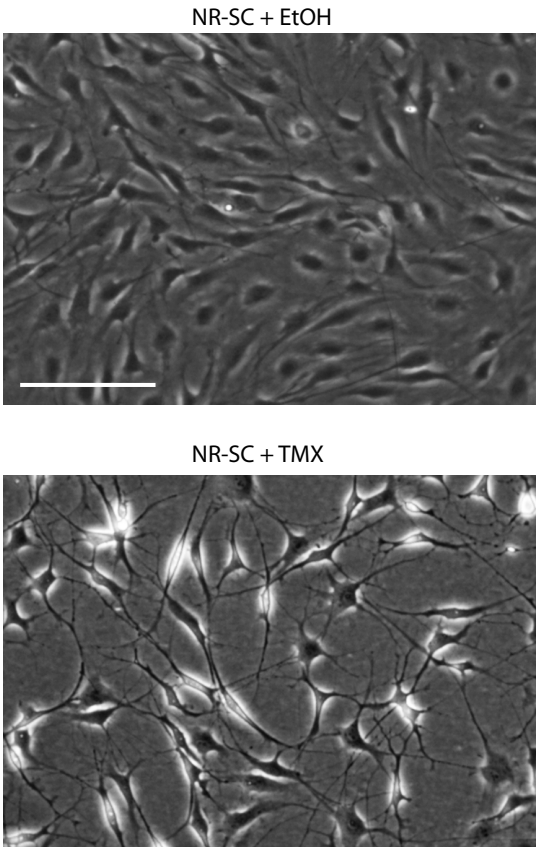

Figure 4.9. Raf-activation is sufficient to induce loss of cell-cell recognition between Schwann cells.
Representative phase-contrast images of Schwann expressing a Raf-inducible construct (NR-SC) in the presence of control solvent EtOH (monolayer) and TMX (loss of monolayer).

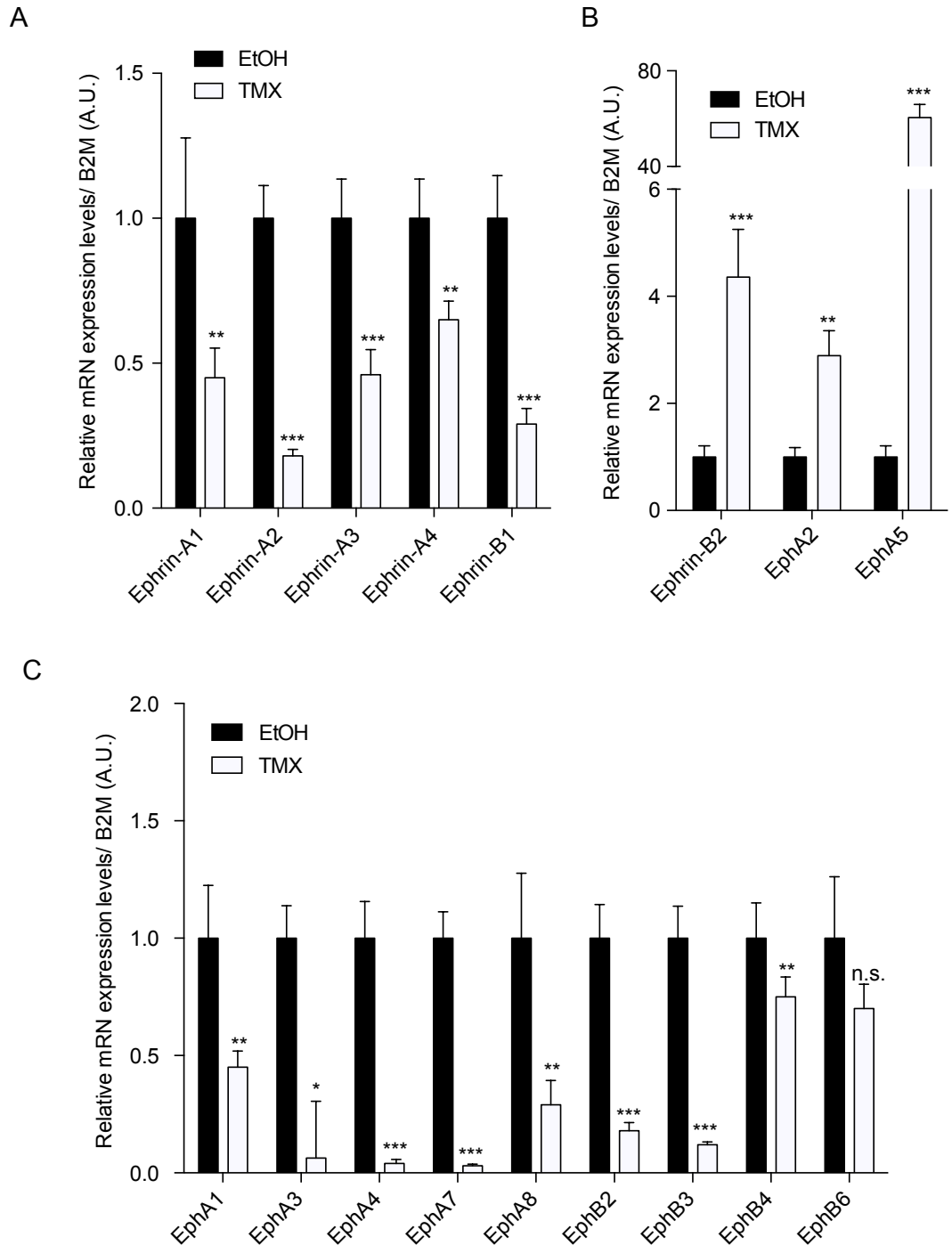

Figure 4.10. Raf activation is sufficient to induce changes in mRNA expression levels of the Eph receptor family.

(A-D) Quantitative RT-PCR analysis of Ephrin-A ligands, Ephrin-B ligands, EphA and EphB receptors in NR-SCs treated with TMX relative to controls NR-SCs treated with EtOH, for 36 hours. Bars show the mean ±SEM of three experiments. Statistics: multiple T-Test

not necessarily imply that the CIL signal between these cells is also mediated by Ephrin-B to EphB2 signalling. To test if Ephrin-B to EphB2 signalling mediates heterotypic CIL between fibroblasts and Schwann cells, my colleague Dr. Victor Quereda treated Schwann cells either with scrambled siRNA or EphB2 siRNA for 36 hours before co-culturing with primary fibroblasts, live-imaging for 24 hours and analysing CIL. Interestingly, in the vast majority of the cases, upon contact with a fibroblast, Schwann cells appeared to "bounce" off the fibroblasts, a process associated with the retraction of protrusions and a change in the direction of migration suggesting there is heterotypic CIL between Schwann cells fibroblasts (Movie 4.3; Figure 4.11A). In contrast, the EphB2 knockdown Schwann cells appeared to repulse less frequently upon contact with fibroblasts, but rather there was a change in the behaviour of the Schwann cells, with many appearing to no longer migrate away following contact, suggesting the Schwann cells were no longer repulsed by the fibroblasts (Figure 4.11A; Movie 4.3). Dr. Victor Quereda quantified this behaviour and found that knockdown of EphB2 in Schwann cells resulted in a large increase in the number of cells that were not repulsed by fibroblasts. However, in contrast to Ras-expressing cells, the Schwann cells did not invade the fibroblasts suggesting that further signals may be needed for invasion (Figure 4.11A and data not shown). This indicates, that CIL between primary fibroblasts and Schwann cells is mediated through EphB2 signalling.

Given that the EphB2 induced repulsion signal between primary fibroblasts and Schwann cells induces Schwann cells clustering, we reasoned that EphB2 would not mediate CIL between Schwann cells, as this would also be predicted to cause clustering. To confirm this hypothesis, EphB2 was knocked down using siRNA-targeting EphB2 in Schwann cells and the effects on CIL were analysed. As expected, scrambled-treated Schwann cells repulsed upon contact (Figure 4.11B).

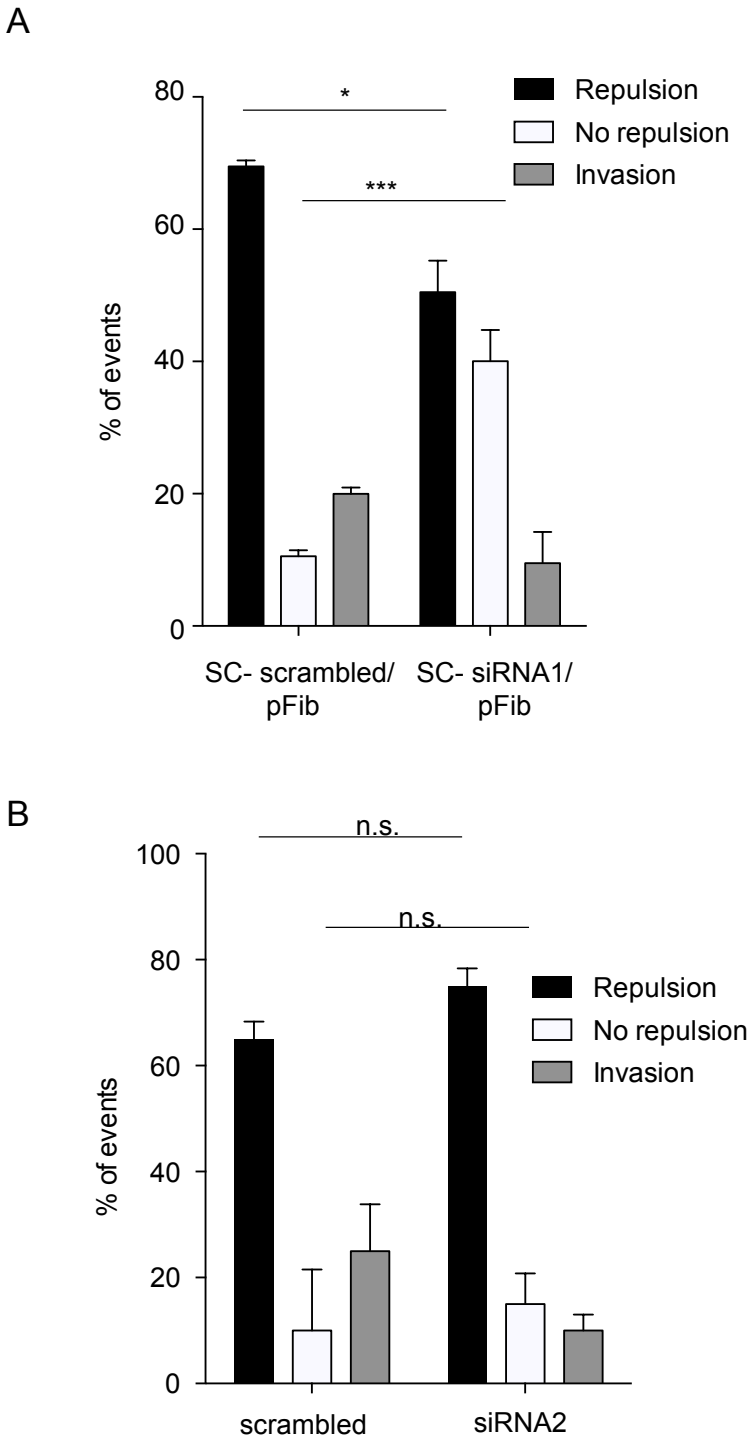

Figure 4.11. Homotypic CIL and heterotypic CIL in Schwann cells are mediated through different mechanisms.

(A) CIL analysis between primary fibroblasts (pFib) and scrambled- or EphB2 siRNA treated Schwann cells. Bars represent mean ±SD of three experiments. **(B)** Quantification of CIL between Schwann cells treated with scrambled siRNA or EphB2 siRNA. 10 cells per condition were quantified. Bars represent mean ±SEM of three experiments. Related to Movie 4.3.

Moreover, EphB2 knockdown cells also appeared to behave like control cells, as they were also repulsed upon contact, suggesting EphB2 is not required for homotypic CIL (Movie 4.3 and quantified in Figure 4.11B). Thus, this data shows that while heterotypic CIL between fibroblasts and Schwann cells is dependent on EphB2 signalling, homotypic CIL is independent of EphB2 signalling. Moreover, N-cad appears to regulate homotypic CIL between Schwann cells by both inhibiting forward protrusion formation and stimulating repulsion, so loss of N-cad results in invasion. In contrast, whilst cells lacking EphB2 are no longer repulsed by fibroblasts they don't invade the cells indicating that the mechanism inhibiting forward protrusion remains intact.

Ephrin-A/EphA signalling has previously been shown to regulate homotypic CIL in PC3 cells by halting forward migration (Astin et al., 2010), and has been shown to play a role in tumour spread of PC3 cells *in vitro*, by mediating repulsion between the cells resulting in outward migration away from the cell mass, which leads to local single cell invasion (Batson et al., 2014). In the previous chapter, we showed that N-cad provides a signal, which is required to induce a repulsion response, but that it is not required for a cell to be repulsed in a N-cad dependent manner. This could suggest that N-cad is involved in presenting a ligand as a repulsion signal to the other cell. Interestingly, though Eph receptor engagement with its ligands can induce bidirectional signalling through both receptor and ligand, Ephrin-A ligands are GPI-linked proteins that do not have a cytoplasmic tail through which they can signal (Lisabeth et al., 2013). However, recent work has shown that Ephrin-A ligands can also signal back into the cell via interactions with the neurotrophin receptors p75, TrKB and Ret to regulate axonal growth (Bonanomi et al., 2012; Lim et al., 2008; Marler et al., 2008). Therefore it remains a possibility that either the Ephrin-A ligand or receptor could act as a repulsion signal.

In initial experiments to test whether EphrinA/EphA signalling may be involved in homotypic CIL, Schwann cells were stimulated with pre-clustered Ephrin-A-Fc chimeras, which by inducing the retraction of cell protrusions (cell rounding), could possibly be an indication of CIL (Astin et al., 2010). The Ephrin-A1 and Ephrin-A4 ligands mRNA expression levels are regulated by Ras in a MEK dependent manner, and their expression correlates with the absence and resumption of CIL in DNp53-RAS treated with PD1184352 (Figures 4.2B and 4.7C), possibly suggesting they could play a role in CIL. Moreover, Ephrin-A1 has been shown to play a role in CIL (Astin et al., 2010), and out of the four Ephrin-A ligands, Ephrin-A1 and Ephrin-A4 appeared to have the highest expression levels based on the mRNA analysis (see Table 4.1).

	Ephrin-A1	Ephrin-A2	Ephrin-A3	Ephrin-A4
DNp53-SC	0.010	0.003	0.001	0.011
DNp53-Ras-SC	0.007	0.000	0.001	0.006

Table 4.1 Expression levels of Ephrin-A ligands in DNp53-Schwann cells and DNp53-Ras-Schwann cells
Shown are the ΔΔCT of the mRNA detection levels of Ephrin-A ligands in DNp53-Schwann cells (DNp53-SCs) and DNp53-Ras-Schwann cells (DNp53-Ras-SCs) normalised to the housekeeping gene B2M. N=3

Therefore it was tested if Ephrin-A1 and/or Ephrin-A4 binding can induce Schwann cell rounding. To test this, Schwann cells were seeded onto laminin-coated coverslips and treated for 20 min with either control-Fc or pre-clustered Ephrin-Fc chimeric ligands, before PFA fixation. Subsequently, the coverslips were stained with phalloidin to visualise the actin cytoskeleton and the morphology of the cells, and immunolabelled for anti-Fc to visualise the EphrinA-Fc and Fc-control chimeras. Images were taken using confocal microscopy and maximal projections are shown (Figure 4.12A). Ephrin-A1 and Ephrin-A4 localised as small puncta in the Schwann cells (insets) (Figure 4.12A middle and right panel), whereas, as might be expected, control-Fc cannot be detected as it cannot bind to a receptor (insets) (Figure 4.12A,

left panel). This suggests that both Ephrin-A1 and Ephrin-A4 can bind to receptors on Schwann cells. However, it appears Ephrin-A4 binds less to Schwann cells than Ephrin-A1, suggesting a differential binding of the ligands. As expected, control-Fc-treated cells had a bipolar morphology and normal actin cytoskeleton organisation, suggesting control-Fc does not have an effect on Schwann cells (Figure 4.12A). Intriguingly, treatment of the cells with Ephrin-A1-Fc appeared to induce a proportion of the cells to round up, suggesting ephrin-A1 binding to the cells induces retraction of the cell periphery a feature of CIL (Figure 4.12A middle panel). Moreover, cell rounding appeared to be associated with a strong rearrangement of the actin cytoskeleton to a more cortical distribution, suggesting Ephrin-A1 ligation regulates the actin cytoskeleton. In contrast, Ephrin-A4-Fc-treated cells appeared less affected, with fewer cells showing a rounded morphology (Figure 4.12A right panel). Moreover, in some of the cells, stress fibres could be observed suggesting Ephrin-A4 binding to the cells induces a change in the actin cytoskeleton (Figure 4.12A right panel). To quantify the effect on cell rounding, the ratio between the length and width of a cell was measured to determine the cell-rounding index. As expected, the majority of the control cells have a low cell-rounding index, consistent with the bipolar morphology of Schwann cells (Figure 4.12B). In contrast, the Ephrin-A1-Fc treated cells showed a marked shift towards a higher cell-rounding index, consistent with a rounding of the cells (Figure 4.12B). In Ephrin-A4-Fc-treated cells, there was a slight trend towards a higher cell-rounding index but the differences were not significant indicating a minor, if any, effect of Ephrin-A4 on cell rounding (Figure 4.12B).

These results show that both Ephrin-A1 and Ephrin-A4 can bind to Schwann cells but the effect of Ephrin-A1 appears to be more potent; Ephrin-A4 induced only a mild response upon binding, while Ephrin-A1 induced retraction of the cell periphery, which was associated with a rearrangement of the actin cytoskeleton. This could

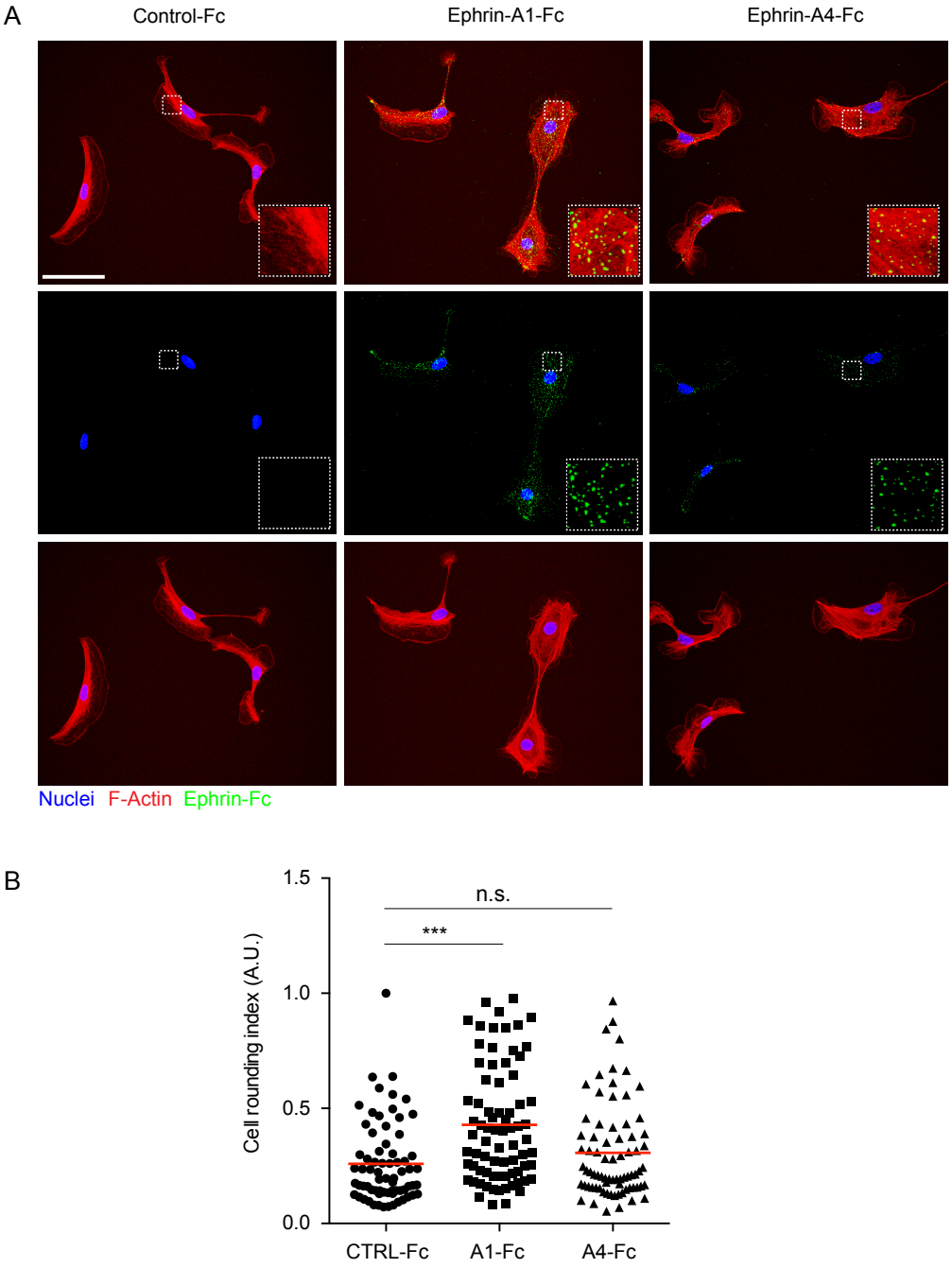

Figure 4.12. Clustered Ephrin-A1 induces Schwann cell rounding.
(A) Representative confocal images of Schwann cells treated with control-Fc, ephrin-A1-Fc or Ephrin-A4-Fc, immunostained for anti-Fc (green) and co-stained with phalloidin (red) to visualise the actin cytoskeleton and Hoechst to stain the nuclei (blue). Insets show a magnification of the actin cytoskeleton and the Ephrin-A ligands. Scale bar 20µm. **(B)** Quantification of (A) in which cell rounding was measured. n=75 cells in three independent experiments. Red line represents mean. Statistics: One-way ANOVA Kruskal-Wallis test.

suggest that Ephrin-A1 may play a role in CIL, however this needs further investigation.

Fyn is a downstream target of Ephrin-A reverse signalling in axons and is important for regulating the repulsion response (Lim et al., 2008). To test if Fyn is important for homotypic CIL between Schwann cells, Fyn was inhibited by adding the Fyn inhibitor SU6656 (250 nM) for one hour before live-imaging the cells for 24 hours. As expected, the majority of control DMSO-treated Schwann cells, were repulsed upon contact (Movie 4.4; Figure 4.13A). However, the SU6656-treated cells behaved similarly to control cells suggesting that Fyn is not required for CIL (Movie 4.4; Figure 4.13A and quantified in 4.13B). However, while Fyn inhibition failed to block CIL, it did block cytokinesis (Movie 4.4) consistent with previous reports (Yasunaga et al., 1996), demonstrating that the inhibitor was active in these experiments.

4.6. Mass spectrometry

In the second approach to identify a potential N-cad dependent repulsion signal, proteins that interact with N-cad in Schwann cells were analysed using Co-IP and mass spectrometry (Mass Spec). Moreover, to identify interactions that might be disrupted upon the activation of the Ras/Raf/ERK pathway, the interactions were compared to those of cells with an activated ERK pathway. To do this, NR-SCs were used which allowed a switch between repulsion and invasive behaviours by TMX induced Raf activation (Figure 4.10). In order to retain as many interactions as possible, preliminary Co-IP experiments were performed in different detergents to determine the least stringent conditions in which known interactions could be preserved. For these experiments, the NR-SCs were seeded at low density, as upon high confluency control NR-SC form stable junctions possibly disrupting interactions

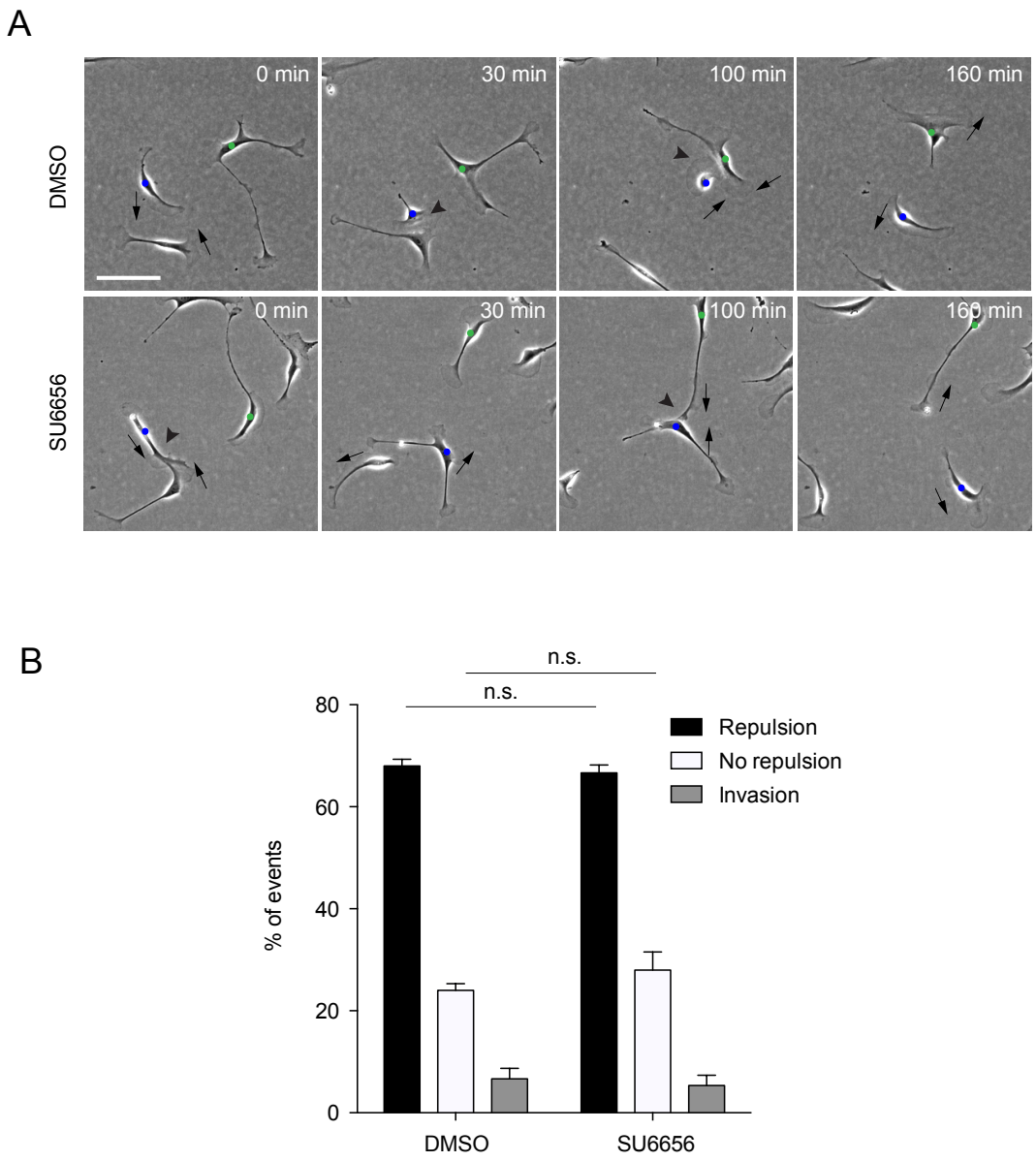

Figure 4.13. Fyn inhibition does not affect CIL.
(A) Representative still images from time-lapse microscopy of a CIL assay in which Schwann cells were treated with DMSO or the Fyn inhibitor SU6646 (250nM) for one hour before starting imaging. Cells of interest are indicated by green and blue dots. Arrows show the direction of migration, arrowheads indicate repulsion events. **(B)** Quantification of (A), 30 cells per condition per experiment were quantified. Bars represent mean ±SEM of three experiments. Related to Movie 4.4.

of N-cad with a potential repulsion signal. NR-SCs were cultured for 36 hours either in the presence of TMX or control solvent (ETOH). Subsequently, protein was harvested using different lysis buffers and immunoprecipitation of N-cad was performed followed by Western blotting to detect interacting proteins. For all

detergents tested, the interaction between N-cad and the known adherence junction complex components could only be detected in the 1% NP40 buffer. Therefore, the results for the 1% NP40 lysis buffer are shown, as these were the conditions used for later experiments.

N-cad could be detected in similar amounts in all conditions in the input lanes (Figure 4.14) and similar amounts of N-cad were detected in the EtOH and TMX conditions following IP of N-cad, consistent with the similar levels of N-cad in these cells. As expected, N-cad was not detected in IgG control (Figure 4.14). In these conditions, interactions with the known interacting proteins β-catenin, α-catenin and p120-catenin could all be detected. Consistent with the findings described in chapter 3, these interactions were unaffected by activation of the Raf/MEK/ERK signalling pathway confirming that activation of this pathway does not affect either the levels of N-cad or the ability of N-cad to interact with these junctional proteins.

These conditions were then used to prepare samples for qualitative Mass Spec analysis. The Co-IP was performed on one sample per condition using 1mg protein as input, and the proteins were eluted from the beads using Laemmli buffer. The proteins were then separated on a gel, the proteins were extracted from the gel, digested with trypsin and analysed using the LTQ Orbitrap Velos Pro Mass-spec systems (Performed by Proteomics Facility, University of Dundee). The obtained data was analysed using the Mascot search engine using the Uniprot DB with rat as the taxonomic filter (performed by the Proteomics Facility, University of Dundee).

The obtained data, showed that in the control (repulsing) cells, there were 622 proteins identified in the N-cad sample, whereas 588 proteins were identified in the IgG control that can be considered background levels (See Table 4.2 and appendix for complete lists Tables 1 and 2). In the cells treated with TMX (invasive cells), 531 proteins were identified in the IgG control, while 672 proteins were

identified in the N-cad sample (See Table 4.2 and appendix Tables 3 and 4 for complete lists).

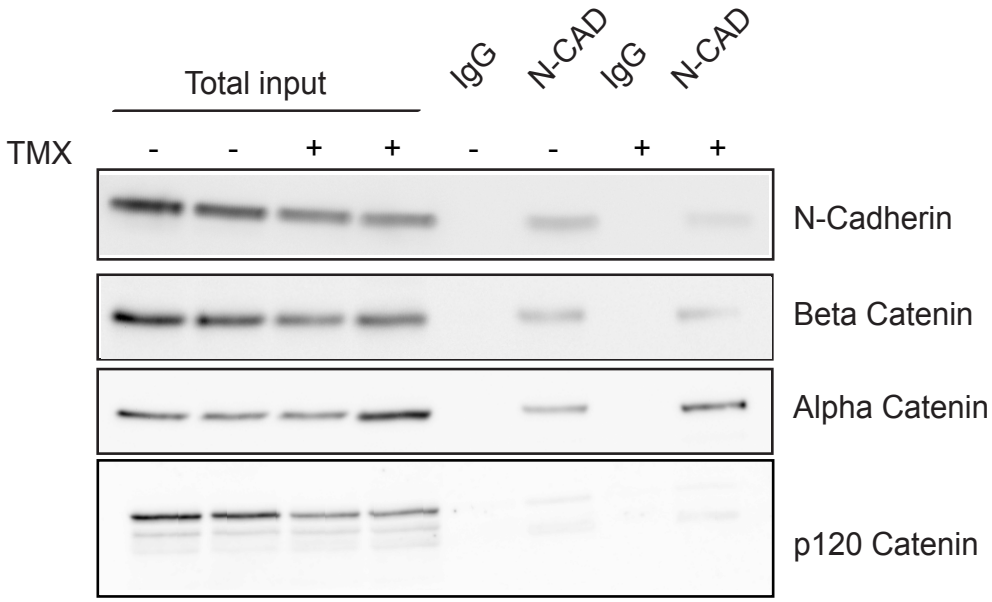

Figure 4.14. Raf-activation does not affect the adherence junction complex. Western blot analysis of Co-IP using an antibody to N-cad or control IgG of NR-SCs that were treated for 36 hours with EtOH (-) or TMX (+). Blots were probed for N-cad, beta-catenin, alpha-catenin or p120-catenin. Shown is a representative blot of three independent experiments with similar results.

To filter for background, N-cad pulled down lists were compared to the IgG control protein lists using http://www.cmbi.ru.nl/cdd/biovenn/ and the background proteins were removed. However, there is a caveat to this approach: N-cad and β-catenin were identified specifically in N-cad samples of both the EtOH and TMX conditions which was consistent with what was found in the Co-IP (Figure 4.14), while α-catenin and p120-catenin were also detected in the IgG controls. Thus, by excluding α-catenin and p120-catenin, which are known interacting proteins of N-cad, valuable data of unknown proteins that could be interacting with N-cad could be lost. To avoid this, proteins associated with a relatively low score in the IgG controls could be excluded from the analysis. The proteins identified on the lists are associated with a score in a range from 1–11,000, in which the higher the score the greater

confidence that the protein ID is correct and a higher likelihood of a higher abundance in the sample. α-catenin and p120-catenin in the IgG were associated with a low score (p120-catenin: EtOH [61] and TMX [116]; α-catenin: EtOH [157]), while in the N-cad samples these proteins were associated with a higher score (p120-catenin: EtOH [116] and TMX [309]; α-catenin: EtOH [2947.42]) (Appendix Tables 1-4). However, we reasoned that the repulsion signal might have a temporal or weak interaction with N-cad, and thus might be present in a low abundance and potentially have a low score. Therefore we decided to take two parallel approaches: first, we included all proteins with a low score and filtered for background by removing all proteins on the IgG control protein lists; second, we included all proteins with a low score and included all proteins with a large score difference between the N-cad samples and IgG controls, using an offset of 2.5 fold difference based on the lowest difference between the scores in the N-cad samples and IgG controls of p120-catenin (12.91 fold increase and 2.66 fold increase in EtOH and TMX samples respectively) and α-catenin (18.74 fold increase in the EtOH-treated samples) (Appendix Tables 5 and 6).

	IgG (♯ proteins)	N-cad (♯ proteins)
EtOH	588	622
TMX	531	672

Table 4.2. Summary of identified proteins.
Table showing the total number of proteins identified in the IgG controls or in the N-cad samples in NR-SCs treated with TMX and EtOH. n=1

The resulting protein lists of the first approach showed that there were 207 proteins identified in the control (EtOH) condition, while there were 262 proteins identified in the TMX condition (Appendix Table 7-9). In the second approach in which we include all proteins with a ≥2.5 fold difference in N-cad samples, five extra proteins were identified in the control cells including α- and p120-catenin and the

junction plakoglobin, while in the TMX treated cells an additional 22 proteins, including p120-catenin were identified, but most appeared to be background (Appendix Tables 5 and 6). Subsequently, the lists obtained from EtOH and TMX samples from the first approach were compared to each other to see differences and similarities in interactions between the two conditions. Surprisingly, relatively few proteins were detected in both conditions, with only 55 proteins being identified (Figure 4.15). These proteins included N-cad and β-catenin as expected, and in addition included other proteins related to the cytoskeleton such as vimentin, F-actin-capping protein subunit beta and Myo18 (Appendix Table 7 red highlighted). However, nothing was identified that had previously been reported to be involved in repulsion signals. In the control (EtOH) condition, 147 proteins were identified (Figure 4.15; Appendix Table 8), while in the invading cells (TMX) there were 207 proteins identified to be interacting with N-cad (Figure 4.15 and Appendix Table 9). This suggests that N-cad has a different interacting profile in repulsing (EtOH) and invading (TMX) cells, which could contribute to the loss of CIL in ERK activated cells. To identify candidates that might be interacting with N-cad to regulate CIL, a functional classification analysis was performed based on the protein class, for proteins present in the overlapping group, as well as proteins that are unique to EtOH or N-cad samples, using http://pantherdb.org. Most of the proteins were mapped and classified based on protein function, which included cell adhesion molecules, cell junction proteins, and cytoskeletal proteins, however there was nothing identified which could suggest a possible role in CIL (Figure 4.16-4.18 and Table 4.4). Moreover, molecules that have previously been described to play a role in CIL such as Wnt, Slit and Robo could not be detected in any condition. Importantly, while we found that Ephrin-A1 induces cell rounding, Ephrin-A1 and other ephrins or Eph receptors also were not identified in either the control or TMX condition. Moreover,

the FGF receptor, which has previously been reported to bind to N-cad could not be detected in the screen, although it has been reported to be expressed by Schwann cells (Grothe and Nikkhah, 2001; Williams et al., 2001). This preliminary data suggests that N-cad does not interact with these classes of molecules; however, an alternate possibility is that the conditions were not appropriate for detecting these interactions.

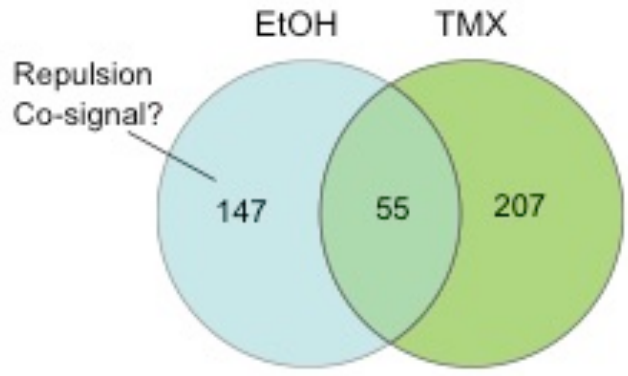

Figure 4.15. Mass Spec analysis of N-cad complexes.

Venn diagram showing the numbers of proteins interacting with N-cad specific to NR-SCs treated with EtOH or TMX and interacting proteins present in both of the conditions. n=1.

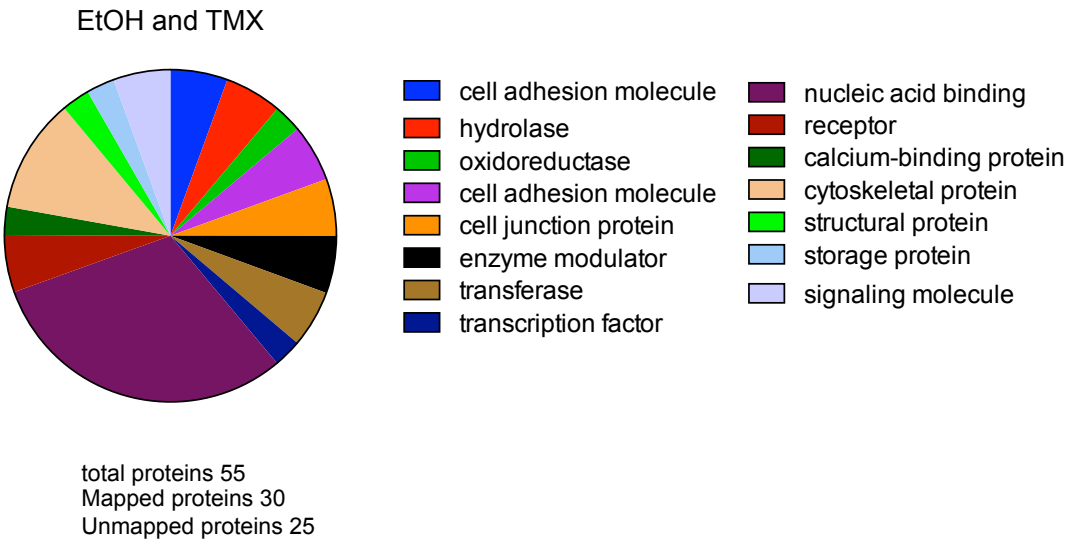

Figure 4.16. Functional classification of proteins overlapping TMX and EtOH samples.
Pie charts showing the functional classification of proteins identified to be interacting in both repulsing (EtOH) and invading (TMX) NR-SCs. A total number of 55 peptides were classified, of which 30 were mapped to a protein ID whereas 25 proteins could not be mapped. n=1.

Cytokeletal proteins	
Accession	**Description**
D3ZFD0	Uncharacterised protein (Myo18a)
Q9WU82	Catenin Beta
P31000	Vimentin
Q5XI32	F-actin-capping protein subunit beta
Cell Junction	
Accession	**Description**
G3V803	Cadherin-2
D3ZFD0	Uncharacterised protein (Myo18a)
Cell Adhesion	
Accession	**Description**
Q9WU82	Catenin Beta
G3V803	Cadherin-2

Table 4.3. Overview of proteins overlapping TMX and EtOH samples.
Table showing proteins mapped in three different protein classes that were identified in both EtOH and TMX treated NR-SCs. n=1

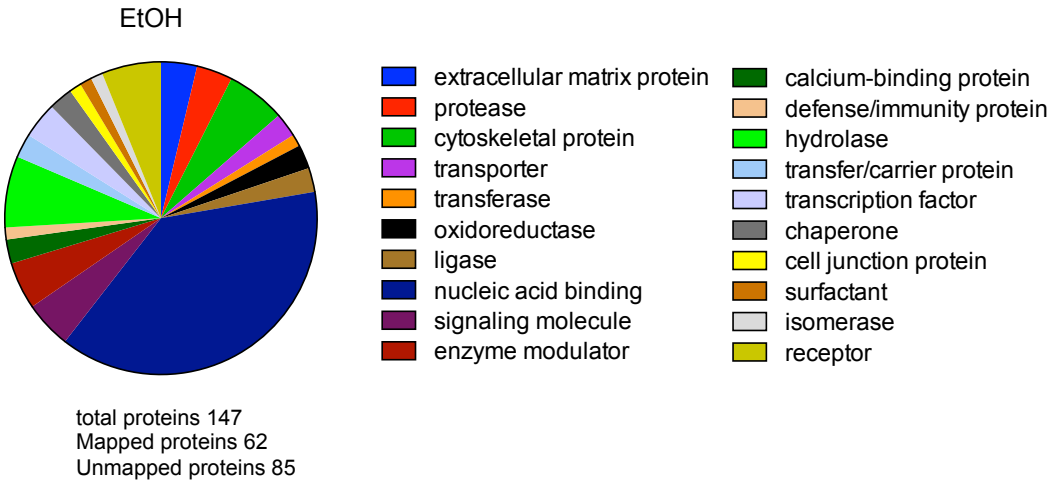

Figure 4.17. Functional classification of proteins interacting with N-cad in EtOH treated samples.

Pie charts showing the functional classification of proteins identified as interacting only in repulsing (EtOH) NR-SCs. A total of 147 proteins were classified of which 62 were mapped to a protein ID whereas 85 proteins could not be mapped. n=1.

Cytokeletal proteins	
Accession	**Description**
Q3KRE8	Tubulin beta-2B chain
P68370	Tubulin alpha-1A chain
D4AAG4	Protein Kif23
P63259	Actin, cytoplasmic 2
Q68FR6	Sorting and assembly machinery component 50 homolog
Cell Junction	
Accession	**Description**
F1M4A0	Protein Tjp1
Cytokeletal proteins	
Accession	**Description**
Q3KRE8	Tubulin beta-2B chain
P68370	Tubulin alpha-1A chain
D4AAG4	Protein Kif23
P63259	Actin, cytoplasmic 2
Q68FR6	Sorting and assembly machinery component 50 homolog

Table 4.4. Overview of proteins interacting with N-cad in EtOH treated samples.

Table showing proteins mapped to three different protein classes that were identified in both EtOH and TMX treated NR-SCs. n=1

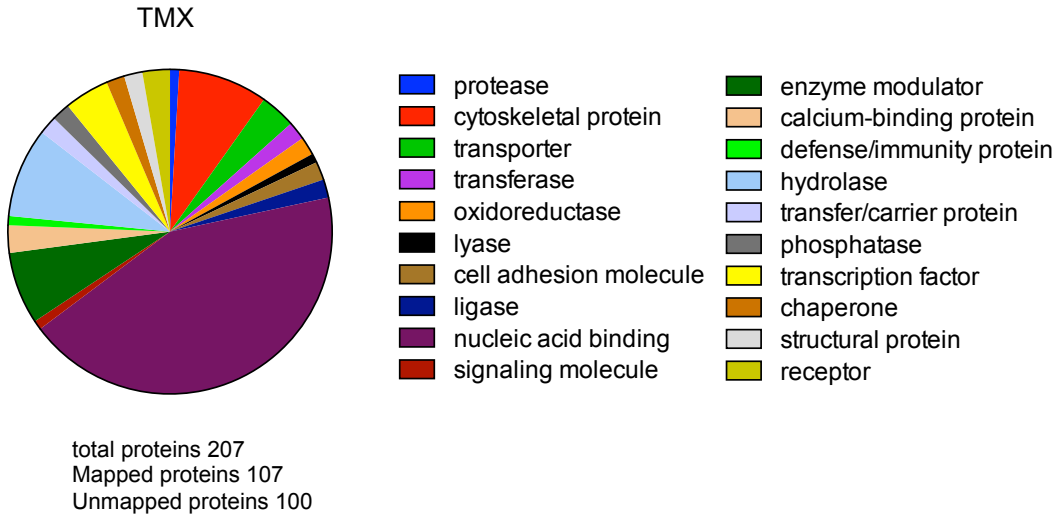

Figure 4.18. Functional classification of proteins interacting with N-cad in TMX treated samples.
Pie charts showing the functional classification of proteins identified as interacting in non-repulsing (TMX) NR-SCs. A total of 207 proteins were identified of which 107 were mapped to a protein ID whereas 100 proteins could not be mapped. n=1.

Cell Adhesion	
Accession	**Description**
G3V852	Protein Tln1
Q5U302	Alpha-catenin
Cytokeletal proteins	
Accession	**Description**
Q5U302	Alpha-catenin
G3V852	Protein Tln1
P38650	Cytoplasmic dynein 1 heavy chain 1
F1LMV9	Coronin (Fragment)
Q6IFU8	Keratin, type I cytoskeletal 17
P30427	Plectin
O88656	Actin-related protein 2/3 complex subunit 1B
Q3T1K5	F-actin-capping protein subunit alpha-2
D3ZLC1	Protein Lmnb2
Q6AYZ1	Tubulin alpha-1C chain
Receptor	
Accession	**Description**
B5DFB2	Protein Rbbp4
P15999	ATP synthase subunit alpha
Q5XI13	Glutamate-rich WD repeat-containing protein 1

Table 4-5. Overview of proteins interacting with N-cad in TMX treated samples.
Table showing proteins mapped to three different protein classes that were identified in TMX treated NR-SCs. n=1.

There were many proteins that could not be mapped for protein ID (TMX specific (100), EtOH specific (85); EtOH and TMX (26)) and whilst the majority of these proteins appeared to be related to mRNA processing and thus appeared to be background, some of these proteins appeared to be related to cytoskeletal proteins and cell junction proteins (Figure 4.16-4.18; Appendix Tables 7-9 See blue highlighted and yellow highlighted). One protein, glypican-4, identified specifically in the control (repulsing) cells, was of particular interest (Appendix Table 8 red highlighted). Glypicans are GPI-linked, heparan sulphate proteoglycan (HSPG) proteins located at the cell surface, and have been described to modulate the signalling of Wnt, Hedgehog, fibroblast growth factor, bone morphogenetic proteins and Slit and Robo either by promoting or inhibiting signalling (Filmus et al., 2008). Moreover, glypicans have been shown to play a role in axonal guidance by mediating repulsion, suggesting it could play a role in CIL in Schwann cells (Blanchette et al., 2015; Filmus et al., 2008). Importantly, glypican-4 is only identified in the repulsing cells and not in the invading cells (TMX), suggesting that the interaction is lost upon Raf-activation, which correlates with the loss of CIL in ERK activated cells.

To test a potential role of glypican-4 in CIL in Schwann cells, we performed some preliminary experiments. We initially set up a siRNA knockdown in Schwann cells using two independent oligos, and for both siRNA1 and siRNA2 an efficient knockdown (≥80%) of mRNA was detected by RT-qPCR at 36 hours (Figure 4.19). However, the knockdown could not be detected at protein levels due to the lack of an available antibody.

To determine the role of glypican-4 in homotypic CIL in Schwann cells, scrambled, siRNA1 and siRNA2 treated cells were seeded at low density and as we do not know the turnover rate of glypican-4 protein levels in Schwann cells, cells were imaged for 72 hours following treatment with the siRNAs for 24 hours.

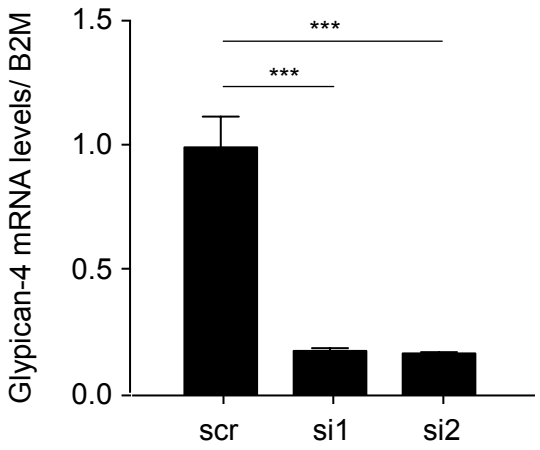

Figure 4.19. Glypican-4 siRNA knockdown is efficient.
Graph showing RT-qPCR analysis of the mRNA expression levels of glypican-4 in scrambled-treated, or glypican-4 knockdown cells, treated with either siRNA 1 or siRNA2 for 36 hours. Results are shown relative to the expression in scrambled-treated cells. Bars represent the mean of three experiments ±SEM. Two-way ANOVA Dunnett's-multiple comparison test.

Interestingly, the siRNA1 or siRNA2 treated cells appeared to be initially repulsed upon contact, however, many of the glypican-4 knockdown cells changed their behaviour around 48 hours after knockdown, when they appeared to be no longer repulsed upon contact, but adhered together and formed clusters, suggesting a role for glypican-4 in CIL (Figure 4.20 and Movie 4.5). This loss of CIL was quantified and strikingly, there was a marked decrease in repulsion events (siRNA1 ≥15%; siRNA2 ≥40%), and a dramatic increase in no-repulsion events (siRNA1 ≥20%; siRNA2 ≥ 40%), while there was no change in invasion events, suggesting glypican-4 is required for CIL (Figure 4.20B). Moreover, this was not due to a decrease in velocity (Figure 4.20C). Surprisingly however, in contrast to the N-cad knockdown cells, which were invasive, glypican-4 knockdown cells appeared to be more adhesive, suggesting glypican-4 knockdown cells form adherence junctions. To test if glypican-4 affected N-cad at the cell-cell junctions, glypican-4 knockdown cells were seeded onto coverslips and immunolabelled for N-cad. As expected, scrambled-treated cells

formed N-cad junctions between them (Figure 4.21). Interestingly, there appeared to be no increase of N-cad levels at the cell-cell junctions between glypican-4 knockdown cells, suggesting glypican-4 does not affect N-cad levels (Figure 4.21). However, some of the junctions appeared tighter (arrows) in glypican-4 knockdown cells, suggesting the junctions are more stable, possibly because the repulsion signal is lost. This needs further investigation. These preliminary results show that glypican-4 is required for CIL, by blocking the repulsion response. However, the interaction of N-cad with glypican-4 needs to be validated and further analysis needs to be done to determine the role of glypican-4 in CIL in Schwann cells.

All together these results show that N-cad interacts with its cytoplasmic binding partners β-catenin, α-catenin and p120-catenin both in repulsing and invading cells, which is consistent with the findings in Chapter 3. Moreover, this preliminary data suggests that the Mass Spec specifically identified proteins interacting with N-cad and suggests that N-cad interacts with a different array of proteins in repulsing and invading cells. While this data suggests N-cad does not interact with known molecules that regulate CIL, it did identify a potential candidate, glypican-4, in the repulsing cells, which in preliminary experiments appears to play a role in CIL. This shows that this methodology provides a tractable system to identify proteins that differentially interact with N-cad and that may have a potential role in CIL.

4.7. Chapter conclusions and discussion

In this chapter, we showed that Schwann cells expressing DNp53 have intact CIL, while oncogenic Ras disrupts CIL in an ERK-dependent manner. Reminiscent of N-cad knockdown cells, Schwann cells expressing oncogenic Ras are invasive (Figure 4.19). Interestingly, loss of CIL by Ras-expressing cells is not caused by altered expression or functionality of N-cad, as N-cad can still localise at cell-cell

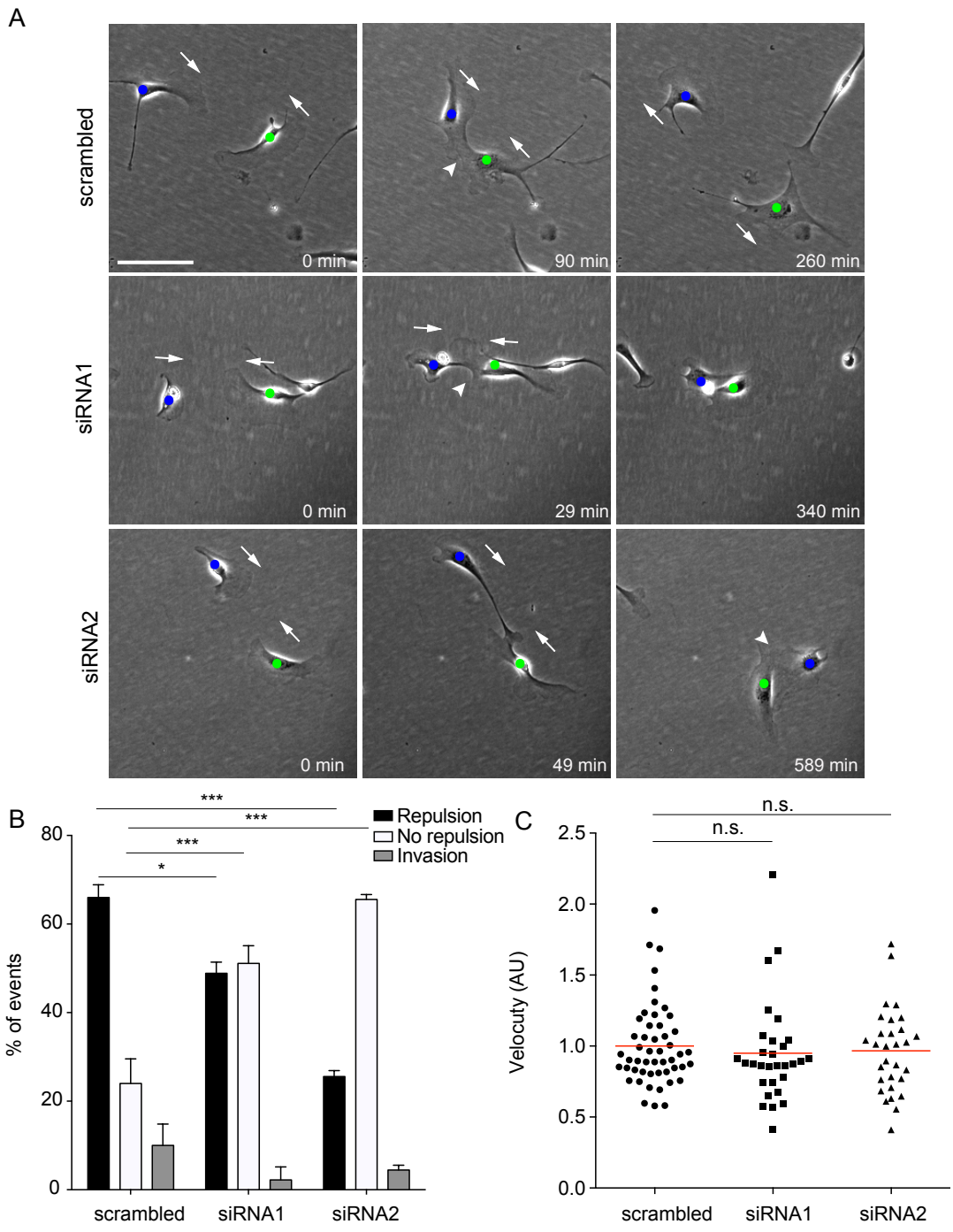

Figure 4.20. Glypican-4 is required for CIL in Schwann cells.

(A) Representative phase-contrast images of time-lapse analysis a CIL assay in which cells were treated with scrambled siRNA or siRNA targeting glypican-4 (siRNA 1 and siRNA 2) for 24 hours before imaging for 72 hours. Shown are images taken between 48 hours and 72 hours after siRNA knockdown. White arrows indicate the direction of migration. Arrowheads indicate repulsion or no-repulsion events. Note that the glypican-4 knockdown cells adhere upon contact. Cells of interest are indicated by blue and green dots. Scale bar 100µm. **(B)** CIL analysis in which repulsion, no-repulsion and invasion were quantified. 30 cells per experiment in each condition were analysed. Related to Movie 4.5. **(C)** Velocity analysis in which <30

cells of three independent cell were quantified. siRNA1 and siRNA2 were tested separately, and were normalised for the average velocity of the Scrambled-treated cells and then combined in one graph. T-Test was performed.

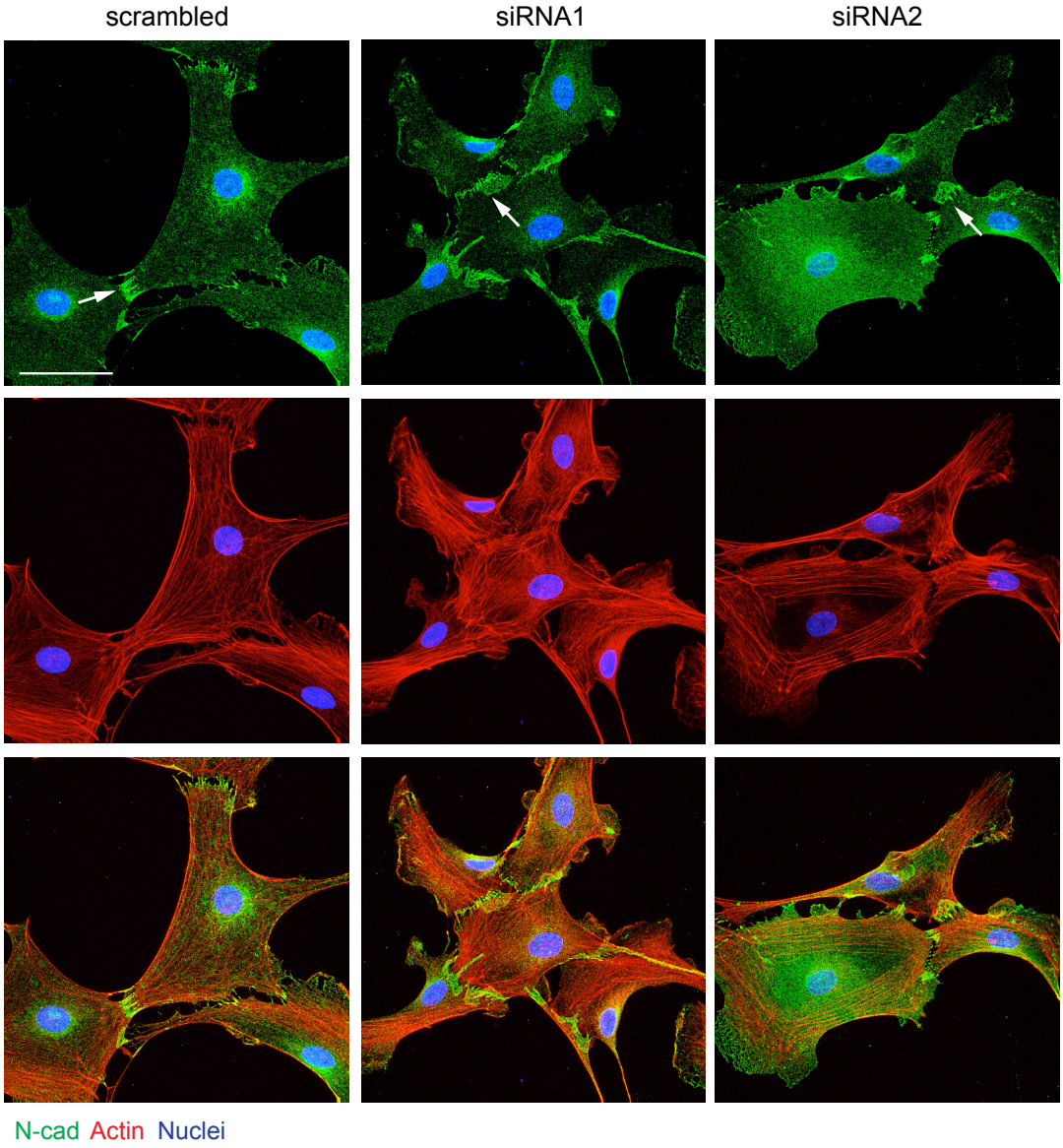

Figure 4.21. Glypican-4 does not appear to affect N-cad levels at membrane junctions.
Representative confocal images of cells treated with scrambled siRNA or siRNA targeting glypican-4 (siRNA 1 and siRNA 2) for 96 hours that were fixed and immunostained for N-cad (green) and costained with Hoechst (blue) and phalloidin to visualise F-actin (red). N-cad positive junctions are indicated with arrows. Scale bar 50µm n=2

contacts, and Raf-activated cells are still able to grab axons, a property of Schwann cells, in an N-cad dependent manner (Figure 4.22). Moreover, the junction components α-catenin, β-catenin and p120-catenin still interact with N-cadherin as detected by Co-IP (Figure 4.22). Rather, oncogenic Ras disrupts CIL through loss of a distinct co-signal. This work, together with others', also showed that N-cad regulates three very distinct processes namely: CIL, cell clustering and axonal grabbing, further suggesting the need for co-signals to mediate these distinct responses. In the case of cell clustering, Ephrin-B/EphB2 can be considered as a co-signal as, via Sox2, it triggers a relocalisation of N-cad to the cell-surface, which in some way is sufficient to overcome the repulsion signals, resulting in the formation of stable cell junctions.

In an attempt to uncover the mechanisms involved, the role of ephrins was explored as these proteins have been shown to be involved in CIL in other systems. The major, unexpected finding was the dramatic and numerous changes in the expression of both the ephrin ligands and their receptors in response to activation of the Ras/Raf/MEK/ERK signalling pathway indicating a likely important role for this pathway in controlling both the transcriptional pattern of expression and based on this, how cells recognise each other and other cell types.

A particularly intriguing finding was that inhibiting MEK was sufficient to fully revert the morphology of Ras-transformed Schwann cells and re-establish cell-cell recognition. This also correlated with the restoration of the expression levels of the majority of the Eph receptors and their ligands, consistent with a potential role in mediating CIL. This may have important implications for the invasive properties of Ras-expressing cancer cells and should be further explored.

We further showed that homotypic and heterotypic CIL involves distinct mechanisms in that while heterotypic CIL between Schwann cells and fibroblasts is

EphB2 dependent, homotypic CIL between Schwann cells is EphB2 independent (Figure 4.23). However, both processes are disrupted by Ras-signalling and the mechanisms behind this remain to be determined, however the strong downregulation of EphB2 levels following Ras expression is likely to play a role in heterotypic CIL between fibroblasts and Schwann cells.

In preliminary experiments to address the potential role of the ephrin-A family in homotypic CIL, we showed that pre-clustered Ephrin-A1 induced retraction of the Schwann cell periphery, which was associated with a change of the actin cytoskeleton, suggesting it was capable of inducing a repulsion signal in Schwann cells. In contrast, while Ephrin-A4 could bind to Schwann cells it appeared to have only a mild effect on the retraction of the cell periphery. This work further showed that Fyn, which has been shown to be a downstream target of Ephrin-A and mediates axonal repulsion, does not mediate CIL between Schwann cells, suggesting reverse signalling through the Ephrin-A ligand is not required for CIL.

Using a combination of Co-IP and mass spectrometry, we attempted to identify a possible N-cad dependent repulsion signal and tested if this was lost in Erk activated Schwann cells. We successfully identified known interacting binding partners such as β-catenin, which was interacting with N-cad both in the repulsing and invading cells showing we could specifically identify proteins interacting with N-cad. However, while we could detect α-catenin and p120-catenin, they were also found in the IgG controls, suggesting further optimisation of the methodology is needed. These preliminary experiments further showed that Raf activation completely changes the interacting profile of N-cad, suggesting that this could possibly be a mechanism by which CIL is lost in ERK activated cells (Figure 4.22). Moreover, a potential candidate, glypican-4, was identified interacting with N-cad in the repulsing cells, which appeared to be lost in invading cells, suggesting it could

play an role important in mediating CIL. In preliminary experiments, we addressed the role of glypican-4 in CIL in Schwann cells using siRNA knockdown, which showed that loss of glypican-4 results in the loss of the repulsion response, which causes the cells to adhere together, suggesting it could play a role in CIL.

Thus, these preliminary experiments show that we have established a robust system to identify the N-cad dependent repulsion signal. However, this needs to be reproduced and further optimisation of the methodology is required to avoid loss of proteins with a temporal or weak interaction perhaps by using a non-membrane permeable cross linker such as 3,3'-Dithiobis(sulfosuccinimidylpropionate) (DTSSP). Moreover, interactions of the extracellular domain with a potential co-signal could be targeted specifically by the use of the extracellular domain tagged with mCherry and Co-IP for mCherry.

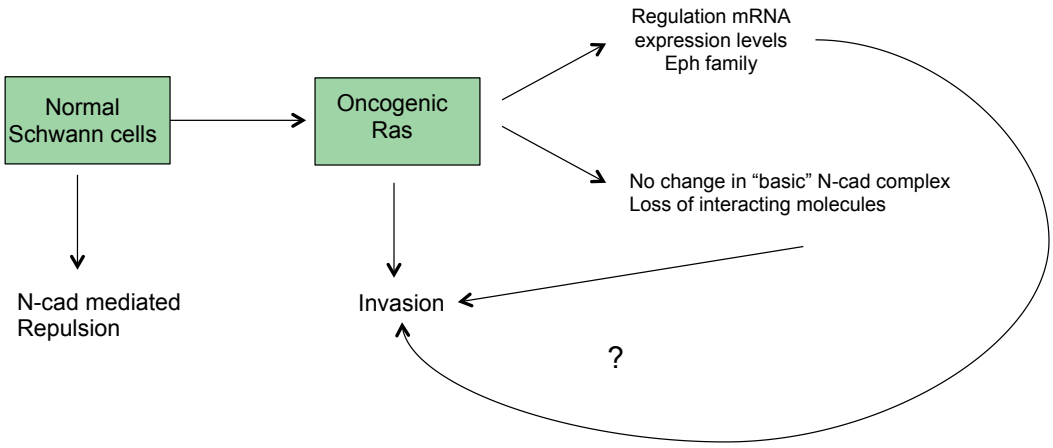

Figure 4.22. Schematic overview of effects of oncogenic Ras on CIL.
A diagram showing that while normal Schwann cells repulse upon contact, following hyperactive signalling of Ras, Schwann cells lose repulsion and become highly invasive. It is unclear how Ras disrupts CIL, however Ras regulates the expression patterns of the Eph receptor and ligands, the majority in a MEK dependent manner. Moreover, Ras does not change the interaction of N-cad with p120-catenin, α-catenin and β-catenin, nor does it appear to change the function of N-cad as Raf activated Schwann cells can still grab axons in an N-cad-dependent manner. However it does appear to change the interaction with glypican-4.

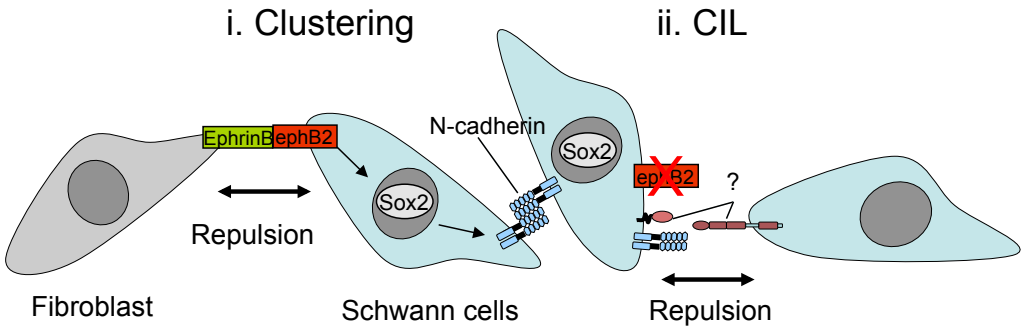

Figure 4.23. Heterotypic and homotypic CIL between Schwann cells and fibroblasts are differentially mediated.
i. Heterotypic interactions between Schwann cells and fibroblasts induces a switch in the behaviour of Schwann cells from repulsive to attractive. Mechanistically, Ephrin-B/EphB2 repulsive signalling induces the activation of Sox-2 that in turn induces the relocalisation of N-cad to the cell-cell junctions, causing Schwann cells to cluster. ii. Schwann cells are repulsed upon contact in a N-cad dependent manner, preliminary data suggests a role for Ephrin-A1 or possibly glypican-4. In contrast, while EphB2 mediates heterotypic CIL between fibroblasts and Schwann cells, homotypic CIL between Schwann cells is EphB2 independent.

4.7.1. Loss of cell-cell recognition in NF1

Losing cell-cell recognition is a hallmark of cancer, which can cause unwanted movement of cells and invasion of tissues, and eventually metastasis (Hanahan and Weinberg, 2011). A longstanding question is how cancer cells lose cell-cell recognition and how this contributes to the formation and progression of tumours and ultimately metastasis. Neurofibromas are benign tumours that are highly disorganised and are thought to resemble the injured nerve (Lassmann et al., 1976; Parrinello and Lloyd, 2009). Neurofibromas have a similar cell composition to the injured nerve, including fibroblasts, mast cells, and dedifferentiated Schwann cells. Additionally, Schwann cells in neurofibromas have the ability to hyperproliferate, and may also be found dissociated from axons (Kim et al., 1997; Parrinello et al., 2010) This suggests, that the heterotypic and homotypic interactions that normally keep

Schwann cells quiescent are lost during the formation of the tumour. Moreover, it suggests that the Schwann cells become migratory. Though it is well established that NF1 results from hyperactive Ras signalling, how heterotypic interactions and homotypic interactions are lost during tumourigenesis of NF1 is unclear. We have recently shown *in vitro*, using DRGs explants with Schwann cells which recapitulates the nerve interactions, that activating Raf in myelinating Schwann cells was sufficient to induce Schwann cell dissociation from the axons (Parrinello et al., 2008). Moreover, we showed that the heterotypic interaction between Schwann cells was mediated by Sema4F, and that loss of Sema4F in Schwann cells was sufficient to induce Schwann cell dissociation. Moreover, loss of these interactions via knockdown of Sema4F resulted in increased proliferation of Schwann cells in the DRG Schwann cell co-cultures. Now we show that in addition to losing heterotypic cell-cell interactions, Schwann cells expressing oncogenic Ras lose homotypic cell-cell recognition in an ERK-dependent manner. We show that loss of cell-cell recognition results from loss of CIL between Schwann cells expressing oncogenic Ras, which become highly invasive and appear to protrude and extend their protrusions more frequently, consistent with previous reports (Dow et al., 2008; Lloyd et al., 1997; Ridley et al., 1988).

How could loss of homotypic CIL contribute to tumourigenesis of NF-1? The mechanisms of tumour cell migration rely on the same principles of cell migration during normal processes such as migration during development and wound healing (Friedl and Alexander, 2011). Likewise, it is thought that while heterotypic CIL between cancer cells and surrounding cells is impaired, allowing invasion of surrounding tissues, homotypic CIL remains intact during tumourigenesis, which could contribute to cancer dissemination (Abercrombie, 1979; Astin et al., 2010; Batson et al., 2014). Recent reports showed that CIL between prostate cancer cells

PC3 remained intact, a process mediated by EphA2/EphA4 (Astin et al., 2010). Moreover, using chamber assays and cancer cell spheroid migrations assays, it was shown that homotypic CIL is required for the cell dispersal of PC3 cells, which could be a potential mechanism of the dispersal of prostate cancer cells from the tumour leading to local single cell invasion (Astin et al., 2010; Batson et al., 2014). In contrast, in this work we showed that homotypic CIL between Schwann cells expressing oncogenic Ras is lost, and the cells become invasive, suggesting loss of CIL of Schwann cells in neurofibromas. Though neurofibromas are benign tumours and do not metastasise, Schwann cells are frequently found dissociated from the axons, suggesting Schwann cells become motile. Interestingly, NF1-/- cells extracted from the peripheral nerve, are more invasive and migratory than their NF1+/+ counter parts *in vitro* (Kim et al., 1997; Sheela et al., 1990). Thus this could suggest that loss of homotypic CIL in Ras Schwann cells could allow Schwann cells to break away from existing contacts, which could contribute to increased migration and local invasion into the surrounding tissues. However, this needs to be further tested.

Ras is thought to play a role in tumourigenesis by inducing hyperproliferation, cell migration and invasion (Pylayeva-Gupta et al., 2011). Ras was originally identified as an oncogene using focus-formation assays which by definition permit a cell to overcome the constraints of a confluent monolayer and proliferate- suggesting a change in cell:cell recognition (Der et al., 1982; Goldfarb et al., 1982; Parada et al., 1982; Santos et al., 1982; Shih and Weinberg, 1982). Since then, multiple studies have shown that oncogenic Ras expression induces loss of cell-cell recognition but the mechanisms remain poorly understood (Pylayeva-Gupta et al., 2011). As for many cells, activation of Ras signalling pathways in Schwann cells results in the cells growing on top of each other, and we showed that this is associated with a loss of CIL, suggesting these two properties may be linked. But how does oncogenic Ras

disrupt CIL in Schwann cells? Following our findings that N-cad knockdown cells also lose CIL, grow on top of each other and somewhat resemble Ras-transformed cells, we considered that inhibition of N-cad was a potential mechanism. Moreover, cadherin switching from E-cad to N-cad expression has been shown to play a major role in regulating migration and invasion in tumour cells and aberrant expression of N-cad is associated with poor prognosis (Berx and van Roy, 2009; Wheelock et al., 2008). However, somewhat to our surprise, we find that Ras-expressing cells maintain similar levels of functional N-cad. However unlike normal cells, Ras Schwann cells appear to be unable to make stable homotypic cell-cell junctions, even though N-cad is localised at transient cell-cell contacts. Intriguingly, while N-cad mediated homotypic CIL is severely impaired, the N-cad mediated heterotypic interaction of axonal grabbing by Schwann cells remains unaffected by hyper-activated Ras/Raf signalling, suggesting N-cad is still functional and that hyperactive Ras/Raf-signalling differentially affects these processes, probably through abrogating a co-signal required for CIL. We also show using a combination of Co-IP and Mass Spec that hyperactive Ras signalling does not affect the interaction of N-cad with the adherence junction components α-catenin, β-catenin and p120-catenin, consistent with our findings that CIL is independent of the intracellular domain, and independent of the intracellular binding partners of N-cad. However, preliminary data from our Mass Spec analysis suggests that hyperactive Raf signalling changes the N-cad interacting profile. Of particular interest is the interaction of N-cad with glypican-4, a HSPGs, which have been suggested to play a role in axonal guidance, directional migration and CIL (Blanchette et al., 2015; Fritz et al., 2015; Matthews et al., 2008).

Interestingly, preliminary results showed that glypican-4 plays a role in CIL mediating a repulsion response. This is consistent with a role of glypican in mediating a netrin/Slit-mediated repulsion response of axons during the larval development in

C. elegans (Blanchette et al., 2015). Intriguingly, in contrast to loss of N-cad, loss of glypican-4 does not result in invasion, rather blocks the repulsion response, which causes the cells to adhere together. This contradictory result is probably due to N-cad still being at the membrane, which might be stabilised in adherence junction complexes upon loss of the repulsion signal. Alternatively, rather than mediating repulsion, glypican-4 may directly regulates the levels of N-cad at the membrane, and the observed adhesiveness in Schwann cells upon loss of glypican-4 is due to increased levels of N-cad at the membrane. Preliminary results argue against this, as there appears no obvious difference of N-cad levels at the junctions between scrambled-treated and glypican-4 knockdown cells. However, it could be that subtle changes in N-cad protein levels and trafficking are missed. This needs further investigation. Moreover, another possibility in the difference between the invasive phenotype in N-cad knockdown cells and the clustering phenotype in glypican-4 knockdown cells may be that the repulsion signal is still present.

What could be the role of glypican-4 in CIL? Glypicans are GPI-linked proteins that have been shown to modulate signalling pathways, by stabilising or interfering with the ligand/receptor interactions of pathways including BMP, FGF and Hedgehogs signalling as well as pathways shown to play a role in CIL such as Wnt, Robo and Slit (Blanchette et al., 2015; Filmus et al., 2008). For example, glypican has been shown to inhibit Hedgehog signalling by competing for the ligand, preventing it from binding to the receptor, or enhance Wnt signalling by stabilising the interactions between ligand and receptor (Capurro et al., 2005; Capurro et al., 2008). This suggests, that glypican-4 may not be the repulsion signal, but possibly stabilises an interaction between N-cad and a repulsion signal (such as Ephrin-A1) and the receptor on the receiving cell. However, the role of glypican-4 in CIL between

Schwann cells needs be further investigated and will be a priority in future experiments.

Aberrant expression of Eph receptors and their ligands have been associated with invasion, metastasis of several tumours including melanoma, prostate, breast and colon cancers and lung carcinoma (Pasquale, 2010). However, the overall picture is somewhat complex and confusing, and future studies are needed to clarify the complexities involved. Ephrins have been reported to be tumour promoting or tumour suppressive, depending on the tumour type and study. Moreover, ephrins have been implicated in boundary formation, cell segregation and CIL, which could all be predicted to have a role in cancer. Here we show that the Ras/Raf/Mek/ERK pathway induces dramatic and several changes in the mRNA expression levels of ephrins, suggesting ephrins have a crucial role in tumourigenesis of the Schwann cells in NF-1. In some compelling studies of the small intestine, the role of ephrins have been shown to have an important role in cell boundary control in normal tissue with loss of these controls associated with the early stages of tumour formation (Batlle et al., 2002). In these studies, it was found that EphB2 and EphB3 are required for compartmentalisation of Paneth cells in the crypt of the normal epithelium by preventing intermingling of the EphB and ephrin-B cell populations. Loss of EphB2 or EphB3 results in the aberrant positioning of Paneth cells, indicating EphB signalling is crucial for boundary formation. Later studies showed, that EphB suppresses tumour progression of adenomas into carcinomas (Batlle et al., 2005; Cortina et al., 2007). EphB2 and EphB3 are required to keep adenomas compartmentalised and prevent growth and migration into the surrounding tissues (Cortina et al., 2007). At the transition of adenomas into carcinomas CRC, EphB2, EphB3 and EphB4 are downregulated, the tumours become highly invasive and invade the surrounding tissues (Batlle et al., 2005). Moreover, later studies showed

that EphB mediates compartmentalisation by cell sorting of Ephrin-B and EphB expressing cells through regulating differential adhesion (Solanas et al., 2011).

Similarly, in a previous study we found that that Ephrin-B/EphB2 signalling between fibroblasts and Schwann cells induces Schwann cell sorting, through N-cad re-localisation to Schwann cell junctions, which is required for the Schwann cells to migrate as a collective following a nerve injury (Parrinello et al., 2010). In this study, we show that Ephrin-B/EphB2 signalling mediates heterotypic CIL between fibroblasts and Schwann cells suggesting this could mediate the cell sorting of the two populations. Moreover, we showed that following hyper-activating Ras, EphB2 and EphB3 are downregulated, and in preliminary data (not shown) my colleague found that Schwann cells expressing oncogenic Ras lose heterotypic CIL, become invasive and migrate over fibroblasts. This could suggest that in neurofibromas, which consist of a mixed cell population including fibroblasts, that loss of heterotypic CIL could contribute to the unwanted movement of the Schwann cells, however this needs to be further tested.

Other studies have shown that EphA2 is frequently upregulated in tumours such as melanoma, prostate, breast and colon cancers and lung carcinoma (Pasquale, 2010). EphA2 induces cells migration and invasion in several cancer cell lines (Pasquale, 2010; Taddei et al., 2011). Interestingly in the breast cancer cell line MCF17, EphA2 is upregulated in a MEK dependent way, while Ephrin-A1 is downregulated by Ras in a MEK dependent manner (Macrae et al., 2005). Similarly, we report here in Schwann cells expressing oncogenic Ras that EphA2 is upregulated, while Ephrin-A1 is slightly down regulated in a MEK dependent manner indicating common regulatory mechanisms in distinct cell types. However, whether aberrant signalling of Eph receptors and their ligands are responsible for the Ras-induced loss of homotypic CIL between Schwann cells remains undetermined.

4.7.2. Repulsion signals

In the previous chapter we showed that N-cad induces a repulsion response independent of the adherence junction complex, independent of *trans*-homodimerisation, and that N-cad is not required for the cell to be repulsed in a N-cad dependent manner. Rather N-cad mediates repulsion through the extracellular domain, by providing a repulsion signal to the other cell. N-cad is not required for the cell to be repulsed in a N-cad dependent manner, thus N-cad induces forward signalling but not "reverse signalling". This is reminiscent of Ephrin-A/EphA signalling, which typically only induces forward signalling, as Ephrin-A is a GPI-linked protein and typically does not induce reverse signalling (Kania and Klein, 2016). Consistent with this hypothesis, we show here that stimulating the Schwann cells with pre-clustered Ephrin-A1, a GPI-linked protein, induces retraction of the cell periphery and reorganises the actin cytoskeleton. This is consistent with previous studies of the prostate cancer cell line PC3, in which pre-clustered Ephrin-A induces cell rounding/ retraction of the cell periphery in a RhoA/MyosinII dependent manner (Astin et al., 2010; Parri et al., 2007). Moreover, it was shown that Ephrin-A1 and Ephrin-A5 can inhibit migration in transwell migration assays, and that Ephrin-A5 is sufficient to induce CIL (Astin et al., 2010). This could suggest that similarly, Ephrin-A1 could mediate CIL between Schwann cells. However, whether Ephrin-A1 does indeed mediate CIL in Schwann cells is unclear. One possibility we considered is that there is a direct interaction between N-cad and Ephrin-A1, with N-cad acting in some way to "present" the signal. Arguing against this hypothesis is that in preliminary data we failed to detect Ephrin-A1 or any other ephrins by Mass Spec, suggesting it does not interact with N-cad. However, as discussed previously, this could be due to a low binding affinity to N-cad, or a very temporal interaction. A further possibility could be

a much more indirect mechanism. In future studies, optimisation of the methodologies will be carried out to search for interacting proteins using the extracellular domain of N-cad as bait. Moreover, the role of Ephrin-A1 and other members of the family will be determined using siRNA studies, inhibitor studies and analysis of downstream effectors such as src, RhoA and MyoII. Moreover, the sufficiency of the signals will be explored using repulsion assays such as stripe assays in which stripes of Ephrin-A are coated using microcontact printing. Moreover, it would be interesting to see if an interaction between glypican-4 and Ephrin-A1 is required to mediate CIL.

Ephrin-A does not typically induce a bidirectional signal, as it is GPI-linked protein, however, there are exceptions which involve Ephrin-A interacting with other cell surface receptors (Bonanomi et al., 2012; Lim et al., 2008; Marler et al., 2008). In axons, Ephrin-A engagement has been shown to induce reverse signalling through interactions with the neurotrophin receptors Ret, TrkB and p75 to mediate repulsion, branching and synaptogenesis of the axons (Bonanomi et al., 2012; Lim et al., 2008; Marler et al., 2008). These studies showed that Ephrin-A2 and Ephrin-A5 can interact with p75, and that this interaction is required for the repulsion of growing axons of retinal ganglion cells explants in response to EphA7 (Lim et al., 2008). The authors propose that p75 transduces the Ephrin-A reverse signal, which results in phosphorylation of Fyn, a known downstream target of Ephrin-A. However, whether Fyn is required for the repulsion of retinal ganglion cells was not reported. In contrast, in a study in PC3 cells, reverse signalling through Ephrin-A ligands was not required to mediate CIL (Astin et al., 2010). In this study we showed that whilst specific Fyn inhibition was able to block cytokinesis in Schwann cells, Fyn is not required for CIL between Schwann cells. This suggests, that CIL is not mediated through Ephrin-A

reverse signalling, consistent with Ephrin-A1 inducing cell rounding, and consistent with N-cad providing a repulsion signal that does not induce reverse signalling.

In conclusion, we propose a model in which N-cad mediates CIL independent of *trans*-homodimerisation, independent of the intracellular domain and the adherence junction components α-, β- and p120-catenin through which N-cad typically signals (Figure 4.24). Rather, N-cad provides a repulsion signal, to the other cell, possibly through interaction of the extracellular domain with a co-signal. Preliminary data indicates that glypican-4 or Ephrin-A1 are potential candidates (Figure 4.24)

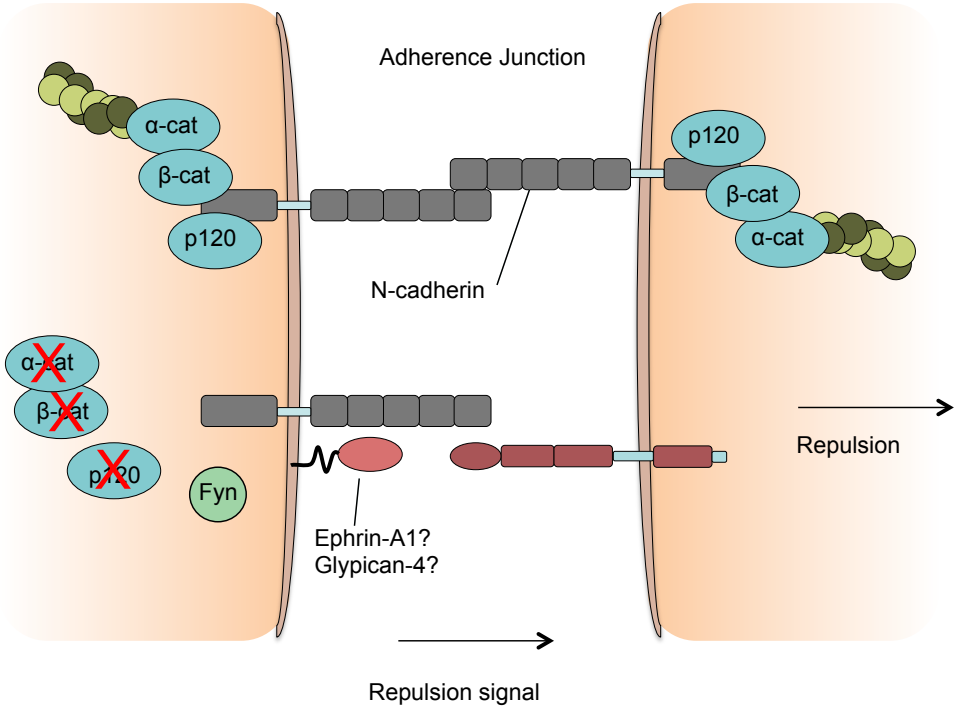

Figure 4.24 N-cad mediates repulsion possibly through interaction with a co-signal.
CIL in Schwann cells is mediated by N-cad through a mechanism independent of *trans*-homodimerisation and of its interacting molecules α-catenin, p120-catenin and β-catenin. Rather, N-cad provides a repulsion signal into the other cell, which is then repulsed. We propose that this co-signal could be Ephrin-A1 which induces cell rounding, or glypican-4 which preliminary work shows to specifically interacts with N-cad in Schwann cells that are repulsive, but this interaction is lost in cells that are invasive.

Chapter Five: Results III

Uncovering the mechanism of heterotypic Schwann cell-endothelial cell interactions

5.1. Chapter introduction

In the previous two chapters we described that the adhesion molecule N-cad mediates CIL by providing a signal to the contacting cell. CIL can polarise cells in the direction of migration and as such can be required for directional migration of individual cells (Carmona-Fontaine et al., 2008). Similarly, in collective migration, CIL mediates polarisation of the leader cells, which is required for the directional migration of the group (Theveneau et al., 2010). The polarity and collective migration of cells is further mediated through soluble factors secreted in the local environment such as cytokines, and through interactions with ECM via adhesion molecules such as integrins (Mayor and Etienne-Manneville, 2016). We have previously shown that upon injury, collective Schwann cell migration is required for axonal regeneration (Parrinello et al., 2010). To achieve this, Schwann cells need to migrate across a new 'bridge' of tissue that forms between the two nerve stumps and consists of inflammatory cells, fibroblasts and ECM. One of the major questions was how Schwann cells could migrate directionally through this densely-packed tissue, and how Schwann cell migration is induced. In recently published work, we showed that polarised blood vessels form in the bridge prior to Schwann cell migration (Cattin et al., 2015). We showed that Schwann cells associate with the blood vessels in the bridge. Moreover, as discussed in the introduction, the polarised blood vessels provide directionality to the migrating Schwann cells, which use the vasculature as a track.

The Schwann cell-endothelial cell interaction could be recapitulated in vitro, by culturing Human Umbilical Vein Endothelial Cells (HUVECs) in fibrin gels together

with GFP-labelled Schwann cells. In these assays, the HUVECs form tubule-like structures and importantly, Schwann cells associated with the tubules and migrated along them {Cattin, 2015 #61}. Correlative light electron microscopy (CLEM) showed that there were discrete but direct interactions between the Schwann cells and endothelial cells suggesting that Schwann cells could migrate via direct interactions with the blood vessel surface. Moreover, Schwann cells within the 3D matrix in the absence of blood vessels failed to migrate. This provides a mechanism to control SC migration within new tissue by limiting migration through the matrix, but permitting migration along the surface of endothelial cells thus providing directionality to this process.

To further understand the nature of the Schwann cell interactions with the endothelial cells and to determine how Schwann cells migrate along the blood vessels, we looked at molecules that could mediate these direct interactions. The work we present here has been published and was done in collaboration with Dr. Anne-Laure Cattin.

5.2. Assessing the role of β1-integrin on Schwann cell migration

From the analysis of time-lapse imaging it appeared that Schwann cells migrating in 3D along HUVEC tubules in fibrin gels appeared to adopt a more amoeboid-like mode of migration, which is characterised by protrusion extension at the front of the cell and an actomyosin dependent contraction of the rear (Cattin et al., 2015; Lammermann and Sixt, 2009; Liu et al., 2015). In contrast, Schwann cells in 2D migrate in a classical adhesion-dependent manner with large lamellipodia forming in the subsequent direction of migration (Figure 3.1. Movie 5.1). Cells adhere and transduce forces to the substratum through focal adhesion complexes, in which integrins link the substratum and the cytoskeleton. Binding to specific types of

substrate is dependent on the types of integrins expressed. Laminin staining of the fibrin tubules showed that they express laminin, suggesting Schwann cells could use this as a substrate to migrate along (Cattin et al., 2015). β1-integrin is required for adhesion to laminin, which is expressed by Schwann cells. Moreover, Schwann cell migration on 2D-laminin is blocked when β1-integrin is inhibited using function-blocking antibodies (Milner et al., 1997). To understand if β1-integrin is required for Schwann cell migration in 2D, we set up a knockdown protocol, treating the cells with two independent siRNAs targeting β1-integrin for 36 hours before harvesting for protein analysis using Western blot analysis. β1-integrin was detected by Western blot in scrambled-treated cells but was efficiently downregulated following treatment with either siRNA1 or siRNA2 (>90%) (Figure 5.1A). Subsequently, scrambled-treated cells or siRNA treated Schwann cells were seeded at low density onto laminin-coated dishes, imaged for 24 hours using time-lapse microscopy and analysed for their migratory behaviour. Scrambled-treated Schwann cells migrated normally with broad lamellipodia (Movie 5.1 and Figure 5.1B). However, the majority of the siRNA1 or siRNA2 treated Schwann cells adopted a rounder morphology and migration was severely impaired, showing that β1-integrin is required for Schwann cell migration on laminin in 2D (Movie 5.1; Figure 5.1B). To quantify this, the speed of migration was measured. Scrambled-treated cells showed a wide distribution of migration velocities, of between 0 and 2.5 arbitrary units (Figure 5.1C). In contrast, the majority of cells treated with siRNA1 showed a decrease in migration speed with an even greater effect seen in the cells treated with siRNA2, with the majority of the cells severely impaired in their migration (Figure 5.1C). However, the effect seen in the quantification of the velocity of the β1-integrin knockdown cells appeared to be less striking than the videos suggested. This is likely due to the movement of the nucleus in the cell, likely causing an overestimation of the velocity in non-migrating

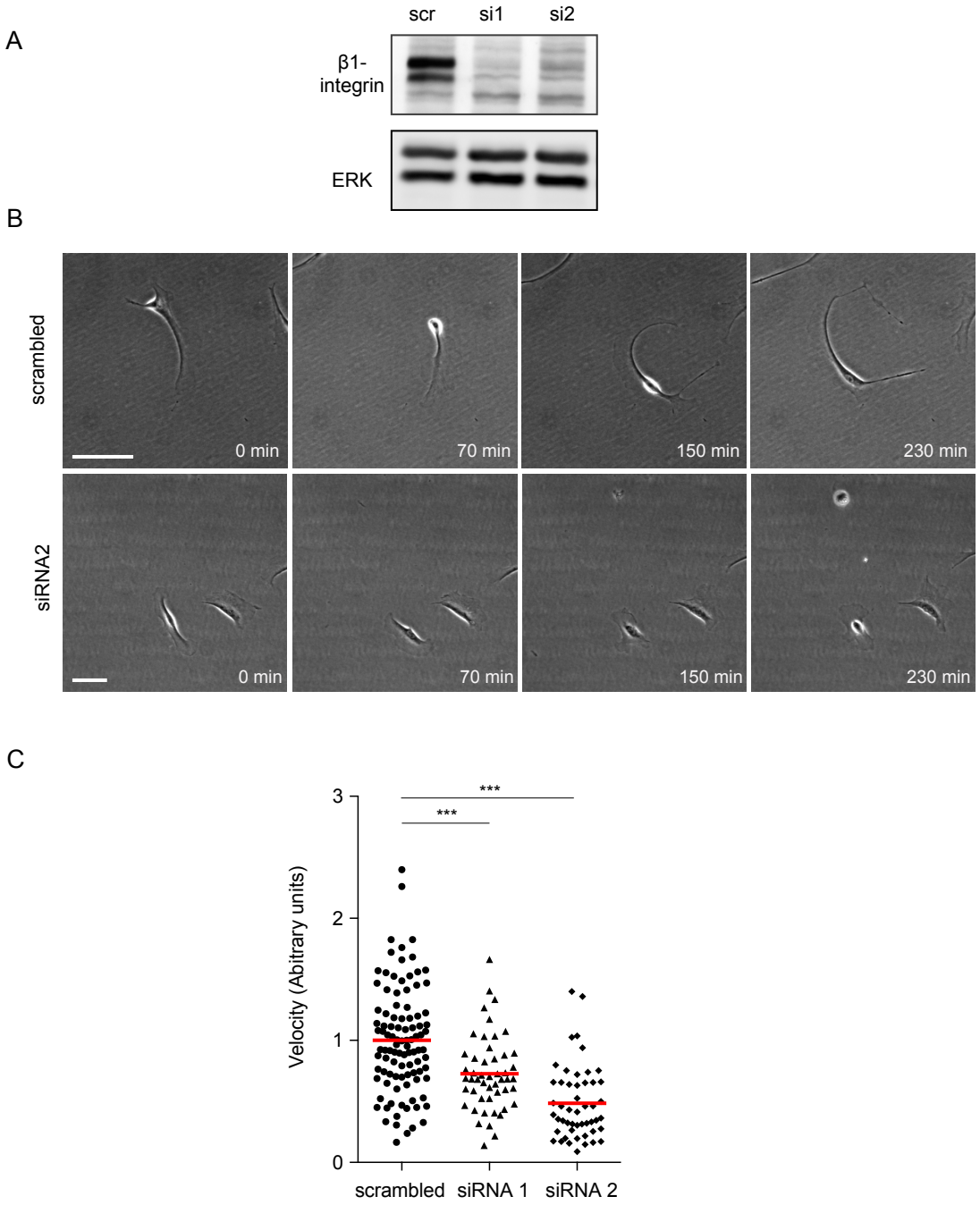

Figure 5.1. β1-integrin is required for 2D Schwann cell migration.
A. Western blot analysis of β1 integrin protein in Schwann cells treated with 5nM scrambled siRNA (scr), siRNA 1 (si1) or siRNA 2 (si2) for 36 hours. This experiment was done by Dr. Anne-Laure Cattin. **B.** Representative still images of time-lapse microscopy of scrambled-treated Schwann cells or β1-integrin knockdown Schwann cells (siRNA2) at 36 hours after knockdown. Note that the β1-integrin knockdown cells do not migrate. **C.** Quantification of cell velocity, in which cells were tracked for 12 hours. A total of 50 cells from two independent experiments were quantified siRNA1 and siRNA2 were tested separately, and were normalised for the average velocity of the Scrambled-treated cells and then combined in one graph. T-Test was performed. Related to movie 5.1.

cells. These results show that Schwann cells migrate on laminin in a β1-integrin dependent manner, which is consistent with previous reports (Milner et al., 1997; Ness et al., 2013).

Focal adhesion complexes are large complexes consisting of integrins, which connect the ECM to the actin cytoskeleton through several adaptor proteins, including talins. To further test if focal adhesion complexes are required for 2D Schwann cells migration, talin 1 and talin 2, were down regulated using siRNA as both talin 1 and 2 are expressed by Schwann cells. Therefore, we used a combination of siRNAs to target both genes to ensure complete disruption of integrin signalling. We set up the siRNAs at several concentrations at different time points (36 hours, 48 hours, 60 hours and 72 hours) and assessed the knockdown efficiency using western blot and immunostaining. It appeared that it took up to 60 hours for the protein to be lost using a total of 8nM siRNA, suggesting a slow turnover of talin (data not shown). Talin has a diffuse cytoplasmic localisation in Schwann cells, but a stronger localisation in puncta, which can be detected at the tip of protrusions (arrows), consistent with localisation in focal adhesion complexes (Figure 5.2A). In contrast, following efficient knockdown of talin 1 and talin 2 using combination siRNA 1, there was a strong decrease in talin immunostaining, and importantly, talin could no longer be detected in the puncta, suggesting talin is no longer present in the focal adhesion complexes (Figure 5.2A). In contrast, knockdown of talin 1 and 2 using combination siRNA 2 was less efficient, as some talin could still be detected in puncta (Figure 5.2A). Next we tested whether knockdown of talin affects Schwann cell migration on 2D laminin. As expected, scrambled-treated Schwann cells migrated with large lamellipodia in the direction of migration (Figure 5.2B; Movie 5.2). Strikingly, the vast majority of Schwan cells treated with siRNA1 became more rounded and appeared to protrude and extend fewer processes than the β1-integrin

knockdown cells and they failed to migrate efficiently, resembling β1-integrin knockdown cells (Figure 5.2B and Movie 5.2). This shows, as might be expected that talin1 and talin2 are required for Schwann cell migration on laminin (Figure 5.2B). In contrast, while the majority of the Schwann cells treated with siRNA2 had impaired migration, some cells migrated normally consistent with the level of knockdown (Figure 5.2A and B; Movie 5.1). This indicates that 2D migration is dependent on and talin 1 and 2, which should block all integrin mediated-migration, and had a strikingly similar effect on Schwann cell migration to β1-integrin knockdown cells, further showing that Schwann cell migration on 2D is integrin-dependent. Moreover, this suggests that in 2D, Schwann cells migrate in an adhesion dependent manner that is mediated through the focal adhesion complex proteins β1-integrin and talin 1 and 2, which is consistent with a mesenchymal mode of migration that is associated with high levels of adhesion and low levels of confinement (Lammermann and Sixt, 2009).

5.3. β1-integrin is not required for Schwann cell migration along blood vessels

To test if Schwann cells require β1-integrin to interact and migrate along the blood vessels in 3D, we used a matrigel assay, in which HUVECs form tubule-like structures within 14 hours, and to which we can add Schwann cells, allowing us to address the effect of the siRNA knockdown of β1-integrin and talin on the migration of Schwann cells along the vasculature. This is in contrast to the fibrin gel system in which the Schwann cells and HUVECs are added together, and the analysis is done after 10 days, which is not suitable for the use of transfected siRNA knockdown cells. To do this, HUVECs were seeded onto matrigel and tubules were allowed to form. Scrambled- or siRNA-treated GFP-labelled Schwann cells were subsequently seeded onto the tubules and imaged for 24 hours using time-lapse microscopy. Scrambled-

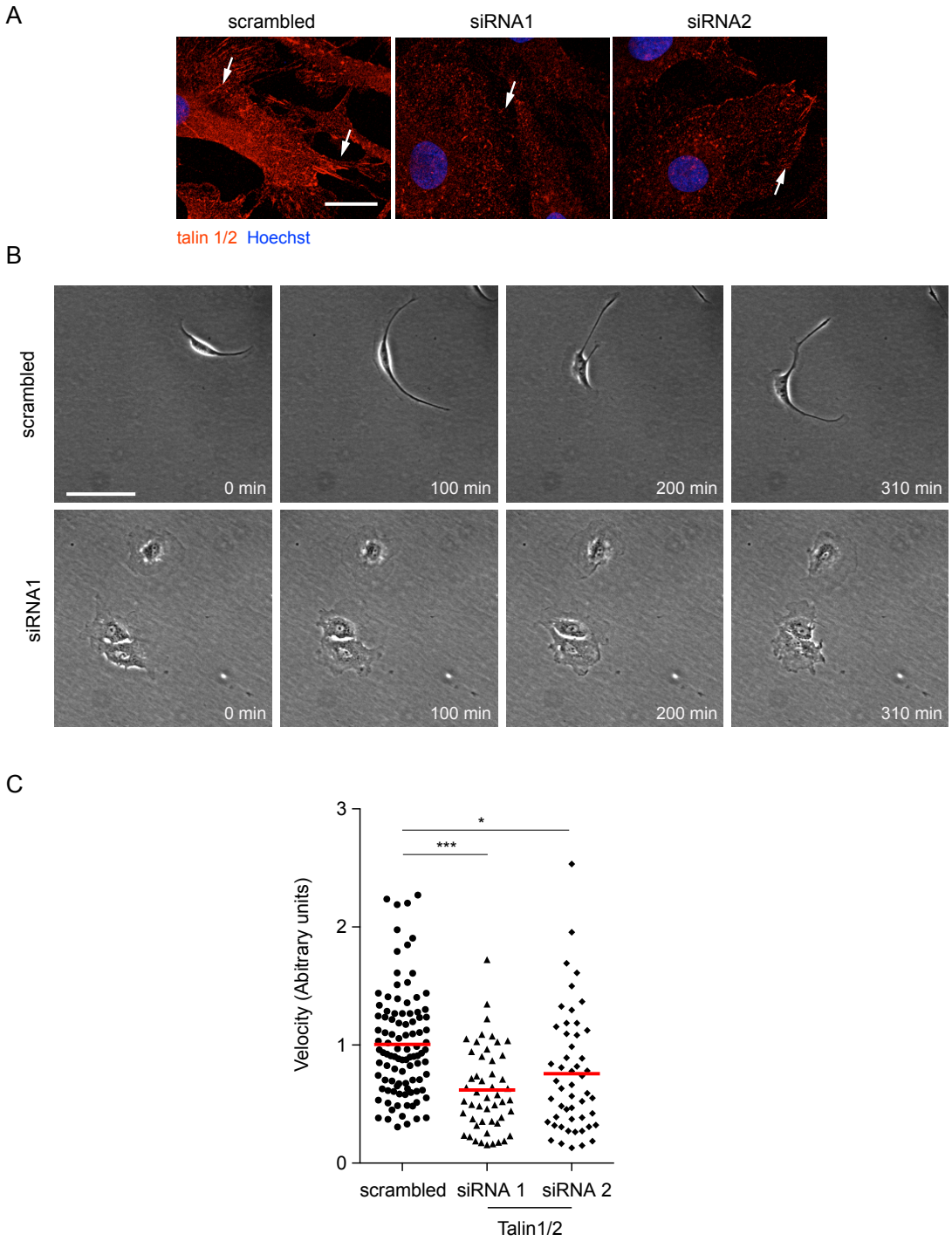

Figure 5.2. Talin 1, talin 2 and β1-integrin are required for 2D Schwann cell migration.

A. Representative confocal images of Schwann cells treated with 8nM scrambled siRNA, combination siRNA 1 (siRNA1) or combination siRNA 2 (siRNA2) for 60 hours immunostained for talin (red) and costained with Hoechst (blue). Arrows indicate stronger talin localisation at focal adhesion foci, which is lost in the talin KD cells. This experiment was done by Dr. Anne-Laure Cattin. **B**. Representative still images of a time-lapse microscopy of scrambled-treated Schwann cells or talin knockdown Schwann cells (siRNA1) at 60 hours after knockdown. **C.** Quantification of the velocity, in which cells were tracked for 12 hours; a total of 50 cells from two

independent experiments were quantified. siRNA1 and siRNA2 were tested separately, and were normalised for the average velocity of the Scrambled-treated cells and then combined in one graph. T-Test was performed.. Related to Movie 5.2.

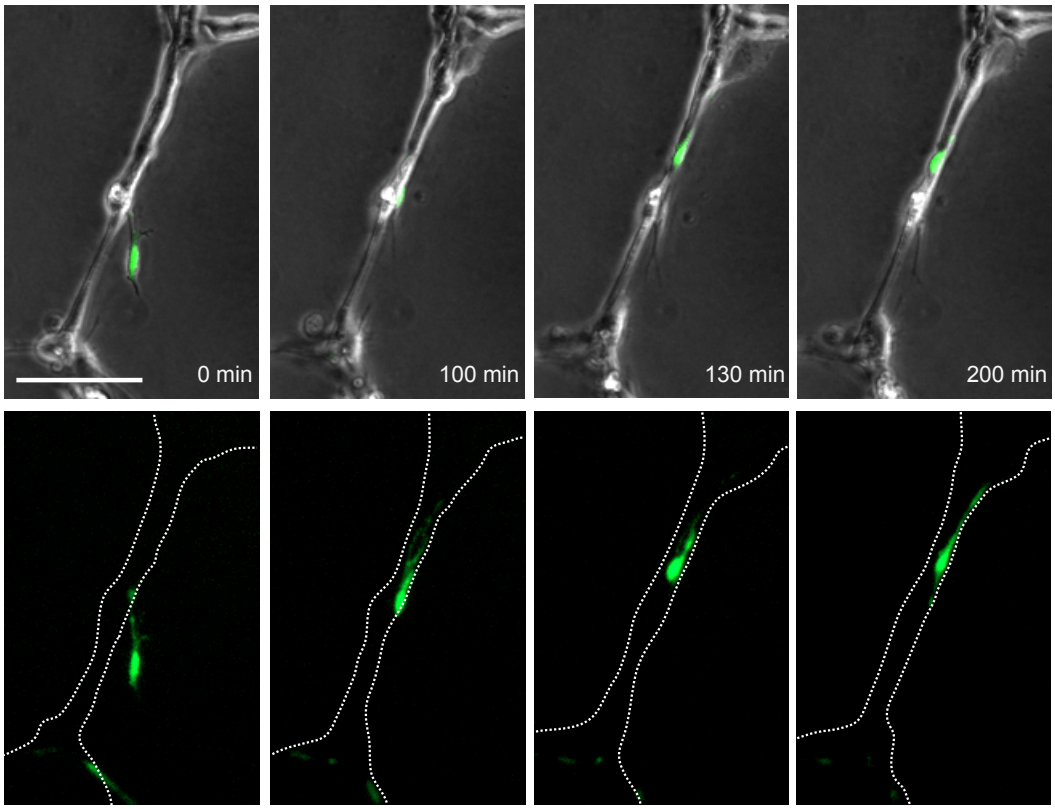

Figure 5.3. Schwann cells migrate along tubules.
Upper panel: Representative phase-contrast still images of time-lapse microscopy of GFP-labelled scrambled-treated Schwann cells migrating along an endothelial cell tubule formed in a matrigel. Lower panel: Representative GFP-images of time-lapse microscopy of GFP-labelled scrambled-treated Schwann cells migrating along the tubule (see outline). Note that the Schwann cells along the tubules adopt a more amoeboid-like morphology. Related to Movie 5.3.

treated GFP-labelled Schwann cells interacted directly with the tubules and the majority migrated along the tubules with forward protrusion extension and rear contraction, causing movements along the tubules, in a similar manner to Schwann cells migrating along blood vessels in fibrin gels (Movie 5.3; Figure 5.3). Interestingly, β1-integrin knockdown cells appeared to interact normally with the HUVECs, showing that loss of β1-integrin does not impair recognition of the tubules (Movie 5.3; Figure 5.3). Surprisingly, whilst β1-integrin knockdown dramatically inhibited 2D migration on laminin, in 3D the majority of the β1-integrin knockdown Schwann cells migrated along the tubules in a similar manner to control cells (Movie 5.3; Figure 5.4). This indicates that in contrast to 2D migration, Schwann cell migration in 3D is not impaired following β1-integrin knockdown. Similarly, we tested whether Schwann cell migration along HUVECs was dependent on talin1 and 2 by seeding talin 1 and talin 2 knockdown cells onto HUVEC tubules. Interestingly, talin 1/2 knockdown cells also interacted with the HUVECs, and the majority migrated along the tubules indistinguishably to control scrambled-treated cells. This indicates that Schwann cells migration in 3D is independent of talin 1 and talin 2 (Movie 5.3; Figure 5.4). Quantification of this showed that scrambled-treated cells have a wide distribution of velocities, but the majority of the cells migrated efficiently along the tubules (Figure 5.6A). Interestingly, β1-integrin knockdown Schwann cells treated with siRNA1, which were unable to migrate in 2D, showed a similar distribution of velocities and importantly there was no significant change in migration speed (Figure 5.6A). Similarly, β1-integrin knockdown Schwann cells treated with siRNA2 migrated at a similar speed to control cells (Figure 5.5A). Thus, this indicates that Schwann cell migration in 3D along the vasculature is independent of β1-integrin, suggesting Schwann cell migration along the vasculature is independent of focal adhesion complexes and is consistent with an amoeboid-like migration, which is associated

with low levels of adhesion (Figure 5.6A). Likewise, while talin knockdown with combination siRNA1 severely impaired 2D migration, there was no significant difference in migration speeds between talin knockdown cells treated with siRNA1 and control cells (Figure 5.6B). Moreover, in siRNA2 treated cells there was a small but not significant change in the migration speed (Figure 5.6B). Thus this indicates that like β1-integrin, talin 1 and talin 2 are not required for Schwann cell migration along the vasculature, indicating that Schwann cell migration along the vasculature is independent of focal adhesion complexes. Consistent with this, focal adhesion complexes could be detected in 2D, but could not be detected in 3D (Cattin et al., 2015).

Taken together, these results show that in contrast to migration in 2D, Schwann cell migration along the vasculature is independent of focal adhesion complexes, which is consistent with an amoeboid-like migration which is associated with low levels of adhesion and high levels of confinement and has previously been reported to be independent of focal adhesion complexes (Lammermann and Sixt, 2009; Liu et al., 2015).

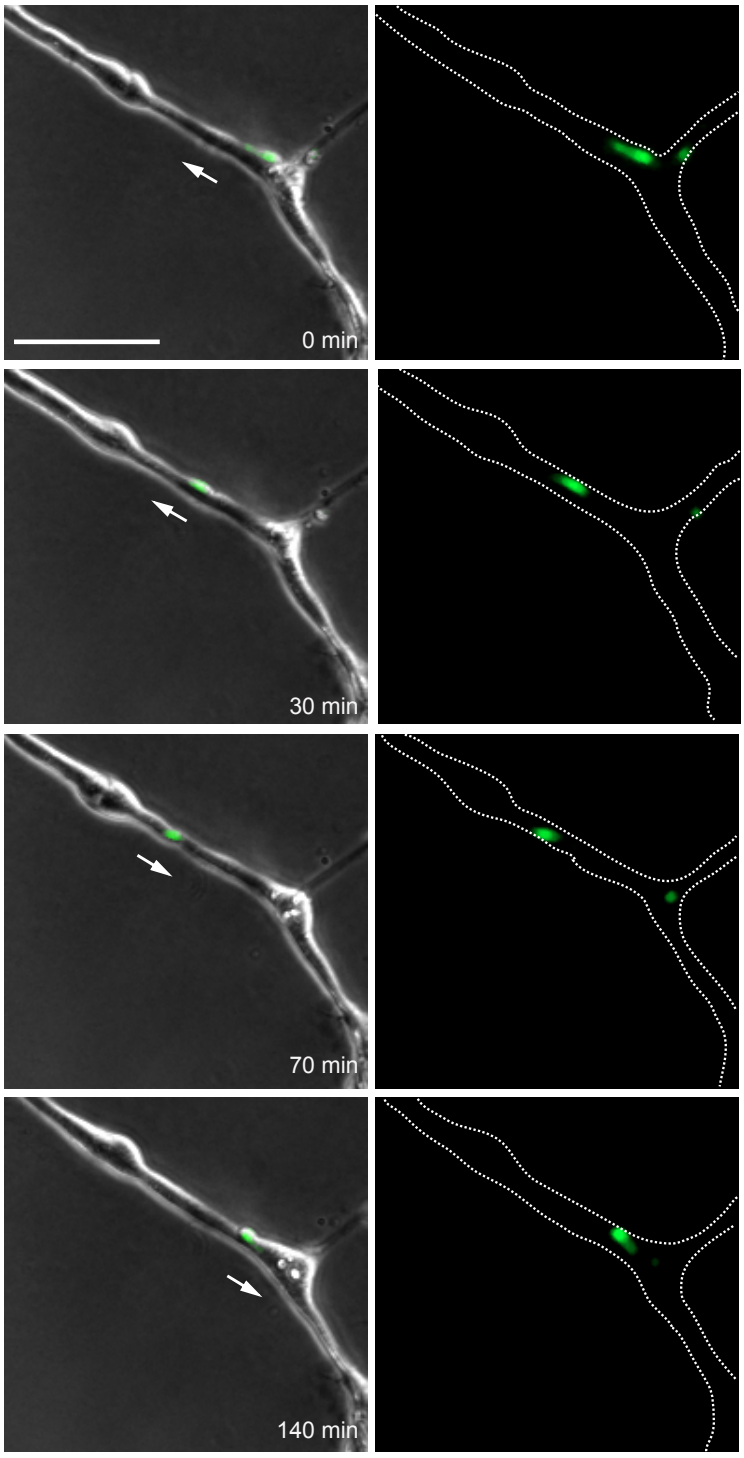

Figure 5.4. Schwann cell migration along endothelial cell tubules is independent of β1-integrin.
Left hand side: Representative phase-contrast still images of time-lapse microscopy of GFP-labelled β1-integrin knockdown Schwann cells migrating along the tubule. Right hand side: Representative GFP-images of time-lapse microscopy of GFP-labelled scrambled-treated Schwann cells migrating along the tubule (see outline). Related to movie 5.3.

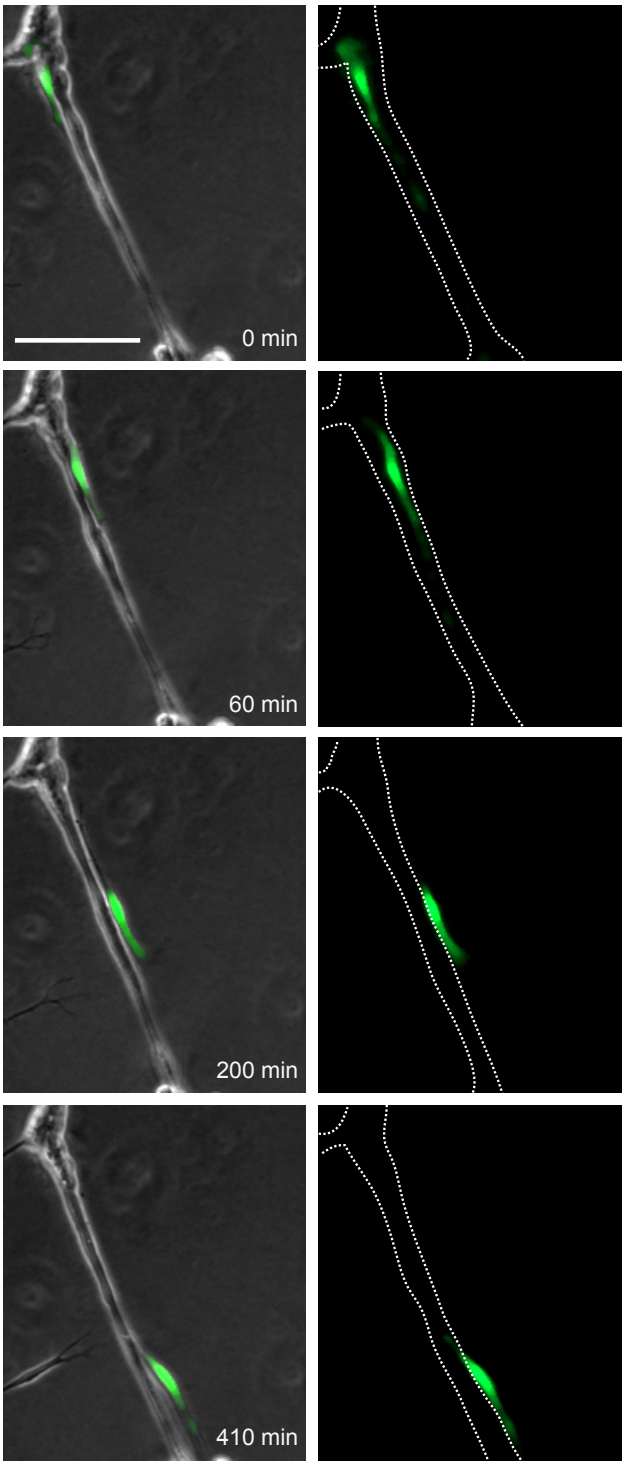

Figure 5.5. Schwann cell migration along endothelial cell tubules is independent of talin.

Left hand sidel: Representative phase-contrast still images of time-lapse microscopy of GFP-labelled talin knockdown Schwann cells migrating along the tubule. Right hand side: Representative GFP-images of time-lapse microscopy of GFP-labelled scrambled-treated Schwann cells migrating along the tubule (see outline). Related to Movie 5.3.

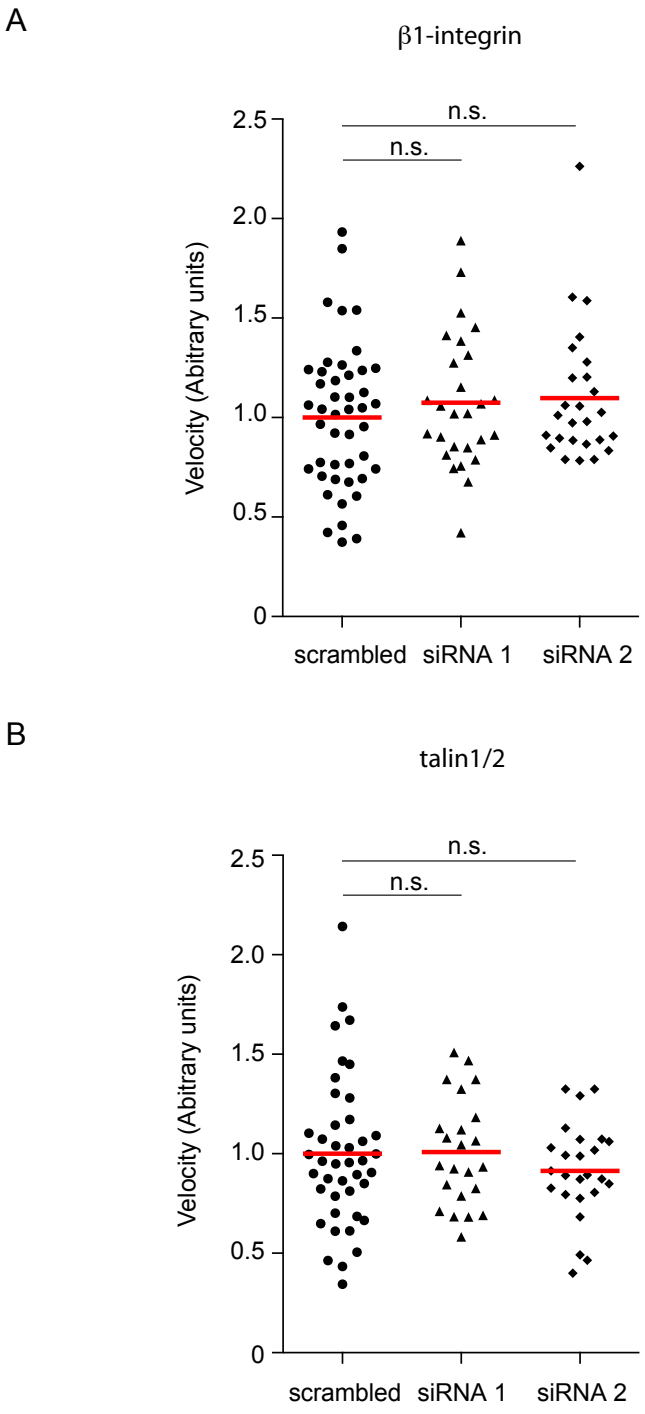

Figure 5.6. Schwann cell migration along blood vessels is independent of focal adhesion complexes.

(A and B) Quantification of Figures 5.2-5.4 in which the scrambled-treated Schwann cells, β1 integrin knockdown cells **(A)** or talin knockdown cells **(B)**, were tracked between 8 and 10 hours. A total of 23 cells per condition were quantified from >3 independent experiments. siRNA1 and siRNA2 were tested in separately, and were normalised for the average velocity of the Scrambled-treated cells and then combined in one graph. T-Test was performed.

5.4. Chapter conclusion

This data demonstrates that Schwann cells use different mechanisms to migrate in 2D versus 3D. In 2D, efficient Schwann cell migration is mediated through β1-integrin and talin 1 and talin 2, consistent with adhesion-dependent migration, which are characteristics of a mesenchymal mode of migration. In contrast in 3D, Schwann cell migration along the vasculature is independent of the focal adhesion complex components β1-integrin and talin 1 and talin 2, which is consistent with an amoeboid–like migration that requires lower levels of adhesion.

Cells can migrate by different mechanisms, which can be broadly divided into two types, mesenchymal migration and a more amoeboid mode of migration which differs in the use of protrusions, contractility and adhesions with the environment (Lammermann and Sixt, 2009). In 2D, in which many cells adopt a mesenchymal mode of migration, adhesion to the substrate, coupled to retrograde forces is required for the cells to migrate. Retrograde forces are generated by actin polymerisation in protrusions such as lamellipodia, which push the membrane forward, coupled with actomyosin-dependent contractility, which causes retraction of the cell rear from the substrate. In 2D, cells are coupled to the substrate via transmembrane receptors such as integrins, which allow traction forces to be exerted onto the surface. In contrast, several studies have shown that an amoeboid mode of migration in 3D is less dependent of adhesion to the substrate, which is consistent with the absence of focal adhesion complexes in 3D (Bergert et al., 2015; Lammermann et al., 2008). Rather, cell locomotion is mediated through a cycle of actin polymerisation-mediated protrusion extension, and actomyosin dependent contraction of the cell rear, that elicits a propulsive type of movement (Lammermann and Sixt, 2009; Liu et al., 2015).

A recent study has shown that cells are able to change their behaviour under high levels of confinement to adopt a more amoeboid mode of migration, which is associated with low levels of adhesion, and that high levels of confinement are required for efficient adhesion-independent migration (Liu et al., 2015). This study further showed that many cell types have the ability and plasticity to switch from a mesenchymal mode of migration to a more amoeboid-mode of migration. This switch in migration mode can be induced by switching from an adhesive and low confinement environment (e.g. 2D migration on a adhesive substrate), to a non-adhesive confined environment (e.g. within a 3D matrix) (Liu et al., 2015). Consistent with these findings, we show here that Schwann cells can also change their mode of migration as in 2D on laminin coated dishes (high adhesion and low confinement), they display a mesenchymal-mode of migration, which is associated with a broad lammellipodia in the direction of migration. In contrast in 3D, Schwann cells in fibrin gels (Cattin et al., 2015) and matrigel, migrate with a cycle of forward protrusion extension and rear contraction (see Figure 5.7). Moreover, we found that rear contraction of Schwann cells migrating along the vasculature is actomyosin dependent (Cattin et al., 2015). Furthermore, an amoeboid-like migration is associated with a more efficient and faster migration (Pankova et al., 2010). Likewise Schwann cells migrate more efficiently along tubules than on 2D laminin (Cattin et al., 2015; Lammermann and Sixt, 2009). Thus, the vasculature provides a track along which Schwann cells can efficiently migrate, providing both directionality and speed.

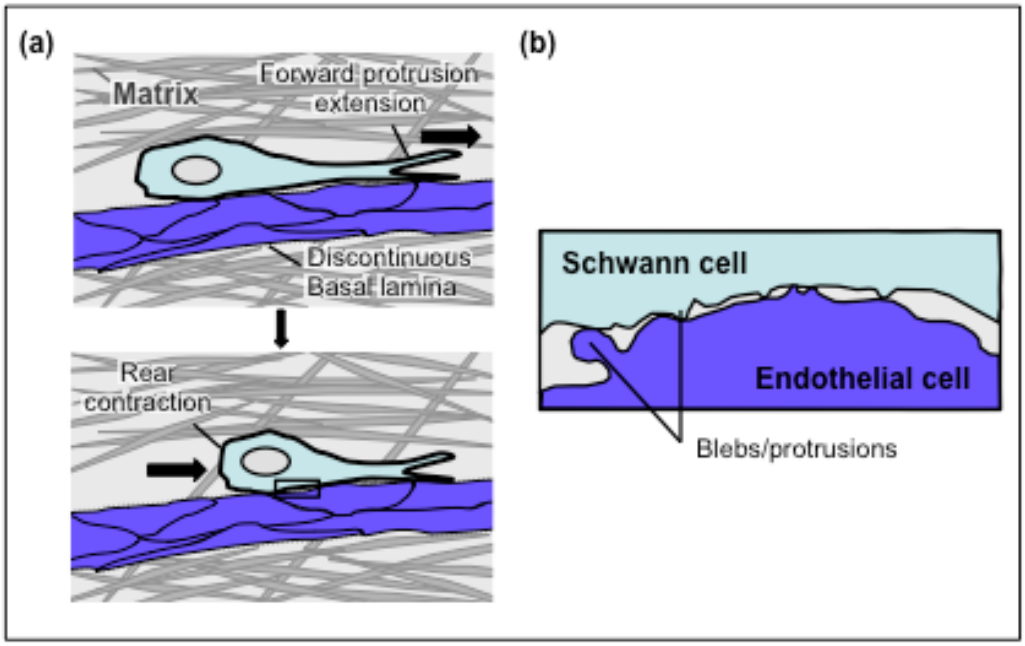

Figure 5.7 Amoeboid-like migration of Schwann cells along the vasculature.
a) Schwann cells migrate along blood vessels in an amoeboid-like fashion that exists out of a cycle of forward protrusion extension and myosin-dependent contraction of the rear of the cell. b) Inset of a) Schwann cell migration along the vasculature is mediated through blebs emerging from both Schwann cells and endothelial cells which provide points of direct contact, and a discontinuous, non-specific surface, through which sufficient forces can be generated to propel the Schwann cells forward; this is consistent with a lower adhesion mode of migration.

How can cells in 3D exert forces required to migrate, independently of adhesion? A recent report shed light into how cells can migrate in the absence of adhesion to the substrate, the authors showed that carcinosarcoma Walker 256 cells, which are unable to migrate in 2D, migrate in 3D in a non-adhesive manner (Bergert et al., 2015). While in 2D, Walker cells have clear focal adhesion foci, in 3D confinement, Walker cells lack these foci. Rather migration is mediated through actomyosin flow from the front to the rear of the cell that is coupled to non-specific friction between the membrane and the matrix, which propels the cell forward. Consistent with this, we found that while 2D migration is dependent on β1-integrin and talin, 3D migration of Schwann cells along endothelial cell tubules is independent of β1-integrin and talin.

Moreover, focal adhesion complexes, which were visualised by paxillin staining, are present in the protrusions of Schwann cells in 2D, but could not be detected in Schwann cells migrating along the vasculature, supporting the idea that Schwann cell migration along the vasculature is independent of adhesion complexes and suggests that Schwann cells may migrate as a result of non-molecular interactions (Cattin et al., 2015).

One striking observation was that while the vast majority of the Schwann cells interact with the HUVEC tubules in fibrin gels, some Schwann cells were found within the matrix and although they were able to form protrusions, they were unable to migrate (Cattin et al., 2015). This suggests that the 3D-matrix environment alone is not sufficient for Schwann cells to migrate. Rather, Schwann cells require the surface of endothelial cells to migrate along. In contrast, fibroblasts (which do not interact with the HUVEC tubules) migrated within the matrix (Cattin et al., 2015), consistent with previous reports (Hakkinen et al., 2011). This indicates that Schwann cells in the matrix cannot generate enough force to migrate. What on the surface of the blood vessels provides an environment for the Schwann cells to efficiently migrate and generate traction forces? High-resolution images of a Schwann cell interacting with an endothelial cell *in vivo*, showed that blebs are emerging from both cells (Cattin et al., 2015). In a recent study a model was created which predicted that blebbing cells in confined spaces migrate more efficiently along a discontinuous surface, as friction between blebs and the discontinuous surface would allow cells to generate traction forces (Tozluoglu et al., 2013). Thus, blebs emerging from both cells could provide points of contact and a discontinuous surface, through which forces could be generated to propel the Schwann cells forward, which is consistent with a non-molecular interaction (Bergert et al., 2015; Liu et al., 2015; Tozluoglu et al., 2013). Moreover, the efficiency of migration is dependent on the density of the ECM and

thus the ECM gap size, as increasing the gap size resulted in weak traction generation and in efficient migration (Tozluoglu et al., 2013). This suggests that Schwann cells within the matrix cannot migrate, as they cannot generate sufficient traction forces to propel themselves forward, possibly due to the density of the matrix. Though specific molecular interactions cannot be excluded, this suggests that blood vessels provide a non-specific discontinuous surface that allows Schwann cells to generate sufficient force to migrate forward.

We propose a model in which the blood vessels in the bridge, in addition to providing directionality to the collectively migrating Schwann cells, provide a frictional surface for the Schwann cells, which allows Schwann cells to generate sufficient forces to efficiently migrate along the blood vessels across the bridge. Though this explains how Schwann cells get their directionality, what triggers the collective migration of Schwann cells following injury is still unknown. Collective migration is often mediated by chemotactic factors, which can induce cell migration (Shellard and Mayor, 2016). Macrophages, in the bridge, are likely to play an important role in the collective migration of Schwann cells, as we showed that macrophages secrete unknown factors that increase Schwann cell migration (Cattin et al., 2015). However, this needs further investigation, which is currently done by colleagues in the lab.

The means by which Schwann cells migrate along the surface of the blood vessels might have broader implications, as several other cell types have been shown to use blood vessels to migrate along. For example a recent study has shown that during the development of the nervous system, oligodendrocyte precursors migrate along the blood vessels (Tsai et al., 2016). Moreover, several cancer cells have been shown to use the vasculature as a substrate and as a mechanism to invade other tissues (Alexander et al., 2013; Bald et al., 2014; Bapat et al., 2011; Carbonell et al., 2009; Farin et al., 2006; Liebig et al., 2009).

Chapter Six: Conclusion

Following severing of the nerve, Schwann cells need to cross a tissue called the bridge, which is formed between the two nerve stumps, in order to guide axons back to their target (Cattin and Lloyd, 2016). We previously showed that Schwann cells migrate as cellular cords, which requires both homotypic interactions, between Schwann cells, as well as heterotypic interactions, with surrounding cells (Cattin et al., 2015; Parrinello et al., 2010). We showed that Schwann cells emerging out of the nerve stumps form clusters when they come in contact with fibroblasts, which is mediated by N-cad (Parrinello et al., 2010). This adhesion is required to mediate the collective migration of Schwann cells as cellular cords. Moreover, recent work from our group showed that in addition to these interactions, interactions of Schwann cells with blood vessels are crucial for directionality and the efficient migration of Schwann cells across the nerve bridge (Cattin et al., 2015). In this current work, we further explored the role of homotypic and heterotypic interactions during the process of peripheral nerve regeneration, and how (the loss of) these interactions are contributing to the tumourigenic process associated with Schwann cell-derived neurofibromas.

We report here that in addition to mediating adhesion, N-cad is also required to mediate CIL in Schwann cells (Parrinello et al., 2010). However, unlike the adherence junction complexes through which N-cad mediates clustering, CIL is independent of the intracellular binding partners α-catenin and p120-catenin, and independent of *trans*-homodimerisation. Rather, we show that the extracellular domain of N-cad is sufficient to revert CIL, and that it presents a repulsion (co-) signal to the other cell. This mechanism provides an explanation as to how N-cad can mediate the seemingly opposing behaviours CIL, which may produce a force to move the cells forward, while at the same time maintaining a cluster through

mediating adhesion. In addition, N-cad is required for initiating remeylination (Lewallen et al., 2011) and in unpublished work by this group, we also showed that N-cad can also mediate CIP and axonal grabbing by Schwann cells (Wingfield-Digby et. al. unpublished thesis; This thesis chapters three and four), further illustrating N-cad has a complex role and can mediate several processes depending on the context. The mechanism, by which N-cad can mediate CIL independent of adhesion, could provide a general mechanism that allows N-cad to play a dual role. Indeed, it has been a longstanding question on how cadherins can mediate adhesion while allowing cellular rearrangements to occur during collective migration or morphogenesis (Etienne-Manneville, 2014; Hong, 2006; Peglion et al., 2014; Theveneau and Mayor, 2010). Moreover, other studies further suggest that similar to in our system in which it appears N-cad is interacting with glypican-4, cadherins could interact with other cells surface proteins to regulate differentiation, axonal growth, cell growth and cell migration (Solanas et al., 2011; Suyama et al., 2002; Trolice et al., 1997; Williams et al., 2001). It would be interesting to see if these processes are also independent of *trans*-homodimerisation and the adherence junction complex.

N-cad is upregulated in various tumours, which is thought to result in the adhesion between tumour cells towards other N-cad expressing tissues such as stroma and the vasculature, resulting in the escape of tumour cells from the tumour mass and invasion of secondary tissues (Berx and van Roy, 2009; Wheelock et al., 2008). Moreover, upregulation of N-cad appears also to be associated with an increase of cell speed, invasion (Hazan et al., 2000; Nieman et al., 1999) and cell growth (Suyama et al., 2002). The latter is dependent on heterotypic interactions in *cis* with growth receptors, causing sustained downstream signalling (Suyama et al.,

2002) This could suggest that other N-cad-mediated adhesion independent mechanisms might also play a role during the tumorigenic process.

We further showed that Schwann cells expressing oncogenic Ras lose CIL in a MEK-dependent manner, which may contribute to development of Schwann cell derived tumours in NF1. However, CIL is not lost through loss of N-cad, as N-cad is functional and the adherence junction complex is unaffected. Instead, oncogenic Ras transforms the mRNA expression levels of the Eph receptors and ephrin ligands and changes the array of proteins interacting with N-cad, thus likely changing the way Schwann cells are interacting with each other and their surrounding cells, and changing the way associated processes are regulated. Interestingly, recent work in perivascular invasion of glioblastoma suggest that loss of NF-1 or expression of oncogenic Ras in these tumour cells, results in a similar change in the expression pattern of the cell surface receptors Eph and their ligands, for example the upregulation of Ephrin-B2 (Krusche et al., 2016). The upregulation of Ephrin-B2 resulted in the attractive signalling of the glioblastoma towards the vasculature, resulting in the perivascular invasion of the normally compartmentalised glioblastomas in the brain. This suggests there might be a general mechanism by which oncogenic Ras regulates the expression of these surface receptors and ligands during the tumorigenic process and the way in which these cells interact between each other and their surrounding cells.

Intriguingly inhibition of the Ras/Raf/ERK pathway in Schwann cells expressing oncogenic Ras, led to the restoration of homotypic Schwann cell interactions, which we showed could revert the loss of CIL. The ability to revert the loss of homotypic interaction between Schwann cells expressing oncogenic Ras, and possibly the interactions with other cells, could provide a possible therapeutic target in patients with MPNSTs and Neurofibromas.

We recently showed that Schwann cells which are unable to migrate through the matrix deposed in the bridge, migrate along the surface of the polarised blood vessels, which form in response to hypoxia (Cattin et al., 2015). Here we show together with the recently published work (Cattin et al., 2015) that, while the focal adhesion components β1-intgerin and talin1 and 2 are required for efficient migration in 2D, they are dispensable for efficient migration along the blood vessel, consistent with an amoeboid-like mode of migration. Instead, we propose that blebs emanating from both Schwann cells and endothelial cells provide direct points of contact and a non-specific frictional surface, which can produce sufficient traction to propel the Schwann cells forward (Cattin et al., 2015). However, the need of other proteins to mediate the heterotypic interactions between Schwann cells and the vasculature cannot be excluded.

A parallel can be drawn between Schwann cells migrating along the vasculature and the spreading of several types of tumour cells along blood vessels or other cell surfaces (Alexander et al., 2013; Bald et al., 2014; Bapat et al., 2011; Carbonell et al., 2009; Farin et al., 2006; Liebig et al., 2009). It would be interesting to see if these tumour cells use similar mechanisms to Schwann cells to migrate along the vasculature. NF1-/- Schwann cells appear to become motile during the tumorigenic process, as they are able to spread along the length of the nerve, become locally invasive and in MPNSTs are able to metastasise (Kim et al., 1997; Sheela et al., 1990). Moreover, neurofibroma formation recapitulates the injury response, in that it has the same cellular components, which could suggest that Schwann cells could use similar mechanisms to migrate along the vasculature, allowing the spreading of the tumour. Another possibility is that oncogenic Ras changes the way in which Schwann cells interact with the vasculature. As mentioned above, glioblastomas with elevated Ras signalling have more attractive signalling

towards the blood vessels, which is mediated by the upregulated ephrin-B2 (Krusche et al., 2016). Similarly, in Schwann cells expressing oncogenic Ras, ephrin-B2 is upregulated, suggesting this could induce the cells to migrate along the vasculature, and allowing the spread of these cells.

How does the amoeboid-like migration of single Schwann cells along the vasculature relate to the collective migration of Schwann cells as cellular cords *in vivo*? It is well established that collective migration relies on the same principles as single migrating cells, in which individual cells within the cell cluster adapt a front to rear polarity, which is mediated through interactions with the cell substrate, such as focal adhesions, as well as through extracellular signals such as chemoattractive factors (Mayor and Etienne-Manneville, 2016). However, recent work in the neural crest showed that only the cells at the edge of the group of cells adapt a front to rear morphology, while the trailing cells (the cells away from the edge of the group) do not have this polarity, which is caused by N-cad-mediated homotypic interactions that can regulate both adhesion and CIL (Theveneau et al., 2010). Thus, one possibility is that within the Schwann cell cords, the leading Schwann cells are polarised, and migrate in a focal adhesion-independent manner. In contrast, the trailing cells might lack this polarity, similar to the neural crest, due to inhibition of the protrusions at the site of cell-cell contact. This is mediated by N-cad, which has a dual role by mediating adhesion allowing the cells to be in constant contact, and in addition induces a repulsion response, which could provide a repulsive force towards the front of the cells, driving the migration of the group forward. Another possibility might be that Schwann cells migrate more as loose stream of cells, in which the cells can escape from the group through repulsive signals. These theories will be tested in future work using both *ex vivo* and *in vivo* live-imaging of Schwann cell cords.

Homotypic and heterotypic interactions between Schwann cells and the surrounding cells play a complex role in regulating the Schwann cells function during the regenerative process and neurofibromatosis. This work highlights that single protein-protein interactions can regulate multiple processes or result in a variety of different Schwann cell responses depending on the context.

References

Abercrombie, M. (1979). Contact inhibition and malignancy. Nature *281*, 259-262.

Abercrombie, M., and Heaysman, J.E. (1953). Observations on the social behaviour of cells in tissue culture. I. Speed of movement of chick heart fibroblasts in relation to their mutual contacts. Experimental cell research *5*, 111-131.

Abercrombie, M., and Heaysman, J.E. (1954a). Invasiveness of sarcoma cells. Nature *174*, 697-698.

Abercrombie, M., and Heaysman, J.E. (1954b). Observations on the social behaviour of cells in tissue culture. II. Monolayering of fibroblasts. Experimental cell research *6*, 293-306.

Aberle, H., Butz, S., Stappert, J., Weissig, H., Kemler, R., and Hoschuetzky, H. (1994). Assembly of the cadherin-catenin complex in vitro with recombinant proteins. Journal of cell science *107 (Pt 12)*, 3655-3663.

Alexander, S., Weigelin, B., Winkler, F., and Friedl, P. (2013). Preclinical intravital microscopy of the tumour-stroma interface: invasion, metastasis, and therapy response. Current opinion in cell biology *25*, 659-671.

Aman, A., and Piotrowski, T. (2010). Cell migration during morphogenesis. Developmental biology *341*, 20-33.

Anastasiadis, P.Z., Moon, S.Y., Thoreson, M.A., Mariner, D.J., Crawford, H.C., Zheng, Y., and Reynolds, A.B. (2000). Inhibition of RhoA by p120 catenin. Nature cell biology *2*, 637-644.

Arthur-Farraj, P., Wanek, K., Hantke, J., Davis, C.M., Jayakar, A., Parkinson, D.B., Mirsky, R., and Jessen, K.R. (2011). Mouse schwann cells need both NRG1 and cyclic AMP to myelinate. Glia *59*, 720-733.

Arthur-Farraj, P.J., Latouche, M., Wilton, D.K., Quintes, S., Chabrol, E., Banerjee, A., Woodhoo, A., Jenkins, B., Rahman, M., Turmaine, M.*, et al.* (2012). c-Jun reprograms Schwann cells of injured nerves to generate a repair cell essential for regeneration. Neuron *75*, 633-647.

Astin, J.W., Batson, J., Kadir, S., Charlet, J., Persad, R.A., Gillatt, D., Oxley, J.D., and Nobes, C.D. (2010). Competition amongst Eph receptors regulates contact inhibition of locomotion and invasiveness in prostate cancer cells. Nature cell biology *12*, 1194-1204.

Bald, T., Quast, T., Landsberg, J., Rogava, M., Glodde, N., Lopez-Ramos, D., Kohlmeyer, J., Riesenberg, S., van den Boorn-Konijnenberg, D., Homig-Holzel, C.*, et al.* (2014). Ultraviolet-radiation-induced inflammation promotes angiotropism and metastasis in melanoma. Nature *507*, 109-113.

Bapat, A.A., Hostetter, G., Von Hoff, D.D., and Han, H. (2011). Perineural invasion and associated pain in pancreatic cancer. Nature reviews Cancer *11*, 695-707.

Bashaw, G.J., and Klein, R. (2010). Signaling from axon guidance receptors. Cold Spring Harbor perspectives in biology *2*, a001941.

Batlle, E., Bacani, J., Begthel, H., Jonkheer, S., Gregorieff, A., van de Born, M., Malats, N., Sancho, E., Boon, E., Pawson, T.*, et al.* (2005). EphB receptor activity suppresses colorectal cancer progression. Nature *435*, 1126-1130.

Batlle, E., Henderson, J.T., Beghtel, H., van den Born, M.M., Sancho, E., Huls, G., Meeldijk, J., Robertson, J., van de Wetering, M., Pawson, T.*, et al.* (2002). Beta-catenin and TCF mediate cell positioning in the intestinal epithelium by controlling the expression of EphB/ephrinB. Cell *111*, 251-263.

Batlle, E., and Wilkinson, D.G. (2012). Molecular mechanisms of cell segregation and boundary formation in development and tumorigenesis. Cold Spring Harbor perspectives in biology *4*, a008227.

Batson, J., Astin, J.W., and Nobes, C.D. (2013). Regulation of contact inhibition of locomotion by Eph-ephrin signalling. Journal of microscopy *251*, 232-241.

Batson, J., Maccarthy-Morrogh, L., Archer, A., Tanton, H., and Nobes, C.D. (2014). EphA receptors regulate prostate cancer cell dissemination through Vav2-RhoA mediated cell-cell repulsion. Biology open *3*, 453-462.

Becker, S.F., Mayor, R., and Kashef, J. (2013). Cadherin-11 mediates contact inhibition of locomotion during Xenopus neural crest cell migration. PloS one *8*, e85717.

Bergert, M., Erzberger, A., Desai, R.A., Aspalter, I.M., Oates, A.C., Charras, G., Salbreux, G., and Paluch, E.K. (2015). Force transmission during adhesion-independent migration. Nature cell biology *17*, 524-529.

Berghs, S., Aggujaro, D., Dirkx, R., Jr., Maksimova, E., Stabach, P., Hermel, J.M., Zhang, J.P., Philbrick, W., Slepnev, V., Ort, T.*, et al.* (2000). betaIV spectrin, a new spectrin localized at axon initial segments and nodes of ranvier in the central and peripheral nervous system. The Journal of cell biology *151*, 985-1002.

Bergoffen, J., Scherer, S.S., Wang, S., Scott, M.O., Bone, L.J., Paul, D.L., Chen, K., Lensch, M.W., Chance, P.F., and Fischbeck, K.H. (1993). Connexin mutations in X-linked Charcot-Marie-Tooth disease. Science *262*, 2039-2042.

Bermingham, J.R., Jr., Shearin, H., Pennington, J., O'Moore, J., Jaegle, M., Driegen, S., van Zon, A., Darbas, A., Ozkaynak, E., Ryu, E.J.*, et al.* (2006). The claw paw mutation reveals a role for Lgi4 in peripheral nerve development. Nature neuroscience *9*, 76-84.

Berti, C., Bartesaghi, L., Ghidinelli, M., Zambroni, D., Figlia, G., Chen, Z.L., Quattrini, A., Wrabetz, L., and Feltri, M.L. (2011). Non-redundant function of dystroglycan and beta1 integrins in radial sorting of axons. Development *138*, 4025-4037.

Berx, G., and van Roy, F. (2009). Involvement of members of the cadherin superfamily in cancer. Cold Spring Harbor perspectives in biology *1*, a003129.

Birchmeier, C. (2009). ErbB receptors and the development of the nervous system. Experimental cell research *315*, 611-618.

Blanchette, C.R., Perrat, P.N., Thackeray, A., and Benard, C.Y. (2015). Glypican Is a Modulator of Netrin-Mediated Axon Guidance. PLoS biology *13*, e1002183.

Bonanomi, D., Chivatakarn, O., Bai, G., Abdesselem, H., Lettieri, K., Marquardt, T., Pierchala, B.A., and Pfaff, S.L. (2012). Ret is a multifunctional coreceptor that integrates diffusible- and contact-axon guidance signals. Cell *148*, 568-582.

Brasch, J., Harrison, O.J., Honig, B., and Shapiro, L. (2012). Thinking outside the cell: how cadherins drive adhesion. Trends in cell biology *22*, 299-310.

Brennan, A., Dean, C.H., Zhang, A.L., Cass, D.T., Mirsky, R., and Jessen, K.R. (2000). Endothelins control the timing of Schwann cell generation in vitro and in vivo. Developmental biology *227*, 545-557.

Britsch, S., Goerich, D.E., Riethmacher, D., Peirano, R.I., Rossner, M., Nave, K.A., Birchmeier, C., and Wegner, M. (2001). The transcription factor Sox10 is a key regulator of peripheral glial development. Genes & development *15*, 66-78.

Buckley, C.D., Tan, J., Anderson, K.L., Hanein, D., Volkmann, N., Weis, W.I., Nelson, W.J., and Dunn, A.R. (2014). Cell adhesion. The minimal cadherin-catenin complex binds to actin filaments under force. Science *346*, 1254211.

Campellone, K.G., and Welch, M.D. (2010). A nucleator arms race: cellular control of actin assembly. Nature reviews Molecular cell biology *11*, 237-251.

Capurro, M.I., Xiang, Y.Y., Lobe, C., and Filmus, J. (2005). Glypican-3 promotes the growth of hepatocellular carcinoma by stimulating canonical Wnt signaling. Cancer research *65*, 6245-6254.

Capurro, M.I., Xu, P., Shi, W., Li, F., Jia, A., and Filmus, J. (2008). Glypican-3 inhibits Hedgehog signaling during development by competing with patched for Hedgehog binding. Developmental cell *14*, 700-711.

Carbonell, W.S., Ansorge, O., Sibson, N., and Muschel, R. (2009). The vascular basement membrane as "soil" in brain metastasis. PloS one *4*, e5857.

Carmona-Fontaine, C., Matthews, H.K., Kuriyama, S., Moreno, M., Dunn, G.A., Parsons, M., Stern, C.D., and Mayor, R. (2008). Contact inhibition of locomotion in vivo controls neural crest directional migration. Nature *456*, 957-961.

Carmona-Fontaine, C., Theveneau, E., Tzekou, A., Tada, M., Woods, M., Page, K.M., Parsons, M., Lambris, J.D., and Mayor, R. (2011). Complement fragment C3a controls mutual cell attraction during collective cell migration. Developmental cell *21*, 1026-1037.

Cattin, A.L., Burden, J.J., Van Emmenis, L., Mackenzie, F.E., Hoving, J.J., Garcia Calavia, N., Guo, Y., McLaughlin, M., Rosenberg, L.H., Quereda, V.*, et al.* (2015). Macrophage-Induced Blood Vessels Guide Schwann Cell-Mediated Regeneration of Peripheral Nerves. Cell *162*, 1127-1139.

Cattin, A.L., and Lloyd, A.C. (2016). The multicellular complexity of peripheral nerve regeneration. Current opinion in neurobiology *39*, 38-46.

Charles, P., Tait, S., Faivre-Sarrailh, C., Barbin, G., Gunn-Moore, F., Denisenko-Nehrbass, N., Guennoc, A.M., Girault, J.A., Brophy, P.J., and Lubetzki, C. (2002). Neurofascin is a glial receptor for the paranodin/Caspr-contactin axonal complex at the axoglial junction. Current biology : CB *12*, 217-220.

Cheng, L., Khan, M., and Mudge, A.W. (1995). Calcitonin gene-related peptide promotes Schwann cell proliferation. The Journal of cell biology *129*, 789-796.

Collins, M.J., Napoli, I., Ribeiro, S., Roberts, S., and Lloyd, A.C. (2012). Loss of Rb cooperates with Ras to drive oncogenic growth in mammalian cells. Current biology : CB *22*, 1765-1773.

Conforti, L., Gilley, J., and Coleman, M.P. (2014). Wallerian degeneration: an emerging axon death pathway linking injury and disease. Nature reviews Neuroscience *15*, 394-409.

Corfas, G., Velardez, M.O., Ko, C.P., Ratner, N., and Peles, E. (2004). Mechanisms and roles of axon-Schwann cell interactions. The Journal of neuroscience : the official journal of the Society for Neuroscience *24*, 9250-9260.

Cornejo, M., Nambi, D., Walheim, C., Somerville, M., Walker, J., Kim, L., Ollison, L., Diamante, G., Vyawahare, S., and de Bellard, M.E. (2010). Effect of NRG1, GDNF, EGF and NGF in the migration of a Schwann cell precursor line. Neurochemical research *35*, 1643-1651.

Cortina, C., Palomo-Ponce, S., Iglesias, M., Fernandez-Masip, J.L., Vivancos, A., Whissell, G., Huma, M., Peiro, N., Gallego, L., Jonkheer, S.*, et al.* (2007). EphB-ephrin-B interactions suppress colorectal cancer progression by compartmentalizing tumor cells. Nature genetics *39*, 1376-1383.

Crawford, A.T., Desai, D., Gokina, P., Basak, S., and Kim, H.A. (2008). E-cadherin expression in postnatal Schwann cells is regulated by the cAMP-dependent protein kinase a pathway. Glia *56*, 1637-1647.

Cunningham, F., Amode, M.R., Barrell, D., Beal, K., Billis, K., Brent, S., Carvalho-Silva, D., Clapham, P., Coates, G., Fitzgerald, S.*, et al.* (2015). Ensembl 2015. Nucleic Acids Res *43*, D662-D669.

Davis, J.R., Luchici, A., Mosis, F., Thackery, J., Salazar, J.A., Mao, Y., Dunn, G.A., Betz, T., Miodownik, M., and Stramer, B.M. (2015). Inter-cellular forces orchestrate contact inhibition of locomotion. Cell *161*, 361-373.

Davis, M.A., Ireton, R.C., and Reynolds, A.B. (2003). A core function for p120-catenin in cadherin turnover. The Journal of cell biology *163*, 525-534.

Davis, S., Gale, N.W., Aldrich, T.H., Maisonpierre, P.C., Lhotak, V., Pawson, T., Goldfarb, M., and Yancopoulos, G.D. (1994). Ligands for EPH-related receptor tyrosine kinases that require membrane attachment or clustering for activity. Science *266*, 816-819.

DeClue, J.E., Papageorge, A.G., Fletcher, J.A., Diehl, S.R., Ratner, N., Vass, W.C., and Lowy, D.R. (1992). Abnormal regulation of mammalian p21ras contributes to

malignant tumor growth in von Recklinghausen (type 1) neurofibromatosis. Cell *69*, 265-273.

Delva, E., and Kowalczyk, A.P. (2009). Regulation of cadherin trafficking. Traffic *10*, 259-267.

Der, C.J., Krontiris, T.G., and Cooper, G.M. (1982). Transforming genes of human bladder and lung carcinoma cell lines are homologous to the ras genes of Harvey and Kirsten sarcoma viruses. Proceedings of the National Academy of Sciences of the United States of America *79*, 3637-3640.

Desai, R., Sarpal, R., Ishiyama, N., Pellikka, M., Ikura, M., and Tepass, U. (2013). Monomeric alpha-catenin links cadherin to the actin cytoskeleton. Nature cell biology *15*, 261-273.

Dow, L.E., Elsum, I.A., King, C.L., Kinross, K.M., Richardson, H.E., and Humbert, P.O. (2008). Loss of human Scribble cooperates with H-Ras to promote cell invasion through deregulation of MAPK signalling. Oncogene *27*, 5988-6001.

Dowsing, B.J., Morrison, W.A., Nicola, N.A., Starkey, G.P., Bucci, T., and Kilpatrick, T.J. (1999). Leukemia inhibitory factor is an autocrine survival factor for Schwann cells. Journal of neurochemistry *73*, 96-104.

Egea, J., Nissen, U.V., Dufour, A., Sahin, M., Greer, P., Kullander, K., Mrsic-Flogel, T.D., Greenberg, M.E., Kiehn, O., Vanderhaeghen, P.*, et al.* (2005). Regulation of EphA 4 kinase activity is required for a subset of axon guidance decisions suggesting a key role for receptor clustering in Eph function. Neuron *47*, 515-528.

Eshed, Y., Feinberg, K., Poliak, S., Sabanay, H., Sarig-Nadir, O., Spiegel, I., Bermingham, J.R., Jr., and Peles, E. (2005). Gliomedin mediates Schwann cell-axon interaction and the molecular assembly of the nodes of Ranvier. Neuron *47*, 215-229.

Etienne-Manneville, S. (2014). Neighborly relations during collective migration. Current opinion in cell biology *30*, 51-59.

Evans, D.G., Baser, M.E., McGaughran, J., Sharif, S., Howard, E., and Moran, A. (2002). Malignant peripheral nerve sheath tumours in neurofibromatosis 1. Journal of medical genetics *39*, 311-314.

Fannon, A.M., Sherman, D.L., Ilyina-Gragerova, G., Brophy, P.J., Friedrich, V.L., Jr., and Colman, D.R. (1995). Novel E-cadherin-mediated adhesion in peripheral nerve: Schwann cell architecture is stabilized by autotypic adherens junctions. The Journal of cell biology *129*, 189-202.

Farin, A., Suzuki, S.O., Weiker, M., Goldman, J.E., Bruce, J.N., and Canoll, P. (2006). Transplanted glioma cells migrate and proliferate on host brain vasculature: a dynamic analysis. Glia *53*, 799-808.

Feltri, M.L., Graus Porta, D., Previtali, S.C., Nodari, A., Migliavacca, B., Cassetti, A., Littlewood-Evans, A., Reichardt, L.F., Messing, A., Quattrini, A.*, et al.* (2002). Conditional disruption of beta 1 integrin in Schwann cells impedes interactions with axons. The Journal of cell biology *156*, 199-209.

Ferner, R.E. (2007). Neurofibromatosis 1 and neurofibromatosis 2: a twenty first century perspective. The Lancet Neurology *6*, 340-351.

Filmus, J., Capurro, M., and Rast, J. (2008). Glypicans. Genome biology *9*, 224.

Fontana, X., Hristova, M., Da Costa, C., Patodia, S., Thei, L., Makwana, M., Spencer-Dene, B., Latouche, M., Mirsky, R., Jessen, K.R.*, et al.* (2012). c-Jun in Schwann cells promotes axonal regeneration and motoneuron survival via paracrine signaling. The Journal of cell biology *198*, 127-141.

Friedl, P., and Alexander, S. (2011). Cancer invasion and the microenvironment: plasticity and reciprocity. Cell *147*, 992-1009.

Fritz, R.D., Menshykau, D., Martin, K., Reimann, A., Pontelli, V., and Pertz, O. (2015). SrGAP2-Dependent Integration of Membrane Geometry and Slit-Robo-Repulsive Cues Regulates Fibroblast Contact Inhibition of Locomotion. Developmental cell *35*, 78-92.

Fujita, Y., Krause, G., Scheffner, M., Zechner, D., Leddy, H.E., Behrens, J., Sommer, T., and Birchmeier, W. (2002). Hakai, a c-Cbl-like protein, ubiquitinates and induces endocytosis of the E-cadherin complex. Nature cell biology *4*, 222-231.

Gale, N.W., Holland, S.J., Valenzuela, D.M., Flenniken, A., Pan, L., Ryan, T.E., Henkemeyer, M., Strebhardt, K., Hirai, H., Wilkinson, D.G.*, et al.* (1996). Eph receptors and ligands comprise two major specificity subclasses and are reciprocally compartmentalized during embryogenesis. Neuron *17*, 9-19.

Glenn, T.D., and Talbot, W.S. (2013). Analysis of Gpr126 function defines distinct mechanisms controlling the initiation and maturation of myelin. Development *140*, 3167-3175.

Goebbels, S., Oltrogge, J.H., Kemper, R., Heilmann, I., Bormuth, I., Wolfer, S., Wichert, S.P., Mobius, W., Liu, X., Lappe-Siefke, C.*, et al.* (2010). Elevated phosphatidylinositol 3,4,5-trisphosphate in glia triggers cell-autonomous membrane wrapping and myelination. The Journal of neuroscience : the official journal of the Society for Neuroscience *30*, 8953-8964.

Goebbels, S., Oltrogge, J.H., Wolfer, S., Wieser, G.L., Nientiedt, T., Pieper, A., Ruhwedel, T., Groszer, M., Sereda, M.W., and Nave, K.A. (2012). Genetic disruption of Pten in a novel mouse model of tomaculous neuropathy. EMBO molecular medicine *4*, 486-499.

Goldfarb, M., Shimizu, K., Perucho, M., and Wigler, M. (1982). Isolation and preliminary characterization of a human transforming gene from T24 bladder carcinoma cells. Nature *296*, 404-409.

Gorelik, R., and Gautreau, A. (2014). Quantitative and unbiased analysis of directional persistence in cell migration. Nature protocols *9*, 1931-1943.

Grosheva, I., Shtutman, M., Elbaum, M., and Bershadsky, A.D. (2001). p120 catenin affects cell motility via modulation of activity of Rho-family GTPases: a link between cell-cell contact formation and regulation of cell locomotion. Journal of cell science *114*, 695-707.

Grothe, C., and Nikkhah, G. (2001). The role of basic fibroblast growth factor in peripheral nerve regeneration. Anatomy and embryology *204*, 171-177.

Gurtner, G.C., Werner, S., Barrandon, Y., and Longaker, M.T. (2008). Wound repair and regeneration. Nature *453*, 314-321.

Hakkinen, K.M., Harunaga, J.S., Doyle, A.D., and Yamada, K.M. (2011). Direct comparisons of the morphology, migration, cell adhesions, and actin cytoskeleton of fibroblasts in four different three-dimensional extracellular matrices. Tissue engineering Part A *17*, 713-724.

Halbleib, J.M., and Nelson, W.J. (2006). Cadherins in development: cell adhesion, sorting, and tissue morphogenesis. Genes & development *20*, 3199-3214.

Hanahan, D., and Weinberg, R.A. (2011). Hallmarks of cancer: the next generation. Cell *144*, 646-674.

Harris, T.J., and Tepass, U. (2010). Adherens junctions: from molecules to morphogenesis. Nature reviews Molecular cell biology *11*, 502-514.

Harrisingh, M.C., Perez-Nadales, E., Parkinson, D.B., Malcolm, D.S., Mudge, A.W., and Lloyd, A.C. (2004). The Ras/Raf/ERK signalling pathway drives Schwann cell dedifferentiation. The EMBO journal *23*, 3061-3071.

Hattori, M., Osterfield, M., and Flanagan, J.G. (2000). Regulated cleavage of a contact-mediated axon repellent. Science *289*, 1360-1365.

Hay, E., Laplantine, E., Geoffroy, V., Frain, M., Kohler, T., Muller, R., and Marie, P.J. (2009). N-cadherin interacts with axin and LRP5 to negatively regulate Wnt/beta-catenin signaling, osteoblast function, and bone formation. Molecular and cellular biology *29*, 953-964.

Hazan, R.B., Phillips, G.R., Qiao, R.F., Norton, L., and Aaronson, S.A. (2000). Exogenous expression of N-cadherin in breast cancer cells induces cell migration, invasion, and metastasis. The Journal of cell biology *148*, 779-790.

Heermann, S., and Krieglstein, K. (2012). Analyzing murine Schwann cell development along growing axons. Journal of visualized experiments : JoVE.

Heermann, S., Schmucker, J., Hinz, U., Rickmann, M., Unterbarnscheidt, T., Schwab, M.H., and Krieglstein, K. (2011). Neuregulin 1 type III/ErbB signaling is crucial for Schwann cell colonization of sympathetic axons. PloS one *6*, e28692.

Heermann, S., and Schwab, M.H. (2013). Molecular control of Schwann cell migration along peripheral axons: keep moving! Cell adhesion & migration *7*, 18-22.

Himanen, J.P., Chumley, M.J., Lackmann, M., Li, C., Barton, W.A., Jeffrey, P.D., Vearing, C., Geleick, D., Feldheim, D.A., Boyd, A.W*., et al.* (2004). Repelling class discrimination: ephrin-A5 binds to and activates EphB2 receptor signaling. Nature neuroscience *7*, 501-509.

Hoke, A. (2006). Mechanisms of Disease: what factors limit the success of peripheral nerve regeneration in humans? Nature clinical practice Neurology *2*, 448-454.

Hung, R.J., and Terman, J.R. (2011). Extracellular inhibitors, repellents, and semaphorin/plexin/MICAL-mediated actin filament disassembly. Cytoskeleton *68*, 415-433.

Huttenlocher, A., and Horwitz, A.R. (2011). Integrins in cell migration. Cold Spring Harbor perspectives in biology *3*, a005074.

Inoue, G., Gaultier, A., Li, X., Mantuano, E., Richardson, G., Takahashi, K., and Campana, W.M. (2010). Erythropoietin promotes Schwann cell migration and assembly of the provisional extracellular matrix by recruiting beta1 integrin to the cell surface. Glia *58*, 399-409.

Jessen, K.R., and Mirsky, R. (2005). The origin and development of glial cells in peripheral nerves. Nature reviews Neuroscience *6*, 671-682.

Jessen, K.R., Mirsky, R., and Lloyd, A.C. (2015). Schwann Cells: Development and Role in Nerve Repair. Cold Spring Harbor perspectives in biology *7*, a020487.

Joseph, N.M., Mosher, J.T., Buchstaller, J., Snider, P., McKeever, P.E., Lim, M., Conway, S.J., Parada, L.F., Zhu, Y., and Morrison, S.J. (2008). The loss of Nf1 transiently promotes self-renewal but not tumorigenesis by neural crest stem cells. Cancer cell *13*, 129-140.

Juarez, P., and Palau, F. (2012). Neural and molecular features on Charcot-Marie-Tooth disease plasticity and therapy. Neural plasticity *2012*, 171636.

Kadir, S., Astin, J.W., Tahtamouni, L., Martin, P., and Nobes, C.D. (2011). Microtubule remodelling is required for the front-rear polarity switch during contact inhibition of locomotion. Journal of cell science *124*, 2642-2653.

Kametani, Y., and Takeichi, M. (2007). Basal-to-apical cadherin flow at cell junctions. Nature cell biology *9*, 92-98.

Kania, A., and Klein, R. (2016). Mechanisms of ephrin-Eph signalling in development, physiology and disease. Nature reviews Molecular cell biology *17*, 240-256.

Kegel, L., Aunin, E., Meijer, D., and Bermingham, J.R. (2013). LGI proteins in the nervous system. ASN neuro *5*, 167-181.

Kim, H.A., Ling, B., and Ratner, N. (1997). Nf1-deficient mouse Schwann cells are angiogenic and invasive and can be induced to hyperproliferate: reversion of some phenotypes by an inhibitor of farnesyl protein transferase. Molecular and cellular biology *17*, 862-872.

Kipanyula, M.J., Woodhoo, A., Rahman, M., Payne, D., Jessen, K.R., and Mirsky, R. (2013). Calcineurin-nuclear factor of activated T cells regulation of Krox-20 expression in Schwann cells requires elevation of intracellular cyclic AMP. Journal of neuroscience research *91*, 105-115.

Kobielak, A., and Fuchs, E. (2004). Alpha-catenin: at the junction of intercellular adhesion and actin dynamics. Nature reviews Molecular cell biology *5*, 614-625.

Kordeli, E., Lambert, S., and Bennett, V. (1995). AnkyrinG. A new ankyrin gene with neural-specific isoforms localized at the axonal initial segment and node of Ranvier. The Journal of biological chemistry *270*, 2352-2359.

Kullander, K., Mather, N.K., Diella, F., Dottori, M., Boyd, A.W., and Klein, R. (2001). Kinase-dependent and kinase-independent functions of EphA4 receptors in major axon tract formation in vivo. Neuron *29*, 73-84.

Lammermann, T., Bader, B.L., Monkley, S.J., Worbs, T., Wedlich-Soldner, R., Hirsch, K., Keller, M., Forster, R., Critchley, D.R., Fassler, R.*, et al.* (2008). Rapid leukocyte migration by integrin-independent flowing and squeezing. Nature *453*, 51-55.

Lammermann, T., and Sixt, M. (2009). Mechanical modes of 'amoeboid' cell migration. Current opinion in cell biology *21*, 636-644.

Laquerriere, A., Maluenda, J., Camus, A., Fontenas, L., Dieterich, K., Nolent, F., Zhou, J., Monnier, N., Latour, P., Gentil, D.*, et al.* (2014). Mutations in CNTNAP1 and ADCY6 are responsible for severe arthrogryposis multiplex congenita with axoglial defects. Human molecular genetics *23*, 2279-2289.

Lassmann, H., Jurecka, W., and Gebhart, W. (1976). Some electron microscopic and autoradiographic results concerning cutaneous neurofibromas in von Recklinghausen's disease. Archives for dermatological research = Archiv fur dermatologische Forschung *255*, 69-81.

le Duc, Q., Shi, Q., Blonk, I., Sonnenberg, A., Wang, N., Leckband, D., and de Rooij, J. (2010). Vinculin potentiates E-cadherin mechanosensing and is recruited to actin-anchored sites within adherens junctions in a myosin II-dependent manner. The Journal of cell biology *189*, 1107-1115.

Lewallen, K.A., Shen, Y.A., De la Torre, A.R., Ng, B.K., Meijer, D., and Chan, J.R. (2011). Assessing the role of the cadherin/catenin complex at the Schwann cell-axon interface and in the initiation of myelination. The Journal of neuroscience : the official journal of the Society for Neuroscience *31*, 3032-3043.

Li, W., Cooper, J., Karajannis, M.A., and Giancotti, F.G. (2012). Merlin: a tumour suppressor with functions at the cell cortex and in the nucleus. EMBO reports *13*, 204-215.

Liebig, C., Ayala, G., Wilks, J.A., Berger, D.H., and Albo, D. (2009). Perineural invasion in cancer: a review of the literature. Cancer *115*, 3379-3391.

Lim, Y.S., McLaughlin, T., Sung, T.C., Santiago, A., Lee, K.F., and O'Leary, D.D. (2008). p75(NTR) mediates ephrin-A reverse signaling required for axon repulsion and mapping. Neuron *59*, 746-758.

Lisabeth, E.M., Falivelli, G., and Pasquale, E.B. (2013). Eph receptor signaling and ephrins. Cold Spring Harbor perspectives in biology *5*.

Liu, Y.J., Le Berre, M., Lautenschlaeger, F., Maiuri, P., Callan-Jones, A., Heuze, M., Takaki, T., Voituriez, R., and Piel, M. (2015). Confinement and low adhesion induce fast amoeboid migration of slow mesenchymal cells. Cell *160*, 659-672.

Lloyd, A.C., Obermuller, F., Staddon, S., Barth, C.F., McMahon, M., and Land, H. (1997). Cooperating oncogenes converge to regulate cyclin/cdk complexes. Genes & development *11*, 663-677.

Lupski, J.R., de Oca-Luna, R.M., Slaugenhaupt, S., Pentao, L., Guzzetta, V., Trask, B.J., Saucedo-Cardenas, O., Barker, D.F., Killian, J.M., Garcia, C.A.*, et al.* (1991). DNA duplication associated with Charcot-Marie-Tooth disease type 1A. Cell *66*, 219-232.

Lyons, D.A., Pogoda, H.M., Voas, M.G., Woods, I.G., Diamond, B., Nix, R., Arana, N., Jacobs, J., and Talbot, W.S. (2005). erbb3 and erbb2 are essential for schwann cell migration and myelination in zebrafish. Current biology : CB *15*, 513-524.

Machacek, M., Hodgson, L., Welch, C., Elliott, H., Pertz, O., Nalbant, P., Abell, A., Johnson, G.L., Hahn, K.M., and Danuser, G. (2009). Coordination of Rho GTPase activities during cell protrusion. Nature *461*, 99-103.

Macrae, M., Neve, R.M., Rodriguez-Viciana, P., Haqq, C., Yeh, J., Chen, C., Gray, J.W., and McCormick, F. (2005). A conditional feedback loop regulates Ras activity through EphA2. Cancer cell *8*, 111-118.

Mann, F., Miranda, E., Weinl, C., Harmer, E., and Holt, C.E. (2003). B-type Eph receptors and ephrins induce growth cone collapse through distinct intracellular pathways. Journal of neurobiology *57*, 323-336.

Marler, K.J., Becker-Barroso, E., Martinez, A., Llovera, M., Wentzel, C., Poopalasundaram, S., Hindges, R., Soriano, E., Comella, J., and Drescher, U. (2008). A TrkB/EphrinA interaction controls retinal axon branching and synaptogenesis. The Journal of neuroscience : the official journal of the Society for Neuroscience *28*, 12700-12712.

Marston, D.J., Dickinson, S., and Nobes, C.D. (2003). Rac-dependent trans-endocytosis of ephrinBs regulates Eph-ephrin contact repulsion. Nature cell biology *5*, 879-888.

Martin, G.A., Viskochil, D., Bollag, G., McCabe, P.C., Crosier, W.J., Haubruck, H., Conroy, L., Clark, R., O'Connell, P., Cawthon, R.M.*, et al.* (1990). The GAP-related domain of the neurofibromatosis type 1 gene product interacts with ras p21. Cell *63*, 843-849.

Mathon, N.F., Malcolm, D.S., Harrisingh, M.C., Cheng, L., and Lloyd, A.C. (2001). Lack of replicative senescence in normal rodent glia. Science *291*, 872-875.

Matthews, H.K., Marchant, L., Carmona-Fontaine, C., Kuriyama, S., Larrain, J., Holt, M.R., Parsons, M., and Mayor, R. (2008). Directional migration of neural crest cells in vivo is regulated by Syndecan-4/Rac1 and non-canonical Wnt signaling/RhoA. Development *135*, 1771-1780.

Maurel, P., Einheber, S., Galinska, J., Thaker, P., Lam, I., Rubin, M.B., Scherer, S.S., Murakami, Y., Gutmann, D.H., and Salzer, J.L. (2007). Nectin-like proteins mediate axon Schwann cell interactions along the internode and are essential for myelination. The Journal of cell biology *178*, 861-874.

Mayor, R., and Carmona-Fontaine, C. (2010). Keeping in touch with contact inhibition of locomotion. Trends in cell biology *20*, 319-328.

Mayor, R., and Etienne-Manneville, S. (2016). The front and rear of collective cell migration. Nature reviews Molecular cell biology *17*, 97-109.

Meier, C., Parmantier, E., Brennan, A., Mirsky, R., and Jessen, K.R. (1999). Developing Schwann cells acquire the ability to survive without axons by establishing an autocrine circuit involving insulin-like growth factor, neurotrophin-3, and platelet-derived growth factor-BB. The Journal of neuroscience : the official journal of the Society for Neuroscience *19*, 3847-3859.

Milner, R., Wilby, M., Nishimura, S., Boylen, K., Edwards, G., Fawcett, J., Streuli, C., Pytela, R., and ffrench-Constant, C. (1997). Division of labor of Schwann cell integrins during migration on peripheral nerve extracellular matrix ligands. Developmental biology *185*, 215-228.

Miyashita, Y., and Ozawa, M. (2007). Increased internalization of p120-uncoupled E-cadherin and a requirement for a dileucine motif in the cytoplasmic domain for endocytosis of the protein. The Journal of biological chemistry *282*, 11540-11548.

Mogha, A., Benesh, A.E., Patra, C., Engel, F.B., Schoneberg, T., Liebscher, I., and Monk, K.R. (2013). Gpr126 functions in Schwann cells to control differentiation and myelination via G-protein activation. The Journal of neuroscience : the official journal of the Society for Neuroscience *33*, 17976-17985.

Monuki, E.S., Weinmaster, G., Kuhn, R., and Lemke, G. (1989). SCIP: a glial POU domain gene regulated by cyclic AMP. Neuron *3*, 783-793.

Moore, R., Theveneau, E., Pozzi, S., Alexandre, P., Richardson, J., Merks, A., Parsons, M., Kashef, J., Linker, C., and Mayor, R. (2013). Par3 controls neural crest migration by promoting microtubule catastrophe during contact inhibition of locomotion. Development *140*, 4763-4775.

Morrison, H., Sherman, L.S., Legg, J., Banine, F., Isacke, C., Haipek, C.A., Gutmann, D.H., Ponta, H., and Herrlich, P. (2001). The NF2 tumor suppressor gene product, merlin, mediates contact inhibition of growth through interactions with CD44. Genes & development *15*, 968-980.

Morrison, H., Sperka, T., Manent, J., Giovannini, M., Ponta, H., and Herrlich, P. (2007). Merlin/neurofibromatosis type 2 suppresses growth by inhibiting the activation of Ras and Rac. Cancer research *67*, 520-527.

Murata, M., Shibuya, Y., Munemoto, S., Takeuchi, J., Kobayashi, M., Suzuki, H., and Komori, T. (2006). Ultrastructural localization of alpha E-catenin in the rat sciatic nerve. The Kobe journal of medical sciences *52*, 77-84.

Nanes, B.A., Chiasson-MacKenzie, C., Lowery, A.M., Ishiyama, N., Faundez, V., Ikura, M., Vincent, P.A., and Kowalczyk, A.P. (2012). p120-catenin binding masks an endocytic signal conserved in classical cadherins. The Journal of cell biology *199*, 365-380.

Napoli, I., Noon, L.A., Ribeiro, S., Kerai, A.P., Parrinello, S., Rosenberg, L.H., Collins, M.J., Harrisingh, M.C., White, I.J., Woodhoo, A.*, et al.* (2012). A central role for the ERK-signaling pathway in controlling Schwann cell plasticity and peripheral nerve regeneration in vivo. Neuron *73*, 729-742.

Narumiya, S., Tanji, M., and Ishizaki, T. (2009). Rho signaling, ROCK and mDia1, in transformation, metastasis and invasion. Cancer metastasis reviews *28*, 65-76.

Navarro, X. (2009). Chapter 27: Neural plasticity after nerve injury and regeneration. International review of neurobiology *87*, 483-505.

Nelson, W.J., and Weis, W.I. (2016). 25 Years of Tension over Actin Binding to the Cadherin Cell Adhesion Complex: The Devil is in the Details. Trends in cell biology *26*, 471-473.

Ness, J.K., Snyder, K.M., and Tapinos, N. (2013). Lck tyrosine kinase mediates beta1-integrin signalling to regulate Schwann cell migration and myelination. Nature communications *4*, 1912.

Nguyen, Q.T., Sanes, J.R., and Lichtman, J.W. (2002). Pre-existing pathways promote precise projection patterns. Nature neuroscience *5*, 861-867.

Nieman, M.T., Prudoff, R.S., Johnson, K.R., and Wheelock, M.J. (1999). N-cadherin promotes motility in human breast cancer cells regardless of their E-cadherin expression. The Journal of cell biology *147*, 631-644.

Nitzan, E., Pfaltzgraff, E.R., Labosky, P.A., and Kalcheim, C. (2013). Neural crest and Schwann cell progenitor-derived melanocytes are two spatially segregated populations similarly regulated by Foxd3. Proceedings of the National Academy of Sciences of the United States of America *110*, 12709-12714.

Nobes, C.D., and Hall, A. (1999). Rho GTPases control polarity, protrusion, and adhesion during cell movement. The Journal of cell biology *144*, 1235-1244.

Noren, N.K., Liu, B.P., Burridge, K., and Kreft, B. (2000). p120 catenin regulates the actin cytoskeleton via Rho family GTPases. The Journal of cell biology *150*, 567-580.

Ozkaynak, E., Abello, G., Jaegle, M., van Berge, L., Hamer, D., Kegel, L., Driegen, S., Sagane, K., Bermingham, J.R., Jr., and Meijer, D. (2010). Adam22 is a major neuronal receptor for Lgi4-mediated Schwann cell signaling. The Journal of neuroscience : the official journal of the Society for Neuroscience *30*, 3857-3864.

Paddock, S.W., and Dunn, G.A. (1986). Analysing collisions between fibroblasts and fibrosarcoma cells: fibrosarcoma cells show an active invasionary response. J Cell Sci *81*, 163-187.

Pankova, K., Rosel, D., Novotny, M., and Brabek, J. (2010). The molecular mechanisms of transition between mesenchymal and amoeboid invasiveness in tumor cells. Cellular and molecular life sciences : CMLS *67*, 63-71.

Parada, L.F., Tabin, C.J., Shih, C., and Weinberg, R.A. (1982). Human EJ bladder carcinoma oncogene is homologue of Harvey sarcoma virus ras gene. Nature *297*, 474-478.

Parkinson, D.B., Bhaskaran, A., Arthur-Farraj, P., Noon, L.A., Woodhoo, A., Lloyd, A.C., Feltri, M.L., Wrabetz, L., Behrens, A., Mirsky, R.*, et al.* (2008). c-Jun is a negative regulator of myelination. The Journal of cell biology *181*, 625-637.

Parri, M., Buricchi, F., Giannoni, E., Grimaldi, G., Mello, T., Raugei, G., Ramponi, G., and Chiarugi, P. (2007). EphrinA1 activates a Src/focal adhesion kinase-mediated motility response leading to rho-dependent actino/myosin contractility. The Journal of biological chemistry *282*, 19619-19628.

Parrinello, S., and Lloyd, A.C. (2009). Neurofibroma development in NF1--insights into tumour initiation. Trends in cell biology *19*, 395-403.

Parrinello, S., Napoli, I., Ribeiro, S., Wingfield Digby, P., Fedorova, M., Parkinson, D.B., Doddrell, R.D., Nakayama, M., Adams, R.H., and Lloyd, A.C. (2010). EphB signaling directs peripheral nerve regeneration through Sox2-dependent Schwann cell sorting. Cell *143*, 145-155.

Parrinello, S., Noon, L.A., Harrisingh, M.C., Wingfield Digby, P., Rosenberg, L.H., Cremona, C.A., Echave, P., Flanagan, A.M., Parada, L.F., and Lloyd, A.C. (2008). NF1 loss disrupts Schwann cell-axonal interactions: a novel role for semaphorin 4F. Genes & development *22*, 3335-3348.

Pasquale, E.B. (2010). Eph receptors and ephrins in cancer: bidirectional signalling and beyond. Nature reviews Cancer *10*, 165-180.

Peglion, F., and Etienne-Manneville, S. (2013). p120catenin alteration in cancer and its role in tumour invasion. Philosophical transactions of the Royal Society of London Series B, Biological sciences *368*, 20130015.

Peglion, F., Llense, F., and Etienne-Manneville, S. (2014). Adherens junction treadmilling during collective migration. Nature cell biology *16*, 639-651.

Pellegatta, M., De Arcangelis, A., D'Urso, A., Nodari, A., Zambroni, D., Ghidinelli, M., Matafora, V., Williamson, C., Georges-Labouesse, E., Kreidberg, J.*, et al.* (2013). alpha6beta1 and alpha7beta1 integrins are required in Schwann cells to sort axons. The Journal of neuroscience : the official journal of the Society for Neuroscience *33*, 17995-18007.

Perrais, M., Chen, X., Perez-Moreno, M., and Gumbiner, B.M. (2007). E-cadherin homophilic ligation inhibits cell growth and epidermal growth factor receptor signaling independently of other cell interactions. Molecular biology of the cell *18*, 2013-2025.

Pertz, O., Hodgson, L., Klemke, R.L., and Hahn, K.M. (2006). Spatiotemporal dynamics of RhoA activity in migrating cells. Nature *440*, 1069-1072.

Petrilli, A.M., and Fernandez-Valle, C. (2016). Role of Merlin/NF2 inactivation in tumor biology. Oncogene *35*, 537-548.

Pokutta, S., and Weis, W.I. (2000). Structure of the dimerization and beta-catenin-binding region of alpha-catenin. Molecular cell *5*, 533-543.

Poss, K.D. (2010). Advances in understanding tissue regenerative capacity and mechanisms in animals. Nature reviews Genetics *11*, 710-722.

Pylayeva-Gupta, Y., Grabocka, E., and Bar-Sagi, D. (2011). RAS oncogenes: weaving a tumorigenic web. Nature reviews Cancer *11*, 761-774.

Raeymaekers, P., Timmerman, V., Nelis, E., De Jonghe, P., Hoogendijk, J.E., Baas, F., Barker, D.F., Martin, J.J., De Visser, M., Bolhuis, P.A.*, et al.* (1991). Duplication in chromosome 17p11.2 in Charcot-Marie-Tooth neuropathy type 1a (CMT 1a). The HMSN Collaborative Research Group. Neuromuscular disorders : NMD *1*, 93-97.

Rasband, M.N., and Peles, E. (2015). The Nodes of Ranvier: Molecular Assembly and Maintenance. Cold Spring Harbor perspectives in biology.

Reig, G., Pulgar, E., and Concha, M.L. (2014). Cell migration: from tissue culture to embryos. Development *141*, 1999-2013.

Rhee, J., Buchan, T., Zukerberg, L., Lilien, J., and Balsamo, J. (2007). Cables links Robo-bound Abl kinase to N-cadherin-bound beta-catenin to mediate Slit-induced modulation of adhesion and transcription. Nature cell biology *9*, 883-892.

Rhee, J., Mahfooz, N.S., Arregui, C., Lilien, J., Balsamo, J., and VanBerkum, M.F. (2002). Activation of the repulsive receptor Roundabout inhibits N-cadherin-mediated cell adhesion. Nature cell biology *4*, 798-805.

Ribeiro, S., Napoli, I., White, I.J., Parrinello, S., Flanagan, A.M., Suter, U., Parada, L.F., and Lloyd, A.C. (2013). Injury signals cooperate with Nf1 loss to relieve the tumor-suppressive environment of adult peripheral nerve. Cell reports *5*, 126-136.

Ridley, A.J., Paterson, H.F., Noble, M., and Land, H. (1988). Ras-mediated cell cycle arrest is altered by nuclear oncogenes to induce Schwann cell transformation. The EMBO journal *7*, 1635-1645.

Riethmacher, D., Sonnenberg-Riethmacher, E., Brinkmann, V., Yamaai, T., Lewin, G.R., and Birchmeier, C. (1997). Severe neuropathies in mice with targeted mutations in the ErbB3 receptor. Nature *389*, 725-730.

Sadok, A., and Marshall, C.J. (2014). Rho GTPases: masters of cell migration. Small GTPases *5*, e29710.

Sagane, K., Hayakawa, K., Kai, J., Hirohashi, T., Takahashi, E., Miyamoto, N., Ino, M., Oki, T., Yamazaki, K., and Nagasu, T. (2005). Ataxia and peripheral nerve hypomyelination in ADAM22-deficient mice. BMC neuroscience *6*, 33.

Salzer, J.L. (2015). Schwann cell myelination. Cold Spring Harbor perspectives in biology *7*, a020529.

Santos, E., Tronick, S.R., Aaronson, S.A., Pulciani, S., and Barbacid, M. (1982). T24 human bladder carcinoma oncogene is an activated form of the normal human homologue of BALB- and Harvey-MSV transforming genes. Nature *298*, 343-347.

Scarpa, E., Szabo, A., Bibonne, A., Theveneau, E., Parsons, M., and Mayor, R. (2015). Cadherin Switch during EMT in Neural Crest Cells Leads to Contact Inhibition of Locomotion via Repolarization of Forces. Developmental cell *34*, 421-434.

Serra, E., Rosenbaum, T., Winner, U., Aledo, R., Ars, E., Estivill, X., Lenard, H.G., and Lazaro, C. (2000). Schwann cells harbor the somatic NF1 mutation in

neurofibromas: evidence of two different Schwann cell subpopulations. Human molecular genetics *9*, 3055-3064.

Shaw, R.J., McClatchey, A.I., and Jacks, T. (1998). Regulation of the neurofibromatosis type 2 tumor suppressor protein, merlin, by adhesion and growth arrest stimuli. The Journal of biological chemistry *273*, 7757-7764.

Sheela, S., Riccardi, V.M., and Ratner, N. (1990). Angiogenic and invasive properties of neurofibroma Schwann cells. The Journal of cell biology *111*, 645-653.

Shellard, A., and Mayor, R. (2016). Chemotaxis during neural crest migration. Seminars in cell & developmental biology.

Shih, C., and Weinberg, R.A. (1982). Isolation of a transforming sequence from a human bladder carcinoma cell line. Cell *29*, 161-169.

Shih, W., and Yamada, S. (2012). N-cadherin-mediated cell-cell adhesion promotes cell migration in a three-dimensional matrix. Journal of cell science *125*, 3661-3670.

Solanas, G., Cortina, C., Sevillano, M., and Batlle, E. (2011). Cleavage of E-cadherin by ADAM10 mediates epithelial cell sorting downstream of EphB signalling. Nature cell biology *13*, 1100-1107.

Spiegel, I., Adamsky, K., Eshed, Y., Milo, R., Sabanay, H., Sarig-Nadir, O., Horresh, I., Scherer, S.S., Rasband, M.N., and Peles, E. (2007). A central role for Necl4 (SynCAM4) in Schwann cell-axon interaction and myelination. Nature neuroscience *10*, 861-869.

Steinberg, M.S. (2007). Differential adhesion in morphogenesis: a modern view. Current opinion in genetics & development *17*, 281-286.

Stewart, H.J., Brennan, A., Rahman, M., Zoidl, G., Mitchell, P.J., Jessen, K.R., and Mirsky, R. (2001). Developmental regulation and overexpression of the transcription factor AP-2, a potential regulator of the timing of Schwann cell generation. The European journal of neuroscience *14*, 363-372.

Stramer, B., Moreira, S., Millard, T., Evans, I., Huang, C.Y., Sabet, O., Milner, M., Dunn, G., Martin, P., and Wood, W. (2010). Clasp-mediated microtubule bundling regulates persistent motility and contact repulsion in Drosophila macrophages in vivo. The Journal of cell biology *189*, 681-689.

Sulaiman, O.A., and Gordon, T. (2009). Role of chronic Schwann cell denervation in poor functional recovery after nerve injuries and experimental strategies to combat it. Neurosurgery *65*, A105-114.

Suter, U., and Scherer, S.S. (2003). Disease mechanisms in inherited neuropathies. Nature reviews Neuroscience *4*, 714-726.

Suyama, K., Shapiro, I., Guttman, M., and Hazan, R.B. (2002). A signaling pathway leading to metastasis is controlled by N-cadherin and the FGF receptor. Cancer cell *2*, 301-314.

Taddei, M.L., Parri, M., Angelucci, A., Bianchini, F., Marconi, C., Giannoni, E., Raugei, G., Bologna, M., Calorini, L., and Chiarugi, P. (2011). EphA2 induces

metastatic growth regulating amoeboid motility and clonogenic potential in prostate carcinoma cells. Molecular cancer research : MCR *9*, 149-160.

Takai, Y., Miyoshi, J., Ikeda, W., and Ogita, H. (2008). Nectins and nectin-like molecules: roles in contact inhibition of cell movement and proliferation. Nature reviews Molecular cell biology *9*, 603-615.

Tanaka, M., Kuriyama, S., and Aiba, N. (2012). Nm23-H1 regulates contact inhibition of locomotion, which is affected by ephrin-B1. Journal of cell science *125*, 4343-4353.

Taveggia, C., Zanazzi, G., Petrylak, A., Yano, H., Rosenbluth, J., Einheber, S., Xu, X., Esper, R.M., Loeb, J.A., Shrager, P.*, et al.* (2005). Neuregulin-1 type III determines the ensheathment fate of axons. Neuron *47*, 681-694.

Theveneau, E., Marchant, L., Kuriyama, S., Gull, M., Moepps, B., Parsons, M., and Mayor, R. (2010). Collective chemotaxis requires contact-dependent cell polarity. Developmental cell *19*, 39-53.

Theveneau, E., and Mayor, R. (2010). Integrating chemotaxis and contact-inhibition during collective cell migration: Small GTPases at work. Small GTPases *1*, 113-117.

Theveneau, E., and Mayor, R. (2012a). Cadherins in collective cell migration of mesenchymal cells. Current opinion in cell biology *24*, 677-684.

Theveneau, E., and Mayor, R. (2012b). Neural crest delamination and migration: from epithelium-to-mesenchyme transition to collective cell migration. Developmental biology *366*, 34-54.

Tozluoglu, M., Tournier, A.L., Jenkins, R.P., Hooper, S., Bates, P.A., and Sahai, E. (2013). Matrix geometry determines optimal cancer cell migration strategy and modulates response to interventions. Nature cell biology *15*, 751-762.

Tricaud, N., Perrin-Tricaud, C., Bruses, J.L., and Rutishauser, U. (2005). Adherens junctions in myelinating Schwann cells stabilize Schmidt-Lanterman incisures via recruitment of p120 catenin to E-cadherin. The Journal of neuroscience : the official journal of the Society for Neuroscience *25*, 3259-3269.

Trolice, M.P., Pappalardo, A., and Peluso, J.J. (1997). Basic fibroblast growth factor and N-cadherin maintain rat granulosa cell and ovarian surface epithelial cell viability by stimulating the tyrosine phosphorylation of the fibroblast growth factor receptors. Endocrinology *138*, 107-113.

Tsai, H.H., Niu, J., Munji, R., Davalos, D., Chang, J., Zhang, H., Tien, A.C., Kuo, C.J., Chan, J.R., Daneman, R.*, et al.* (2016). Oligodendrocyte precursors migrate along vasculature in the developing nervous system. Science *351*, 379-384.

Valentin, G., Haas, P., and Gilmour, D. (2007). The chemokine SDF1a coordinates tissue migration through the spatially restricted activation of Cxcr7 and Cxcr4b. Current biology : CB *17*, 1026-1031.

van Roy, F. (2014). Beyond E-cadherin: roles of other cadherin superfamily members in cancer. Nature reviews Cancer *14*, 121-134.

Wanner, I.B., Guerra, N.K., Mahoney, J., Kumar, A., Wood, P.M., Mirsky, R., and Jessen, K.R. (2006). Role of N-cadherin in Schwann cell precursors of growing nerves. Glia *54*, 439-459.

Wanner, I.B., and Wood, P.M. (2002). N-cadherin mediates axon-aligned process growth and cell-cell interaction in rat Schwann cells. The Journal of neuroscience : the official journal of the Society for Neuroscience *22*, 4066-4079.

Wehrendt, D.P., Carmona, F., Gonzalez Wusener, A.E., Gonzalez, A., Martinez, J.M., and Arregui, C.O. (2016). P120-Catenin Regulates Early Trafficking Stages of the N-Cadherin Precursor Complex. PloS one *11*, e0156758.

Weiner, J.A., and Chun, J. (1999). Schwann cell survival mediated by the signaling phospholipid lysophosphatidic acid. Proceedings of the National Academy of Sciences of the United States of America *96*, 5233-5238.

Wells, A., Chao, Y.L., Grahovac, J., Wu, Q., and Lauffenburger, D.A. (2011). Epithelial and mesenchymal phenotypic switchings modulate cell motility in metastasis. Frontiers in bioscience *16*, 815-837.

Wheelock, M.J., Shintani, Y., Maeda, M., Fukumoto, Y., and Johnson, K.R. (2008). Cadherin switching. Journal of cell science *121*, 727-735.

Williams, E.J., Williams, G., Howell, F.V., Skaper, S.D., Walsh, F.S., and Doherty, P. (2001). Identification of an N-cadherin motif that can interact with the fibroblast growth factor receptor and is required for axonal growth. The Journal of biological chemistry *276*, 43879-43886.

Woodhoo, A., Alonso, M.B., Droggiti, A., Turmaine, M., D'Antonio, M., Parkinson, D.B., Wilton, D.K., Al-Shawi, R., Simons, P., Shen, J.*, et al.* (2009). Notch controls embryonic Schwann cell differentiation, postnatal myelination and adult plasticity. Nature neuroscience *12*, 839-847.

Woodhoo, A., and Sommer, L. (2008). Development of the Schwann cell lineage: from the neural crest to the myelinated nerve. Glia *56*, 1481-1490.

Woodruff, J.M. (1999). Pathology of tumors of the peripheral nerve sheath in type 1 neurofibromatosis. American journal of medical genetics *89*, 23-30.

Wu, J., Williams, J.P., Rizvi, T.A., Kordich, J.J., Witte, D., Meijer, D., Stemmer-Rachamimov, A.O., Cancelas, J.A., and Ratner, N. (2008). Plexiform and dermal neurofibromas and pigmentation are caused by Nf1 loss in desert hedgehog-expressing cells. Cancer cell *13*, 105-116.

Xu, G.F., Lin, B., Tanaka, K., Dunn, D., Wood, D., Gesteland, R., White, R., Weiss, R., and Tamanoi, F. (1990). The catalytic domain of the neurofibromatosis type 1 gene product stimulates ras GTPase and complements ira mutants of S. cerevisiae. Cell *63*, 835-841.

Yamada, S., Pokutta, S., Drees, F., Weis, W.I., and Nelson, W.J. (2005). Deconstructing the cadherin-catenin-actin complex. Cell *123*, 889-901.

Yamauchi, J., Chan, J.R., and Shooter, E.M. (2003). Neurotrophin 3 activation of TrkC induces Schwann cell migration through the c-Jun N-terminal kinase pathway.

Proceedings of the National Academy of Sciences of the United States of America *100*, 14421-14426.

Yamauchi, J., Chan, J.R., and Shooter, E.M. (2004). Neurotrophins regulate Schwann cell migration by activating divergent signaling pathways dependent on Rho GTPases. Proceedings of the National Academy of Sciences of the United States of America *101*, 8774-8779.

Yang, F.C., Ingram, D.A., Chen, S., Hingtgen, C.M., Ratner, N., Monk, K.R., Clegg, T., White, H., Mead, L., Wenning, M.J.*, et al.* (2003). Neurofibromin-deficient Schwann cells secrete a potent migratory stimulus for Nf1+/- mast cells. The Journal of clinical investigation *112*, 1851-1861.

Yang, F.C., Ingram, D.A., Chen, S., Zhu, Y., Yuan, J., Li, X., Yang, X., Knowles, S., Horn, W., Li, Y.*, et al.* (2008). Nf1-dependent tumors require a microenvironment containing Nf1+/-- and c-kit-dependent bone marrow. Cell *135*, 437-448.

Yao, M., Qiu, W., Liu, R., Efremov, A.K., Cong, P., Seddiki, R., Payre, M., Lim, C.T., Ladoux, B., Mege, R.M.*, et al.* (2014). Force-dependent conformational switch of alpha-catenin controls vinculin binding. Nature communications *5*, 4525.

Yap, A.S., Gomez, G.A., and Parton, R.G. (2015). Adherens Junctions Revisualized: Organizing Cadherins as Nanoassemblies. Developmental cell *35*, 12-20.

Yasunaga, M., Yagi, T., Hanzawa, N., Yasuda, M., Yamanashi, Y., Yamamoto, T., Aizawa, S., Miyauchi, Y., and Nishikawa, S. (1996). Involvement of Fyn tyrosine kinase in progression of cytokinesis of B lymphocyte progenitor. The Journal of cell biology *132*, 91-99.

Yonemura, S., Wada, Y., Watanabe, T., Nagafuchi, A., and Shibata, M. (2010). alpha-Catenin as a tension transducer that induces adherens junction development. Nature cell biology *12*, 533-542.

Zheng, H., Chang, L., Patel, N., Yang, J., Lowe, L., Burns, D.K., and Zhu, Y. (2008). Induction of abnormal proliferation by nonmyelinating schwann cells triggers neurofibroma formation. Cancer cell *13*, 117-128.

Zhu, Y., Ghosh, P., Charnay, P., Burns, D.K., and Parada, L.F. (2002). Neurofibromas in NF1: Schwann cell origin and role of tumor environment. Science *296*, 920-922.

Zimmer, M., Palmer, A., Kohler, J., and Klein, R. (2003). EphB-ephrinB bi-directional endocytosis terminates adhesion allowing contact mediated repulsion. Nature cell biology *5*, 869-878.

Zisch, A.H., Kalo, M.S., Chong, L.D., and Pasquale, E.B. (1998). Complex formation between EphB2 and Src requires phosphorylation of tyrosine 611 in the EphB2 juxtamembrane region. Oncogene *16*, 2657-2670.

Zochodne, D.W. (2008). Neurobiology of Peripheral Nerve Regeneration (Cambridge University Press).

Appendix

Time-lapse videos (Located on the CD at the back of the thesis)

Movie 3.1. N-cad is required for CIL
Related to figure 3.2. Time-lapse microscopy Schwann cells treated with either scrambled, or siRNA1 or siRNA2 targeting N-cad. Images were taken every 10 min up to 4 hours. Interacting cells are indicated by a blue and green dot.

Movie 3.2. N-cad is required for contact dependent outward migration
Related to figure 3.3 and 3.4. Time-lapse microscopy of a scratch assay of scrambled-treated Schwann cells or N-cad knockdown Schwann cells imaged every 10 min for 12 hours (7fps).

Movie 3.3. N-cad mediates CIL independent of trans-homodimerisation
Related to figure 3.5 and 3.6. Time-lapse microscopy of scrambled-treated cells (red fluorescent-labelled) mixed with N-cad knockdown cells (green fluorescent labelled). Imaged every 10 min for up to 7 hours (5fps). An interacting N-cad knockdown cell and scrambled-treated cell are indicated by the green and red dot respectively.

Movie 3.4. CIL is independent of α-catenin
Related to figure 3.5 and 3.6. Time-lapse microscopy of scrambled-treated cells or α-catenin knockdown cells, which were imaged every 10 min for 24 hours (5fps). Interacting cells are indicated by a blue and green dot. Shown is representative movie of 9 hours.

Movie 3.5. CIL is independent of p120-catenin
Related to figure 3.5 and 3.6. Time-lapse microscopy of Schwann cells treated with scrambled siRNA or with p120-catenin siRNA1 or siRNA2, which were imaged every 10 min up to 9 hours (5fps). Interacting cells are indicated by a blue and green dot.

Movie 3.6. Extracellular domain of N-cad is sufficient to mediate CIL
Related to figure 3.17 and 3.18 Time-lapse microscopy of N-cad knockdown cells (green or blue dot) with N-cad knockdown cells transfected with cytoplasmic GFP and full-length, extracellular domain or intracellular domain of N-cad tagged with ptdTomato (red dot). The ptdTomato expression is only shown for the first two time points, and is subsequently indicated by a red dot. Cells were imaged every 10 min up to 15 hours (5 fps).

Movie 4.1. DN-p53-Ras Schwann cells lose CIL in a MEK dependent manner
Related to figure 4.4. Time-lapse microscopy of DNp53-SCs or DNp53-Ras-SCs treated with control solvent (DMSO) or MEK inhibitor PD184352 (0.75 μM) for 18 hours, before imaging for a further 24 hours. Interacting cells are indicated by a blue and green dot. Cells were imaged every 10 min for up to 2 hours (5 fps).

Movie 4.2. Restoration of CIL in DNp53-Ras Schwann cells is slow
Related to figure 4.6. Time-lapse microscopy of a time-course of homotypic CIL between DNp53-Ras-SCs imaged for 6 hours before adding the MEK inhibitor PD184352 (0.75μM) and further imaging for another 12 hours. Images were taken every 10 min (5 fps). Cells that are invasive are indicated by a green and blue dot. The cell indicated by a red dot indicate a cell that is initially invasive but becomes repulsive overtime.

Movie 4.3. Homotypic CIL and Heterotypic CIL are regulated through different Mechanisms
Related to figure 4.6. Time-lapse microscopy of a CIL assay between primary fibroblasts (blue dot) and green fluorescent-labelled scrambled or EphB2 siRNA treated Schwann cells (green dot), followed by a movie of EphB2 knockdown cells alone. Cells were imaged every 10 min up to 6 hours (5 fps).

Movie 4.4. Fyn is not required for CIL
Related to figure 4.13. Time-lapse microscopy of a CIL assay in which Schwann cells were treated with DMSO or the Fyn inhibitor SU6646 (250nM) for one hour before starting imaging for a further 24 hours. Cells were imaged every 10 min for 3 hours (5 fps). Interacting cells are indicated by a blue and green dot. Shown is reps

Movie 4.5. Glypican-4 is required for CIL
Related to figure 4.21. Time-lapse microscopy of scrambled-treated cells or Schwann cells treated with Glypican siRNA 1 or siRNA2 for 48 hours before imaging for a further 24 hours. Cells were imaged every 10 min up to 10 hours (5 fps). Interacting cells are indicated by a blue and green dot.

Movie 5.1. β1 *integrin mediates 2D Schwann cell migration*
Related to figure 5.1. Time-lapse microscopy of scrambled-treated cells or Schwann cells treated with β1 integrin siRNA 1 for 36 hours before imaging for a further 24 hours. Cells were imaged every 10 min for 4 hours (5 fps).

Movie 5.2. Talin1 and Talin2 are required for 2D Schwann cell migration
Related to figure 5.2. Time-lapse microscopy of scrambled-treated cells or Schwann cells treated with Talin 1 and 2 siRNA combination 1 for 60 hours before imaging for a further 24 hours. Cells were imaged every 10 min for 4 hours (5 fps).

Movie 5.3. Schwann cell migration along endothelial tubules is independent of focal adhesions
Related to figure 5.3-5.6. Time-lapse microscopy of GFP-labelled scrambled-treated cells, or GFP-labelled Schwann cells treated with β1 integrin siRNA 1, or Talin 1 and 2 siRNA combination 1 for 36 hours, migrating along HUVECs in matrigel. Images were taken every 10 min for 4 hours.

Mass spectrometry data

Located on the CD at the back of the thesis

Table 1	Full Mass Spec list IgG EtOH
Table 2	Full Mass Spec list N-cad EtOH
Table 3	Full Mass Spec list IgG TMX
Table 4	Full Mass Spec list N-cad TMX

Located in thesis

Table 5	Comparison of N-cad EtOH sample to IgG control based on fold increase (≥2.5)
Table 6	Comparison of N-cad TMX sample to IgG control based on fold increase (≥2.5)
Table 7	Proteins overlapping in EtOH and TMX
Table 8	Proteins specifically identified in EtOH samples
Table 9	Proteins specifically identified in TMX samples

Table 5 Comparison of N-cad EtOH sample to IgG control based on fold increase (≥2.5)

N-Cad specific Fold increase EtOH		
Accession	Description	Fold increase Score
D3ZCH7	Adducin 3 (Gamma), isoform CRA_b OS=Rattus norvegicus GN=Add3 PE=4 SV=2 - [D3ZCH7_RAT]	2.55
Q5FVQ2	Peter pan homolog (Drosophila) OS=Rattus norvegicus GN=Ppan PE=2 SV=1 - [Q5FVQ2_RAT]	2.83
Q6P0K8	Junction plakoglobin OS=Rattus norvegicus GN=Jup PE=1 SV=1 - [PLAK_RAT]	7.70
D3ZZZ9	Catenin (Cadherin associated protein), delta 1 (Predicted), isoform CRA_a OS=Rattus norvegicus GN=Ctnnd1 PE=1 SV=1 - [D3ZZZ9_RAT]	12.91
Q5U302	Catenin (Cadherin associated protein), alpha 1 OS=Rattus norvegicus GN=Ctnna1 PE=1 SV=1 - [Q5U302_RAT]	18.74
A0JPL2	Casein kinase 1, alpha 1, isoform CRA_d OS=Rattus norvegicus GN=Csnk1a1 PE=2 SV=1 - [A0JPL2_RAT]	N/A
A2RRU1	Glycogen [starch] synthase, muscle OS=Rattus norvegicus GN=Gys1 PE=2 SV=1 - [GYS1_RAT]	N/A
B0BNF5	Qk protein OS=Rattus norvegicus GN=Qk PE=2 SV=1 - [B0BNF5_RAT]	N/A
B1H237	Terf2 protein OS=Rattus norvegicus GN=Terf2 PE=2 SV=1 - [B1H237_RAT]	N/A
B1VKB4	Synaptopodin OS=Rattus norvegicus GN=Synpo PE=2 SV=1 - [B1VKB4_RAT]	N/A
B2GUU1	YTH domain family 2 (Predicted) OS=Rattus norvegicus GN=Ythdf2 PE=2 SV=1 - [B2GUU1_RAT]	N/A
B2GUY6	Srrm2 protein (Fragment) OS=Rattus norvegicus GN=Srrm2 PE=2 SV=1 - [B2GUY6_RAT]	N/A
B2RYQ5	Enhancer of rudimentary homolog OS=Rattus norvegicus GN=Erh PE=2 SV=1 - [B2RYQ5_RAT]	N/A
B5DF27	Lysyl oxidase homolog 2 OS=Rattus norvegicus GN=Loxl2 PE=2 SV=2 - [LOXL2_RAT]	N/A
D3Z8W1	Uncharacterized protein OS=Rattus norvegicus GN=LOC680384 PE=4 SV=1 - [D3Z8W1_RAT]	N/A
D3ZEI6	Nuclear receptor coactivator 5 (Predicted) OS=Rattus norvegicus GN=Ncoa5 PE=4 SV=1 - [D3ZEI6_RAT]	N/A
D3ZFD0	Uncharacterized protein OS=Rattus norvegicus GN=Myo18a PE=1 SV=2 - [D3ZFD0_RAT]	N/A
D3ZHB3	40S ribosomal protein S12 OS=Rattus norvegicus GN=LOC100360573 PE=3 SV=2 - [D3ZHB3_RAT]	N/A
D3ZI68	PRP31 pre-mRNA processing factor 31 homolog (Yeast) (Predicted) OS=Rattus norvegicus GN=Prpf31 PE=4 SV=1 - [D3ZI68_RAT]	N/A
D3ZIX4	Protein H1fx OS=Rattus norvegicus GN=H1fx PE=3 SV=1 - [D3ZIX4_RAT]	N/A
D3ZJ67	Protein Sun2 OS=Rattus norvegicus GN=Sun2 PE=4 SV=1 - [D3ZJ67_RAT]	N/A
D3ZJU5	Protein Smarcc1 OS=Rattus norvegicus GN=Smarcc1 PE=4 SV=1 - [D3ZJU5_RAT]	N/A
D3ZN76	Protein Sec16a OS=Rattus norvegicus GN=Sec16a PE=4 SV=1 - [D3ZN76_RAT]	N/A
D3ZNH2	Protein Utp18 OS=Rattus norvegicus GN=Utp18 PE=4 SV=2 - [D3ZNH2_RAT]	N/A
D3ZNP7	Protein LOC100909685 OS=Rattus norvegicus GN=Myo1b PE=4 SV=2 - [D3ZNP7_RAT]	N/A
D3ZQG1	Protein Nufip2 OS=Rattus norvegicus GN=LOC687994 PE=4 SV=2 - [D3ZQG1_RAT]	N/A
D3ZR53	Protein phosphatase 1 regulatory subunit 12 OS=Rattus norvegicus GN=Ppp1r12a PE=1 SV=2 - [D3ZR53_RAT]	N/A

D3ZRT6	Protein Plekha7 OS=Rattus norvegicus GN=Plekha7 PE=4 SV=1 - [D3ZRT6_RAT]	N/A
D3ZUK4	Protein Trim33 (Fragment) OS=Rattus norvegicus GN=Trim33 PE=4 SV=2 - [D3ZUK4_RAT]	N/A
D3ZWZ6	Protein Igf2bp2 (Fragment) OS=Rattus norvegicus GN=Igf2bp2 PE=4 SV=2 - [D3ZWZ6_RAT]	N/A
D3ZYT2	Mitochondrial ribosomal protein S5 (Predicted) OS=Rattus norvegicus GN=Mrps5 PE=3 SV=1 - [D3ZYT2_RAT]	N/A
D3ZZM1	Uncharacterized protein (Fragment) OS=Rattus norvegicus PE=4 SV=2 - [D3ZZM1_RAT]	N/A
D3ZZR5	Protein Snrpa1 OS=Rattus norvegicus GN=Snrpa1 PE=4 SV=1 - [D3ZZR5_RAT]	N/A
D4A2B0	Polymerase (DNA-directed), delta interacting protein 3 (Predicted), isoform CRA_a OS=Rattus norvegicus GN=Poldip3 PE=4 SV=1 - [D4A2B0_RAT]	N/A
D4A2Z8	DEAH (Asp-Glu-Ala-His) box polypeptide 36 (Predicted), isoform CRA_a OS=Rattus norvegicus GN=Dhx36 PE=4 SV=1 - [D4A2Z8_RAT]	N/A
D4A554	Eukaryotic translation initiation factor 4 gamma, 3 (Predicted), isoform CRA_a OS=Rattus norvegicus GN=Eif4g3 PE=4 SV=2 - [D4A554_RAT]	N/A
D4A5G2	Protein Nop14 OS=Rattus norvegicus GN=Nop14 PE=4 SV=1 - [D4A5G2_RAT]	N/A
D4A5K7	Protein Rbm28 OS=Rattus norvegicus GN=Rbm28 PE=4 SV=1 - [D4A5K7_RAT]	N/A
D4A5S9	Protein Prpf39 OS=Rattus norvegicus GN=Prpf39 PE=4 SV=1 - [D4A5S9_RAT]	N/A
D4AAG4	Protein Kif23 OS=Rattus norvegicus GN=Kif23 PE=3 SV=2 - [D4AAG4_RAT]	N/A
D4AAW2	Protein transport protein Sec16B OS=Rattus norvegicus GN=Sec16b PE=4 SV=2 - [D4AAW2_RAT]	N/A
D4ABR6	Annexin (Fragment) OS=Rattus norvegicus GN=Anxa6 PE=3 SV=2 - [D4ABR6_RAT]	N/A
D4ACV3	Histone H2A OS=Rattus norvegicus GN=Hist2h2ac PE=3 SV=1 - [D4ACV3_RAT]	N/A
D4AE65	Protein Rrp7a OS=Rattus norvegicus GN=Rrp7a PE=4 SV=1 - [D4AE65_RAT]	N/A
D4JQY2	Chaperone protein DnaK n=3 Tax=root RepID=D4JQY2_9FIRM	N/A
E9PT66	Protein Sf3b3 OS=Rattus norvegicus GN=Sf3b3 PE=4 SV=2 - [E9PT66_RAT]	N/A
F1LNF1	Heterogeneous nuclear ribonucleoproteins A2/B1 (Fragment) OS=Rattus norvegicus GN=Hnrnpa2b1 PE=4 SV=1 - [F1LNF1_RAT]	N/A
F1LQB2	Structural maintenance of chromosomes protein 3 OS=Rattus norvegicus GN=Smc3 PE=4 SV=1 - [F1LQB2_RAT]	N/A
F1LS65	Signal-induced proliferation-associated 1-like protein 1 (Fragment) OS=Rattus norvegicus GN=Sipa1l1 PE=4 SV=2 - [F1LS65_RAT]	N/A
F1LSL1	Transcription factor Pur-beta OS=Rattus norvegicus GN=Purb PE=4 SV=2 - [F1LSL1_RAT]	N/A
F1LSL2	Nuclear pore complex protein Nup107 OS=Rattus norvegicus GN=Nup107 PE=4 SV=2 - [F1LSL2_RAT]	N/A
F1LSS1	Structural maintenance of chromosomes protein OS=Rattus norvegicus GN=Smc1a PE=3 SV=2 - [F1LSS1_RAT]	N/A
F1LX68	Protein Spats2 OS=Rattus norvegicus GN=Spats2 PE=4 SV=2 - [F1LX68_RAT]	N/A
F1M0V4	Protein Thoc2 OS=Rattus norvegicus GN=Thoc2 PE=4 SV=2 - [F1M0V4_RAT]	N/A
F1M3H2	Uncharacterized protein (Fragment) OS=Rattus norvegicus GN=LOC100360367 PE=4 SV=2 - [F1M3H2_RAT]	N/A
F1M3K6	Protein Bag4 (Fragment) OS=Rattus norvegicus GN=Bag4 PE=4 SV=2 - [F1M3K6_RAT]	N/A

F1M4A0	Protein Tjp1 OS=Rattus norvegicus GN=Tjp1 PE=1 SV=2 - [F1M4A0_RAT]	N/A
F1M4U9	Protein Baz1a (Fragment) OS=Rattus norvegicus GN=Baz1a PE=4 SV=2 - [F1M4U9_RAT]	N/A
F1MAA5	Protein Rangap1 OS=Rattus norvegicus GN=Rangap1 PE=4 SV=2 - [F1MAA5_RAT]	N/A
F1MAA7	Protein Lamc1 OS=Rattus norvegicus GN=Lamc1 PE=4 SV=1 - [F1MAA7_RAT]	N/A
F1SW39	PC4 and SFRS1 interacting protein 1 OS=Rattus norvegicus GN=Psip1 PE=2 SV=1 - [F1SW39_RAT]	N/A
F7EM03	Protein Krt31 OS=Rattus norvegicus GN=Krt34 PE=3 SV=1 - [F7EM03_RAT]	N/A
G3V6A4	Heterogeneous nuclear ribonucleoprotein D, isoform CRA_b OS=Rattus norvegicus GN=Hnrpd PE=1 SV=1 - [G3V6A4_RAT]	N/A
G3V702	Smu-1 suppressor of mec-8 and unc-52 homolog (C. elegans) OS=Rattus norvegicus GN=Smu1 PE=4 SV=1 - [G3V702_RAT]	N/A
G3V727	DEAD (Asp-Glu-Ala-Asp) box polypeptide 47, isoform CRA_a OS=Rattus norvegicus GN=Ddx47 PE=3 SV=1 - [G3V727_RAT]	N/A
G3V7J2	Interferon-inducible double-stranded RNA-dependent protein kinase activator A OS=Rattus norvegicus GN=Prkra PE=1 SV=1 - [G3V7J2_RAT]	N/A
G3V7K3	Ceruloplasmin OS=Rattus norvegicus GN=Cp PE=4 SV=1 - [G3V7K3_RAT]	N/A
G3V7N0	Heparan sulfate 2-O-sulfotransferase 1, isoform CRA_a OS=Rattus norvegicus GN=Hs2st1 PE=4 SV=1 - [G3V7N0_RAT]	N/A
G3V803	Cadherin-2 OS=Rattus norvegicus GN=Cdh2 PE=4 SV=1 - [G3V803_RAT]	N/A
G3V8B3	Histone H2B OS=Rattus norvegicus GN=LOC100910200 PE=3 SV=1 - [G3V8B3_RAT]	N/A
G3V8B4	Brix domain containing 2, isoform CRA_a OS=Rattus norvegicus GN=Brix1 PE=4 SV=1 - [G3V8B4_RAT]	N/A
G3V8T4	DNA damage-binding protein 1 OS=Rattus norvegicus GN=Ddb1 PE=4 SV=1 - [G3V8T4_RAT]	N/A
G3V9F3	Myosin phosphatase Rho-interacting protein OS=Rattus norvegicus GN=Mprip PE=4 SV=1 - [G3V9F3_RAT]	N/A
G3V9R0	LUC7-like (S. cerevisiae) OS=Rattus norvegicus GN=Luc7l PE=2 SV=2 - [G3V9R0_RAT]	N/A
M0R7L9	Protein LOC100911677 OS=Rattus norvegicus GN=LOC100911677 PE=4 SV=1 - [M0R7L9_RAT]	N/A
M0R7Z0	Uncharacterized protein OS=Rattus norvegicus PE=4 SV=1 - [M0R7Z0_RAT]	N/A
M0R8U4	Protein Rpl13a-ps1 OS=Rattus norvegicus GN=Rpl13a-ps1 PE=3 SV=1 - [M0R8U4_RAT]	N/A
M0R907	Protein Snrpd3 OS=Rattus norvegicus GN=Snrpd3 PE=4 SV=1 - [M0R907_RAT]	N/A
M0RCH1	Uncharacterized protein (Fragment) OS=Rattus norvegicus PE=3 SV=1 - [M0RCH1_RAT]	N/A
M0RD14	Pyruvate kinase OS=Rattus norvegicus PE=3 SV=1 - [M0RD14_RAT]	N/A
P04692-7	Isoform 7 of Tropomyosin alpha-1 chain n=1 Tax=Rattus norvegicus RepID=P04692-7	N/A
P05942	Protein S100-A4 OS=Rattus norvegicus GN=S100a4 PE=2 SV=1 - [S10A4_RAT]	N/A
P15865	Histone H1.4 OS=Rattus norvegicus GN=Hist1h1e PE=1 SV=3 - [H14_RAT]	N/A
P19637	Tissue-type plasminogen activator OS=Rattus norvegicus GN=Plat PE=2 SV=2 - [TPA_RAT]	N/A
P23785	Granulins OS=Rattus norvegicus GN=Grn PE=1 SV=3 - [GRN_RAT]	N/A
P24049	60S ribosomal protein L17 OS=Rattus norvegicus GN=Rpl17 PE=2 SV=3 - [RL17_RAT]	N/A
P31000	Vimentin OS=Rattus norvegicus GN=Vim PE=1 SV=2 - [VIME_RAT]	N/A

P61354	60S ribosomal protein L27 OS=Rattus norvegicus GN=Rpl27 PE=2 SV=2 - [RL27_RAT]	N/A
P62260	14-3-3 protein epsilon OS=Rattus norvegicus GN=Ywhae PE=1 SV=1 - [1433E_RAT]	N/A
P62755	40S ribosomal protein S6 OS=Rattus norvegicus GN=Rps6 PE=1 SV=1 - [RS6_RAT]	N/A
P62912	60S ribosomal protein L32 OS=Rattus norvegicus GN=Rpl32 PE=1 SV=2 - [RL32_RAT]	N/A
P63259	Actin, cytoplasmic 2 OS=Rattus norvegicus GN=Actg1 PE=1 SV=1 - [ACTG_RAT]	N/A
P68370	Tubulin alpha-1A chain OS=Rattus norvegicus GN=Tuba1a PE=1 SV=1 - [TBA1A_RAT]	N/A
P81795	Eukaryotic translation initiation factor 2 subunit 3 OS=Rattus norvegicus GN=Eif2s3 PE=1 SV=2 - [IF2G_RAT]	N/A
P84092	AP-2 complex subunit mu OS=Rattus norvegicus GN=Ap2m1 PE=1 SV=1 - [AP2M1_RAT]	N/A
Q05962	ADP/ATP translocase 1 OS=Rattus norvegicus GN=Slc25a4 PE=1 SV=3 - [ADT1_RAT]	N/A
Q1JU68	Eukaryotic translation initiation factor 3 subunit A OS=Rattus norvegicus GN=Eif3a PE=2 SV=2 - [EIF3A_RAT]	N/A
Q3KRE8	Tubulin beta-2B chain OS=Rattus norvegicus GN=Tubb2b PE=1 SV=1 - [TBB2B_RAT]	N/A
Q3MHS8	Sin3-associated polypeptide 18 OS=Rattus norvegicus GN=Sap18 PE=2 SV=1 - [Q3MHS8_RAT]	N/A
Q498M4	WD repeat-containing protein 5 OS=Rattus norvegicus GN=Wdr5 PE=1 SV=1 - [WDR5_RAT]	N/A
Q4FZS2	Budding uninhibited by benzimidazoles 3 homolog (S. cerevisiae) OS=Rattus norvegicus GN=Bub3 PE=2 SV=1 - [Q4FZS2_RAT]	N/A
Q4KLJ1	RCG61762, isoform CRA_a OS=Rattus norvegicus GN=Srsf7 PE=2 SV=1 - [Q4KLJ1_RAT]	N/A
Q4KLJ3	Guanine nucleotide binding protein-like 2 (Nucleolar) OS=Rattus norvegicus GN=Gnl2 PE=2 SV=1 - [Q4KLJ3_RAT]	N/A
Q4KLM7	Protein Specc1 OS=Rattus norvegicus GN=Specc1 PE=2 SV=1 - [Q4KLM7_RAT]	N/A
Q4KLN3	SFRS protein kinase 1 OS=Rattus norvegicus GN=Srpk1 PE=2 SV=1 - [Q4KLN3_RAT]	N/A
Q4QQW4	Histone deacetylase 1 OS=Rattus norvegicus GN=Hdac1 PE=1 SV=1 - [HDAC1_RAT]	N/A
Q4QR75	Exosome complex component RRP45 OS=Rattus norvegicus GN=Exosc9 PE=2 SV=1 - [EXOS9_RAT]	N/A
Q4V7D7	Pre-mRNA-splicing factor RBM22 OS=Rattus norvegicus GN=Rbm22 PE=2 SV=1 - [RBM22_RAT]	N/A
Q4V8J6	Protein Ythdf1 OS=Rattus norvegicus GN=Ythdf1 PE=2 SV=1 - [Q4V8J6_RAT]	N/A
Q562C2	Ribosome biogenesis protein BOP1 OS=Rattus norvegicus GN=Bop1 PE=2 SV=1 - [BOP1_RAT]	N/A
Q56A18-4	Isoform 4 of SWI/SNF-related matrix-associated actin-dependent regulator of chromatin subfamily E member 1 n=2 Tax=Rattus norvegicus RepID=Q56A18-4	N/A
Q56A27	Nuclear cap-binding protein subunit 1 OS=Rattus norvegicus GN=Ncbp1 PE=2 SV=1 - [NCBP1_RAT]	N/A
Q56B11	Proline-, glutamic acid- and leucine-rich protein 1 OS=Rattus norvegicus GN=Pelp1 PE=2 SV=2 - [PELP1_RAT]	N/A
Q56R17	Importin subunit alpha OS=Rattus norvegicus GN=Kpna4 PE=2 SV=1 - [Q56R17_RAT]	N/A
Q5EB93	Gatad2a protein OS=Rattus norvegicus GN=Gatad2a PE=2 SV=1 - [Q5EB93_RAT]	N/A
Q5I0H3	Small ubiquitin-related modifier 1 OS=Rattus norvegicus GN=Sumo1 PE=1 SV=1 - [SUMO1_RAT]	N/A
Q5M7V3	LOC367586 protein OS=Rattus norvegicus GN=LOC367586 PE=2 SV=1 - [Q5M7V3_RAT]	N/A
Q5RJM0	MKI67 FHA domain-interacting nucleolar phosphoprotein OS=Rattus norvegicus GN=Nifk PE=2 SV=1 - [MK67I_RAT]	N/A

Q5U2W5	Transducin beta-like protein 3 OS=Rattus norvegicus GN=Tbl3 PE=2 SV=1 - [TBL3_RAT]	N/A
Q5XI01	La-related protein 7 OS=Rattus norvegicus GN=Larp7 PE=1 SV=2 - [LARP7_RAT]	N/A
Q5XI32	F-actin-capping protein subunit beta OS=Rattus norvegicus GN=Capzb PE=1 SV=1 - [CAPZB_RAT]	N/A
Q5XIG8	Serine-threonine kinase receptor-associated protein OS=Rattus norvegicus GN=Strap PE=1 SV=1 - [STRAP_RAT]	N/A
Q63009	Protein arginine N-methyltransferase 1 OS=Rattus norvegicus GN=Prmt1 PE=1 SV=1 - [ANM1_RAT]	N/A
Q642B0	Glypican 4 OS=Rattus norvegicus GN=Gpc4 PE=2 SV=1 - [Q642B0_RAT]	N/A
Q66HD0	Endoplasmin OS=Rattus norvegicus GN=Hsp90b1 PE=1 SV=2 - [ENPL_RAT]	N/A
Q66HT5	Cysteine rich protein 61 OS=Rattus norvegicus GN=Cyr61 PE=2 SV=1 - [Q66HT5_RAT]	N/A
Q68FP1-2	Isoform 2 of Gelsolin n=2 Tax=Rattus norvegicus RepID=Q68FP1-2	N/A
Q68FR6	Elongation factor 1-gamma OS=Rattus norvegicus GN=Eef1g PE=1 SV=3 - [EF1G_RAT]	N/A
Q6AXV4	Sorting and assembly machinery component 50 homolog OS=Rattus norvegicus GN=Samm50 PE=1 SV=1 - [SAM50_RAT]	N/A
Q6AYA1	H/ACA ribonucleoprotein complex subunit 1 OS=Rattus norvegicus GN=Gar1 PE=2 SV=1 - [GAR1_RAT]	N/A
Q6AYL5	Splicing factor 3B subunit 4 OS=Rattus norvegicus GN=Sf3b4 PE=2 SV=1 - [SF3B4_RAT]	N/A
Q6AYT6	DEAD (Asp-Glu-Ala-Asp) box polypeptide 56 OS=Rattus norvegicus GN=Ddx56 PE=2 SV=1 - [Q6AYT6_RAT]	N/A
Q6AYU2	Pcbp2 protein OS=Rattus norvegicus GN=Pcbp2 PE=2 SV=1 - [Q6AYU2_RAT]	N/A
Q6AZ26	C-terminal binding protein 1 OS=Rattus norvegicus GN=Ctbp1 PE=1 SV=1 - [Q6AZ26_RAT]	N/A
Q6GMN8	Actn1 protein OS=Rattus norvegicus GN=Actn1 PE=2 SV=1 - [Q6GMN8_RAT]	N/A
Q6MG10	Mitochondrial ribosomal protein S18B OS=Rattus norvegicus GN=Mrps18b PE=2 SV=1 - [Q6MG10_RAT]	N/A
Q6P136	Hyou1 protein OS=Rattus norvegicus GN=Hyou1 PE=2 SV=1 - [Q6P136_RAT]	N/A
Q6P3V8	Eukaryotic translation initiation factor 4A1 OS=Rattus norvegicus GN=Eif4a1 PE=1 SV=1 - [Q6P3V8_RAT]	N/A
Q6P6G9	Hnrpa1 protein OS=Rattus norvegicus GN=Hnrnpa1 PE=2 SV=1 - [Q6P6G9_RAT]	N/A
Q6P7R0	Coronin OS=Rattus norvegicus GN=Coro1b PE=2 SV=1 - [Q6P7R0_RAT]	N/A
Q6P9U7	L-lactate dehydrogenase OS=Rattus norvegicus GN=Ldha PE=2 SV=1 - [Q6P9U7_RAT]	N/A
Q6QLN3	Glioma tumor suppressor candidate region gene 2 OS=Rattus norvegicus GN=Gltscr2 PE=2 SV=1 - [Q6QLN3_RAT]	N/A
Q6TXE9	LRRGT00050 OS=Rattus norvegicus GN=Eprs PE=1 SV=1 - [Q6TXE9_RAT]	N/A
Q6U6G5	Zinc finger CCCH domain-containing protein 15 OS=Rattus norvegicus GN=Zc3h15 PE=2 SV=1 - [ZC3HF_RAT]	N/A
Q925G0	Putative RNA-binding protein 3 OS=Rattus norvegicus GN=Rbm3 PE=1 SV=2 - [RBM3_RAT]	N/A
Q9JKL8	Activity-dependent neuroprotector homeobox protein OS=Rattus norvegicus GN=Adnp PE=2 SV=1 - [ADNP_RAT]	N/A
Q9QZK5	Serine protease HTRA1 OS=Rattus norvegicus GN=Htra1 PE=2 SV=1 - [HTRA1_RAT]	N/A
Q9R1E9	Connective tissue growth factor OS=Rattus norvegicus GN=Ctgf PE=2 SV=1 - [CTGF_RAT]	N/A
Q9WU82	Catenin beta-1 OS=Rattus norvegicus GN=Ctnnb1 PE=1 SV=1 - [CTNB1_RAT]	N/A

Q9WUW5	Collagen type XVIII, alpha (I) chain (Fragment) OS=Rattus norvegicus GN=Col18a1 PE=2 SV=1 - [Q9WUW5_RAT]	N/A
T1SRT4	Radixin isoform OS=Rattus norvegicus GN=Rdx PE=2 SV=1 - [T1SRT4_RAT]	N/A
UPI0000180AB4	PREDICTED: luc7-like protein 3 isoform X2 n=1 Tax=Rattus norvegicus RepID=UPI0000180AB4	N/A
UPI00001C8B75	PREDICTED: plasminogen activator inhibitor 1 RNA-binding protein isoform X2 n=1 Tax=Rattus norvegicus RepID=UPI00001C8B75	N/A
UPI00001D0F5B	PREDICTED: cytokine receptor-like factor 1 isoform X2 n=1 Tax=Rattus norvegicus RepID=UPI00001D0F5B	N/A
UPI0000250BD6	PREDICTED: 60S ribosomal protein L13-like n=1 Tax=Rattus norvegicus RepID=UPI0000250BD6	N/A
UPI0000250FE4	PREDICTED: myosin-14 isoform X2 n=1 Tax=Rattus norvegicus RepID=UPI0000250FE4	N/A
UPI0000500E84	PREDICTED: C-Jun-amino-terminal kinase-interacting protein 4 isoform X5 n=1 Tax=Rattus norvegicus RepID=UPI0000500E84	N/A
UPI0000503905	PREDICTED: DEAH (Asp-Glu-Ala-Asp/His) box polypeptide 57 isoform X2 n=1 Tax=Rattus norvegicus RepID=UPI0000503905	N/A
UPI0000DA1CD8	PREDICTED: AP-2 complex subunit alpha-1 isoform X4 n=1 Tax=Rattus norvegicus RepID=UPI0000DA1CD8	N/A
UPI0000DA285F	PREDICTED: MAP7 domain-containing protein 1 isoform X5 n=1 Tax=Rattus norvegicus RepID=UPI0000DA285F	N/A
UPI0000DA38FD	PREDICTED: homeobox protein cut-like 1 isoform X8 n=1 Tax=Rattus norvegicus RepID=UPI0000DA38FD	N/A
UPI0000DBF3AC	PREDICTED: fibronectin isoform X4 n=1 Tax=Rattus norvegicus RepID=UPI0000DBF3AC	N/A
UPI0000DBF7D2	PREDICTED: heterogeneous nuclear ribonucleoprotein M isoform X1 n=1 Tax=Rattus norvegicus RepID=UPI0000DBF7D2	N/A
UPI000154E9E5	PREDICTED: E3 ubiquitin-protein ligase TRIM56 n=1 Tax=Rattus norvegicus RepID=UPI000154E9E5	N/A
UPI000154F802	programmed cell death 6-interacting protein n=1 Tax=Rattus norvegicus RepID=UPI000154F802	N/A
UPI0001550CCB	PREDICTED: histone H1.2 n=1 Tax=Rattus norvegicus RepID=UPI0001550CCB	N/A
UPI0001551E07	PREDICTED: DNA-directed RNA polymerases I, II, and III subunit RPABC1 isoform X3 n=1 Tax=Rattus norvegicus RepID=UPI0001551E07	N/A
UPI0001B7B713	PREDICTED: AT-rich interactive domain-containing protein 1A isoform X1 n=1 Tax=Rattus norvegicus RepID=UPI0001B7B713	N/A
UPI0001CF3CF5	PREDICTED: catenin alpha-3 isoform X1 n=2 Tax=Rattus norvegicus RepID=UPI0001CF3CF5	N/A
UPI0001CF3F9F	YLP motif-containing protein 1 n=1 Tax=Rattus norvegicus RepID=UPI0001CF3F9F	N/A
UPI0001CF734A	PREDICTED: protein AHNAK2 n=1 Tax=Rattus norvegicus RepID=UPI0001CF734A	N/A
UPI0003D077B6	PREDICTED: alpha-actinin-4 isoform X3 n=1 Tax=Rattus norvegicus RepID=UPI0003D077B6	N/A
UPI0003D0839D	PREDICTED: apoptotic chromatin condensation inducer 1 isoform X5 n=1 Tax=Rattus norvegicus RepID=UPI0003D0839D	N/A
UPI0003D0841E	PREDICTED: SH3 and PX domain-containing protein 2A isoform X4 n=1 Tax=Rattus norvegicus RepID=UPI0003D0841E	N/A
UPI0003D088F0	PREDICTED: polypyrimidine tract-binding protein 3 isoform X2 n=2 Tax=Rattus norvegicus RepID=UPI0003D088F0	N/A
UPI0003D08BCF	PREDICTED: bcl-2-associated transcription factor 1 isoform X4 n=1 Tax=Rattus norvegicus RepID=UPI0003D08BCF	N/A
UPI0003D093A2	PREDICTED: protein SON isoform X3 n=1 Tax=Rattus norvegicus RepID=UPI0003D093A2	N/A
UPI0003D09F77	PREDICTED: probable ATP-dependent RNA helicase DDX52 isoform X1 n=1 Tax=Rattus norvegicus RepID=UPI0003D09F77	N/A
UPI0003D09FC6	PREDICTED: serine/threonine-protein kinase DCLK1 isoform X2 n=2 Tax=Rattus norvegicus RepID=UPI0003D09FC6	N/A

UPI0003D0AC45	PREDICTED: protein transport protein Sec24D isoform X2 n=1 Tax=Rattus norvegicus RepID=UPI0003D0AC45	N/A
UPI0003D0B550	PREDICTED: serine/arginine repetitive matrix protein 1 isoform X5 n=1 Tax=Rattus norvegicus RepID=UPI0003D0B550	N/A
UPI0003D0B91E	PREDICTED: SWI/SNF-related matrix-associated actin-dependent regulator of chromatin subfamily B member 1 isoform X3 n=1 Tax=Rattus norvegicus RepID=UPI0003D0B91E	N/A
UPI0003D0BC78	PREDICTED: keratin, type I cytoskeletal 16 isoform X1 n=1 Tax=Rattus norvegicus RepID=UPI0003D0BC78	N/A
UPI0003D0C0AC	PREDICTED: protein DEK isoform X1 n=1 Tax=Rattus norvegicus RepID=UPI0003D0C0AC	N/A
UPI0003D0C20D	PREDICTED: PERQ amino acid-rich with GYF domain-containing protein 2-like isoform X6 n=1 Tax=Rattus norvegicus RepID=UPI0003D0C20D	N/A
UPI0003D0C2CD	PREDICTED: myelin expression factor 2 isoform X4 n=1 Tax=Rattus norvegicus RepID=UPI0003D0C2CD	N/A
UPI0003D0C949	PREDICTED: centrosomal protein of 170 kDa isoform X11 n=1 Tax=Rattus norvegicus RepID=UPI0003D0C949	N/A
UPI0003D0E282	PREDICTED: guanine nucleotide-binding protein G(i) subunit alpha-2 isoform X2 n=1 Tax=Rattus norvegicus RepID=UPI0003D0E282	N/A
UPI0003D0E362	PREDICTED: protein FAM98B isoform X2 n=1 Tax=Rattus norvegicus RepID=UPI0003D0E362	N/A
UPI0003D0E707	PREDICTED: nucleolar and coiled-body phosphoprotein 1 isoform X1 n=1 Tax=Rattus norvegicus RepID=UPI0003D0E707	N/A
UPI0003D0E753	PREDICTED: 39S ribosomal protein L39, mitochondrial n=1 Tax=Rattus norvegicus RepID=UPI0003D0E753	N/A
UPI0003D0EC97	PREDICTED: RNA-binding protein 42 isoform X1 n=1 Tax=Rattus norvegicus RepID=UPI0003D0EC97	N/A
UPI0003D0F01C	PREDICTED: SUN domain-containing protein 1 isoform X4 n=1 Tax=Rattus norvegicus RepID=UPI0003D0F01C	N/A
UPI0003D0F450	PREDICTED: 28S ribosomal protein S35, mitochondrial isoform X2 n=1 Tax=Rattus norvegicus RepID=UPI0003D0F450	N/A
UPI0003D0F60C	PREDICTED: protein polybromo-1-like isoform X20 n=1 Tax=Rattus norvegicus RepID=UPI0003D0F60C	N/A
UPI0003D0F9C8	PREDICTED: microtubule-actin cross-linking factor 1 isoform X10 n=1 Tax=Rattus norvegicus RepID=UPI0003D0F9C8	N/A
UPI0003D0FC8D	PREDICTED: rho guanine nucleotide exchange factor 17 n=1 Tax=Rattus norvegicus RepID=UPI0003D0FC8D	N/A
UPI0003D0FD46	PREDICTED: protein PRRC2A isoform X5 n=1 Tax=Rattus norvegicus RepID=UPI0003D0FD46	N/A
UPI0003D1005E	PREDICTED: reversion-inducing cysteine-rich protein with Kazal motifs isoform X2 n=1 Tax=Rattus norvegicus RepID=UPI0003D1005E	N/A
UPI0004E4726C	PREDICTED: serine/threonine-protein phosphatase 1 regulatory subunit 10 isoform X1 n=1 Tax=Rattus norvegicus RepID=UPI0004E4726C	N/A
UPI0004E472EA	PREDICTED: tenascin isoform X5 n=1 Tax=Rattus norvegicus RepID=UPI0004E472EA	N/A
UPI0004E47558	PREDICTED: drebrin isoform X4 n=1 Tax=Rattus norvegicus RepID=UPI0004E47558	N/A
UPI0004E47B0A	PREDICTED: ribosome-binding protein 1 isoform X2 n=1 Tax=Rattus norvegicus RepID=UPI0004E47B0A	N/A
UPI0004E47BB8	PREDICTED: methyl-CpG-binding domain protein 3 isoform X4 n=1 Tax=Rattus norvegicus RepID=UPI0004E47BB8	N/A
UPI0004E48EAA	PREDICTED: LOW QUALITY PROTEIN: uncharacterized protein LOC100910366 n=1 Tax=Rattus norvegicus RepID=UPI0004E48EAA	N/A
UPI0004E491F4	PREDICTED: replication factor C subunit 1 isoform X3 n=1 Tax=Rattus norvegicus RepID=UPI0004E491F4	N/A
UPI0004E49349	PREDICTED: ATP-dependent RNA helicase DDX3Y isoform X2 n=1 Tax=Rattus norvegicus RepID=UPI0004E49349	N/A

Table 6 Comparison of N-cad TMX sample to IgG control based on fold increase (≥2.5)

N-Cad specific Fold increase TMX		
Accession	Description	Fold increase score
G3V8T5	Protein Ruvbl2 OS=Rattus norvegicus GN=Ruvbl2 PE=4 SV=1 - [G3V8T5_RAT]	2.59
D3ZZZ9	Catenin (Cadherin associated protein), delta 1 (Predicted), isoform CRA_a OS=Rattus norvegicus GN=Ctnnd1 PE=1 SV=1 - [D3ZZZ9_RAT]	2.66
P40615	H/ACA ribonucleoprotein complex subunit 4 OS=Rattus norvegicus GN=Dkc1 PE=1 SV=4 - [DKC1_RAT]	2.74
P22509	rRNA 2'-O-methyltransferase fibrillarin OS=Rattus norvegicus GN=Fbl PE=1 SV=2 - [FBRL_RAT]	2.77
D4A563	Protein RGD1312026 OS=Rattus norvegicus GN=Peak1 PE=1 SV=1 - [D4A563_RAT]	2.86
F1LV13	Heterogeneous nuclear ribonucleoprotein M OS=Rattus norvegicus GN=Hnrnpm PE=4 SV=1 - [F1LV13_RAT]	3.08
A9CMB7	Aspartyl-tRNA synthetase OS=Rattus norvegicus GN=Dars PE=3 SV=1 - [A9CMB7_RAT]	3.18
Q5XHY0	DEAD (Asp-Glu-Ala-Asp) box polypeptide 18 OS=Rattus norvegicus GN=Ddx18 PE=2 SV=1 - [Q5XHY0_RAT]	3.20
D4AAG8	Protein Smchd1 OS=Rattus norvegicus GN=Smchd1 PE=4 SV=1 - [D4AAG8_RAT]	3.30
UPI0003D08B80	PREDICTED: pre-mRNA-processing factor 6 isoform X1 n=1 Tax=Rattus norvegicus RepID=UPI0003D08B80	3.44
Q9QZ86	Nucleolar protein 58 OS=Rattus norvegicus GN=Nop58 PE=1 SV=1 - [NOP58_RAT]	3.72
D4AEB4	Protein Nat10 OS=Rattus norvegicus GN=Nat10 PE=4 SV=1 - [D4AEB4_RAT]	3.87
F1LR02	Procollagen, type XVIII, alpha 1, isoform CRA_a OS=Rattus norvegicus GN=Col18a1 PE=4 SV=2 - [F1LR02_RAT]	3.92
D3ZNI3	Protein Pdcd11 OS=Rattus norvegicus GN=Pdcd11 PE=4 SV=1 - [D3ZNI3_RAT]	3.98
UPI000154F802	programmed cell death 6-interacting protein n=1 Tax=Rattus norvegicus RepID=UPI000154F802	4.23
Q5FVM4	Non-POU domain-containing octamer-binding protein OS=Rattus norvegicus GN=Nono PE=1 SV=3 - [NONO_RAT]	4.26
F1LW91	Protein Numa1 (Fragment) OS=Rattus norvegicus GN=Numa1 PE=4 SV=1 - [F1LW91_RAT]	4.36
P62845	40S ribosomal protein S15 OS=Rattus norvegicus GN=Rps15 PE=1 SV=2 - [RS15_RAT]	4.37
D3ZD24	Protein Syne3 OS=Rattus norvegicus GN=Syne3 PE=4 SV=2 - [D3ZD24_RAT]	4.74
G3V6H2	Pre-mRNA processing factor 8, isoform CRA_a OS=Rattus norvegicus GN=Prpf8 PE=4 SV=1 - [G3V6H2_RAT]	4.85
Q14TE9	DNA topoisomerase 2 OS=Rattus norvegicus GN=Top2b PE=2 SV=1 - [Q14TE9_RAT]	5.14
G3V7U4	Lamin-B1 OS=Rattus norvegicus GN=Lmnb1 PE=3 SV=1 - [G3V7U4_RAT]	8.91
Q09073	ADP/ATP translocase 2 OS=Rattus norvegicus GN=Slc25a5 PE=1 SV=3 - [ADT2_RAT]	N/A
A1A5P2	Ribosome biogenesis regulatory protein homolog OS=Rattus norvegicus GN=Rrs1 PE=2 SV=1 - [RRS1_RAT]	N/A
A2RRU3	U3 small nucleolar RNA-associated protein 15 homolog OS=Rattus norvegicus GN=Utp15 PE=2 SV=1 - [UTP15_RAT]	N/A
B0BMU2	NOP16 nucleolar protein homolog (Yeast) OS=Rattus norvegicus GN=Nop16 PE=2 SV=1 - [B0BMU2_RAT]	N/A
B0BMV8	Dihydrofolate reductase OS=Rattus norvegicus GN=Dhfr PE=2 SV=1 - [B0BMV8_RAT]	N/A
B0BN90	DIM1 dimethyladenosine transferase 1-like (S. cerevisiae) OS=Rattus norvegicus GN=Dimt1 PE=2 SV=1 - [B0BN90_RAT]	N/A

B0BND5	Protein Rrp9 OS=Rattus norvegicus GN=Rrp9 PE=2 SV=1 - [B0BND5_RAT]	N/A
B0BNF5	Qk protein OS=Rattus norvegicus GN=Qk PE=2 SV=1 - [B0BNF5_RAT]	N/A
B1H227	LOC682908 protein OS=Rattus norvegicus GN=Rcc1 PE=2 SV=1 - [B1H227_RAT]	N/A
B1H269	Ddx27 protein OS=Rattus norvegicus GN=Ddx27 PE=2 SV=1 - [B1H269_RAT]	N/A
B2GUZ3	Mthfd1l protein OS=Rattus norvegicus GN=Mthfd1l PE=2 SV=1 - [B2GUZ3_RAT]	N/A
B2GV01	Metastasis-associated gene family, member 2 OS=Rattus norvegicus GN=Mta2 PE=2 SV=1 - [B2GV01_RAT]	N/A
B2GV02	Protein LOC100909901 OS=Rattus norvegicus GN=Racgap1 PE=2 SV=1 - [B2GV02_RAT]	N/A
B2RYQ5	Enhancer of rudimentary homolog OS=Rattus norvegicus GN=Erh PE=2 SV=1 - [B2RYQ5_RAT]	N/A
B5DFB2	Protein Rbbp4 OS=Rattus norvegicus GN=Rbbp4 PE=2 SV=1 - [B5DFB2_RAT]	N/A
B5DFG2	Hnrnpl protein (Fragment) OS=Rattus norvegicus GN=Hnrnpl PE=2 SV=1 - [B5DFG2_RAT]	N/A
B5DFJ3	Ddx23 protein (Fragment) OS=Rattus norvegicus GN=Ddx23 PE=2 SV=1 - [B5DFJ3_RAT]	N/A
B6RIU0	FIP1-like 1 OS=Rattus norvegicus GN=Fip1l1 PE=2 SV=1 - [B6RIU0_RAT]	N/A
D3ZAY8	Protein Pnn OS=Rattus norvegicus GN=Pnn PE=4 SV=1 - [D3ZAY8_RAT]	N/A
D3ZAZ0	Eukaryotic translation initiation factor 3 subunit M OS=Rattus norvegicus GN=Eif3m PE=3 SV=1 - [D3ZAZ0_RAT]	N/A
D3ZBS9	Protein Smarcd1 OS=Rattus norvegicus GN=Smarcd1 PE=4 SV=1 - [D3ZBS9_RAT]	N/A
D3ZC82	Protein Nufip2 OS=Rattus norvegicus GN=LOC687994 PE=4 SV=2 - [D3ZC82_RAT]	N/A
D3ZC84	Ubiquitin carboxyl-terminal hydrolase OS=Rattus norvegicus GN=Usp9x PE=3 SV=1 - [D3ZC84_RAT]	N/A
D3ZD73	Protein Ddx6 OS=Rattus norvegicus GN=Ddx6 PE=3 SV=1 - [D3ZD73_RAT]	N/A
D3ZD97	DEAH (Asp-Glu-Ala-His) box polypeptide 15 (Predicted), isoform CRA_b OS=Rattus norvegicus GN=Dhx15 PE=4 SV=1 - [D3ZD97_RAT]	N/A
D3ZDS4	EMG1 nucleolar protein homolog (S. cerevisiae) (Predicted), isoform CRA_b OS=Rattus norvegicus GN=Emg1 PE=4 SV=1 - [D3ZDS4_RAT]	N/A
D3ZEI6	Nuclear receptor coactivator 5 (Predicted) OS=Rattus norvegicus GN=Ncoa5 PE=4 SV=1 - [D3ZEI6_RAT]	N/A
D3ZF07	Protein RGD1562402 OS=Rattus norvegicus GN=RGD1562402 PE=3 SV=1 - [D3ZF07_RAT]	N/A
D3ZF52	Ribosomal protein L15 OS=Rattus norvegicus GN=RGD1565767 PE=3 SV=1 - [D3ZF52_RAT]	N/A
D3ZF89	Protein Ubap2 OS=Rattus norvegicus GN=Ubap2 PE=4 SV=2 - [D3ZF89_RAT]	N/A
D3ZFD0	Uncharacterized protein OS=Rattus norvegicus GN=Myo18a PE=1 SV=2 - [D3ZFD0_RAT]	N/A
D3ZGE6	Protein Cttn OS=Rattus norvegicus GN=Cttn PE=4 SV=2 - [D3ZGE6_RAT]	N/A
D3ZGQ8	Protein Rsf1 OS=Rattus norvegicus GN=Rsf1 PE=4 SV=1 - [D3ZGQ8_RAT]	N/A
D3ZGV8	Protein Prrc2c OS=Rattus norvegicus GN=Prrc2c PE=1 SV=2 - [D3ZGV8_RAT]	N/A
D3ZI68	PRP31 pre-mRNA processing factor 31 homolog (Yeast) (Predicted) OS=Rattus norvegicus GN=Prpf31 PE=4 SV=1 - [D3ZI68_RAT]	N/A
D3ZJ67	Protein Sun2 OS=Rattus norvegicus GN=Sun2 PE=4 SV=1 - [D3ZJ67_RAT]	N/A

D3ZL86	HEAT repeat containing 1 (Predicted) OS=Rattus norvegicus GN=Heatr1 PE=4 SV=1 - [D3ZL86_RAT]	N/A
D3ZLC1	Protein Lmnb2 OS=Rattus norvegicus GN=Lmnb2 PE=4 SV=1 - [D3ZLC1_RAT]	N/A
D3ZN76	Protein Sec16a OS=Rattus norvegicus GN=Sec16a PE=4 SV=1 - [D3ZN76_RAT]	N/A
D3ZNU1	Protein Cebpz OS=Rattus norvegicus GN=Cebpz PE=4 SV=1 - [D3ZNU1_RAT]	N/A
D3ZUM5	Protein Trim33 (Fragment) OS=Rattus norvegicus GN=Trim33 PE=4 SV=2 - [D3ZUM5_RAT]	N/A
D3ZUV3	Eukaryotic translation initiation factor 2 subunit 1 OS=Rattus norvegicus GN=Eif2a PE=4 SV=2 - [D3ZUV3_RAT]	N/A
D3ZUX5	Coiled-coil-helix-coiled-coil-helix domain containing 3 (Predicted), isoform CRA_a OS=Rattus norvegicus GN=Chchd3 PE=4 SV=1 - [D3ZUX5_RAT]	N/A
D3ZV54	Protein Pwp2 OS=Rattus norvegicus GN=Pwp2 PE=4 SV=1 - [D3ZV54_RAT]	N/A
D3ZY44	Protein Mrps2 OS=Rattus norvegicus GN=Mrps2 PE=3 SV=1 - [D3ZY44_RAT]	N/A
D3ZZY2	Protein Utp14a OS=Rattus norvegicus GN=Utp14a PE=4 SV=2 - [D3ZZY2_RAT]	N/A
D3ZZZ0	Protein Ahctf1 OS=Rattus norvegicus GN=Ahctf1 PE=4 SV=1 - [D3ZZZ0_RAT]	N/A
D4A054	Protein LOC100911178 OS=Rattus norvegicus GN=Ranbp2 PE=1 SV=1 - [D4A054_RAT]	N/A
D4A0E8	Protein arginine N-methyltransferase 5 OS=Rattus norvegicus GN=Prmt5 PE=3 SV=1 - [D4A0E8_RAT]	N/A
D4A0H5	Cleavage and polyadenylation specific factor 1, 160kDa (Predicted), isoform CRA_a OS=Rattus norvegicus GN=Cpsf1 PE=4 SV=1 - [D4A0H5_RAT]	N/A
D4A1K2	Protein Rpl7l1 OS=Rattus norvegicus GN=Rpl7l1 PE=3 SV=1 - [D4A1K2_RAT]	N/A
D4A512	Protein Nemf OS=Rattus norvegicus GN=Nemf PE=4 SV=2 - [D4A512_RAT]	N/A
D4A5S9	Protein Prpf39 OS=Rattus norvegicus GN=Prpf39 PE=4 SV=1 - [D4A5S9_RAT]	N/A
D4A7J8	PRP4 pre-mRNA processing factor 4 homolog (Yeast) OS=Rattus norvegicus GN=Prpf4 PE=4 SV=1 - [D4A7J8_RAT]	N/A
D4ACW0	Protein Rbm6 OS=Rattus norvegicus GN=Rbm6 PE=4 SV=1 - [D4ACW0_RAT]	N/A
D4AE41	RNA binding motif protein, X-linked-like-1 OS=Rattus norvegicus GN=Rbmxl1 PE=3 SV=1 - [RMXL1_RAT]	N/A
D4AE65	Protein Rrp7a OS=Rattus norvegicus GN=Rrp7a PE=4 SV=1 - [D4AE65_RAT]	N/A
D4AEC0	Histone H2A OS=Rattus norvegicus GN=LOC685909 PE=3 SV=1 - [D4AEC0_RAT]	N/A
E9PTI6	Protein Raly OS=Rattus norvegicus GN=Raly PE=4 SV=1 - [E9PTI6_RAT]	N/A
E9PU01	Protein Chd4 OS=Rattus norvegicus GN=Chd4 PE=4 SV=2 - [E9PU01_RAT]	N/A
F1LMV9	Coronin (Fragment) OS=Rattus norvegicus GN=Coro2b PE=3 SV=2 - [F1LMV9_RAT]	N/A
F1LP60	Moesin (Fragment) OS=Rattus norvegicus GN=Msn PE=4 SV=1 - [F1LP60_RAT]	N/A
F1LPQ3	Alpha-mannosidase 2C1 OS=Rattus norvegicus GN=Man2c1 PE=4 SV=1 - [F1LPQ3_RAT]	N/A
F1LR39	RCG29171, isoform CRA_a OS=Rattus norvegicus GN=Wdr18 PE=4 SV=2 - [F1LR39_RAT]	N/A
F1LRJ2	Protein Srrm2 OS=Rattus norvegicus GN=Srrm2 PE=1 SV=2 - [F1LRJ2_RAT]	N/A
F1LSL2	Nuclear pore complex protein Nup107 OS=Rattus norvegicus GN=Nup107 PE=4 SV=2 - [F1LSL2_RAT]	N/A

F1LSL3	Inositol 1,4,5-trisphosphate receptor type 3 OS=Rattus norvegicus GN=Itpr3 PE=4 SV=2 - [F1LSL3_RAT]	N/A
F1LSS1	Structural maintenance of chromosomes protein OS=Rattus norvegicus GN=Smc1a PE=3 SV=2 - [F1LSS1_RAT]	N/A
F1LU69	Protein Rps27l3 OS=Rattus norvegicus GN=Rps27l3 PE=4 SV=2 - [F1LU69_RAT]	N/A
F1LVD0	Protein LOC690134 (Fragment) OS=Rattus norvegicus GN=LOC690134 PE=3 SV=2 - [F1LVD0_RAT]	N/A
F1LYI5	Protein RGD1564138 (Fragment) OS=Rattus norvegicus GN=RGD1564138 PE=4 SV=2 - [F1LYI5_RAT]	N/A
F1M0V4	Protein Thoc2 OS=Rattus norvegicus GN=Thoc2 PE=4 SV=2 - [F1M0V4_RAT]	N/A
F1M3H2	Uncharacterized protein (Fragment) OS=Rattus norvegicus GN=LOC100360367 PE=4 SV=2 - [F1M3H2_RAT]	N/A
F1M3K6	Protein Bag4 (Fragment) OS=Rattus norvegicus GN=Bag4 PE=4 SV=2 - [F1M3K6_RAT]	N/A
F1M4U9	Protein Baz1a (Fragment) OS=Rattus norvegicus GN=Baz1a PE=4 SV=2 - [F1M4U9_RAT]	N/A
F1M5V2	Protein Glipr2 OS=Rattus norvegicus GN=Glipr2 PE=4 SV=2 - [F1M5V2_RAT]	N/A
F1M6V1	Heterochromatin protein 1-binding protein 3 OS=Rattus norvegicus GN=Hp1bp3 PE=3 SV=2 - [F1M6V1_RAT]	N/A
F1M779	Clathrin heavy chain OS=Rattus norvegicus GN=Cltc PE=3 SV=1 - [F1M779_RAT]	N/A
F1M7A0	DNA topoisomerase 2 (Fragment) OS=Rattus norvegicus GN=Top2a PE=3 SV=2 - [F1M7A0_RAT]	N/A
F1M8H5	Protein Abcf2 OS=Rattus norvegicus GN=Abcf2 PE=4 SV=2 - [F1M8H5_RAT]	N/A
F1MA04	Protein Wdr36 (Fragment) OS=Rattus norvegicus GN=Wdr36 PE=4 SV=2 - [F1MA04_RAT]	N/A
F1MA52	Nuclear RNA export factor 1 OS=Rattus norvegicus GN=Nxf1 PE=4 SV=1 - [F1MA52_RAT]	N/A
F1SW39	PC4 and SFRS1 interacting protein 1 OS=Rattus norvegicus GN=Psip1 PE=2 SV=1 - [F1SW39_RAT]	N/A
F7FFV2	Keratin, type II cytoskeletal 5 (Fragment) OS=Rattus norvegicus GN=Krt5 PE=3 SV=1 - [F7FFV2_RAT]	N/A
G3V661	Bromodomain adjacent to zinc finger domain protein 1B OS=Rattus norvegicus GN=Baz1b PE=4 SV=1 - [G3V661_RAT]	N/A
G3V6A8	Golgi autoantigen, golgin subfamily b, macrogolgin 1, isoform CRA_c OS=Rattus norvegicus GN=Golgb1 PE=1 SV=1 - [G3V6A8_RAT]	N/A
G3V6D3	ATP synthase subunit beta OS=Rattus norvegicus GN=Atp5b PE=3 SV=1 - [G3V6D3_RAT]	N/A
G3V702	Smu-1 suppressor of mec-8 and unc-52 homolog (C. elegans) OS=Rattus norvegicus GN=Smu1 PE=4 SV=1 - [G3V702_RAT]	N/A
G3V7B7	DNA-directed RNA polymerase OS=Rattus norvegicus GN=Polr1a PE=3 SV=1 - [G3V7B7_RAT]	N/A
G3V7G3	Activity-dependent neuroprotector homeobox protein OS=Rattus norvegicus GN=Adnp PE=4 SV=1 - [G3V7G3_RAT]	N/A
G3V7G9	Eukaryotic translation initiation factor 3 subunit L OS=Rattus norvegicus GN=Eif3l PE=2 SV=2 - [G3V7G9_RAT]	N/A
G3V803	Cadherin-2 OS=Rattus norvegicus GN=Cdh2 PE=4 SV=1 - [G3V803_RAT]	N/A
G3V852	Protein Tln1 OS=Rattus norvegicus GN=Tln1 PE=1 SV=1 - [G3V852_RAT]	N/A
G3V8B3	Histone H2B OS=Rattus norvegicus GN=LOC100910200 PE=3 SV=1 - [G3V8B3_RAT]	N/A
G3V8G5	Golgi apparatus protein 1 OS=Rattus norvegicus GN=Glg1 PE=4 SV=1 - [G3V8G5_RAT]	N/A
G3V920	Protein Wdr43 OS=Rattus norvegicus GN=Wdr43 PE=4 SV=1 - [G3V920_RAT]	N/A
G3V9R0	LUC7-like (S. cerevisiae) OS=Rattus norvegicus GN=Luc7l PE=2 SV=2 - [G3V9R0_RAT]	N/A

G3V9R8	Heterogeneous nuclear ribonucleoprotein C (C1/C2) OS=Rattus norvegicus GN=Hnrnpc PE=1 SV=2 - [G3V9R8_RAT]	N/A
M0R3M8	Protein Rrp12 OS=Rattus norvegicus GN=Rrp12 PE=4 SV=1 - [M0R3M8_RAT]	N/A
M0R3Z8	Protein Rbm15 OS=Rattus norvegicus GN=Rbm15 PE=1 SV=1 - [M0R3Z8_RAT]	N/A
M0R440	Zinc finger protein 326 (Fragment) OS=Rattus norvegicus GN=Zfp326 PE=4 SV=1 - [M0R440_RAT]	N/A
M0R548	Protein LOC100912029 OS=Rattus norvegicus GN=LOC100912029 PE=4 SV=1 - [M0R548_RAT]	N/A
M0R7D1	La-related protein 7 OS=Rattus norvegicus GN=Larp7 PE=4 SV=1 - [M0R7D1_RAT]	N/A
M0R8A7	tRNA selenocysteine 1-associated protein 1 OS=Rattus norvegicus GN=Trnau1ap PE=4 SV=1 - [M0R8A7_RAT]	N/A
M0R9Q1	Protein LOC100911677 OS=Rattus norvegicus GN=LOC100911677 PE=4 SV=1 - [M0R9Q1_RAT]	N/A
M0RB74	Protein Ipo5 OS=Rattus norvegicus GN=Ipo5 PE=4 SV=1 - [M0RB74_RAT]	N/A
M0RD14	Pyruvate kinase OS=Rattus norvegicus PE=3 SV=1 - [M0RD14_RAT]	N/A
M0RDD7	RCG29880 OS=Rattus norvegicus GN=Chtop PE=4 SV=1 - [M0RDD7_RAT]	N/A
M0RDF7	Bystin OS=Rattus norvegicus GN=Bysl PE=4 SV=1 - [M0RDF7_RAT]	N/A
O88656	Actin-related protein 2/3 complex subunit 1B OS=Rattus norvegicus GN=Arpc1b PE=2 SV=3 - [ARC1B_RAT]	N/A
O88791	High mobility group AT-hook 2 OS=Rattus norvegicus GN=Hmga2 PE=2 SV=1 - [O88791_RAT]	N/A
P04256	Heterogeneous nuclear ribonucleoprotein A1 OS=Rattus norvegicus GN=Hnrnpa1 PE=1 SV=3 - [ROA1_RAT]	N/A
P05942	Protein S100-A4 OS=Rattus norvegicus GN=S100a4 PE=2 SV=1 - [S10A4_RAT]	N/A
P07943	Aldose reductase OS=Rattus norvegicus GN=Akr1b1 PE=1 SV=3 - [ALDR_RAT]	N/A
P09895	60S ribosomal protein L5 OS=Rattus norvegicus GN=Rpl5 PE=1 SV=3 - [RL5_RAT]	N/A
P15999	ATP synthase subunit alpha, mitochondrial OS=Rattus norvegicus GN=Atp5a1 PE=1 SV=2 - [ATPA_RAT]	N/A
P17136	Small nuclear ribonucleoprotein-associated protein B (Fragment) OS=Rattus norvegicus GN=Snrpb PE=2 SV=1 - [RSMB_RAT]	N/A
P23785	Granulins OS=Rattus norvegicus GN=Grn PE=1 SV=3 - [GRN_RAT]	N/A
P24049	60S ribosomal protein L17 OS=Rattus norvegicus GN=Rpl17 PE=2 SV=3 - [RL17_RAT]	N/A
P30427	Plectin OS=Rattus norvegicus GN=Plec PE=1 SV=2 - [PLEC_RAT]	N/A
P31000	Vimentin OS=Rattus norvegicus GN=Vim PE=1 SV=2 - [VIME_RAT]	N/A
P38650	Cytoplasmic dynein 1 heavy chain 1 OS=Rattus norvegicus GN=Dync1h1 PE=1 SV=1 - [DYHC1_RAT]	N/A
P54313	Guanine nucleotide-binding protein G(I)/G(S)/G(T) subunit beta-2 OS=Rattus norvegicus GN=Gnb2 PE=1 SV=4 - [GBB2_RAT]	N/A
P55770	NHP2-like protein 1 OS=Rattus norvegicus GN=Nhp2l1 PE=2 SV=4 - [NH2L1_RAT]	N/A
P61354	60S ribosomal protein L27 OS=Rattus norvegicus GN=Rpl27 PE=2 SV=2 - [RL27_RAT]	N/A
P62138	Serine/threonine-protein phosphatase PP1-alpha catalytic subunit OS=Rattus norvegicus GN=Ppp1ca PE=1 SV=1 - [PP1A_RAT]	N/A
P62142	Serine/threonine-protein phosphatase PP1-beta catalytic subunit OS=Rattus norvegicus GN=Ppp1cb PE=1 SV=3 - [PP1B_RAT]	N/A
P62275	40S ribosomal protein S29 OS=Rattus norvegicus GN=Rps29 PE=1 SV=2 - [RS29_RAT]	N/A

P62828	GTP-binding nuclear protein Ran OS=Rattus norvegicus GN=Ran PE=1 SV=3 - [RAN_RAT]	N/A
P62859	40S ribosomal protein S28 OS=Rattus norvegicus GN=Rps28 PE=1 SV=1 - [RS28_RAT]	N/A
P62912	60S ribosomal protein L32 OS=Rattus norvegicus GN=Rpl32 PE=1 SV=2 - [RL32_RAT]	N/A
P68255	14-3-3 protein theta OS=Rattus norvegicus GN=Ywhaq PE=1 SV=1 - [1433T_RAT]	N/A
P70501	RNA-binding protein 10 OS=Rattus norvegicus GN=Rbm10 PE=2 SV=1 - [RBM10_RAT]	N/A
P70565	Plakoglobin OS=Rattus norvegicus GN=Jup PE=2 SV=1 - [P70565_RAT]	N/A
P70625	Zonula occludens 2 protein (Fragment) OS=Rattus norvegicus GN=ZO-2 PE=2 SV=2 - [P70625_RAT]	N/A
P81795	Eukaryotic translation initiation factor 2 subunit 3 OS=Rattus norvegicus GN=Eif2s3 PE=1 SV=2 - [IF2G_RAT]	N/A
P97690	Structural maintenance of chromosomes protein 3 OS=Rattus norvegicus GN=Smc3 PE=1 SV=1 - [SMC3_RAT]	N/A
Q05096-3	Isoform C of Unconventional myosin-Ib n=1 Tax=Rattus norvegicus RepID=Q05096-3	N/A
Q0D2G9	RGD1308290 protein (Fragment) OS=Rattus norvegicus GN=RGD1308290 PE=2 SV=1 - [Q0D2G9_RAT]	N/A
Q14V05	Tat-binding protein-1 OS=Rattus rattus GN=TBP-1 PE=2 SV=1 - [Q14V05_RATRT]	N/A
Q1JU68	Eukaryotic translation initiation factor 3 subunit A OS=Rattus norvegicus GN=Eif3a PE=2 SV=2 - [EIF3A_RAT]	N/A
Q27W01	RNA-binding protein 8A OS=Rattus norvegicus GN=Rbm8a PE=2 SV=1 - [RBM8A_RAT]	N/A
Q3KRE0	ATPase family AAA domain-containing protein 3 OS=Rattus norvegicus GN=Atad3 PE=1 SV=1 - [ATAD3_RAT]	N/A
Q3T1K5	F-actin-capping protein subunit alpha-2 OS=Rattus norvegicus GN=Capza2 PE=1 SV=1 - [CAZA2_RAT]	N/A
Q498C9	Protein Zfp207 OS=Rattus norvegicus GN=Zfp207 PE=2 SV=1 - [Q498C9_RAT]	N/A
Q4FZT9	26S proteasome non-ATPase regulatory subunit 2 OS=Rattus norvegicus GN=Psmd2 PE=2 SV=1 - [PSMD2_RAT]	N/A
Q4KLH7	Protein Rad21 OS=Rattus norvegicus GN=Rad21 PE=2 SV=1 - [Q4KLH7_RAT]	N/A
Q4KLI7	Protein Sf3a3 OS=Rattus norvegicus GN=Sf3a3 PE=2 SV=1 - [Q4KLI7_RAT]	N/A
Q4QQT3	CUGBP Elav-like family member 1 OS=Rattus norvegicus GN=Celf1 PE=2 SV=1 - [CELF1_RAT]	N/A
Q4QQW4	Histone deacetylase 1 OS=Rattus norvegicus GN=Hdac1 PE=1 SV=1 - [HDAC1_RAT]	N/A
Q4V8E1	GATA zinc finger domain containing 2B OS=Rattus norvegicus GN=Gatad2b PE=2 SV=1 - [Q4V8E1_RAT]	N/A
Q56A18-4	Isoform 4 of SWI/SNF-related matrix-associated actin-dependent regulator of chromatin subfamily E member 1 n=2 Tax=Rattus norvegicus RepID=Q56A18-4	N/A
Q56A27	Nuclear cap-binding protein subunit 1 OS=Rattus norvegicus GN=Ncbp1 PE=2 SV=1 - [NCBP1_RAT]	N/A
Q5EB56	MAK16 homolog (S. cerevisiae) OS=Rattus norvegicus GN=Mak16 PE=2 SV=1 - [Q5EB56_RAT]	N/A
Q5EEY3	GTP-binding protein G-alpha-i2 splice variant b OS=Rattus norvegicus GN=Gnai2 PE=2 SV=1 - [Q5EEY3_RAT]	N/A
Q5M7V8	Thyroid hormone receptor-associated protein 3 OS=Rattus norvegicus GN=Thrap3 PE=1 SV=1 - [TR150_RAT]	N/A
Q5M920	EBNA1 binding protein 2 OS=Rattus norvegicus GN=Ebna1bp2 PE=2 SV=1 - [Q5M920_RAT]	N/A
Q5RKJ9	RAB10, member RAS oncogene family OS=Rattus norvegicus GN=Rab10 PE=2 SV=1 - [Q5RKJ9_RAT]	N/A
Q5U2W5	Transducin beta-like protein 3 OS=Rattus norvegicus GN=Tbl3 PE=2 SV=1 - [TBL3_RAT]	N/A

Q5U2Y1-2	Isoform 2 of General transcription factor II-I n=2 Tax=Rattus norvegicus RepID=Q5U2Y1-2	N/A
Q5U302	Catenin (Cadherin associated protein), alpha 1 OS=Rattus norvegicus GN=Ctnna1 PE=1 SV=1 - [Q5U302_RAT]	N/A
Q5XI13	Glutamate-rich WD repeat-containing protein 1 OS=Rattus norvegicus GN=Grwd1 PE=2 SV=1 - [GRWD1_RAT]	N/A
Q5XI32	F-actin-capping protein subunit beta OS=Rattus norvegicus GN=Capzb PE=1 SV=1 - [CAPZB_RAT]	N/A
Q5XIB5	Coiled-coil domain-containing protein 86 OS=Rattus norvegicus GN=Ccdc86 PE=2 SV=1 - [CCD86_RAT]	N/A
Q62636	Ras-related protein Rap-1b OS=Rattus norvegicus GN=Rap1b PE=2 SV=2 - [RAP1B_RAT]	N/A
Q62940	E3 ubiquitin-protein ligase NEDD4 OS=Rattus norvegicus GN=Nedd4 PE=1 SV=1 - [NEDD4_RAT]	N/A
Q63009	Protein arginine N-methyltransferase 1 OS=Rattus norvegicus GN=Prmt1 PE=1 SV=1 - [ANM1_RAT]	N/A
Q63413	Spliceosome RNA helicase Ddx39b OS=Rattus norvegicus GN=Ddx39b PE=1 SV=3 - [DX39B_RAT]	N/A
Q63692	Hsp90 co-chaperone Cdc37 OS=Rattus norvegicus GN=Cdc37 PE=1 SV=2 - [CDC37_RAT]	N/A
Q63716	Peroxiredoxin-1 OS=Rattus norvegicus GN=Prdx1 PE=1 SV=1 - [PRDX1_RAT]	N/A
Q641X8	Eukaryotic translation initiation factor 3 subunit E OS=Rattus norvegicus GN=Eif3e PE=2 SV=1 - [EIF3E_RAT]	N/A
Q66HD0	Endoplasmin OS=Rattus norvegicus GN=Hsp90b1 PE=1 SV=2 - [ENPL_RAT]	N/A
Q66HG8	Protein Red OS=Rattus norvegicus GN=Ik PE=1 SV=1 - [RED_RAT]	N/A
Q6AXU3	Interferon-stimulated 20 kDa exonuclease-like 2 OS=Rattus norvegicus GN=Isg20l2 PE=2 SV=1 - [I20L2_RAT]	N/A
Q6AY87	THO complex subunit 6 homolog OS=Rattus norvegicus GN=Thoc6 PE=2 SV=1 - [THOC6_RAT]	N/A
Q6AYD3	Proliferation-associated 2G4 OS=Rattus norvegicus GN=Pa2g4 PE=2 SV=1 - [Q6AYD3_RAT]	N/A
Q6AYU2	Pcbp2 protein OS=Rattus norvegicus GN=Pcbp2 PE=2 SV=1 - [Q6AYU2_RAT]	N/A
Q6AYZ1	Tubulin alpha-1C chain OS=Rattus norvegicus GN=Tuba1c PE=1 SV=1 - [TBA1C_RAT]	N/A
Q6IFU8	Keratin, type I cytoskeletal 17 OS=Rattus norvegicus GN=Krt17 PE=2 SV=1 - [K1C17_RAT]	N/A
Q6P9U7	L-lactate dehydrogenase OS=Rattus norvegicus GN=Ldha PE=2 SV=1 - [Q6P9U7_RAT]	N/A
Q6QLN3	Glioma tumor suppressor candidate region gene 2 OS=Rattus norvegicus GN=Gltscr2 PE=2 SV=1 - [Q6QLN3_RAT]	N/A
Q6VEU8	DEAD (Asp-Glu-Ala-Asp) box polypeptide 24 OS=Rattus norvegicus GN=Ddx24 PE=2 SV=1 - [Q6VEU8_RAT]	N/A
Q8CHN6	Sphingosine-1-phosphate lyase 1 OS=Rattus norvegicus GN=Sgpl1 PE=2 SV=1 - [SGPL1_RAT]	N/A
Q8K585-2	Isoform HMG-Y of High mobility group protein HMG-I/HMG-Y n=1 Tax=Rattus norvegicus RepID=Q8K585-2	N/A
Q925G0	Putative RNA-binding protein 3 OS=Rattus norvegicus GN=Rbm3 PE=1 SV=2 - [RBM3_RAT]	N/A
Q9ESY8	Stau1 protein OS=Rattus norvegicus GN=Stau1 PE=2 SV=1 - [Q9ESY8_RAT]	N/A
Q9QYW0	Protein AATF OS=Rattus norvegicus GN=Aatf PE=1 SV=1 - [AATF_RAT]	N/A
Q9R1T1	Barrier-to-autointegration factor OS=Rattus norvegicus GN=Banf1 PE=1 SV=1 - [BAF_RAT]	N/A
Q9R1Z0	Voltage-dependent anion-selective channel protein 3 OS=Rattus norvegicus GN=Vdac3 PE=1 SV=2 - [VDAC3_RAT]	N/A
Q9WU82	Catenin beta-1 OS=Rattus norvegicus GN=Ctnnb1 PE=1 SV=1 - [CTNB1_RAT]	N/A

Q9WUC8	Pleiotropic regulator 1 OS=Rattus norvegicus GN=Plrg1 PE=2 SV=1 - [PLRG1_RAT]	N/A
Q9Z118	Polypyrimidine tract-binding protein 3 OS=Rattus norvegicus GN=Ptbp3 PE=2 SV=1 - [PTBP3_RAT]	N/A
UPI000017E2CF	PREDICTED: nucleolar protein 14 isoform X1 n=1 Tax=Rattus norvegicus RepID=UPI000017E2CF	N/A
UPI000017F893	proline-, glutamic acid- and leucine-rich protein 1 n=1 Tax=Rattus norvegicus RepID=UPI000017F893	N/A
UPI00001CFDCB	PREDICTED: polymerase delta-interacting protein 3 isoform X1 n=1 Tax=Rattus norvegicus RepID=UPI00001CFDCB	N/A
UPI00001D0F5B	PREDICTED: cytokine receptor-like factor 1 isoform X2 n=1 Tax=Rattus norvegicus RepID=UPI00001D0F5B	N/A
UPI0000503E75	PREDICTED: ribonucleases P/MRP protein subunit POP1 isoform X1 n=1 Tax=Rattus norvegicus RepID=UPI0000503E75	N/A
UPI0000DA267A	PREDICTED: filamin-C isoform X1 n=1 Tax=Rattus norvegicus RepID=UPI0000DA267A	N/A
UPI0000DA3509	PREDICTED: RNA-binding protein 25 n=1 Tax=Rattus norvegicus RepID=UPI0000DA3509	N/A
UPI0000DA3DFF	PREDICTED: rho GTPase-activating protein 22 isoform X4 n=1 Tax=Rattus norvegicus RepID=UPI0000DA3DFF	N/A
UPI0000DA4524	LAS1-like n=2 Tax=Rattus norvegicus RepID=UPI0000DA4524	N/A
UPI0000DBFEDB	PREDICTED: pumilio homolog 1 isoform X11 n=1 Tax=Rattus norvegicus RepID=UPI0000DBFEDB	N/A
UPI000150B091	PREDICTED: drebrin isoform X3 n=1 Tax=Rattus norvegicus RepID=UPI000150B091	N/A
UPI000154D8C8	nuclear pore complex protein Nup160 n=1 Tax=Rattus norvegicus RepID=UPI000154D8C8	N/A
UPI0001551D2B	PREDICTED: uncharacterized protein C9orf114 homolog isoform X1 n=1 Tax=Rattus norvegicus RepID=UPI0001551D2B	N/A
UPI0001551E07	PREDICTED: DNA-directed RNA polymerases I, II, and III subunit RPABC1 isoform X3 n=1 Tax=Rattus norvegicus RepID=UPI0001551E07	N/A
UPI0001552819	PREDICTED: 5""-3"" exoribonuclease 2 isoform X2 n=1 Tax=Rattus norvegicus RepID=UPI0001552819	N/A
UPI0001B79CC2	PREDICTED: probable ATP-dependent RNA helicase YTHDC2 n=1 Tax=Rattus norvegicus RepID=UPI0001B79CC2	N/A
UPI0001B7B713	PREDICTED: AT-rich interactive domain-containing protein 1A isoform X1 n=1 Tax=Rattus norvegicus RepID=UPI0001B7B713	N/A
UPI0001CF3F9F	YLP motif-containing protein 1 n=1 Tax=Rattus norvegicus RepID=UPI0001CF3F9F	N/A
UPI0001CF735C	neuroblast differentiation-associated protein AHNAK n=1 Tax=Rattus norvegicus RepID=UPI0001CF735C	N/A
UPI000268808A	zinc finger RNA-binding protein n=1 Tax=Rattus norvegicus RepID=UPI000268808A	N/A
UPI0003D0721E	PREDICTED: fibronectin isoform X10 n=1 Tax=Rattus norvegicus RepID=UPI0003D0721E	N/A
UPI0003D07514	PREDICTED: poly(U)-binding-splicing factor PUF60 isoform X5 n=1 Tax=Rattus norvegicus RepID=UPI0003D07514	N/A
UPI0003D07629	PREDICTED: 28S ribosomal protein S29, mitochondrial isoform X1 n=1 Tax=Rattus norvegicus RepID=UPI0003D07629	N/A
UPI0003D0803D	PREDICTED: pre-mRNA-processing factor 40 homolog A isoform X4 n=1 Tax=Rattus norvegicus RepID=UPI0003D0803D	N/A
UPI0003D080F2	PREDICTED: lupus La protein homolog isoform X3 n=1 Tax=Rattus norvegicus RepID=UPI0003D080F2	N/A
UPI0003D0841E	PREDICTED: SH3 and PX domain-containing protein 2A isoform X4 n=1 Tax=Rattus norvegicus RepID=UPI0003D0841E	N/A
UPI0003D084DB	PREDICTED: E3 ubiquitin-protein ligase TRIP12 isoform X11 n=1 Tax=Rattus norvegicus RepID=UPI0003D084DB	N/A
UPI0003D0853E	PREDICTED: tripeptidyl-peptidase 2 isoform X3 n=1 Tax=Rattus norvegicus RepID=UPI0003D0853E	N/A
UPI0003D08BBF	PREDICTED: protein KRI1 homolog n=1 Tax=Rattus norvegicus RepID=UPI0003D08BBF	N/A

UPI0003D08BCF	PREDICTED: bcl-2-associated transcription factor 1 isoform X4 n=1 Tax=Rattus norvegicus RepID=UPI0003D08BCF	N/A
UPI0003D08D2D	PREDICTED: RNA-binding motif, single-stranded-interacting protein 1 isoform X2 n=1 Tax=Rattus norvegicus RepID=UPI0003D08D2D	N/A
UPI0003D093A2	PREDICTED: protein SON isoform X3 n=1 Tax=Rattus norvegicus RepID=UPI0003D093A2	N/A
UPI0003D09498	PREDICTED: U3 small nucleolar RNA-associated protein 6 homolog n=1 Tax=Rattus norvegicus RepID=UPI0003D09498	N/A
UPI0003D09676	PREDICTED: unconventional myosin-VI isoform X4 n=1 Tax=Rattus norvegicus RepID=UPI0003D09676	N/A
UPI0003D09A07	PREDICTED: nuclear pore complex protein Nup98-Nup96 isoform X3 n=1 Tax=Rattus norvegicus RepID=UPI0003D09A07	N/A
UPI0003D09C9B	PREDICTED: heat shock 70 kDa protein 4 isoform X1 n=1 Tax=Rattus norvegicus RepID=UPI0003D09C9B	N/A
UPI0003D0A336	PREDICTED: cell division cycle and apoptosis regulator protein 1 isoform X5 n=1 Tax=Rattus norvegicus RepID=UPI0003D0A336	N/A
UPI0003D0A51A	PREDICTED: zinc finger CCHC domain-containing protein 8 isoform X2 n=1 Tax=Rattus norvegicus RepID=UPI0003D0A51A	N/A
UPI0003D0A55E	PREDICTED: C-Jun-amino-terminal kinase-interacting protein 4 isoform X9 n=1 Tax=Rattus norvegicus RepID=UPI0003D0A55E	N/A
UPI0003D0A726	PREDICTED: UPF0568 protein C14orf166 homolog isoform X2 n=1 Tax=Rattus norvegicus RepID=UPI0003D0A726	N/A
UPI0003D0AB54	PREDICTED: telomere-associated protein RIF1-like n=1 Tax=Rattus norvegicus RepID=UPI0003D0AB54	N/A
UPI0003D0AB89	PREDICTED: ribosomal RNA processing protein 1 homolog B isoform X2 n=1 Tax=Rattus norvegicus RepID=UPI0003D0AB89	N/A
UPI0003D0AC45	PREDICTED: protein transport protein Sec24D isoform X2 n=1 Tax=Rattus norvegicus RepID=UPI0003D0AC45	N/A
UPI0003D0B550	PREDICTED: serine/arginine repetitive matrix protein 1 isoform X5 n=1 Tax=Rattus norvegicus RepID=UPI0003D0B550	N/A
UPI0003D0BDBD	PREDICTED: SWI/SNF complex subunit SMARCC2-like isoform X10 n=1 Tax=Rattus norvegicus RepID=UPI0003D0BDBD	N/A
UPI0003D0BE42	PREDICTED: methionine--tRNA ligase, cytoplasmic isoform X2 n=1 Tax=Rattus norvegicus RepID=UPI0003D0BE42	N/A
UPI0003D0C20D	PREDICTED: PERQ amino acid-rich with GYF domain-containing protein 2-like isoform X6 n=1 Tax=Rattus norvegicus RepID=UPI0003D0C20D	N/A
UPI0003D0C2CD	PREDICTED: myelin expression factor 2 isoform X4 n=1 Tax=Rattus norvegicus RepID=UPI0003D0C2CD	N/A
UPI0003D0C521	PREDICTED: LOW QUALITY PROTEIN: deoxynucleotidyltransferase terminal-interacting protein 2-like n=1 Tax=Rattus norvegicus RepID=UPI0003D0C521	N/A
UPI0003D0CF50	PREDICTED: ubiquitin-associated and SH3 domain-containing protein B isoform X4 n=1 Tax=Rattus norvegicus RepID=UPI0003D0CF50	N/A
UPI0003D0CF50	PREDICTED: ubiquitin-associated and SH3 domain-containing protein B isoform X4 n=1 Tax=Rattus norvegicus RepID=UPI0003D0CF50	N/A
UPI0003D0D1B4	PREDICTED: serrate RNA effector molecule homolog isoform X1 n=1 Tax=Rattus norvegicus RepID=UPI0003D0D1B4	N/A
UPI0003D0E753	PREDICTED: 39S ribosomal protein L39, mitochondrial n=1 Tax=Rattus norvegicus RepID=UPI0003D0E753	N/A
UPI0003D0F25F	PREDICTED: nestin-like, partial n=1 Tax=Rattus norvegicus RepID=UPI0003D0F25F	N/A
UPI0003D0F9C8	PREDICTED: microtubule-actin cross-linking factor 1 isoform X10 n=1 Tax=Rattus norvegicus RepID=UPI0003D0F9C8	N/A
UPI0004E473EA	PREDICTED: plectin isoform X4 n=1 Tax=Rattus norvegicus RepID=UPI0004E473EA	N/A
UPI0004E4745E	PREDICTED: TATA-binding protein-associated factor 2N-like isoform X1 n=1 Tax=Rattus norvegicus RepID=UPI0004E4745E	N/A
UPI0004E477F8	PREDICTED: band 4.1-like protein 2 isoform X7 n=1 Tax=Rattus norvegicus RepID=UPI0004E477F8	N/A

UPI0004E4789B	PREDICTED: cirhin isoform X2 n=1 Tax=Rattus norvegicus RepID=UPI0004E4789B	N/A
UPI0004E48548	PREDICTED: nuclear pore complex protein Nup153 isoform X1 n=1 Tax=Rattus norvegicus RepID=UPI0004E48548	N/A
UPI0004E4880A	PREDICTED: ATP-dependent RNA helicase DHX36 isoform X1 n=1 Tax=Rattus norvegicus RepID=UPI0004E4880A	N/A
UPI0004E48819	PREDICTED: LOW QUALITY PROTEIN: eukaryotic translation initiation factor 4 gamma 2-like isoform X1, partial n=1 Tax=Rattus norvegicus RepID=UPI0004E48819	N/A
UPI0004E4891E	PREDICTED: tumor suppressor p53-binding protein 1 isoform X1 n=1 Tax=Rattus norvegicus RepID=UPI0004E4891E	N/A
UPI0004E4894C	PREDICTED: nucleolar protein 6 isoform X2 n=1 Tax=Rattus norvegicus RepID=UPI0004E4894C	N/A
UPI0004E489DA	PREDICTED: zinc finger CCCH domain-containing protein 14 isoform X2 n=1 Tax=Rattus norvegicus RepID=UPI0004E489DA	N/A
UPI0004E48B1F	PREDICTED: ataxin-2 isoform X14 n=1 Tax=Rattus norvegicus RepID=UPI0004E48B1F	N/A
UPI0004E48EAA	PREDICTED: LOW QUALITY PROTEIN: uncharacterized protein LOC100910366 n=1 Tax=Rattus norvegicus RepID=UPI0004E48EAA	N/A
UPI0004E48EB3	PREDICTED: U4/U6 small nuclear ribonucleoprotein Prp3 isoform X3 n=1 Tax=Rattus norvegicus RepID=UPI0004E48EB3	N/A
UPI0004E48EEF	PREDICTED: tight junction protein ZO-1 isoform X4 n=1 Tax=Rattus norvegicus RepID=UPI0004E48EEF	N/A
UPI0004E48FAD	PREDICTED: la-related protein 4 isoform X6 n=2 Tax=Rattus norvegicus RepID=UPI0004E48FAD	N/A
UPI0004E494D5	PREDICTED: splicing factor 3B subunit 2 isoform X1 n=1 Tax=Rattus norvegicus RepID=UPI0004E494D5	N/A

Table 7 Proteins overlapping in EtOH and TMX

Mapped proteins
Unmapped proteins
Unmapped proteins related to cytoskeleton
Known N-cad interacting proteins

EtOH and TMX			
Accession	Description	EtOH score	TMX score
B0BNF5	Qk protein OS=Rattus norvegicus GN=Qk PE=2 SV=1 - [B0BNF5_RAT]	126.42	117.77
B2RYQ5	Enhancer of rudimentary homolog OS=Rattus norvegicus GN=Erh PE=2 SV=1 - [B2RYQ5_RAT]	77.84	87.17
D3ZEI6	Nuclear receptor coactivator 5 (Predicted) OS=Rattus norvegicus GN=Ncoa5 PE=4 SV=1 - [D3ZEI6_RAT]	88.43	112.87
D3ZFD0	Uncharacterized protein OS=Rattus norvegicus GN=Myo18a PE=1 SV=2 - [D3ZFD0_RAT]	202.13	64.01
D3ZI68	PRP31 pre-mRNA processing factor 31 homolog (Yeast) (Predicted) OS=Rattus norvegicus GN=Prpf31 PE=4 SV=1 - [D3ZI68_RAT]	124.86	93.36
D3ZJ67	Protein Sun2 OS=Rattus norvegicus GN=Sun2 PE=4 SV=1 - [D3ZJ67_RAT]	160.04	142.52
D3ZN76	Protein Sec16a OS=Rattus norvegicus GN=Sec16a PE=4 SV=1 - [D3ZN76_RAT]	1165.42	1682.02
D4A5S9	Protein Prpf39 OS=Rattus norvegicus GN=Prpf39 PE=4 SV=1 - [D4A5S9_RAT]	317.49	294.02
D4AE65	Protein Rrp7a OS=Rattus norvegicus GN=Rrp7a PE=4 SV=1 - [D4AE65_RAT]	75.01	96.31
F1LSL2	Nuclear pore complex protein Nup107 OS=Rattus norvegicus GN=Nup107 PE=4 SV=2 - [F1LSL2_RAT]	88.97	158.34
F1LSS1	Structural maintenance of chromosomes protein OS=Rattus norvegicus GN=Smc1a PE=3 SV=2 - [F1LSS1_RAT]	162.50	151.80
F1M0V4	Protein Thoc2 OS=Rattus norvegicus GN=Thoc2 PE=4 SV=2 - [F1M0V4_RAT]	123.79	306.07
F1M3H2	Uncharacterized protein (Fragment) OS=Rattus norvegicus GN=LOC100360367 PE=4 SV=2 - [F1M3H2_RAT]	240.77	298.65
F1M3K6	Protein Bag4 (Fragment) OS=Rattus norvegicus GN=Bag4 PE=4 SV=2 - [F1M3K6_RAT]	137.31	161.37
F1M4U9	Protein Baz1a (Fragment) OS=Rattus norvegicus GN=Baz1a PE=4 SV=2 - [F1M4U9_RAT]	117.66	115.19
F1SW39	PC4 and SFRS1 interacting protein 1 OS=Rattus norvegicus GN=Psip1 PE=2 SV=1 - [F1SW39_RAT]	323.58	159.30
G3V702	Smu-1 suppressor of mec-8 and unc-52 homolog (C. elegans) OS=Rattus norvegicus GN=Smu1 PE=4 SV=1 - [G3V702_RAT]	95.96	169.31
G3V803	Cadherin-2 OS=Rattus norvegicus GN=Cdh2 PE=4 SV=1 - [G3V803_RAT]	1026.61	1052.41
G3V8B3	Histone H2B OS=Rattus norvegicus GN=LOC100910200 PE=3 SV=1 - [G3V8B3_RAT]	971.68	995.15
G3V9R0	LUC7-like (S. cerevisiae) OS=Rattus norvegicus GN=Luc7l PE=2 SV=2 - [G3V9R0_RAT]	73.56	91.16
M0RD14	Pyruvate kinase OS=Rattus norvegicus PE=3 SV=1 - [M0RD14_RAT]	75.95	466.68
P05942	Protein S100-A4 OS=Rattus norvegicus GN=S100a4 PE=2 SV=1 - [S10A4_RAT]	91.17	90.76
P23785	Granulins OS=Rattus norvegicus GN=Grn PE=1 SV=3 - [GRN_RAT]	117.79	126.53
P24049	60S ribosomal protein L17 OS=Rattus norvegicus GN=Rpl17 PE=2 SV=3 - [RL17_RAT]	254.48	221.55

P31000	Vimentin OS=Rattus norvegicus GN=Vim PE=1 SV=2 - [VIME_RAT]	7580.16	6419.78
P61354	60S ribosomal protein L27 OS=Rattus norvegicus GN=Rpl27 PE=2 SV=2 - [RL27_RAT]	73.15	105.86
P62912	60S ribosomal protein L32 OS=Rattus norvegicus GN=Rpl32 PE=1 SV=2 - [RL32_RAT]	65.07	92.89
P81795	Eukaryotic translation initiation factor 2 subunit 3 OS=Rattus norvegicus GN=Eif2s3 PE=1 SV=2 - [IF2G_RAT]	222.99	303.15
Q1JU68	Eukaryotic translation initiation factor 3 subunit A OS=Rattus norvegicus GN=Eif3a PE=2 SV=2 - [EIF3A_RAT]	329.28	333.31
Q4QQW4	Histone deacetylase 1 OS=Rattus norvegicus GN=Hdac1 PE=1 SV=1 - [HDAC1_RAT]	147.99	71.86
Q56A18-4	Isoform 4 of SWI/SNF-related matrix-associated actin-dependent regulator of chromatin subfamily E member 1 n=2 Tax=Rattus norvegicus RepID=Q56A18-4	239.69	192.18
Q56A27	Nuclear cap-binding protein subunit 1 OS=Rattus norvegicus GN=Ncbp1 PE=2 SV=1 - [NCBP1_RAT]	118.52	81.67
Q5U2W5	Transducin beta-like protein 3 OS=Rattus norvegicus GN=Tbl3 PE=2 SV=1 - [TBL3_RAT]	68.34	69.92
Q5XI32	F-actin-capping protein subunit beta OS=Rattus norvegicus GN=Capzb PE=1 SV=1 - [CAPZB_RAT]	179.83	156.20
Q63009	Protein arginine N-methyltransferase 1 OS=Rattus norvegicus GN=Prmt1 PE=1 SV=1 - [ANM1_RAT]	471.77	532.23
Q66HD0	Endoplasmin OS=Rattus norvegicus GN=Hsp90b1 PE=1 SV=2 - [ENPL_RAT]	274.06	428.47
Q6AYU2	Pcbp2 protein OS=Rattus norvegicus GN=Pcbp2 PE=2 SV=1 - [Q6AYU2_RAT]	181.77	320.72
Q6P9U7	L-lactate dehydrogenase OS=Rattus norvegicus GN=Ldha PE=2 SV=1 - [Q6P9U7_RAT]	81.64	85.65
Q6QLN3	Glioma tumor suppressor candidate region gene 2 OS=Rattus norvegicus GN=Gltscr2 PE=2 SV=1 - [Q6QLN3_RAT]	148.05	110.43
Q925G0	Putative RNA-binding protein 3 OS=Rattus norvegicus GN=Rbm3 PE=1 SV=2 - [RBM3_RAT]	169.16	157.57
Q9WU82	Catenin beta-1 OS=Rattus norvegicus GN=Ctnnb1 PE=1 SV=1 - [CTNB1_RAT]	2612.40	2529.22
UPI00001D0F5B	PREDICTED: cytokine receptor-like factor 1 isoform X2 n=1 Tax=Rattus norvegicus RepID=UPI00001D0F5B	57.57	62.08
UPI0001551E07	PREDICTED: DNA-directed RNA polymerases I, II, and III subunit RPABC1 isoform X3 n=1 Tax=Rattus norvegicus RepID=UPI0001551E07	87.32	139.85
UPI0001B7B713	PREDICTED: AT-rich interactive domain-containing protein 1A isoform X1 n=1 Tax=Rattus norvegicus RepID=UPI0001B7B713	232.56	124.20
UPI0001CF3F9F	YLP motif-containing protein 1 n=1 Tax=Rattus norvegicus RepID=UPI0001CF3F9F	58.41	70.11
UPI0003D0841E	PREDICTED: SH3 and PX domain-containing protein 2A isoform X4 n=1 Tax=Rattus norvegicus RepID=UPI0003D0841E	83.31	108.07
UPI0003D08BCF	PREDICTED: bcl-2-associated transcription factor 1 isoform X4 n=1 Tax=Rattus norvegicus RepID=UPI0003D08BCF	60.70	44.87
UPI0003D093A2	PREDICTED: protein SON isoform X3 n=1 Tax=Rattus norvegicus RepID=UPI0003D093A2	74.42	109.66
UPI0003D0AC45	PREDICTED: protein transport protein Sec24D isoform X2 n=1 Tax=Rattus norvegicus RepID=UPI0003D0AC45	134.04	140.73

UPI0003D0B550	PREDICTED: serine/arginine repetitive matrix protein 1 isoform X5 n=1 Tax=Rattus norvegicus RepID=UPI0003D0B550	58.87	69.56
UPI0003D0C20D	PREDICTED: PERQ amino acid-rich with GYF domain-containing protein 2-like isoform X6 n=1 Tax=Rattus norvegicus RepID=UPI0003D0C20D	69.98	95.36
UPI0003D0C2CD	PREDICTED: myelin expression factor 2 isoform X4 n=1 Tax=Rattus norvegicus RepID=UPI0003D0C2CD	130.39	279.93
UPI0003D0E753	PREDICTED: 39S ribosomal protein L39, mitochondrial n=1 Tax=Rattus norvegicus RepID=UPI0003D0E753	91.23	121.50
UPI0003D0F9C8	PREDICTED: microtubule-actin cross-linking factor 1 isoform X10 n=1 Tax=Rattus norvegicus RepID=UPI0003D0F9C8	292.24	190.22
UPI0004E48EAA	PREDICTED: LOW QUALITY PROTEIN: uncharacterized protein LOC100910366 n=1 Tax=Rattus norvegicus RepID=UPI0004E48EAA	460.84	537.82

Table 8 Proteins specifically identified in EtOH samples

Mapped proteins
Unmapped proteins
Unmapped proteins related to cytoskeleton
Protein of interest

EtOH specific		
Accession	Description	Score
A0JPL2	Casein kinase 1, alpha 1, isoform CRA_d OS=Rattus norvegicus GN=Csnk1a1 PE=2 SV=1 - [A0JPL2_RAT]	112.73
A2RRU1	Glycogen [starch] synthase, muscle OS=Rattus norvegicus GN=Gys1 PE=2 SV=1 - [GYS1_RAT]	91.73
B1H237	Terf2 protein OS=Rattus norvegicus GN=Terf2 PE=2 SV=1 - [B1H237_RAT]	87.48
B1VKB4	Synaptopodin OS=Rattus norvegicus GN=Synpo PE=2 SV=1 - [B1VKB4_RAT]	344.34
B2GUU1	YTH domain family 2 (Predicted) OS=Rattus norvegicus GN=Ythdf2 PE=2 SV=1 - [B2GUU1_RAT]	112.64
B2GUY6	Srrm2 protein (Fragment) OS=Rattus norvegicus GN=Srrm2 PE=2 SV=1 - [B2GUY6_RAT]	166.32
B5DF27	Lysyl oxidase homolog 2 OS=Rattus norvegicus GN=Loxl2 PE=2 SV=2 - [LOXL2_RAT]	157.53
D3Z8W1	Uncharacterized protein OS=Rattus norvegicus GN=LOC680384 PE=4 SV=1 - [D3Z8W1_RAT]	73.47
D3ZHB3	40S ribosomal protein S12 OS=Rattus norvegicus GN=LOC100360573 PE=3 SV=2 - [D3ZHB3_RAT]	78.65
D3ZIX4	Protein H1fx OS=Rattus norvegicus GN=H1fx PE=3 SV=1 - [D3ZIX4_RAT]	75.06
D3ZJU5	Protein Smarcc1 OS=Rattus norvegicus GN=Smarcc1 PE=4 SV=1 - [D3ZJU5_RAT]	322.41
D3ZNH2	Protein Utp18 OS=Rattus norvegicus GN=Utp18 PE=4 SV=2 - [D3ZNH2_RAT]	134.72
D3ZNP7	Protein LOC100909685 OS=Rattus norvegicus GN=Myo1b PE=4 SV=2 - [D3ZNP7_RAT]	331.22
D3ZQG1	Protein Nufip2 OS=Rattus norvegicus GN=LOC687994 PE=4 SV=2 - [D3ZQG1_RAT]	273.92
D3ZR53	Protein phosphatase 1 regulatory subunit 12 OS=Rattus norvegicus GN=Ppp1r12a PE=1 SV=2 - [D3ZR53_RAT]	532.54
D3ZRT6	Protein Plekha7 OS=Rattus norvegicus GN=Plekha7 PE=4 SV=1 - [D3ZRT6_RAT]	96.39
D3ZUK4	Protein Trim33 (Fragment) OS=Rattus norvegicus GN=Trim33 PE=4 SV=2 - [D3ZUK4_RAT]	284.91
D3ZWZ6	Protein Igf2bp2 (Fragment) OS=Rattus norvegicus GN=Igf2bp2 PE=4 SV=2 - [D3ZWZ6_RAT]	263.64
D3ZYT2	Mitochondrial ribosomal protein S5 (Predicted) OS=Rattus norvegicus GN=Mrps5 PE=3 SV=1 - [D3ZYT2_RAT]	110.26
D3ZZM1	Uncharacterized protein (Fragment) OS=Rattus norvegicus PE=4 SV=2 - [D3ZZM1_RAT]	323.52
D3ZZR5	Protein Snrpa1 OS=Rattus norvegicus GN=Snrpa1 PE=4 SV=1 - [D3ZZR5_RAT]	146.28
D4A2B0	Polymerase (DNA-directed), delta interacting protein 3 (Predicted), isoform CRA_a OS=Rattus norvegicus GN=Poldip3 PE=4 SV=1 - [D4A2B0_RAT]	211.77
D4A2Z8	DEAH (Asp-Glu-Ala-His) box polypeptide 36 (Predicted), isoform CRA_a OS=Rattus norvegicus GN=Dhx36 PE=4 SV=1 - [D4A2Z8_RAT]	126.60
D4A554	Eukaryotic translation initiation factor 4 gamma, 3 (Predicted), isoform CRA_a OS=Rattus norvegicus GN=Eif4g3 PE=4 SV=2 - [D4A554_RAT]	70.55
D4A5G2	Protein Nop14 OS=Rattus norvegicus GN=Nop14 PE=4 SV=1 - [D4A5G2_RAT]	102.37
D4A5K7	Protein Rbm28 OS=Rattus norvegicus GN=Rbm28 PE=4 SV=1 - [D4A5K7_RAT]	77.36

D4AAG4	Protein Kif23 OS=Rattus norvegicus GN=Kif23 PE=3 SV=2 - [D4AAG4_RAT]	59.73
D4AAW2	Protein transport protein Sec16B OS=Rattus norvegicus GN=Sec16b PE=4 SV=2 - [D4AAW2_RAT]	68.83
D4ABR6	Annexin (Fragment) OS=Rattus norvegicus GN=Anxa6 PE=3 SV=2 - [D4ABR6_RAT]	214.32
D4ACV3	Histone H2A OS=Rattus norvegicus GN=Hist2h2ac PE=3 SV=1 - [D4ACV3_RAT]	348.54
D4JQY2	Chaperone protein DnaK n=3 Tax=root RepID=D4JQY2_9FIRM	125.33
E9PT66	Protein Sf3b3 OS=Rattus norvegicus GN=Sf3b3 PE=4 SV=2 - [E9PT66_RAT]	290.42
F1LNF1	Heterogeneous nuclear ribonucleoproteins A2/B1 (Fragment) OS=Rattus norvegicus GN=Hnrnpa2b1 PE=4 SV=1 - [F1LNF1_RAT]	1428.52
F1LQB2	Structural maintenance of chromosomes protein 3 OS=Rattus norvegicus GN=Smc3 PE=4 SV=1 - [F1LQB2_RAT]	387.08
F1LS65	Signal-induced proliferation-associated 1-like protein 1 (Fragment) OS=Rattus norvegicus GN=Sipa1l1 PE=4 SV=2 - [F1LS65_RAT]	130.45
F1LSL1	Transcription factor Pur-beta OS=Rattus norvegicus GN=Purb PE=4 SV=2 - [F1LSL1_RAT]	139.40
F1LX68	Protein Spats2 OS=Rattus norvegicus GN=Spats2 PE=4 SV=2 - [F1LX68_RAT]	170.56
F1M4A0	Protein Tjp1 OS=Rattus norvegicus GN=Tjp1 PE=1 SV=2 - [F1M4A0_RAT]	155.69
F1MAA5	Protein Rangap1 OS=Rattus norvegicus GN=Rangap1 PE=4 SV=2 - [F1MAA5_RAT]	95.73
F1MAA7	Protein Lamc1 OS=Rattus norvegicus GN=Lamc1 PE=4 SV=1 - [F1MAA7_RAT]	293.77
F7EM03	Protein Krt31 OS=Rattus norvegicus GN=Krt34 PE=3 SV=1 - [F7EM03_RAT]	118.76
G3V6A4	Heterogeneous nuclear ribonucleoprotein D, isoform CRA_b OS=Rattus norvegicus GN=Hnrpd PE=1 SV=1 - [G3V6A4_RAT]	313.89
G3V727	DEAD (Asp-Glu-Ala-Asp) box polypeptide 47, isoform CRA_a OS=Rattus norvegicus GN=Ddx47 PE=3 SV=1 - [G3V727_RAT]	100.43
G3V7J2	Interferon-inducible double-stranded RNA-dependent protein kinase activator A OS=Rattus norvegicus GN=Prkra PE=1 SV=1 - [G3V7J2_RAT]	77.11
G3V7K3	Ceruloplasmin OS=Rattus norvegicus GN=Cp PE=4 SV=1 - [G3V7K3_RAT]	102.86
G3V7N0	Heparan sulfate 2-O-sulfotransferase 1, isoform CRA_a OS=Rattus norvegicus GN=Hs2st1 PE=4 SV=1 - [G3V7N0_RAT]	128.76
G3V8B4	Brix domain containing 2, isoform CRA_a OS=Rattus norvegicus GN=Brix1 PE=4 SV=1 - [G3V8B4_RAT]	67.15
G3V8T4	DNA damage-binding protein 1 OS=Rattus norvegicus GN=Ddb1 PE=4 SV=1 - [G3V8T4_RAT]	91.56
G3V9F3	Myosin phosphatase Rho-interacting protein OS=Rattus norvegicus GN=Mprip PE=4 SV=1 - [G3V9F3_RAT]	587.26
M0R7L9	Protein LOC100911677 OS=Rattus norvegicus GN=LOC100911677 PE=4 SV=1 - [M0R7L9_RAT]	391.30
M0R7Z0	Uncharacterized protein OS=Rattus norvegicus PE=4 SV=1 - [M0R7Z0_RAT]	128.03
M0R8U4	Protein Rpl13a-ps1 OS=Rattus norvegicus GN=Rpl13a-ps1 PE=3 SV=1 - [M0R8U4_RAT]	60.65
M0R907	Protein Snrpd3 OS=Rattus norvegicus GN=Snrpd3 PE=4 SV=1 - [M0R907_RAT]	88.64
M0RCH1	Uncharacterized protein (Fragment) OS=Rattus norvegicus PE=3 SV=1 - [M0RCH1_RAT]	80.38
P04692-7	Isoform 7 of Tropomyosin alpha-1 chain n=1 Tax=Rattus norvegicus RepID=P04692-7	86.79
P15865	Histone H1.4 OS=Rattus norvegicus GN=Hist1h1e PE=1 SV=3 - [H14_RAT]	506.37
P19637	Tissue-type plasminogen activator OS=Rattus norvegicus GN=Plat PE=2 SV=2 - [TPA_RAT]	136.66

P62260	14-3-3 protein epsilon OS=Rattus norvegicus GN=Ywhae PE=1 SV=1 - [1433E_RAT]	82.49
P62755	40S ribosomal protein S6 OS=Rattus norvegicus GN=Rps6 PE=1 SV=1 - [RS6_RAT]	483.61
P63259	Actin, cytoplasmic 2 OS=Rattus norvegicus GN=Actg1 PE=1 SV=1 - [ACTG_RAT]	3505.13
P68370	Tubulin alpha-1A chain OS=Rattus norvegicus GN=Tuba1a PE=1 SV=1 - [TBA1A_RAT]	277.70
P84092	AP-2 complex subunit mu OS=Rattus norvegicus GN=Ap2m1 PE=1 SV=1 - [AP2M1_RAT]	73.22
Q05962	ADP/ATP translocase 1 OS=Rattus norvegicus GN=Slc25a4 PE=1 SV=3 - [ADT1_RAT]	201.52
Q3KRE8	Tubulin beta-2B chain OS=Rattus norvegicus GN=Tubb2b PE=1 SV=1 - [TBB2B_RAT]	444.06
Q3MHS8	Sin3-associated polypeptide 18 OS=Rattus norvegicus GN=Sap18 PE=2 SV=1 - [Q3MHS8_RAT]	136.24
Q498M4	WD repeat-containing protein 5 OS=Rattus norvegicus GN=Wdr5 PE=1 SV=1 - [WDR5_RAT]	114.30
Q4FZS2	Budding uninhibited by benzimidazoles 3 homolog (S. cerevisiae) OS=Rattus norvegicus GN=Bub3 PE=2 SV=1 - [Q4FZS2_RAT]	89.30
Q4KLJ1	RCG61762, isoform CRA_a OS=Rattus norvegicus GN=Srsf7 PE=2 SV=1 - [Q4KLJ1_RAT]	146.37
Q4KLJ3	Guanine nucleotide binding protein-like 2 (Nucleolar) OS=Rattus norvegicus GN=Gnl2 PE=2 SV=1 - [Q4KLJ3_RAT]	101.70
Q4KLM7	Protein Specc1 OS=Rattus norvegicus GN=Specc1 PE=2 SV=1 - [Q4KLM7_RAT]	101.70
Q4KLN3	SFRS protein kinase 1 OS=Rattus norvegicus GN=Srpk1 PE=2 SV=1 - [Q4KLN3_RAT]	97.64
Q4QR75	Exosome complex component RRP45 OS=Rattus norvegicus GN=Exosc9 PE=2 SV=1 - [EXOS9_RAT]	89.84
Q4V7D7	Pre-mRNA-splicing factor RBM22 OS=Rattus norvegicus GN=Rbm22 PE=2 SV=1 - [RBM22_RAT]	96.10
Q4V8J6	Protein Ythdf1 OS=Rattus norvegicus GN=Ythdf1 PE=2 SV=1 - [Q4V8J6_RAT]	142.52
Q562C2	Ribosome biogenesis protein BOP1 OS=Rattus norvegicus GN=Bop1 PE=2 SV=1 - [BOP1_RAT]	73.22
Q56B11	Proline-, glutamic acid- and leucine-rich protein 1 OS=Rattus norvegicus GN=Pelp1 PE=2 SV=2 - [PELP1_RAT]	62.22
Q56R17	Importin subunit alpha OS=Rattus norvegicus GN=Kpna4 PE=2 SV=1 - [Q56R17_RAT]	74.09
Q5EB93	Gatad2a protein OS=Rattus norvegicus GN=Gatad2a PE=2 SV=1 - [Q5EB93_RAT]	158.30
Q5I0H3	Small ubiquitin-related modifier 1 OS=Rattus norvegicus GN=Sumo1 PE=1 SV=1 - [SUMO1_RAT]	61.54
Q5I0K8	28S ribosomal protein S7, mitochondrial OS=Rattus norvegicus GN=Mrps7 PE=2 SV=2 - [RT07_RAT]	69.19
Q5RJM0	MKI67 FHA domain-interacting nucleolar phosphoprotein OS=Rattus norvegicus GN=Nifk PE=2 SV=1 - [MK67I_RAT]	204.44
Q5XI01	Glypican 4 OS=Rattus norvegicus GN=Gpc4 PE=2 SV=1 - [Q642B0_RAT]	92.19
Q5XIG8	Serine-threonine kinase receptor-associated protein OS=Rattus norvegicus GN=Strap PE=1 SV=1 - [STRAP_RAT]	
Q642B0	Cysteine rich protein 61 OS=Rattus norvegicus GN=Cyr61 PE=2 SV=1 - [Q66HT5_RAT]	77.65
Q66HT5	Isoform 2 of Gelsolin n=2 Tax=Rattus norvegicus RepID=Q68FP1-2	63.28
Q68FP1-2	Elongation factor 1-gamma OS=Rattus norvegicus GN=Eef1g PE=1 SV=3 - [EF1G_RAT]	90.09
Q68FR6	Sorting and assembly machinery component 50 homolog OS=Rattus norvegicus GN=Samm50 PE=1 SV=1 - [SAM50_RAT]	83.39
Q6AXV4	H/ACA ribonucleoprotein complex subunit 1 OS=Rattus norvegicus GN=Gar1 PE=2 SV=1 - [GAR1_RAT]	55.32

Q6AYA1	Splicing factor 3B subunit 4 OS=Rattus norvegicus GN=Sf3b4 PE=2 SV=1 - [SF3B4_RAT]	120.45
Q6AYL5	DEAD (Asp-Glu-Ala-Asp) box polypeptide 56 OS=Rattus norvegicus GN=Ddx56 PE=2 SV=1 - [Q6AYT6_RAT]	176.73
Q6AYT6	C-terminal binding protein 1 OS=Rattus norvegicus GN=Ctbp1 PE=1 SV=1 - [Q6AZ26_RAT]	72.22
Q6AZ26	Actn1 protein OS=Rattus norvegicus GN=Actn1 PE=2 SV=1 - [Q6GMN8_RAT]	747.57
Q6GMN8	Mitochondrial ribosomal protein S18B OS=Rattus norvegicus GN=Mrps18b PE=2 SV=1 - [Q6MG10_RAT]	87.56
Q6MG10	Junction plakoglobin OS=Rattus norvegicus GN=Jup PE=1 SV=1 - [PLAK_RAT]	929.77
Q6P136	Eukaryotic translation initiation factor 4A1 OS=Rattus norvegicus GN=Eif4a1 PE=1 SV=1 - [Q6P3V8_RAT]	272.79
Q6P3V8	Heterochromatin protein 1-binding protein 3 OS=Rattus norvegicus GN=Hp1bp3 PE=2 SV=1 - [HP1B3_RAT]	224.63
Q6P6G9	Hnrpa1 protein OS=Rattus norvegicus GN=Hnrnpa1 PE=2 SV=1 - [Q6P6G9_RAT]	1160.15
Q6P7R0	La-related protein 7 OS=Rattus norvegicus GN=Larp7 PE=1 SV=2 - [LARP7_RAT]	183.16
Q6TXE9	LRRGT00050 OS=Rattus norvegicus GN=Eprs PE=1 SV=1 - [Q6TXE9_RAT]	506.61
Q6U6G5	Zinc finger CCCH domain-containing protein 15 OS=Rattus norvegicus GN=Zc3h15 PE=2 SV=1 - [ZC3HF_RAT]	136.84
Q9QZK5	Serine protease HTRA1 OS=Rattus norvegicus GN=Htra1 PE=2 SV=1 - [HTRA1_RAT]	86.10
Q9QZK5	Serine protease HTRA1 OS=Rattus norvegicus GN=Htra1 PE=2 SV=1 - [HTRA1_RAT]	86.10
Q9R1E9	Connective tissue growth factor OS=Rattus norvegicus GN=Ctgf PE=2 SV=1 - [CTGF_RAT]	62.16
Q9WUW5	Collagen type XVIII, alpha (I) chain (Fragment) OS=Rattus norvegicus GN=Col18a1 PE=2 SV=1 - [Q9WUW5_RAT]	86.51
T1SRT4	Radixin isoform OS=Rattus norvegicus GN=Rdx PE=2 SV=1 - [T1SRT4_RAT]	93.78
UPI0000180AB4	PREDICTED: luc7-like protein 3 isoform X2 n=1 Tax=Rattus norvegicus RepID=UPI0000180AB4	118.10
UPI00001C8B75	PREDICTED: plasminogen activator inhibitor 1 RNA-binding protein isoform X2 n=1 Tax=Rattus norvegicus RepID=UPI00001C8B75	304.36
UPI0000250BD6	PREDICTED: 60S ribosomal protein L13-like n=1 Tax=Rattus norvegicus RepID=UPI0000250BD6	255.04
UPI0000250FE4	PREDICTED: myosin-14 isoform X2 n=1 Tax=Rattus norvegicus RepID=UPI0000250FE4	266.65
UPI0000500E84	PREDICTED: C-Jun-amino-terminal kinase-interacting protein 4 isoform X5 n=1 Tax=Rattus norvegicus RepID=UPI0000500E84	358.11
UPI0000503905	PREDICTED: DEAH (Asp-Glu-Ala-Asp/His) box polypeptide 57 isoform X2 n=1 Tax=Rattus norvegicus RepID=UPI0000503905	97.38
UPI0000DA1CD8	PREDICTED: AP-2 complex subunit alpha-1 isoform X4 n=1 Tax=Rattus norvegicus RepID=UPI0000DA1CD8	259.15
UPI0000DA285F	PREDICTED: MAP7 domain-containing protein 1 isoform X5 n=1 Tax=Rattus norvegicus RepID=UPI0000DA285F	98.05
UPI0000DA38FD	PREDICTED: homeobox protein cut-like 1 isoform X8 n=1 Tax=Rattus norvegicus RepID=UPI0000DA38FD	63.55
UPI0000DBF3AC	PREDICTED: fibronectin isoform X4 n=1 Tax=Rattus norvegicus RepID=UPI0000DBF3AC	1087.27
UPI0000DBF7D2	PREDICTED: heterogeneous nuclear ribonucleoprotein M isoform X1 n=1 Tax=Rattus norvegicus RepID=UPI0000DBF7D2	1804.26
UPI000154E9E5	PREDICTED: E3 ubiquitin-protein ligase TRIM56 n=1 Tax=Rattus norvegicus RepID=UPI000154E9E5	71.29
UPI000154F802	programmed cell death 6-interacting protein n=1 Tax=Rattus norvegicus RepID=UPI000154F802	
UPI0001550CCB	PREDICTED: histone H1.2 n=1 Tax=Rattus norvegicus RepID=UPI0001550CCB	484.41

UPI0001CF3CF5	PREDICTED: catenin alpha-3 isoform X1 n=2 Tax=Rattus norvegicus RepID=UPI0001CF3CF5	159.76
UPI0001CF734A	PREDICTED: protein AHNAK2 n=1 Tax=Rattus norvegicus RepID=UPI0001CF734A	78.76
UPI0003D077B6	PREDICTED: alpha-actinin-4 isoform X3 n=1 Tax=Rattus norvegicus RepID=UPI0003D077B6	874.43
UPI0003D0839D	PREDICTED: apoptotic chromatin condensation inducer 1 isoform X5 n=1 Tax=Rattus norvegicus RepID=UPI0003D0839D	188.92
UPI0003D088F0	PREDICTED: polypyrimidine tract-binding protein 3 isoform X2 n=2 Tax=Rattus norvegicus RepID=UPI0003D088F0	179.42
UPI0003D09F77	PREDICTED: probable ATP-dependent RNA helicase DDX52 isoform X1 n=1 Tax=Rattus norvegicus RepID=UPI0003D09F77	81.50
UPI0003D09FC6	PREDICTED: serine/threonine-protein kinase DCLK1 isoform X2 n=2 Tax=Rattus norvegicus RepID=UPI0003D09FC6	144.34
UPI0003D0B91E	PREDICTED: SWI/SNF-related matrix-associated actin-dependent regulator of chromatin subfamily B member 1 isoform X3 n=1 Tax=Rattus norvegicus RepID=UPI0003D0B91E	101.21
UPI0003D0BC78	PREDICTED: keratin, type I cytoskeletal 16 isoform X1 n=1 Tax=Rattus norvegicus RepID=UPI0003D0BC78	197.49
UPI0003D0C0AC	PREDICTED: protein DEK isoform X1 n=1 Tax=Rattus norvegicus RepID=UPI0003D0C0AC	69.08
UPI0003D0C949	PREDICTED: centrosomal protein of 170 kDa isoform X11 n=1 Tax=Rattus norvegicus RepID=UPI0003D0C949	68.39
UPI0003D0E282	PREDICTED: guanine nucleotide-binding protein G(i) subunit alpha-2 isoform X2 n=1 Tax=Rattus norvegicus RepID=UPI0003D0E282	353.58
UPI0003D0E362	PREDICTED: protein FAM98B isoform X2 n=1 Tax=Rattus norvegicus RepID=UPI0003D0E362	141.04
UPI0003D0E707	PREDICTED: nucleolar and coiled-body phosphoprotein 1 isoform X1 n=1 Tax=Rattus norvegicus RepID=UPI0003D0E707	95.26
UPI0003D0EC97	PREDICTED: RNA-binding protein 42 isoform X1 n=1 Tax=Rattus norvegicus RepID=UPI0003D0EC97	101.17
UPI0003D0F01C	PREDICTED: SUN domain-containing protein 1 isoform X4 n=1 Tax=Rattus norvegicus RepID=UPI0003D0F01C	68.73
UPI0003D0F450	PREDICTED: 28S ribosomal protein S35, mitochondrial isoform X2 n=1 Tax=Rattus norvegicus RepID=UPI0003D0F450	114.55
UPI0003D0F60C	PREDICTED: protein polybromo-1-like isoform X20 n=1 Tax=Rattus norvegicus RepID=UPI0003D0F60C	56.13
UPI0003D0FC8D	PREDICTED: rho guanine nucleotide exchange factor 17 n=1 Tax=Rattus norvegicus RepID=UPI0003D0FC8D	116.54
UPI0003D0FD46	PREDICTED: protein PRRC2A isoform X5 n=1 Tax=Rattus norvegicus RepID=UPI0003D0FD46	196.40
UPI0003D1005E	PREDICTED: reversion-inducing cysteine-rich protein with Kazal motifs isoform X2 n=1 Tax=Rattus norvegicus RepID=UPI0003D1005E	106.68
UPI0004E4726C	PREDICTED: serine/threonine-protein phosphatase 1 regulatory subunit 10 isoform X1 n=1 Tax=Rattus norvegicus RepID=UPI0004E4726C	75.97
UPI0004E472EA	PREDICTED: tenascin isoform X5 n=1 Tax=Rattus norvegicus RepID=UPI0004E472EA	436.20
UPI0004E47558	PREDICTED: drebrin isoform X4 n=1 Tax=Rattus norvegicus RepID=UPI0004E47558	230.32
UPI0004E47B0A	PREDICTED: ribosome-binding protein 1 isoform X2 n=1 Tax=Rattus norvegicus RepID=UPI0004E47B0A	1004.40
UPI0004E47BB8	PREDICTED: methyl-CpG-binding domain protein 3 isoform X4 n=1 Tax=Rattus norvegicus RepID=UPI0004E47BB8	144.46
UPI0004E491F4	PREDICTED: replication factor C subunit 1 isoform X3 n=1 Tax=Rattus norvegicus RepID=UPI0004E491F4	157.82
UPI0004E49349	PREDICTED: ATP-dependent RNA helicase DDX3Y isoform X2 n=1 Tax=Rattus norvegicus RepID=UPI0004E49349	1520.85

Table 9 Proteins specifically identified in TMX samples

Mapped proteins
Unmapped proteins
Unmapped proteins related to cytoskeleton

TMX specific		
Accession	Description	Score
A1A5P2	Ribosome biogenesis regulatory protein homolog OS=Rattus norvegicus GN=Rrs1 PE=2 SV=1 - [RRS1_RAT]	225.91
A2RRU3	U3 small nucleolar RNA-associated protein 15 homolog OS=Rattus norvegicus GN=Utp15 PE=2 SV=1 - [UTP15_RAT]	73.45
B0BMU2	NOP16 nucleolar protein homolog (Yeast) OS=Rattus norvegicus GN=Nop16 PE=2 SV=1 - [B0BMU2_RAT]	81.47
B0BMV8	Dihydrofolate reductase OS=Rattus norvegicus GN=Dhfr PE=2 SV=1 - [B0BMV8_RAT]	57.83
B0BN90	DIM1 dimethyladenosine transferase 1-like (S. cerevisiae) OS=Rattus norvegicus GN=Dimt1 PE=2 SV=1 - [B0BN90_RAT]	130.63
B0BND5	Protein Rrp9 OS=Rattus norvegicus GN=Rrp9 PE=2 SV=1 - [B0BND5_RAT]	83.85
B1H227	LOC682908 protein OS=Rattus norvegicus GN=Rcc1 PE=2 SV=1 - [B1H227_RAT]	101.18
B1H269	Ddx27 protein OS=Rattus norvegicus GN=Ddx27 PE=2 SV=1 - [B1H269_RAT]	305.69
B2GUZ3	Mthfd1l protein OS=Rattus norvegicus GN=Mthfd1l PE=2 SV=1 - [B2GUZ3_RAT]	111.47
B2GV01	Metastasis-associated gene family, member 2 OS=Rattus norvegicus GN=Mta2 PE=2 SV=1 - [B2GV01_RAT]	68.68
B2GV02	Protein LOC100909901 OS=Rattus norvegicus GN=Racgap1 PE=2 SV=1 - [B2GV02_RAT]	179.67
B5DFB2	Protein Rbbp4 OS=Rattus norvegicus GN=Rbbp4 PE=2 SV=1 - [B5DFB2_RAT]	172.55
B5DFG2	Hnrnpl protein (Fragment) OS=Rattus norvegicus GN=Hnrnpl PE=2 SV=1 - [B5DFG2_RAT]	971.96
B5DFJ3	Ddx23 protein (Fragment) OS=Rattus norvegicus GN=Ddx23 PE=2 SV=1 - [B5DFJ3_RAT]	111.47
B6RIU0	FIP1-like 1 OS=Rattus norvegicus GN=Fip1l1 PE=2 SV=1 - [B6RIU0_RAT]	67.5
D3ZAY8	Protein Pnn OS=Rattus norvegicus GN=Pnn PE=4 SV=1 - [D3ZAY8_RAT]	176.85
D3ZAZ0	Eukaryotic translation initiation factor 3 subunit M OS=Rattus norvegicus GN=Eif3m PE=3 SV=1 - [D3ZAZ0_RAT]	220.99
D3ZBS9	Protein Smarcd1 OS=Rattus norvegicus GN=Smarcd1 PE=4 SV=1 - [D3ZBS9_RAT]	120.52
D3ZC82	Protein Nufip2 OS=Rattus norvegicus GN=LOC687994 PE=4 SV=2 - [D3ZC82_RAT]	302.48
D3ZC84	Ubiquitin carboxyl-terminal hydrolase OS=Rattus norvegicus GN=Usp9x PE=3 SV=1 - [D3ZC84_RAT]	100.41
D3ZD73	Protein Ddx6 OS=Rattus norvegicus GN=Ddx6 PE=3 SV=1 - [D3ZD73_RAT]	114.07
D3ZD97	DEAH (Asp-Glu-Ala-His) box polypeptide 15 (Predicted), isoform CRA_b OS=Rattus norvegicus GN=Dhx15 PE=4 SV=1 - [D3ZD97_RAT]	395.81
D3ZDS4	EMG1 nucleolar protein homolog (S. cerevisiae) (Predicted), isoform CRA_b OS=Rattus norvegicus GN=Emg1 PE=4 SV=1 - [D3ZDS4_RAT]	165.69
D3ZF07	Protein RGD1562402 OS=Rattus norvegicus GN=RGD1562402 PE=3 SV=1 - [D3ZF07_RAT]	105.24
D3ZF52	Ribosomal protein L15 OS=Rattus norvegicus GN=RGD1565767 PE=3 SV=1 - [D3ZF52_RAT]	75.88
D3ZF89	Protein Ubap2 OS=Rattus norvegicus GN=Ubap2 PE=4 SV=2 - [D3ZF89_RAT]	733.71
D3ZGE6	Protein Cttn OS=Rattus norvegicus GN=Cttn PE=4 SV=2 - [D3ZGE6_RAT]	293.15
D3ZGQ8	Protein Rsf1 OS=Rattus norvegicus GN=Rsf1 PE=4 SV=1 - [D3ZGQ8_RAT]	86.80

D3ZGV8	Protein Prrc2c OS=Rattus norvegicus GN=Prrc2c PE=1 SV=2 - [D3ZGV8_RAT]	156.03
D3ZL86	HEAT repeat containing 1 (Predicted) OS=Rattus norvegicus GN=Heatr1 PE=4 SV=1 - [D3ZL86_RAT]	107.62
D3ZLC1	Protein Lmnb2 OS=Rattus norvegicus GN=Lmnb2 PE=4 SV=1 - [D3ZLC1_RAT]	285.36
D3ZNU1	Protein Cebpz OS=Rattus norvegicus GN=Cebpz PE=4 SV=1 - [D3ZNU1_RAT]	223.53
D3ZUM5	Protein Trim33 (Fragment) OS=Rattus norvegicus GN=Trim33 PE=4 SV=2 - [D3ZUM5_RAT]	170.29
D3ZUV3	Eukaryotic translation initiation factor 2 subunit 1 OS=Rattus norvegicus GN=Eif2a PE=4 SV=2 - [D3ZUV3_RAT]	66.78
D3ZUX5	Coiled-coil-helix-coiled-coil-helix domain containing 3 (Predicted), isoform CRA_a OS=Rattus norvegicus GN=Chchd3 PE=4 SV=1 - [D3ZUX5_RAT]	82
D3ZV54	Protein Pwp2 OS=Rattus norvegicus GN=Pwp2 PE=4 SV=1 - [D3ZV54_RAT]	103.74
D3ZY44	Protein Mrps2 OS=Rattus norvegicus GN=Mrps2 PE=3 SV=1 - [D3ZY44_RAT]	104.14
D3ZZY2	Protein Utp14a OS=Rattus norvegicus GN=Utp14a PE=4 SV=2 - [D3ZZY2_RAT]	164.01
D3ZZZ0	Protein Ahctf1 OS=Rattus norvegicus GN=Ahctf1 PE=4 SV=1 - [D3ZZZ0_RAT]	106.31
D4A054	Protein LOC100911178 OS=Rattus norvegicus GN=Ranbp2 PE=1 SV=1 - [D4A054_RAT]	618.38
D4A0E8	Protein arginine N-methyltransferase 5 OS=Rattus norvegicus GN=Prmt5 PE=3 SV=1 - [D4A0E8_RAT]	60.82
D4A0H5	Cleavage and polyadenylation specific factor 1, 160kDa (Predicted), isoform CRA_a OS=Rattus norvegicus GN=Cpsf1 PE=4 SV=1 - [D4A0H5_RAT]	96.85
D4A1K2	Protein Rpl7l1 OS=Rattus norvegicus GN=Rpl7l1 PE=3 SV=1 - [D4A1K2_RAT]	59.47
D4A512	Protein Nemf OS=Rattus norvegicus GN=Nemf PE=4 SV=2 - [D4A512_RAT]	130.66
D4A7J8	PRP4 pre-mRNA processing factor 4 homolog (Yeast) OS=Rattus norvegicus GN=Prpf4 PE=4 SV=1 - [D4A7J8_RAT]	69.15
D4ACW0	Protein Rbm6 OS=Rattus norvegicus GN=Rbm6 PE=4 SV=1 - [D4ACW0_RAT]	65.49
D4AE41	RNA binding motif protein, X-linked-like-1 OS=Rattus norvegicus GN=Rbmxl1 PE=3 SV=1 - [RMXL1_RAT]	309.16
D4AEC0	Histone H2A OS=Rattus norvegicus GN=LOC685909 PE=3 SV=1 - [D4AEC0_RAT]	146.52
E9PTI6	Protein Raly OS=Rattus norvegicus GN=Raly PE=4 SV=1 - [E9PTI6_RAT]	110.3
E9PU01	Protein Chd4 OS=Rattus norvegicus GN=Chd4 PE=4 SV=2 - [E9PU01_RAT]	215.01
F1LMV9	Coronin (Fragment) OS=Rattus norvegicus GN=Coro2b PE=3 SV=2 - [F1LMV9_RAT]	158.8
F1LP60	Moesin (Fragment) OS=Rattus norvegicus GN=Msn PE=4 SV=1 - [F1LP60_RAT]	101.22
F1LPQ3	Alpha-mannosidase 2C1 OS=Rattus norvegicus GN=Man2c1 PE=4 SV=1 - [F1LPQ3_RAT]	135.14
F1LR39	RCG29171, isoform CRA_a OS=Rattus norvegicus GN=Wdr18 PE=4 SV=2 - [F1LR39_RAT]	107.57
F1LRJ2	Protein Srrm2 OS=Rattus norvegicus GN=Srrm2 PE=1 SV=2 - [F1LRJ2_RAT]	358.01
F1LSL3	Inositol 1,4,5-trisphosphate receptor type 3 OS=Rattus norvegicus GN=Itpr3 PE=4 SV=2 - [F1LSL3_RAT]	134.52
F1LU69	Protein Rps27l3 OS=Rattus norvegicus GN=Rps27l3 PE=4 SV=2 - [F1LU69_RAT]	122.83
F1LVD0	Protein LOC690134 (Fragment) OS=Rattus norvegicus GN=LOC690134 PE=3 SV=2 - [F1LVD0_RAT]	104.42
F1LYI5	Protein RGD1564138 (Fragment) OS=Rattus norvegicus GN=RGD1564138 PE=4 SV=2 - [F1LYI5_RAT]	62.79
F1M5V2	Protein Glipr2 OS=Rattus norvegicus GN=Glipr2 PE=4 SV=2 - [F1M5V2_RAT]	128.89

F1M6V1	Heterochromatin protein 1-binding protein 3 OS=Rattus norvegicus GN=Hp1bp3 PE=3 SV=2 - [F1M6V1_RAT]	238.55
F1M779	Clathrin heavy chain OS=Rattus norvegicus GN=Cltc PE=3 SV=1 - [F1M779_RAT]	459.49
F1M7A0	DNA topoisomerase 2 (Fragment) OS=Rattus norvegicus GN=Top2a PE=3 SV=2 - [F1M7A0_RAT]	123.77
F1M8H5	Protein Abcf2 OS=Rattus norvegicus GN=Abcf2 PE=4 SV=2 - [F1M8H5_RAT]	62.84
F1MA04	Protein Wdr36 (Fragment) OS=Rattus norvegicus GN=Wdr36 PE=4 SV=2 - [F1MA04_RAT]	99.43
F1MA52	Nuclear RNA export factor 1 OS=Rattus norvegicus GN=Nxf1 PE=4 SV=1 - [F1MA52_RAT]	187.82
F7FFV2	Keratin, type II cytoskeletal 5 (Fragment) OS=Rattus norvegicus GN=Krt5 PE=3 SV=1 - [F7FFV2_RAT]	361.29
G3V661	Bromodomain adjacent to zinc finger domain protein 1B OS=Rattus norvegicus GN=Baz1b PE=4 SV=1 - [G3V661_RAT]	176.36
G3V6A8	Golgi autoantigen, golgin subfamily b, macrogolgin 1, isoform CRA_c OS=Rattus norvegicus GN=Golgb1 PE=1 SV=1 - [G3V6A8_RAT]	63.1
G3V6D3	ATP synthase subunit beta OS=Rattus norvegicus GN=Atp5b PE=3 SV=1 - [G3V6D3_RAT]	103.05
G3V7B7	DNA-directed RNA polymerase OS=Rattus norvegicus GN=Polr1a PE=3 SV=1 - [G3V7B7_RAT]	119.52
G3V7G3	Activity-dependent neuroprotector homeobox protein OS=Rattus norvegicus GN=Adnp PE=4 SV=1 - [G3V7G3_RAT]	75.42
G3V7G9	Eukaryotic translation initiation factor 3 subunit L OS=Rattus norvegicus GN=Eif3l PE=2 SV=2 - [G3V7G9_RAT]	111.6
G3V852	Protein Tln1 OS=Rattus norvegicus GN=Tln1 PE=1 SV=1 - [G3V852_RAT]	343.86
G3V8G5	Golgi apparatus protein 1 OS=Rattus norvegicus GN=Glg1 PE=4 SV=1 - [G3V8G5_RAT]	67.53
G3V920	Protein Wdr43 OS=Rattus norvegicus GN=Wdr43 PE=4 SV=1 - [G3V920_RAT]	178.54
G3V9R8	Heterogeneous nuclear ribonucleoprotein C (C1/C2) OS=Rattus norvegicus GN=Hnrnpc PE=1 SV=2 - [G3V9R8_RAT]	719.77
M0R3M8	Protein Rrp12 OS=Rattus norvegicus GN=Rrp12 PE=4 SV=1 - [M0R3M8_RAT]	243.03
M0R3Z8	Protein Rbm15 OS=Rattus norvegicus GN=Rbm15 PE=1 SV=1 - [M0R3Z8_RAT]	106.55
M0R440	Zinc finger protein 326 (Fragment) OS=Rattus norvegicus GN=Zfp326 PE=4 SV=1 - [M0R440_RAT]	90.43
M0R548	Protein LOC100912029 OS=Rattus norvegicus GN=LOC100912029 PE=4 SV=1 - [M0R548_RAT]	129.59
M0R7D1	La-related protein 7 OS=Rattus norvegicus GN=Larp7 PE=4 SV=1 - [M0R7D1_RAT]	175.62
M0R8A7	tRNA selenocysteine 1-associated protein 1 OS=Rattus norvegicus GN=Trnau1ap PE=4 SV=1 - [M0R8A7_RAT]	78.07
M0R9Q1	Protein LOC100911677 OS=Rattus norvegicus GN=LOC100911677 PE=4 SV=1 - [M0R9Q1_RAT]	561.89
M0RB74	Protein Ipo5 OS=Rattus norvegicus GN=Ipo5 PE=4 SV=1 - [M0RB74_RAT]	94.41
M0RDD7	RCG29880 OS=Rattus norvegicus GN=Chtop PE=4 SV=1 - [M0RDD7_RAT]	157.28
M0RDF7	Bystin OS=Rattus norvegicus GN=Bysl PE=4 SV=1 - [M0RDF7_RAT]	101.76
O88656	Actin-related protein 2/3 complex subunit 1B OS=Rattus norvegicus GN=Arpc1b PE=2 SV=3 - [ARC1B_RAT]	79.63
O88791	High mobility group AT-hook 2 OS=Rattus norvegicus GN=Hmga2 PE=2 SV=1 - [O88791_RAT]	193.05
P04256	Heterogeneous nuclear ribonucleoprotein A1 OS=Rattus norvegicus GN=Hnrnpa1 PE=1 SV=3 - [ROA1_RAT]	1111.8
P07943	Aldose reductase OS=Rattus norvegicus GN=Akr1b1 PE=1 SV=3 - [ALDR_RAT]	68.28
P09895	60S ribosomal protein L5 OS=Rattus norvegicus GN=Rpl5 PE=1 SV=3 - [RL5_RAT]	403.43

P15999	ATP synthase subunit alpha, mitochondrial OS=Rattus norvegicus GN=Atp5a1 PE=1 SV=2 - [ATPA_RAT]	213.57
P17136	Small nuclear ribonucleoprotein-associated protein B (Fragment) OS=Rattus norvegicus GN=Snrpb PE=2 SV=1 - [RSMB_RAT]	67.32
P30427	Plectin OS=Rattus norvegicus GN=Plec PE=1 SV=2 - [PLEC_RAT]	10108.38
P38650	Cytoplasmic dynein 1 heavy chain 1 OS=Rattus norvegicus GN=Dync1h1 PE=1 SV=1 - [DYHC1_RAT]	447.17
P54313	Guanine nucleotide-binding protein G(I)/G(S)/G(T) subunit beta-2 OS=Rattus norvegicus GN=Gnb2 PE=1 SV=4 - [GBB2_RAT]	260.48
P55770	NHP2-like protein 1 OS=Rattus norvegicus GN=Nhp2l1 PE=2 SV=4 - [NH2L1_RAT]	89.96
P62138	Serine/threonine-protein phosphatase PP1-alpha catalytic subunit OS=Rattus norvegicus GN=Ppp1ca PE=1 SV=1 - [PP1A_RAT]	304.89
P62142	Serine/threonine-protein phosphatase PP1-beta catalytic subunit OS=Rattus norvegicus GN=Ppp1cb PE=1 SV=3 - [PP1B_RAT]	316.31
P62275	40S ribosomal protein S29 OS=Rattus norvegicus GN=Rps29 PE=1 SV=2 - [RS29_RAT]	64.98
P62828	GTP-binding nuclear protein Ran OS=Rattus norvegicus GN=Ran PE=1 SV=3 - [RAN_RAT]	66.6
P62859	40S ribosomal protein S28 OS=Rattus norvegicus GN=Rps28 PE=1 SV=1 - [RS28_RAT]	66
P68255	14-3-3 protein theta OS=Rattus norvegicus GN=Ywhaq PE=1 SV=1 - [1433T_RAT]	124.26
P70501	RNA-binding protein 10 OS=Rattus norvegicus GN=Rbm10 PE=2 SV=1 - [RBM10_RAT]	105.63
P70565	Plakoglobin OS=Rattus norvegicus GN=Jup PE=2 SV=1 - [P70565_RAT]	1053.15
P70625	Zonula occludens 2 protein (Fragment) OS=Rattus norvegicus GN=ZO-2 PE=2 SV=2 - [P70625_RAT]	74.88
P97690	Structural maintenance of chromosomes protein 3 OS=Rattus norvegicus GN=Smc3 PE=1 SV=1 - [SMC3_RAT]	201.58
Q05096-3	Isoform C of Unconventional myosin-Ib n=1 Tax=Rattus norvegicus RepID=Q05096-3	232.36
Q09073	ADP/ATP translocase 2 OS=Rattus norvegicus GN=Slc25a5 PE=1 SV=3 - [ADT2_RAT]	274.1
Q0D2G9	RGD1308290 protein (Fragment) OS=Rattus norvegicus GN=RGD1308290 PE=2 SV=1 - [Q0D2G9_RAT]	123.28
Q14V05	Tat-binding protein-1 OS=Rattus rattus GN=TBP-1 PE=2 SV=1 - [Q14V05_RATRT]	78.51
Q27W01	RNA-binding protein 8A OS=Rattus norvegicus GN=Rbm8a PE=2 SV=1 - [RBM8A_RAT]	129.97
Q3KRE0	ATPase family AAA domain-containing protein 3 OS=Rattus norvegicus GN=Atad3 PE=1 SV=1 - [ATAD3_RAT]	83.55
Q3T1K5	F-actin-capping protein subunit alpha-2 OS=Rattus norvegicus GN=Capza2 PE=1 SV=1 - [CAZA2_RAT]	92.99
Q498C9	Protein Zfp207 OS=Rattus norvegicus GN=Zfp207 PE=2 SV=1 - [Q498C9_RAT]	66.03
Q4FZT9	26S proteasome non-ATPase regulatory subunit 2 OS=Rattus norvegicus GN=Psmd2 PE=2 SV=1 - [PSMD2_RAT]	117.94
Q4KLH7	Protein Rad21 OS=Rattus norvegicus GN=Rad21 PE=2 SV=1 - [Q4KLH7_RAT]	86.19
Q4KLI7	Protein Sf3a3 OS=Rattus norvegicus GN=Sf3a3 PE=2 SV=1 - [Q4KLI7_RAT]	76.83
Q4QQT3	CUGBP Elav-like family member 1 OS=Rattus norvegicus GN=Celf1 PE=2 SV=1 - [CELF1_RAT]	78.57
Q4V8E1	GATA zinc finger domain containing 2B OS=Rattus norvegicus GN=Gatad2b PE=2 SV=1 - [Q4V8E1_RAT]	121.64
Q5EB56	MAK16 homolog (S. cerevisiae) OS=Rattus norvegicus GN=Mak16 PE=2 SV=1 - [Q5EB56_RAT]	75.62
Q5EEY3	GTP-binding protein G-alpha-i2 splice variant b OS=Rattus norvegicus GN=Gnai2 PE=2 SV=1 - [Q5EEY3_RAT]	248.22
Q5M7V8	Thyroid hormone receptor-associated protein 3 OS=Rattus norvegicus GN=Thrap3 PE=1 SV=1 - [TR150_RAT]	164.51

Q5M920	EBNA1 binding protein 2 OS=Rattus norvegicus GN=Ebna1bp2 PE=2 SV=1 - [Q5M920_RAT]	138.38
Q5RKJ9	RAB10, member RAS oncogene family OS=Rattus norvegicus GN=Rab10 PE=2 SV=1 - [Q5RKJ9_RAT]	69.11
Q5U2Y1-2	Isoform 2 of General transcription factor II-I n=2 Tax=Rattus norvegicus RepID=Q5U2Y1-2	93.22
Q5U302	Catenin (Cadherin associated protein), alpha 1 OS=Rattus norvegicus GN=Ctnna1 PE=1 SV=1 - [Q5U302_RAT]	2959.13
Q5XI13	Glutamate-rich WD repeat-containing protein 1 OS=Rattus norvegicus GN=Grwd1 PE=2 SV=1 - [GRWD1_RAT]	82.5
Q5XIB5	Coiled-coil domain-containing protein 86 OS=Rattus norvegicus GN=Ccdc86 PE=2 SV=1 - [CCD86_RAT]	58.31
Q62636	Ras-related protein Rap-1b OS=Rattus norvegicus GN=Rap1b PE=2 SV=2 - [RAP1B_RAT]	94.76
Q62940	E3 ubiquitin-protein ligase NEDD4 OS=Rattus norvegicus GN=Nedd4 PE=1 SV=1 - [NEDD4_RAT]	152.79
Q63413	Spliceosome RNA helicase Ddx39b OS=Rattus norvegicus GN=Ddx39b PE=1 SV=3 - [DX39B_RAT]	131.1
Q63692	Hsp90 co-chaperone Cdc37 OS=Rattus norvegicus GN=Cdc37 PE=1 SV=2 - [CDC37_RAT]	81.21
Q63716	Peroxiredoxin-1 OS=Rattus norvegicus GN=Prdx1 PE=1 SV=1 - [PRDX1_RAT]	110.87
Q641X8	Eukaryotic translation initiation factor 3 subunit E OS=Rattus norvegicus GN=Eif3e PE=2 SV=1 - [EIF3E_RAT]	208.94
Q66HG8	Protein Red OS=Rattus norvegicus GN=Ik PE=1 SV=1 - [RED_RAT]	178.45
Q6AXU3	Interferon-stimulated 20 kDa exonuclease-like 2 OS=Rattus norvegicus GN=Isg20l2 PE=2 SV=1 - [I20L2_RAT]	278.57
Q6AY87	THO complex subunit 6 homolog OS=Rattus norvegicus GN=Thoc6 PE=2 SV=1 - [THOC6_RAT]	101.05
Q6AYD3	Proliferation-associated 2G4 OS=Rattus norvegicus GN=Pa2g4 PE=2 SV=1 - [Q6AYD3_RAT]	152.33
Q6AYZ1	Tubulin alpha-1C chain OS=Rattus norvegicus GN=Tuba1c PE=1 SV=1 - [TBA1C_RAT]	625.13
Q6IFU8	Keratin, type I cytoskeletal 17 OS=Rattus norvegicus GN=Krt17 PE=2 SV=1 - [K1C17_RAT]	188.42
Q6VEU8	DEAD (Asp-Glu-Ala-Asp) box polypeptide 24 OS=Rattus norvegicus GN=Ddx24 PE=2 SV=1 - [Q6VEU8_RAT]	355.19
Q8CHN6	Sphingosine-1-phosphate lyase 1 OS=Rattus norvegicus GN=Sgpl1 PE=2 SV=1 - [SGPL1_RAT]	90.04
Q8K585-2	Isoform HMG-Y of High mobility group protein HMG-I/HMG-Y n=1 Tax=Rattus norvegicus RepID=Q8K585-2	86.88
Q9ESY8	Stau1 protein OS=Rattus norvegicus GN=Stau1 PE=2 SV=1 - [Q9ESY8_RAT]	170.06
Q9QYW0	Protein AATF OS=Rattus norvegicus GN=Aatf PE=1 SV=1 - [AATF_RAT]	88.82
Q9R1T1	Barrier-to-autointegration factor OS=Rattus norvegicus GN=Banf1 PE=1 SV=1 - [BAF_RAT]	110.13
Q9R1Z0	Voltage-dependent anion-selective channel protein 3 OS=Rattus norvegicus GN=Vdac3 PE=1 SV=2 - [VDAC3_RAT]	62.63
Q9WUC8	Pleiotropic regulator 1 OS=Rattus norvegicus GN=Plrg1 PE=2 SV=1 - [PLRG1_RAT]	83.1
Q9Z118	Polypyrimidine tract-binding protein 3 OS=Rattus norvegicus GN=Ptbp3 PE=2 SV=1 - [PTBP3_RAT]	154.24
UPI000017E2CF	PREDICTED: nucleolar protein 14 isoform X1 n=1 Tax=Rattus norvegicus RepID=UPI000017E2CF	127.69
UPI000017F893	proline-, glutamic acid- and leucine-rich protein 1 n=1 Tax=Rattus norvegicus RepID=UPI000017F893	144.82
UPI00001CFDCB	PREDICTED: polymerase delta-interacting protein 3 isoform X1 n=1 Tax=Rattus norvegicus RepID=UPI00001CFDCB	89.79
UPI0000503E75	PREDICTED: ribonucleases P/MRP protein subunit POP1 isoform X1 n=1 Tax=Rattus norvegicus RepID=UPI0000503E75	62.62
UPI0000DA267A	PREDICTED: filamin-C isoform X1 n=1 Tax=Rattus norvegicus RepID=UPI0000DA267A	382.84

UPI0000DA3509	PREDICTED: RNA-binding protein 25 n=1 Tax=Rattus norvegicus RepID=UPI0000DA3509	90.36
UPI0000DA3DFF	PREDICTED: rho GTPase-activating protein 22 isoform X4 n=1 Tax=Rattus norvegicus RepID=UPI0000DA3DFF	91.37
UPI0000DA4524	LAS1-like n=2 Tax=Rattus norvegicus RepID=UPI0000DA4524	179.85
UPI0000DBFEDB	PREDICTED: pumilio homolog 1 isoform X11 n=1 Tax=Rattus norvegicus RepID=UPI0000DBFEDB	60.06
UPI000150B091	PREDICTED: drebrin isoform X3 n=1 Tax=Rattus norvegicus RepID=UPI000150B091	368.84
UPI000154D8C8	nuclear pore complex protein Nup160 n=1 Tax=Rattus norvegicus RepID=UPI000154D8C8	80.87
UPI0001551D2B	PREDICTED: uncharacterized protein C9orf114 homolog isoform X1 n=1 Tax=Rattus norvegicus RepID=UPI0001551D2B	62.13
UPI0001552819	PREDICTED: 5""-3"" exoribonuclease 2 isoform X2 n=1 Tax=Rattus norvegicus RepID=UPI0001552819	272.67
UPI0001B79CC2	PREDICTED: probable ATP-dependent RNA helicase YTHDC2 n=1 Tax=Rattus norvegicus RepID=UPI0001B79CC2	57.63
UPI0001CF735C	neuroblast differentiation-associated protein AHNAK n=1 Tax=Rattus norvegicus RepID=UPI0001CF735C	123.47
UPI000268808A	zinc finger RNA-binding protein n=1 Tax=Rattus norvegicus RepID=UPI000268808A	351.66
UPI0003D0721E	PREDICTED: fibronectin isoform X10 n=1 Tax=Rattus norvegicus RepID=UPI0003D0721E	974.83
UPI0003D07514	PREDICTED: poly(U)-binding-splicing factor PUF60 isoform X5 n=1 Tax=Rattus norvegicus RepID=UPI0003D07514	250.38
UPI0003D07629	PREDICTED: 28S ribosomal protein S29, mitochondrial isoform X1 n=1 Tax=Rattus norvegicus RepID=UPI0003D07629	267.18
UPI0003D0803D	PREDICTED: pre-mRNA-processing factor 40 homolog A isoform X4 n=1 Tax=Rattus norvegicus RepID=UPI0003D0803D	109.22
UPI0003D080F2	PREDICTED: lupus La protein homolog isoform X3 n=1 Tax=Rattus norvegicus RepID=UPI0003D080F2	277.66
UPI0003D084DB	PREDICTED: E3 ubiquitin-protein ligase TRIP12 isoform X11 n=1 Tax=Rattus norvegicus RepID=UPI0003D084DB	233.48
UPI0003D0853E	PREDICTED: tripeptidyl-peptidase 2 isoform X3 n=1 Tax=Rattus norvegicus RepID=UPI0003D0853E	129.52
UPI0003D08BBF	PREDICTED: protein KRI1 homolog n=1 Tax=Rattus norvegicus RepID=UPI0003D08BBF	127.28
UPI0003D08D2D	PREDICTED: RNA-binding motif, single-stranded-interacting protein 1 isoform X2 n=1 Tax=Rattus norvegicus RepID=UPI0003D08D2D	166.92
UPI0003D09498	PREDICTED: U3 small nucleolar RNA-associated protein 6 homolog n=1 Tax=Rattus norvegicus RepID=UPI0003D09498	60.17
UPI0003D09676	PREDICTED: unconventional myosin-VI isoform X4 n=1 Tax=Rattus norvegicus RepID=UPI0003D09676	77.78
UPI0003D09A07	PREDICTED: nuclear pore complex protein Nup98-Nup96 isoform X3 n=1 Tax=Rattus norvegicus RepID=UPI0003D09A07	130.13
UPI0003D0A336	PREDICTED: cell division cycle and apoptosis regulator protein 1 isoform X5 n=1 Tax=Rattus norvegicus RepID=UPI0003D0A336	118.36
UPI0003D0A51A	PREDICTED: zinc finger CCHC domain-containing protein 8 isoform X2 n=1 Tax=Rattus norvegicus RepID=UPI0003D0A51A	144.9
UPI0003D0A55E	PREDICTED: C-Jun-amino-terminal kinase-interacting protein 4 isoform X9 n=1 Tax=Rattus norvegicus RepID=UPI0003D0A55E	265.06
UPI0003D0A726	PREDICTED: UPF0568 protein C14orf166 homolog isoform X2 n=1 Tax=Rattus norvegicus RepID=UPI0003D0A726	383.1
UPI0003D0AB54	PREDICTED: telomere-associated protein RIF1-like n=1 Tax=Rattus norvegicus RepID=UPI0003D0AB54	217.61
UPI0003D0AB89	PREDICTED: ribosomal RNA processing protein 1 homolog B isoform X2 n=1 Tax=Rattus norvegicus RepID=UPI0003D0AB89	175.37
UPI0003D0BDBD	PREDICTED: SWI/SNF complex subunit SMARCC2-like isoform X10 n=1 Tax=Rattus norvegicus RepID=UPI0003D0BDBD	360.50
UPI0003D0BE0D	PREDICTED: trinucleotide repeat-containing gene 6A protein isoform X4 n=1 Tax=Rattus norvegicus RepID=UPI0003D0BE0D	205.97

UPI0003D0BE42	PREDICTED: methionine--tRNA ligase, cytoplasmic isoform X2 n=1 Tax=Rattus norvegicus RepID=UPI0003D0BE42	187.43
UPI0003D0C521	PREDICTED: LOW QUALITY PROTEIN: deoxynucleotidyltransferase terminal-interacting protein 2-like n=1 Tax=Rattus norvegicus RepID=UPI0003D0C521	319.34
UPI0003D0CF50	PREDICTED: ubiquitin-associated and SH3 domain-containing protein B isoform X4 n=1 Tax=Rattus norvegicus RepID=UPI0003D0CF50	126.63
UPI0003D0D1B4	PREDICTED: serrate RNA effector molecule homolog isoform X1 n=1 Tax=Rattus norvegicus RepID=UPI0003D0D1B4	164.05
UPI0003D0F25F	PREDICTED: nestin-like, partial n=1 Tax=Rattus norvegicus RepID=UPI0003D0F25F	2840.27
UPI0004E473EA	PREDICTED: plectin isoform X4 n=1 Tax=Rattus norvegicus RepID=UPI0004E473EA	10302.63
UPI0004E4745E	PREDICTED: TATA-binding protein-associated factor 2N-like isoform X1 n=1 Tax=Rattus norvegicus RepID=UPI0004E4745E	294.9
UPI0004E477F8	PREDICTED: band 4.1-like protein 2 isoform X7 n=1 Tax=Rattus norvegicus RepID=UPI0004E477F8	120.66
UPI0004E4789B	PREDICTED: cirhin isoform X2 n=1 Tax=Rattus norvegicus RepID=UPI0004E4789B	66.53
UPI0004E48548	PREDICTED: nuclear pore complex protein Nup153 isoform X1 n=1 Tax=Rattus norvegicus RepID=UPI0004E48548	94.36
UPI0004E4880A	PREDICTED: ATP-dependent RNA helicase DHX36 isoform X1 n=1 Tax=Rattus norvegicus RepID=UPI0004E4880A	135.6
UPI0004E48819	PREDICTED: LOW QUALITY PROTEIN: eukaryotic translation initiation factor 4 gamma 2-like isoform X1, partial n=1 Tax=Rattus norvegicus RepID=UPI0004E48819	63.71
UPI0004E4891E	PREDICTED: tumor suppressor p53-binding protein 1 isoform X1 n=1 Tax=Rattus norvegicus RepID=UPI0004E4891E	164.65
UPI0004E4894C	PREDICTED: nucleolar protein 6 isoform X2 n=1 Tax=Rattus norvegicus RepID=UPI0004E4894C	148.76
UPI0004E489DA	PREDICTED: zinc finger CCCH domain-containing protein 14 isoform X2 n=1 Tax=Rattus norvegicus RepID=UPI0004E489DA	148.34
UPI0004E48B1F	PREDICTED: ataxin-2 isoform X14 n=1 Tax=Rattus norvegicus RepID=UPI0004E48B1F	114.19
UPI0004E48EB3	PREDICTED: U4/U6 small nuclear ribonucleoprotein Prp3 isoform X3 n=1 Tax=Rattus norvegicus RepID=UPI0004E48EB3	111.24
UPI0004E48EEF	PREDICTED: tight junction protein ZO-1 isoform X4 n=1 Tax=Rattus norvegicus RepID=UPI0004E48EEF	101.32
UPI0004E48FAD	PREDICTED: la-related protein 4 isoform X6 n=2 Tax=Rattus norvegicus RepID=UPI0004E48FAD	129.83
UPI0004E494D5	PREDICTED: splicing factor 3B subunit 2 isoform X1 n=1 Tax=Rattus norvegicus RepID=UPI0004E494D5	268.27